

SITES FOR WIND POWER INSTALLATIONS:
Physical Modeling of the Influence of Hills
Ridges and Complex Terrain on
Wind Speed and Turbulence

by

R.N. Meroney and V.A. Sandborn
Principal Investigators

R.J.B. Bouwmeester, H.C. Chien, M. Rider
Associate Investigators

FINAL REPORT: PART II

APPENDIX

Fluid Mechanics and Wind Engineering Program
Civil Engineering Department
Colorado State University
Fort Collins, Colorado 80523

June 1978

Engineering Sciences

AUG 24 '79

Branch Library

Prepared for the United States
Department of Energy
Division of Distributed Solar Technology
Federal Wind Energy Program

DOE Contract No. EY-76-S-06-2438, A001

NOTICE

This report was prepared as an account of work sponsored by an agency of the United States Government. Neither the United States nor any agency thereof, nor any of their employees, makes any warranty, expressed or implied, or assumes any legal liability or responsibility for any third party's use or the results of such use of any information, apparatus, product or process disclosed in this report, or represents that its use by such third party would not infringe privately owned rights.

ACKNOWLEDGEMENT

The authors wish to express their appreciation to Drs. William Pennell and Ronald Drake of Battelle, Pacific Northwest Laboratories, for their technical review and advice, to Ms. Pamela Partch for her careful editorial review and criticism, and to Mrs. Louise Warren for her patience during typing many revisions of this report. Special thanks is given to George Tennyson and Louis Divone of the Department of Energy Wind Systems Branch for their support and advice.

TABLE OF CONTENTS - APPENDICES

	<u>PAGE</u>
APPENDIX A: MEASUREMENTS OF THE MEAN AND LONGITUDINAL TURBULENT VELOCITIES OVER VARYING HILL SHAPES . . .	1
SUMMARY	1
INTRODUCTION	1
TEST SETUP	1
FLOW VISUALIZATION	2
RESULTS	2
CONCLUDING REMARKS	3
REFERENCES	3
TABLES	4
FIGURES	11
APPENDIX B: BOUNDARY LAYER TURBULENCE OVER TWO-DIMENSIONAL HILLS	30
SUMMARY	30
INTRODUCTION	30
THEORETICAL BACKGROUND	31
Surface Shear Stress Evaluation	32
Shear Stress Distribution Evaluation	34
TURBULENT VELOCITY COMPONENT SIMILARITY	36
BOUNDARY CONDITIONS	38
EXPERIMENTAL SETUP	39
Wind Tunnel Facility	39
Model Description	40
Instrumentation	40
Static Pressure Measurements	40
Velocity Measurements	41
Turbulence and Shear Stress Measurements	42
RESULTS AND DISCUSSION	42
Mean Velocity	43
Longitudinal Turbulent Velocities	43
Vertical Turbulent Component	44
Shear Stress Distribution and Surface Static Pressure	44
CONCLUSIONS	46
REFERENCES	46
FIGURES	48
TABLES	52

	<u>PAGE</u>
APPENDIX C: MEASUREMENTS OF MEAN AND TURBULENT VELOCITIES AND TEMPERATURE FOR THERMALLY STRATIFIED FLOWS	
SUMMARY	134
INTRODUCTION	134
MEASUREMENTS	134
RESULTS	136
TABLES	138
FIGURES	145
APPENDIX D: MEASUREMENTS OF FLOW OVER MODEL THREE-DIMENSIONAL HILLS	161
SUMMARY	161
INTRODUCTION	161
EXPERIMENTAL SETUP	161
Wind Tunnel Facility	162
Model Description	162
Instrumentation	162
STATIC PRESSURE MEASUREMENTS	162
VELOCITY MEASUREMENTS	162
RESULTS	163
CONCLUDING REMARKS	164
REFERENCES	164
TABLES	165
FIGURES	176
APPENDIX E: EFFECTS OF ALTERNATE RIDGE SHAPES	189
SUMMARY	189
INTRODUCTION	189
BLUFF RIDGES	189
TABLES	191
FIGURES	194

LIST OF TABLES

<u>Table</u>		<u>Page</u>
AI	Measured mean and turbulent velocity distributions	4
BI	Tabulated data for Flow Case I: 1:2 hill model . . .	48
CI	1 to 4 ridge data	138
CII	1 to 6 ridge data	143
DI	Static pressure on the surface of Gaussian hill . . .	165
DII	Static pressure on the surface of 1:4 cone hill . . .	166
DIII	Tabulated upstream velocity profiles for each hill .	167
DIV	Tabulated velocity profiles	168
DV	Tabulated velocity profiles	172
DVI	TABulated velocity profiles	175
EI	Velocity profiles. Bluff step ridge	191
EII	Velocity profiles 1:1.5 slope ridge	192

LIST OF FIGURES

<u>Figure</u>		<u>Page</u>
A1	Transpiration wind tunnel	11
A2	Wind tunnel setup	12
A3	Hill shapes	13
A4	Flow visualization	14
A5	Velocity profile for hill models	16
A6	Velocity speedup between approach flow and crest . .	22
A7	Longitudinal turbulent component hill model	23
A8	Comparison of data from two similar triangular hills.	29
B1	Comparison of Ludwig-Tillmann equation and shear-stress meter (4)	70
B2	Comparison of shear stress evaluated by Ludwig- Tillmann equation and "law of the wall" of flat plate	71
B3	Comparison of shear-stress distribution, for zero pressure gradient flow, with values determined from equation (A-15) (7)	72
B4	Comparison of shear stress measurements by Klebanoff and Zoric (10)	73
B5	Comparison of flat plate longitudinal turbulent velocity distribution of Klebanoff and Zoric (10) . .	74
B6	Comparison of flat plate vertical turbulent velocity distribution of Klebanoff, Zoric and Tieleman (10) .	75
B7	Shear stress evaluated by the "law of the wall" for standard coordinates and curvilinear coordinates . .	76
B8	Meteorological wind tunnel	77
B9	Tunnel setup for Flow Case I	78
B10	Tunnel setup for Flow Case II	79
B11	Schematic of probes	80

LIST OF FIGURES (continued)

<u>Figure</u>		<u>Page</u>
B12	Model description and instrumentation location dimensions listed in cm	81
B13	Schematic of equipment setup	82
B14	Velocity similarity profiles for both flow cases .	83
B15	Upstream similarity velocity profiles and velocity at the crest	84
B16	Velocity profiles Flow Case I	86
B17	Velocity profiles Flow Case II	89
B18	Upstream measurements compared to measurements at crest (Flow Case I)	91
B19	Upstream measurements compared to measurements at crest (Flow Case II)	93
B20	Profiles Flow Case I	94
B21	Profiles Flow Case II	102
B22	Comparison of upstream measurements to those of Zoric and Klebanoff. Flow Case I	109
B23	Comparison of upstream measurements to those of Zoric and Klebanoff. Flow Case II	110
B24	Upstream measurements compared to measurements at crest. Flow Case I	111
B25	Profiles Flow Case I	113
B26	Comparison of measurements to those of Zoric and Tieleman. Flow Case I	121
B27	Wall, shear stress, and static pressure distribu- tion	123
B28	Shear stress distribution Flow Case I	125
B29	Comparison of upstream shear stress distribution to that of Zoric. Flow Case I	133
B30	Comparison of upstream shear stress distribution to that of Zoric. Flow Case II	133

LIST OF FIGURES (continued)

<u>Figure</u>		<u>Page</u>
C1	Velocity distributions over the 1 to 4 slope ridge	145
C2	Velocity distribution over the 1 to 6 slope ridge	148
C3	Temperature distribution over the 1 to 4 slope ridge	150
C4	Temperature distributions over the 1 to 6 slope ridge	153
C5	Longitudinal turbulence over the 1 to 4 slope ridge	155
C6	Longitudinal turbulence over the 1 to 6 slope ridge	157
C7	Temperature fluctuations over the 1 to 4 slope ridge	158
C8	Temperature fluctuations over the 1 to 6 slope ridge	159
D1	Dimension of 3 dimensional hills and location of static taps on their surfaces (Real scale) . . .	176
D2	Surface oil streak patterns over the Gaussian hill (top view)	178
D3	Smoke streak patterns over the Gaussian hill . .	179
D4	Upstream velocity profiles	180
D5	Velocity profiles for Hill No. 1	181
D6	Velocity profiles for Hill No. 1	182
D7	Velocity profiles for Hill No. 1	183
D8	Velocity profiles for Hill No. 1	184
D9	Velocity profiles for Hill No. 2	185
D10	Velocity profiles for Hill No. 2	186

LIST OF FIGURES (continued)

<u>Figure</u>		<u>Page</u>
D11	Velocity profiles for Hill No. 2	187
D12	Velocity profiles for Hill No. 3	188
E1	Velocity profiles along the top of a bluff-step ridge	194
E2	Measured separation bubble extent at the forward edge of a bluff-step ridge	196
E3	Velocity distributions over a bluff-step sloped ridge	197

NOMENCLATURE

A	Hot wire calibration constant
A_1	Constant in the boundary layer logarithmic velocity profile
A_2	Boundary layer similarity parameter
B	Hot wire calibration constant
B_1	Constant in the boundary layer logarithmic velocity profile
B_2	Boundary layer similarity parameter
b	Test model cord length, cm
C	Hot wire calibration constant
C_1	Constant in the boundary layer logarithmic velocity profile
C_f	Skin friction coefficient
C_p	Pressure coefficient
DE/DU	Hot wire sensitivity to velocity v , volts/m/s
DELTA	Boundary layer thickness, cm
E	Hot wire voltage, volts
e	Time varying part of the hot wire voltage, volts
f_v	Mean velocity function
$f_{\rho v}$	Mean mass flow function
H	Model maximum height, cm
H^*	Boundary layer form factor
I	Hot wire current, amps
L	One fourth the model cord length, cm
P	Pressure, N/m^2

NOMENCLATURE (continued)

R	Radial distance in polar coordinates, cm
Re	Reynolds number
Ri	Richardson number
RMS	Root-mean-square
RMSU	Root-mean-square of the velocity fluctuation in the longitudinal direction, m/s ²
RMSV	Root-mean-square of the velocity fluctuation in the vertical direction, m/s ²
Ro	Hot wire resistance at temperature T _o , ohms
ROE	Air density, Kg/m ³
S _t	Hot wire sensitivity to temperature, volts/degree c
S _u	Hot wire sensitivity to longitudinal velocity, volts/m/s
S _v	Hot wire sensitivity to normal velocity, volts/m/s
T	Temperature °C
To	Reference temperature, °C
t'	Time varying temperature, °C
TRMS	Root-mean-square of the temperature, °C
U	Local mean longitudinal velocity, m/s
U _e	Characteristic velocity
U _(ref)	Reference velocity
U _{RMS}	Root-mean-square of the longitudinal velocity, m/s
U _τ	Shear stress velocity, m/s
UN	Ratio of local to freestream velocity
U*	Ratio of local to reference velocity
u	Time dependent longitudinal velocity, m/s

NOMENCLATURE (continued)

V	Local mean velocity in the vertical direction, m/s
v	Time dependent velocity in the vertical direction, m/s
W	One half the model cord length, cm
x	Longitudinal direction coordinate length, cm
Y, Y_N Y^*	} Ratio of local vertical distance to boundary layer thickness
y	Vertical direction coordinate length, cm
α	Thermal coefficient of resistance, per $^{\circ}\text{C}$
δ	Boundary layer thickness, cm
δ_e	Characteristic boundary layer length, cm
δ^*	Boundary layer displacement thickness, cm
η	Non-dimensional boundary layer length coordinate
θ	Angular measure in polar coordinates, degrees
θ^*	Boundary layer momentum thickness, cm

APPENDIX A
MEASUREMENTS OF THE MEAN AND LONGITUDINAL TURBULENT
VELOCITIES OVER VARYING HILL SHAPES

by
Michael A. Rider
and
V. A. Sandborn

SUMMARY

A systematic wind-tunnel study of flow over two-dimensional hills was made. The flow over six different two-dimensional hills were evaluated for identical approach conditions. The results indicated that the triangular and sinusoidal hills produced the greatest speedup of the airstream in the region near the surface. The more abrupt models produced less of an increase in local velocity.

INTRODUCTION

Site selection for wind turbine installations is a major criteria for the success of a wind system. Topography is known to have very strong effects on the atmospheric winds. Particularly, in the lower atmosphere, the influence of the local terrain is extremely evident. Different hills or ridges will produce different degrees of speedup of the airstream as the flow approaches the summit. Thus, it is important to find the most likely location for the greatest possible power production.

A series of tests were conducted in a small wind tunnel to estimate the change in flow properties of a turbulent boundary layer as it moved over six different ridge models. Models of the same relief but different slope were investigated. The hills varied geometrically from triangular to sinusoidal and finally to box shape.

TEST SETUP

The measurements were made in a small 0.37 x 0.37 meter (transpiration) wind tunnel located at the Fluid Dynamics and Diffusion Laboratory at Colorado State University (see Figure A1). All tests were conducted with a zero pressure gradient.

As the flow entered the test section a series of five fences, 2.54 cm in height and spaced 10 cm apart were used to initiate the growth of the turbulent boundary layer (see Figures A2). The last fence was followed by a 1.22 m reach of roughness. The roughness made from 0.5 cm diameter spheres ended 2.54 cm from the base of the models.

The center of the models were positioned 1.35 m from the last boundary-layer roughness. A false floor covered the total test section as shown in Figure A2. A horizontal hot-wire probe sampled the mean and the longitudinal velocities. Profiles were taken at locations 10.16 cm in front of the crest, at the foot of the hills, and at the crest of the hills.

The hill models shapes shown in Figure A3 were constructed from 0.32 cm masonite (see Figure 3). All of the models were 43 cm in length. A traverse mounted on the underside of the tunnel was used to survey the flow. The traverse entered the tunnel behind the models and along the center line of the tunnel.

FLOW VISUALIZATION

To aid in the investigation, several photographs were taken of smoke passing over the hills. The smoke, titanium tetrachloride was released a few centimeters upstream of the foot of the hill models. All of the photographs were taken with a tunnel velocity of about 3 m/s. The shutter speed was varied to give different perspectives of the flow. Figure A4 shows typical flow patterns obtained with the smoke.

RESULTS

Of the shapes tested the triangular hill produced the greatest speedup at the crest. Table AI lists the measured mean and turbulent velocity profiles for each hill. The approach profile was measured only once and was assumed to remain the same for all the tests. Figures A5a) to A5f) are plots of the measured nondimensional mean velocity distributions. For all the figures the initial upstream profile is the same. With the exception of the rectangular hill (bluff body) a decrease in velocity always occurs at the foot of the hill and a speedup at the crest. The boundary layer upstream of the foot of the hills experienced an increasing pressure gradient, which is indicated in the smoke pictures by a local separation bubble for the bluff body. (Note that the smoke pictures of Figure A4 can be somewhat misleading as a result of shadow effects both along the upstream and downstream junctions between the model and the floor.)

Figure A6 is a plot of the fractional speedup:

$$\Delta S \equiv \frac{\bar{U}\left(\frac{y}{10H}\right)_{\text{crest}} - \bar{U}\left(\frac{y}{10H}\right)_{\text{approach}}}{\bar{U}\left(\frac{y}{10H}\right)_{\text{approach}}} \quad (\text{A-1})$$

The triangular and sinusoidal hills produce the greatest speedup effect. It is somewhat surprising that hill number 4 shows considerably less speedup than the same sloped triangular hill. The smoke pictures indicate that the separation effect in the lee of the triangular

hills forces the flow outward near the crest. Thus, to the approach flow the hill appears higher than the actual physical height.

Figure A7 is a plot of the longitudinal turbulent intensity distributions for the six hills. With the exception of the rectangular hill the turbulent intensities are greatly reduced at the crest of the hills. Rider (1) noted that a reduction in the longitudinal turbulent velocity component would be predicted from the theory for turbulence undergoing a contraction. The reduction in the longitudinal turbulence will be accompanied by a proportional increase in the vertical turbulent component.

The present study made in a small wind tunnel was limited to the use of boundary-layer trips and roughness to increase the equivalent Reynolds-number-approach velocity profile. The equivalent Reynolds number was estimated from the value of skin friction coefficient for the approach profile to be approximately 10^7 . A comparison of the present results for the triangular hill with similar results reported by Rider (1) for a much longer boundary-layer development length ($Re \sim 10^8$) are shown in Figure A8. The fractional speedup for both cases is quite similar. The larger flow facility velocity profile is somewhat fuller than the one employed in the small wind tunnel.

CONCLUDING REMARKS

Evaluation of the velocity speedup over different shaped hills shows that triangular and sinusoidal geometry is preferred for wind-power sites. The flat top hill does not give as large a speedup to the crease because of absence of the separation that occurs for the "sharp" crested models. The present feasibility study suggests that reasonably small-scale flow systems may be employed to determine the gross features of hill shapes on the speedup.

REFERENCES

- Rider, Michael A. Boundary Layer Turbulence Over Two-Dimensional Hills. M.S. Thesis, Colorado State University, Fort Collins, Colorado, 1977. (see Appendix B this report)

Table AI Measured Mean and Turbulent Velocity Distributions

a) Initial Approach Profiles

FREE STREAM VELOCITY 17.87M/S
 TUNNEL TEMP. 73.0F
 DENSITY .9896E+00 KG/M³

POSITION 10.16CM FROM CREST
 BAROMETRIC PRESSURE 24.70IN HG
 DATE 4/26/76 TIME 2.30

A= 11.533 B= 3.333 C= .50

Y CM	E VOLTS	RMS MV	DE/DU M/S	U M/S	RMSU	YN	UN
.40	4.488	171.20	.0719	6.67	2.381	.016	.373
1.47	4.713	141.00	.0552	10.26	2.555	.058	.574
3.42	4.821	115.00	.0492	12.34	2.337	.135	.691
6.17	4.896	100.20	.0456	13.92	2.197	.243	.779
8.71	4.946	92.00	.0434	15.05	2.118	.343	.842
11.47	4.999	79.50	.0413	16.30	1.925	.451	.912
14.26	5.034	57.70	.0400	17.16	1.444	.561	.960
16.64	5.054	35.10	.0392	17.67	.895	.655	.989
19.99	5.062	17.90	.0389	17.87	.460	.787	1.000

Table AI (Continued) Measured Mean and Turbulent Velocity Distributions
b)

FOR HILL 1

FREE STREAM VELOCITY 17.67M/S

TUNNEL TEMP. 72.0F

DENSITY .9896E+00 KG/M³

A= 11.533 B= 3.333 C= .50

POSITION 10.16CM FROM CREST

BAROMETRIC PRESSURE 24.74IN HG

DATE 4/26/76 TIME 11.30

Y CM	E VOLTS	RMS MV	DE/DU M/S	U M/S	RMSU	YN	UN
1.53	4.351	187.80	.0863	4.93	2.176	.021	.279
1.63	4.625	155.80	.0609	8.75	2.557	.064	.495
4.42	4.803	113.10	.0501	11.98	2.256	.174	.678
6.82	4.871	95.00	.0468	13.38	2.031	.268	.757
9.68	4.948	89.20	.0434	15.09	2.058	.357	.854
11.03	4.963	80.40	.0427	15.44	1.882	.434	.874
12.39	4.991	73.10	.0416	16.11	1.757	.488	.911
14.42	5.019	57.40	.0405	16.79	1.416	.568	.950
16.53	5.041	38.10	.0397	17.34	.960	.651	.981
18.54	5.048	23.10	.0394	17.51	.586	.730	.991
20.00	5.054	19.80	.0392	17.67	.505	.788	1.000

FOR HILL 1

FREE STREAM VELOCITY 18.15M/S

TUNNEL TEMP. 73.0F

DENSITY .9844E+00 KG/M³

A= 11.334 B= 3.333 C= .50

POSITION 0.00CM FROM CREST

BAROMETRIC PRESSURE 24.66IN HG

DATE 4/27/76 TIME 11. 0

Y CM	E VOLTS	RMS MV	DE/DU M/S	U M/S	RMSU	YN	UN
.17	4.927	83.00	.0436	15.08	1.906	.007	.831
.36	4.927	85.00	.0436	15.08	1.952	.014	.831
1.51	4.927	94.00	.0436	15.08	2.158	.059	.831
3.21	4.943	88.00	.0429	15.45	2.052	.126	.851
5.98	4.968	84.00	.0419	16.04	2.006	.236	.884
8.41	5.005	79.00	.0405	16.94	1.953	.331	.933
11.08	5.024	64.00	.0398	17.41	1.610	.436	.959
13.64	5.044	42.00	.0390	17.92	1.076	.537	.987
16.19	5.051	23.00	.0388	18.10	.543	.637	.997
18.95	5.052	16.00	.0387	18.12	.413	.730	.998
20.43	5.053	13.00	.0387	18.15	.336	.804	1.000

Table AI (Continued) Measured Mean and Turbulent Velocity Distributions
c)

FOR HILL 2

FREE STREAM VELOCITY 17.75M/S

TUNNEL TEMP. 72.0F

DENSITY .9896E+00 KG/M³

A= 11.533 B= 3.333 C= .150

POSITION 10.16CM FROM CREST

BAROMETRIC PRESSURE 24.74IN HG

DATE 4/26/76 TIME 12.0

Y CM	E VOLTS	RMS MV	DE/DU M/S	U M/S	RMSU	YN	UN
.30	4.243	162.50	.1012	3.77	1.606	.012	.212
.75	4.501	162.80	.0707	6.85	2.302	.010	.386
2.50	4.694	130.50	.0564	9.92	2.316	.049	.559
3.83	4.781	114.60	.0513	11.54	2.234	.151	.650
5.61	4.852	98.10	.0477	12.98	2.058	.221	.731
7.01	4.881	93.00	.0463	13.60	2.009	.276	.766
9.98	4.942	86.30	.0436	14.95	1.979	.377	.843
11.75	4.986	76.70	.0418	15.99	1.835	.462	.901
14.06	5.010	59.40	.0409	16.57	1.454	.554	.933
16.01	5.039	41.90	.0398	17.29	1.053	.630	.974
18.45	5.050	23.00	.0394	17.56	.584	.726	.989
19.97	5.057	19.30	.0391	17.74	.493	.786	1.000

FOR HILL 2

FREE STREAM VELOCITY 18.56M/S

TUNNEL TEMP. 73.0F

DENSITY .9844E+00 KG/M³

A= 11.334 B= 3.333 C= .150

POSITION 0.00CM FROM CREST

BAROMETRIC PRESSURE 24.66IN HG

DATE 4/27/76 TIME 10.30

Y CM	E VOLTS	RMS MV	DE/DU M/S	U M/S	RMSU	YN	UN
.17	4.920	86.00	.0439	14.92	1.961	.007	.804
.46	4.926	88.00	.0436	15.05	2.018	.018	.811
2.88	4.941	91.00	.0430	15.40	2.118	.035	.830
2.25	4.952	95.00	.0425	15.66	2.234	.089	.844
4.38	4.964	87.00	.0420	15.94	2.069	.172	.859
6.35	4.994	83.00	.0409	16.66	2.031	.250	.898
9.10	5.016	75.00	.0400	17.21	1.873	.358	.927
11.63	5.048	60.00	.0389	18.02	1.543	.458	.971
13.79	5.061	43.00	.0384	18.36	1.119	.543	.989
16.47	5.066	24.00	.0383	18.49	.627	.648	.996
20.43	5.069	17.00	.0382	18.56	.446	.804	1.000

Table AI (Continued) Measured Mean and Turbulent Velocity Distributions
d)

FOR HILL 3
FREE STREAM VELOCITY 17.75M/S
TUNNEL TEMP. 73.0F
DENSITY .9896E+00 KG/M³

POSITION 10.16CM FROM CREST
BAROMETRIC PRESSURE 24.72IN HG
DATE 4/26/76 TIME 12.45

A= 11.533 B= 3.333 C= .50

Y CM	E VOLTS	RMS MV	DE/DU M/S	U M/S	RMSU	YN	UN
.35	4.236	167.40	.1023	3.70	1.637	.014	.208
1.20	4.564	157.30	.0655	7.78	2.418	.050	.438
2.71	4.714	123.40	.0551	10.28	2.238	.107	.579
4.19	4.801	106.90	.0502	11.94	2.128	.165	.673
6.91	4.888	94.60	.0460	13.75	2.057	.272	.775
9.73	4.941	88.20	.0436	14.93	2.021	.383	.841
12.09	4.995	71.30	.0414	16.20	1.720	.476	.913
13.88	5.024	60.40	.0403	16.91	1.497	.546	.953
15.45	5.038	43.70	.0398	17.26	1.098	.628	.972
18.15	5.047	26.20	.0395	17.49	.664	.714	.985
19.98	5.057	17.40	.0391	17.74	.445	.787	1.000

FOR HILL 3
FREE STREAM VELOCITY 18.46M/S
TUNNEL TEMP. 73.0F
DENSITY .9844E+00 KG/M³

POSITION 0.00CM FROM CREST
BAROMETRIC PRESSURE 24.66IN HG
DATE 4/27/76 TIME 9.10

A= 11.334 B= 3.333 C= .50

Y CM	E VOLTS	RMS MV	DE/DU M/S	U M/S	RMSU	YN	UN
.14	5.011	81.00	.0402	17.08	2.013	.006	.925
.37	4.990	82.00	.0410	16.57	1.999	.015	.897
.62	4.966	85.00	.0420	15.99	2.026	.024	.866
.76	4.957	90.00	.0423	15.77	2.127	.030	.855
1.83	4.934	94.00	.0433	15.24	2.173	.072	.825
2.76	4.943	90.00	.0429	15.45	2.098	.109	.837
4.72	4.961	85.70	.0422	15.87	2.033	.186	.860
6.63	4.972	81.90	.0417	16.13	1.963	.261	.874
8.74	5.007	75.30	.0404	16.98	1.865	.344	.920
11.07	5.031	62.50	.0395	17.59	1.582	.436	.953
13.71	5.054	43.10	.0387	18.17	1.114	.540	.985
15.43	5.057	28.10	.0386	18.25	.729	.607	.989
18.07	5.063	20.90	.0384	18.41	.545	.712	.997
20.41	5.065	12.30	.0383	18.46	.321	.804	1.000

Table AI (Continued) Measured Mean and Turbulent Velocity Distributions
e)

FOR HILL 4

FREE STREAM VELOCITY 17.52M/S

TUNNEL TEMP. 73.0F

DENSITY .9896E+00 KG/M³

A= 11.533 B= 3.333 C= .150

POSITION 10.16CM FROM CREST

BAROMETRIC PRESSURE 24.72IN HG

DATE 4/26/76 TIME 1.15

Y CM	E VOLTS	RMS MV	DE/DU M/S	U M/S	RMSU	YN	UN
0.77	4.185	193.30	.1110	3.22	1.742	.030	.184
1.60	4.453	178.80	.0752	6.19	2.378	.063	.354
3.16	4.715	124.40	.0551	10.30	2.259	.142	.588
4.813	4.813	103.70	.0496	12.18	2.090	.203	.695
6.55	4.886	93.00	.0461	13.71	2.019	.245	.782
8.47	4.936	85.60	.0439	14.82	1.952	.276	.846
10.47	4.988	78.20	.0425	15.56	1.839	.452	.888
12.52	5.012	61.40	.0408	16.62	1.505	.555	.948
14.65	5.036	39.60	.0399	17.21	.993	.650	.982
16.85	5.044	23.50	.0396	17.41	.594	.726	.994
19.99	5.048	19.20	.0394	17.51	.487	.787	1.000

FOR HILL 4

FREE STREAM VELOCITY 18.23M/S

TUNNEL TEMP. 73.0F

DENSITY .9844E+00 KG/M³

A= 11.334 B= 3.333 C= .50

POSITION 0.00CM FROM CREST

BAROMETRIC PRESSURE 24.66IN HG

DATE 4/27/76 TIME 10.10

Y CM	E VOLTS	RMS MV	DE/DU M/S	U M/S	RMSU	YN	UN
0.14	4.680	120.20	.0562	10.05	2.141	.005	.552
0.33	4.794	118.00	.0497	12.21	2.373	.021	.670
0.72	4.858	107.00	.0466	13.54	2.296	.068	.743
1.44	4.912	95.00	.0442	14.73	2.150	.136	.808
2.72	4.954	85.00	.0424	15.70	2.026	.225	.861
4.26	4.985	80.00	.0412	16.45	1.941	.299	.902
6.00	5.008	71.00	.0403	17.01	1.760	.392	.933
7.96	5.041	56.00	.0391	17.84	1.431	.484	.979
10.29	5.048	39.00	.0389	18.02	1.003	.560	.988
12.91	5.051	26.00	.0388	18.10	.670	.640	.993
15.86	5.053	18.00	.0387	18.15	.465	.735	.996
19.67	5.056	14.00	.0386	18.23	.363	.804	1.000

Table AI (Continued) Measured Mean and Turbulent Velocity Distributions
f)

FOR HILL 5
FREE STREAM VELOCITY 17.85M/S
TUNNEL TEMP. 73.0F
DENSITY .9896E+00 KG/M³

POSITION 10.16CM FROM CREST
BAROMETRIC PRESSURE 24.70IN HG
DATE 4/26/76 TIME 2.50

A= 11.533 B= 3.333 C= .50

Y CM	E VOLTS	RMS MV	DE/DU M/S	U M/S	RMSU	YN	UN
.41	4.282	196.00	.0954	4.16	2.055	.016	.233
1.94	4.637	159.00	.0601	8.94	2.579	.076	.501
3.42	4.749	124.00	.0531	10.90	2.336	.135	.612
5.93	4.848	102.00	.0479	12.90	2.131	.234	.722
8.63	4.917	90.70	.0447	14.39	2.030	.340	.806
11.05	4.968	81.00	.0425	15.56	1.905	.435	.872
13.62	5.015	66.90	.0407	16.69	1.845	.536	.935
15.85	5.044	45.30	.0396	17.41	1.744	.624	.975
18.34	5.056	27.10	.0392	17.72	.692	.722	.993
19.99	5.061	20.00	.0390	17.84	.513	.767	1.000

FOR HILL 5
FREE STREAM VELOCITY 18.23M/S
TUNNEL TEMP. 73.0F
DENSITY .9844E+00 KG/M³

POSITION 0.00CM FROM CREST
BAROMETRIC PRESSURE 24.66IN HG
DATE 4/27/76 TIME 10.0

A= 11.334 B= 3.333 C= .50

Y CM	E VOLTS	RMS MV	DE/DU M/S	U M/S	RMSU	YN	UN
.24	4.864	90.00	.0463	13.67	1.943	.009	.750
.53	4.854	90.00	.0468	13.46	1.923	.021	.738
1.58	4.862	100.00	.0464	13.63	2.154	.062	.748
3.25	4.905	94.00	.0445	14.58	2.113	.128	.800
5.36	4.933	88.00	.0433	15.21	2.032	.211	.835
7.83	4.974	80.00	.0416	16.18	1.921	.308	.888
10.30	5.009	68.00	.0403	17.03	1.687	.406	.934
12.91	5.042	50.00	.0391	17.87	1.279	.508	.980
15.84	5.052	28.00	.0387	18.12	.723	.624	.994
18.49	5.055	17.60	.0386	18.20	.456	.728	.998
20.43	5.056	13.50	.0386	18.23	.350	.804	1.000

Table AI (Completed) Measured Mean and Turbulent Velocity Distributions
g)

FOR HILL 6
FREE STREAM VELOCITY 17.75M/S
TUNNEL TEMP. 73.0F
DENSITY .9896E+00 KG/M³

POSITION 10.16CM FROM CREST
BAROMETRIC PRESSURE 24.70IN HG
DATE 4/26/76 TIME 2.10

A= 11.533 B= 3.333 C= .50

Y CM	E VOLTS	RMS MV	DE/DU M/S	U M/S	RMSU	YN	UN
2.99	4.806	88.00	.0500	12.04	1.761	.118	.678
3.30	4.821	94.00	.0492	12.34	1.910	.130	.695
5.39	4.878	97.10	.0464	13.53	2.091	.212	.762
8.14	4.930	89.80	.0441	14.68	2.036	.320	.827
10.62	4.974	81.30	.0423	15.70	1.923	.418	.885
12.68	5.005	71.80	.0411	16.44	1.749	.499	.926
14.52	5.032	59.70	.0400	17.11	1.491	.572	.964
16.64	5.050	40.20	.0394	17.56	1.021	.655	.989
18.47	5.055	27.10	.0392	17.69	.691	.727	.997
19.99	5.057	19.10	.0391	17.74	.488	.787	1.000

FOR HILL 6
FREE STREAM VELOCITY 18.51M/S
TUNNEL TEMP. 73.0F
DENSITY .9844E+00 KG/M³

POSITION 0.00CM FROM CREST
BAROMETRIC PRESSURE 24.66IN HG
DATE 4/27/76 TIME 9.30

A= 11.334 B= 3.333 C= .50

Y CM	E VOLTS	RMS MV	DE/DU M/S	U M/S	RMSU	YN	UN
.29	4.580	196.00	.0629	8.37	3.117	.012	.452
.68	4.640	200.00	.0587	9.36	3.407	.027	.506
1.53	4.770	183.00	.0510	11.74	3.589	.060	.634
3.11	4.881	126.00	.0456	14.04	2.766	.123	.759
4.81	4.940	100.00	.0430	15.38	2.325	.189	.831
6.95	4.977	87.00	.0415	16.25	2.095	.274	.878
9.01	5.006	76.00	.0404	16.96	1.880	.355	.916
11.60	5.041	64.00	.0391	17.84	1.635	.457	.964
13.76	5.054	46.00	.0387	18.17	1.189	.542	.982
16.21	5.065	30.00	.0383	18.46	.784	.638	.997
18.52	5.066	19.00	.0383	18.49	.497	.729	.999
20.42	5.067	15.00	.0382	18.51	.392	.804	1.000

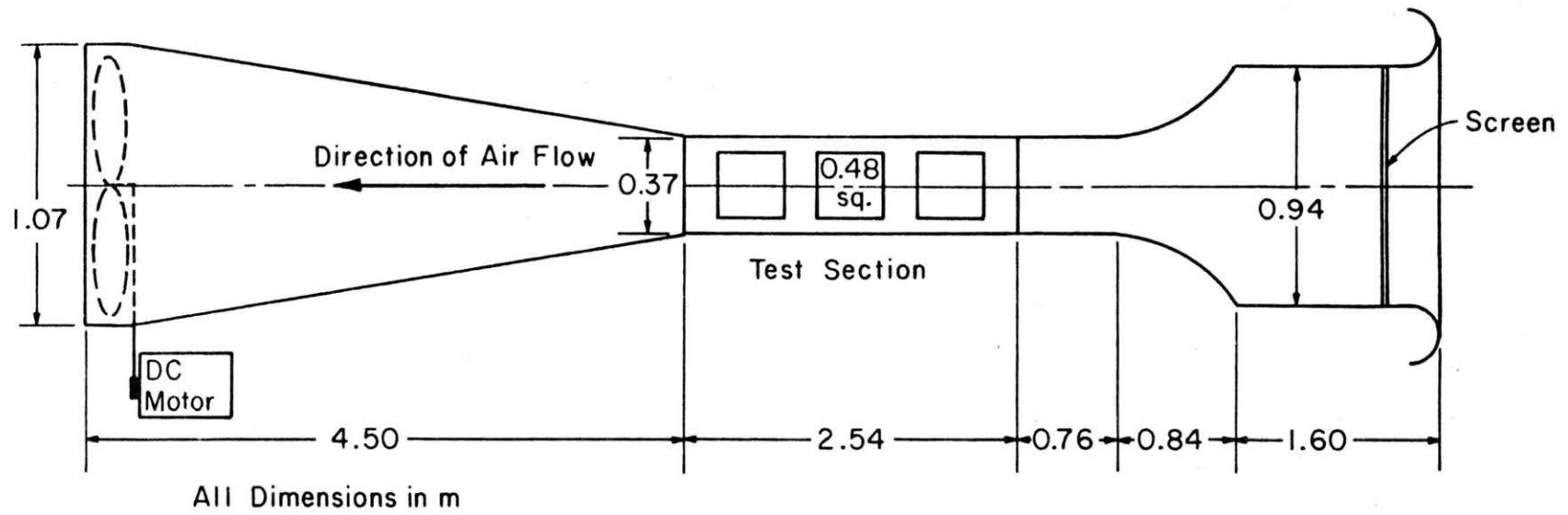


Figure A1 TRANSPARATION WIND TUNNEL
FLUID DYNAMICS & DIFFUSION LABORATORY
COLORADO STATE UNIVERSITY

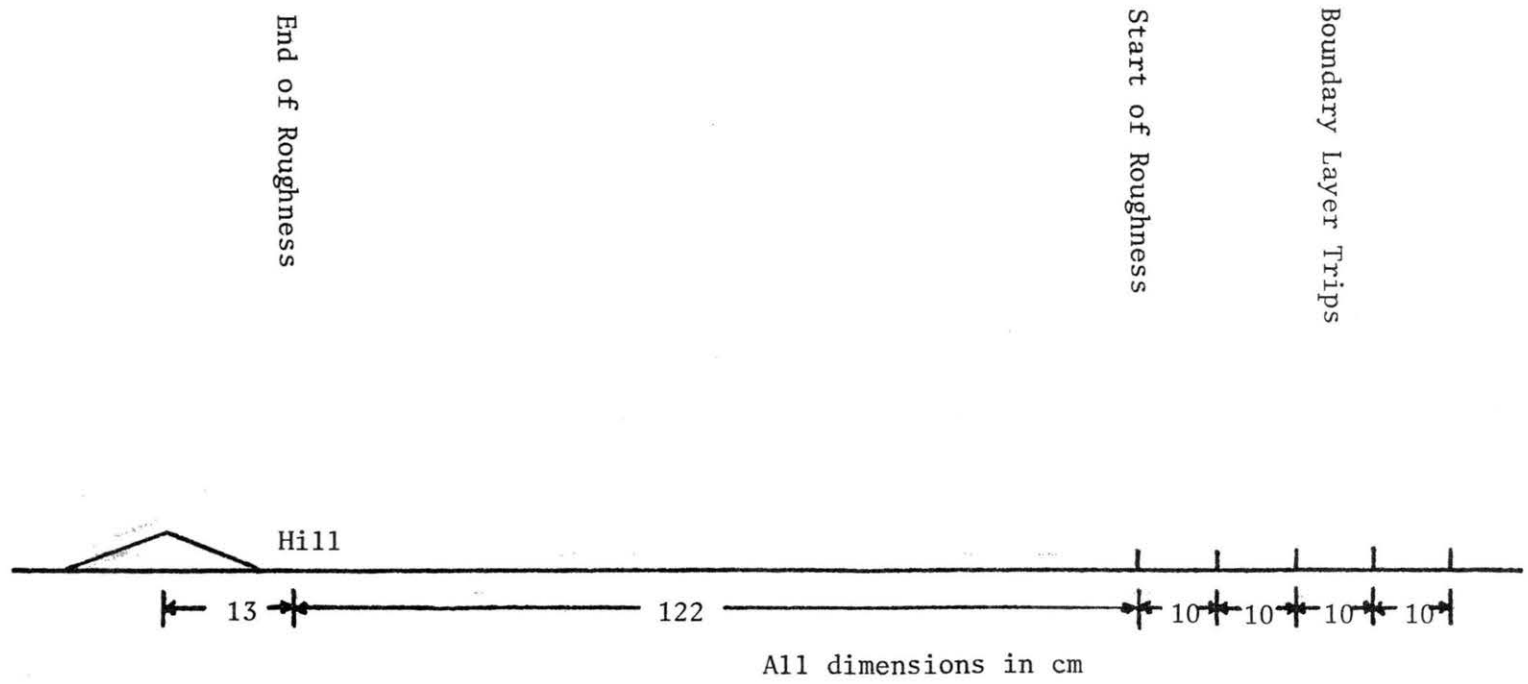


Figure A2 Wind Tunnel Setup

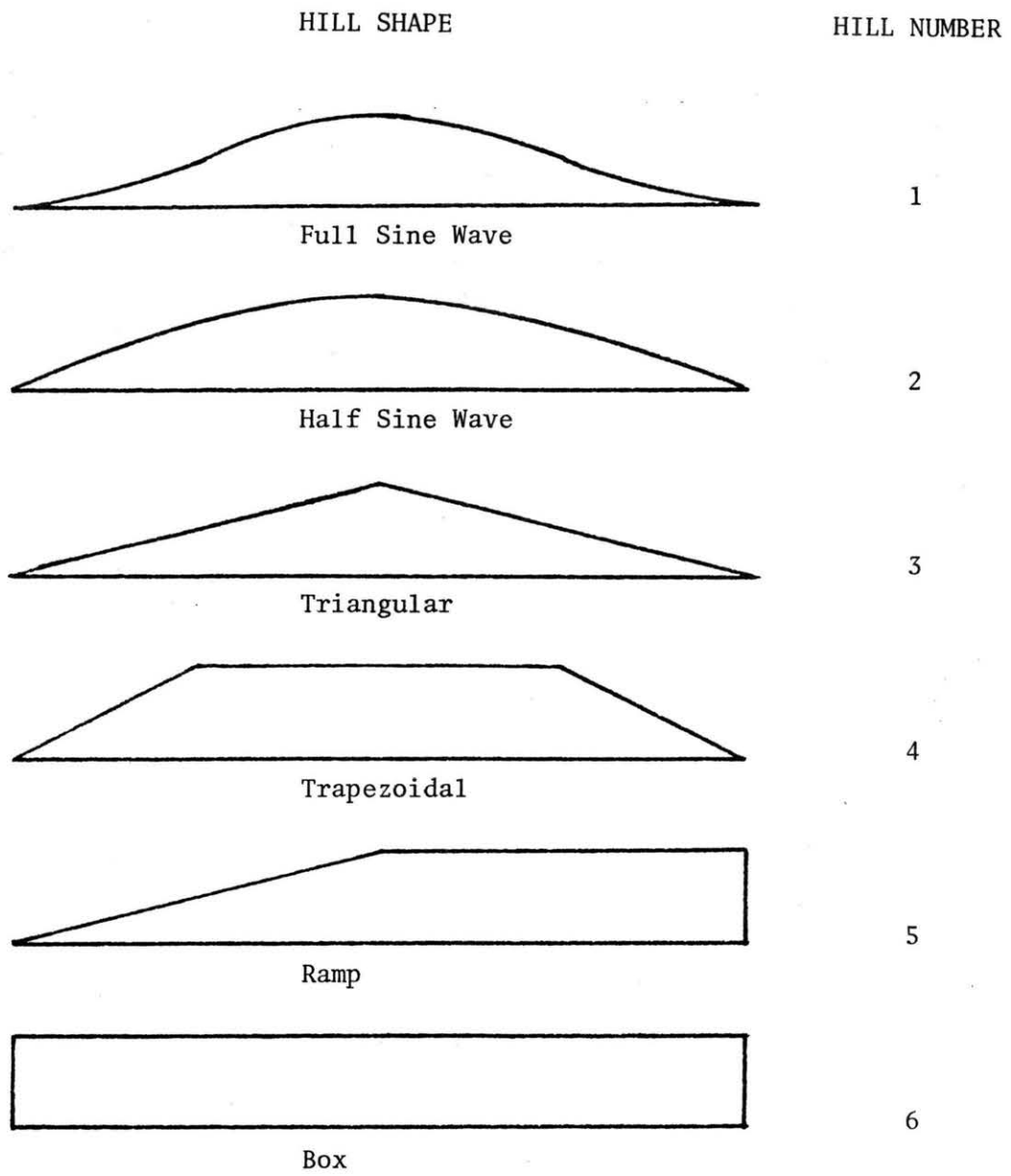
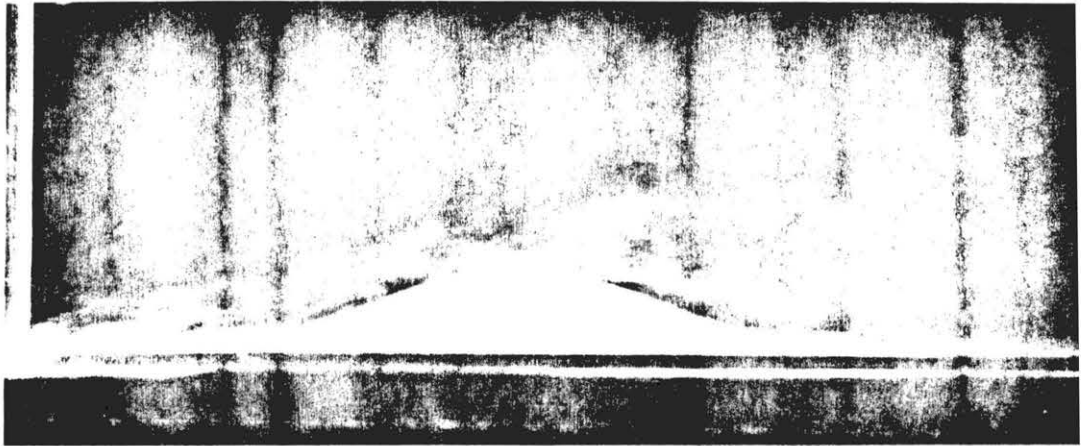
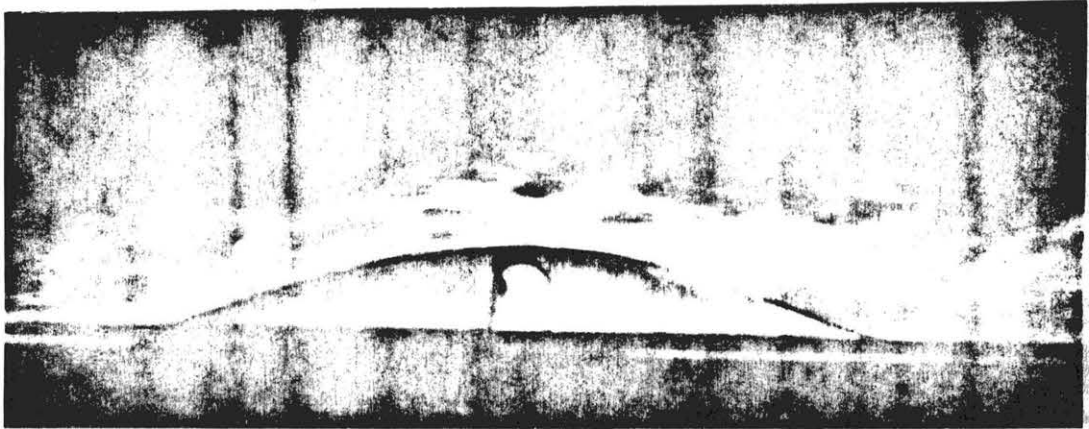


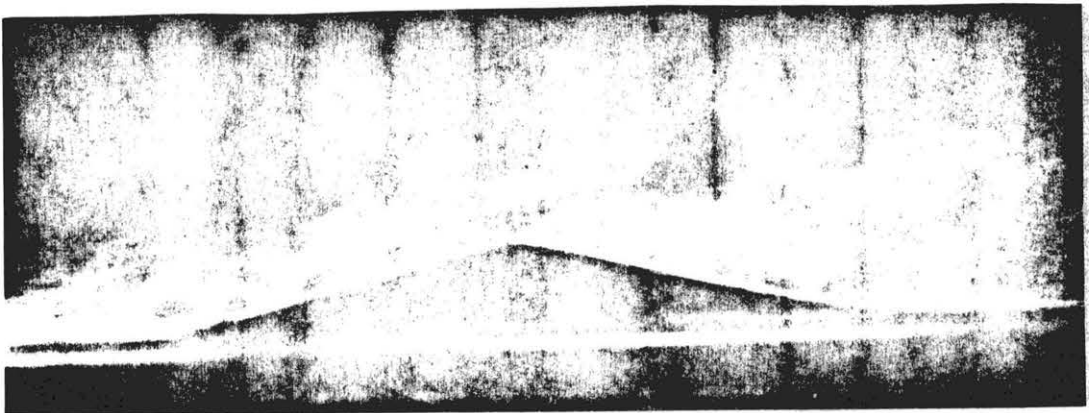
Figure A3 Hill Shapes



a) Full Sine Wave

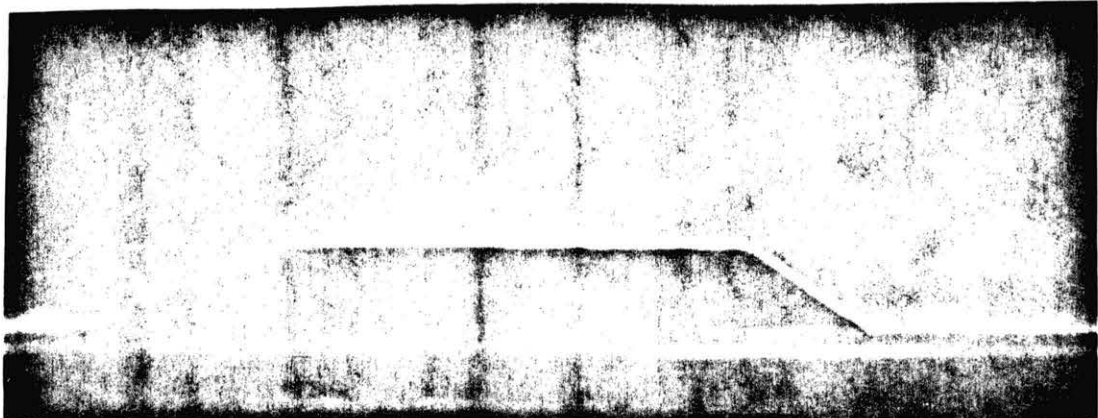


b) Half Sine Wave

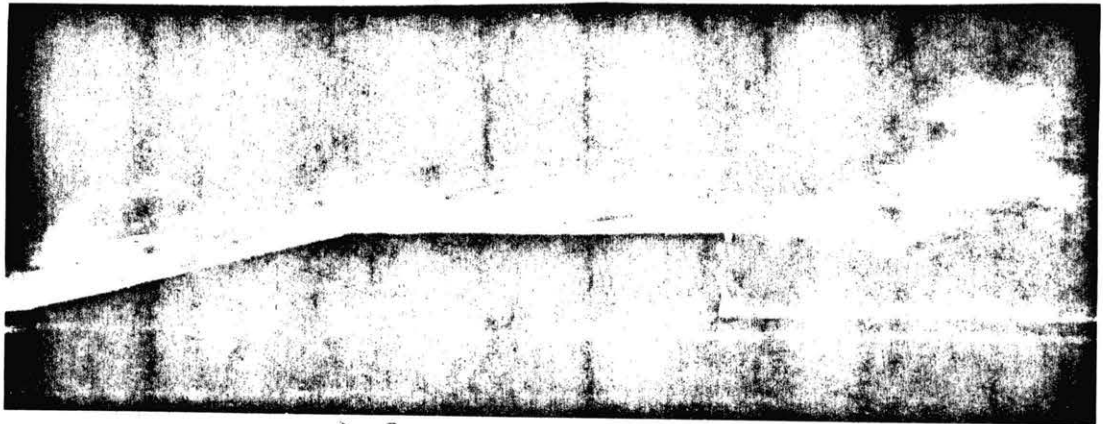


c) Triangular

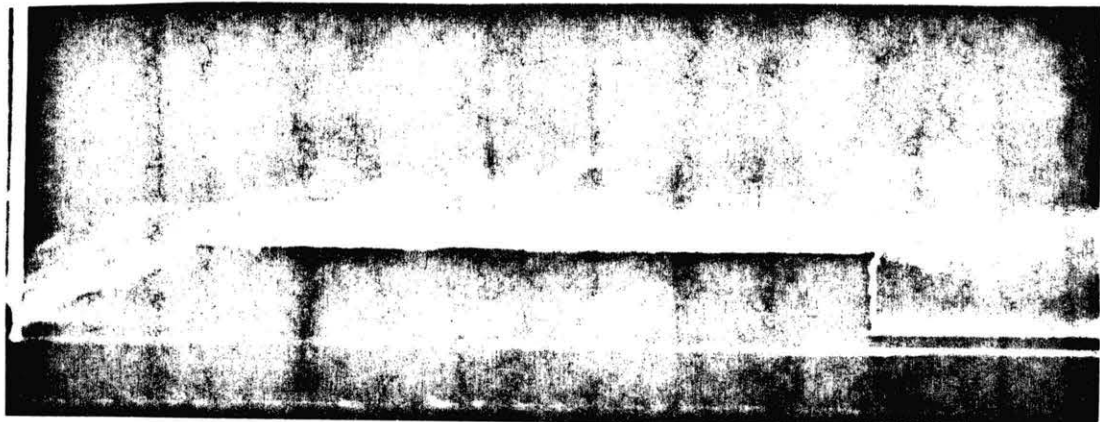
Figures A4 Flow Visualization



d) Trapezoidal

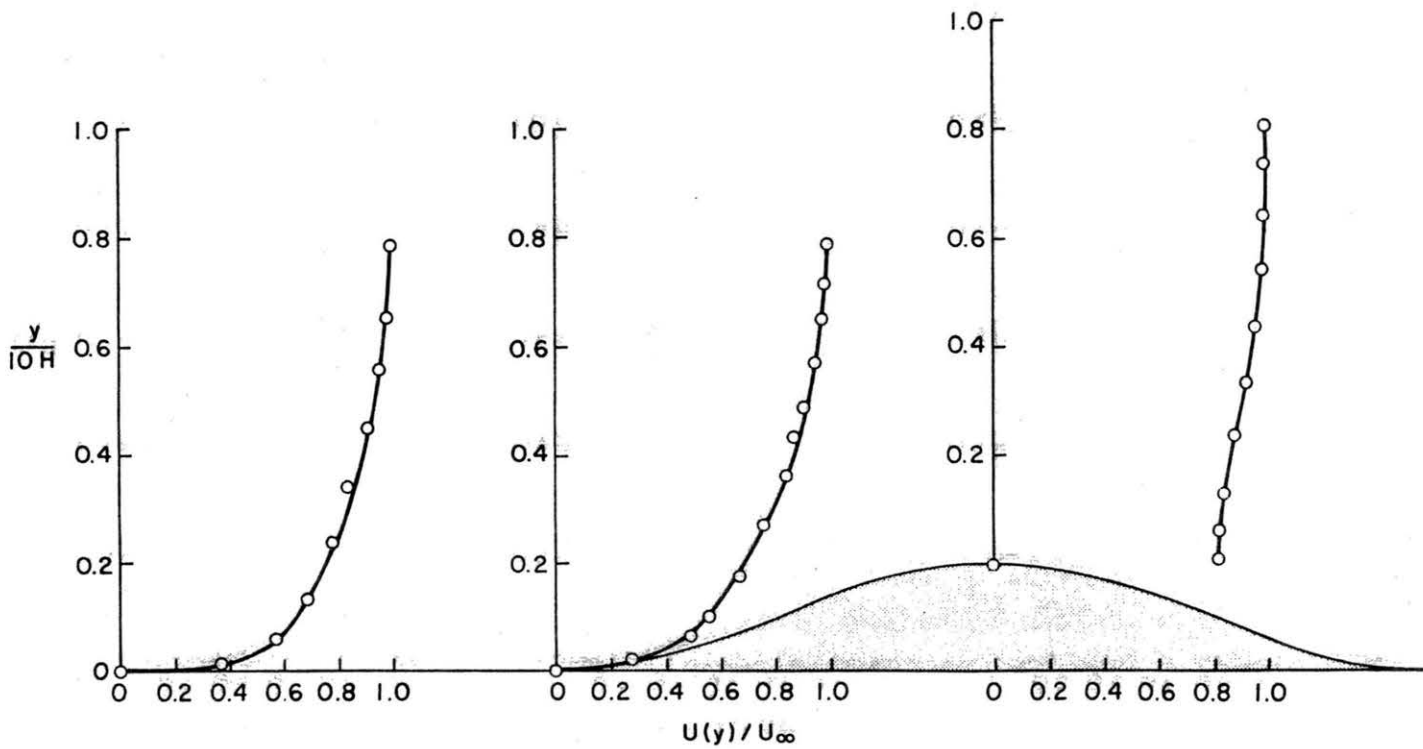


e) Ramp



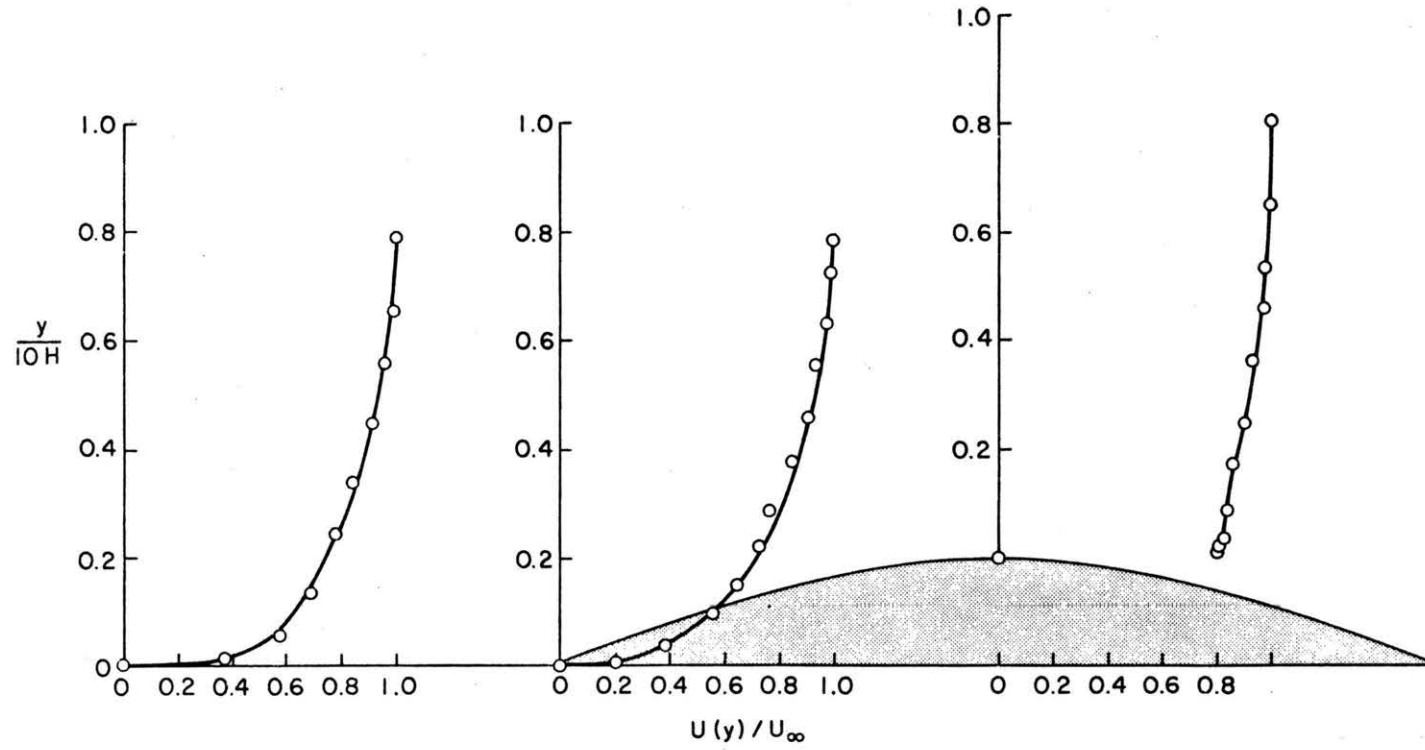
f) Box

Figures A4 (concluded) Flow Visualization



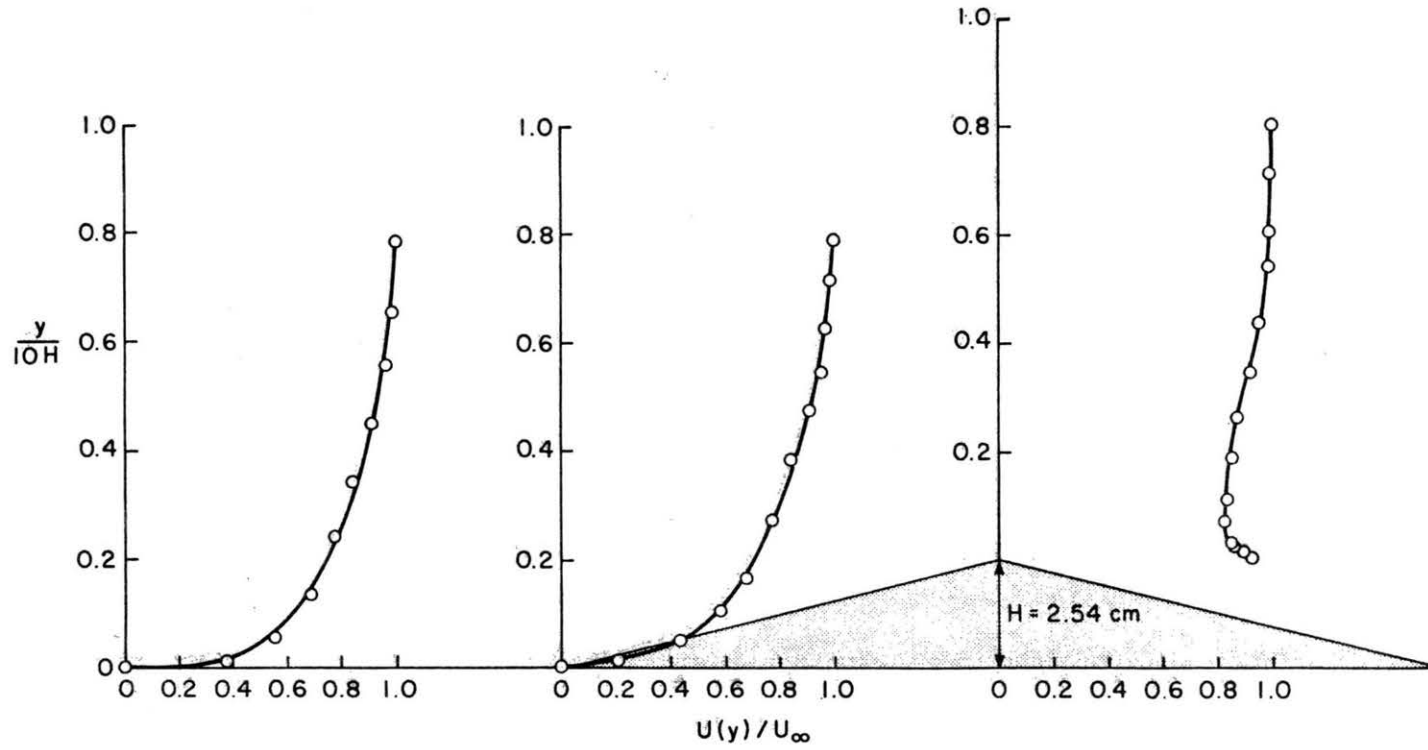
a) Full Sine Wave

Figure A5 Velocity Profile for Hill Models



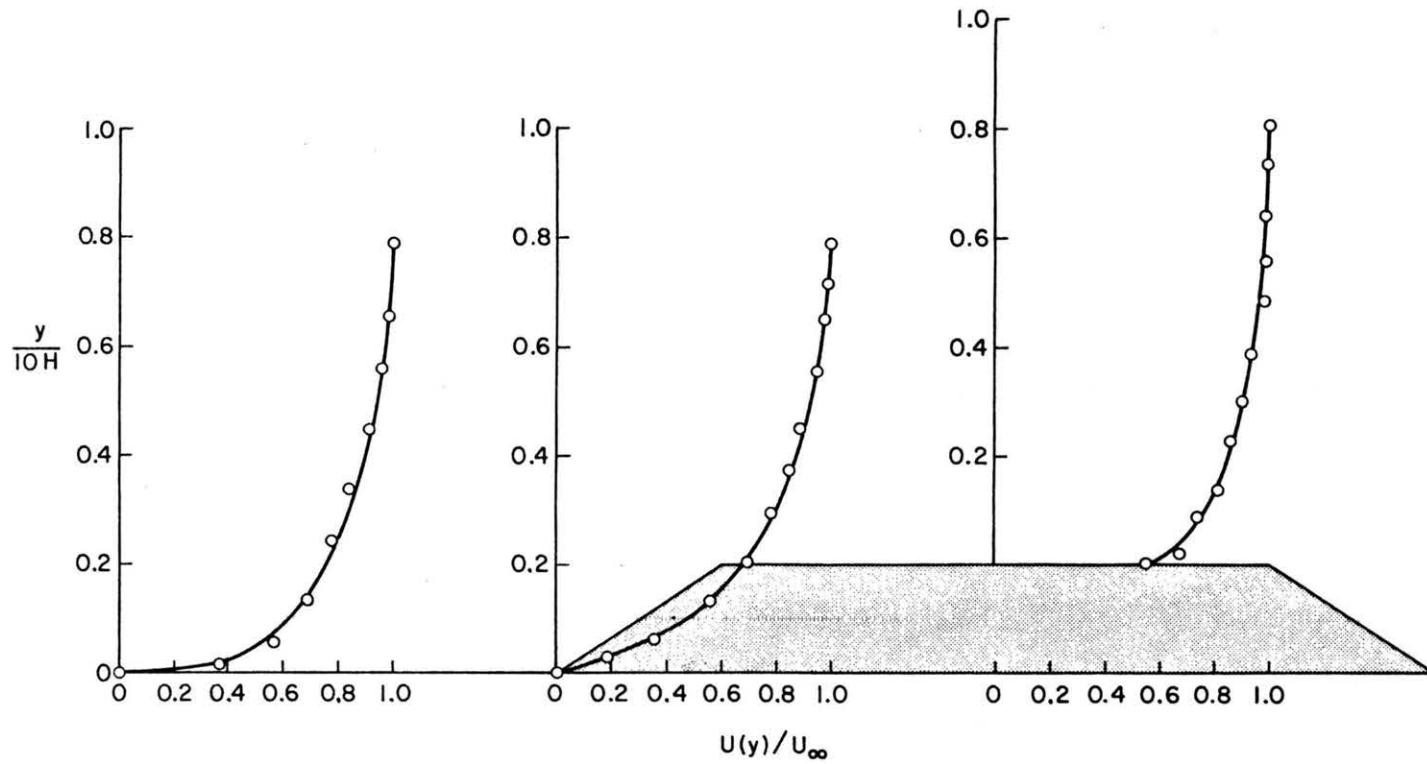
b) Half Sine Wave

Figure A5 (continued) Velocity Profile for Hill Models



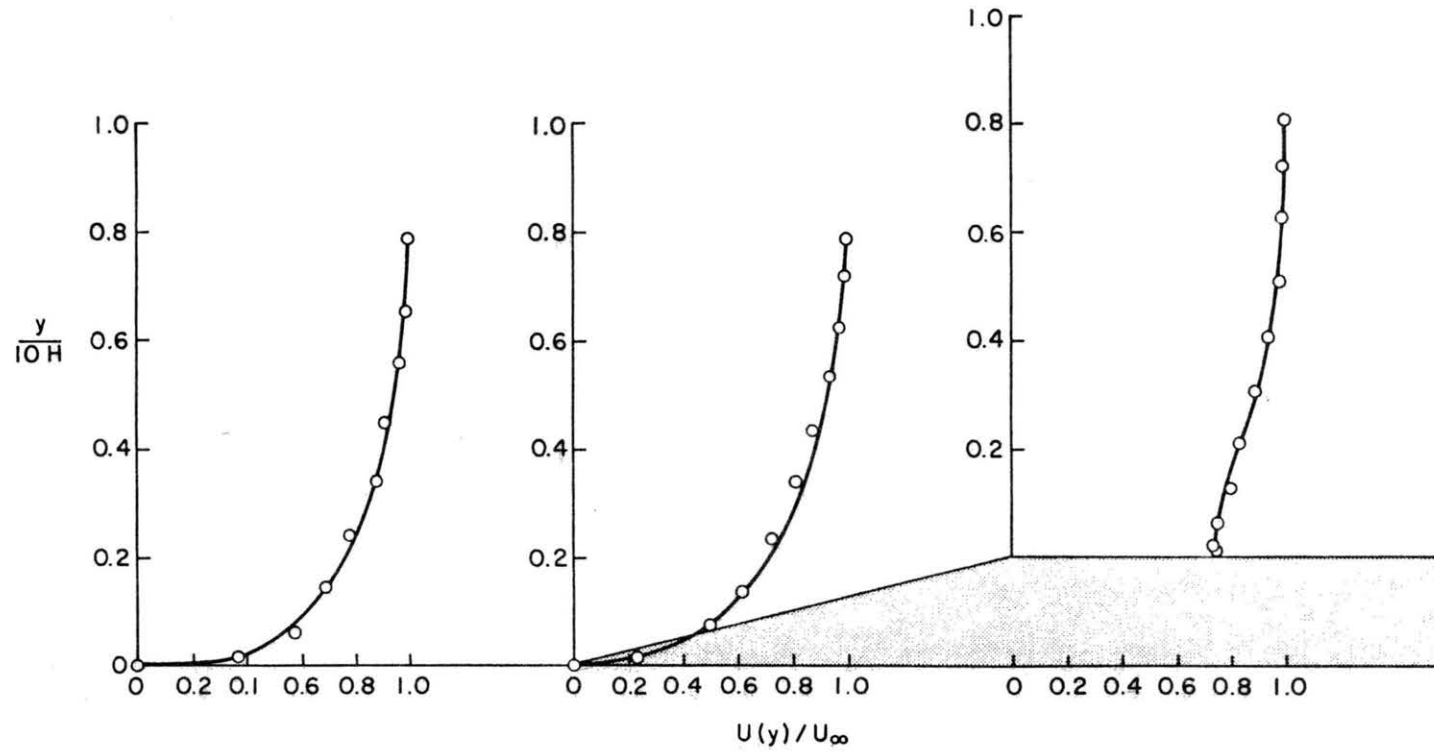
c) Triangular

Figure A5 (continued) Velocity Profile for Hill Models



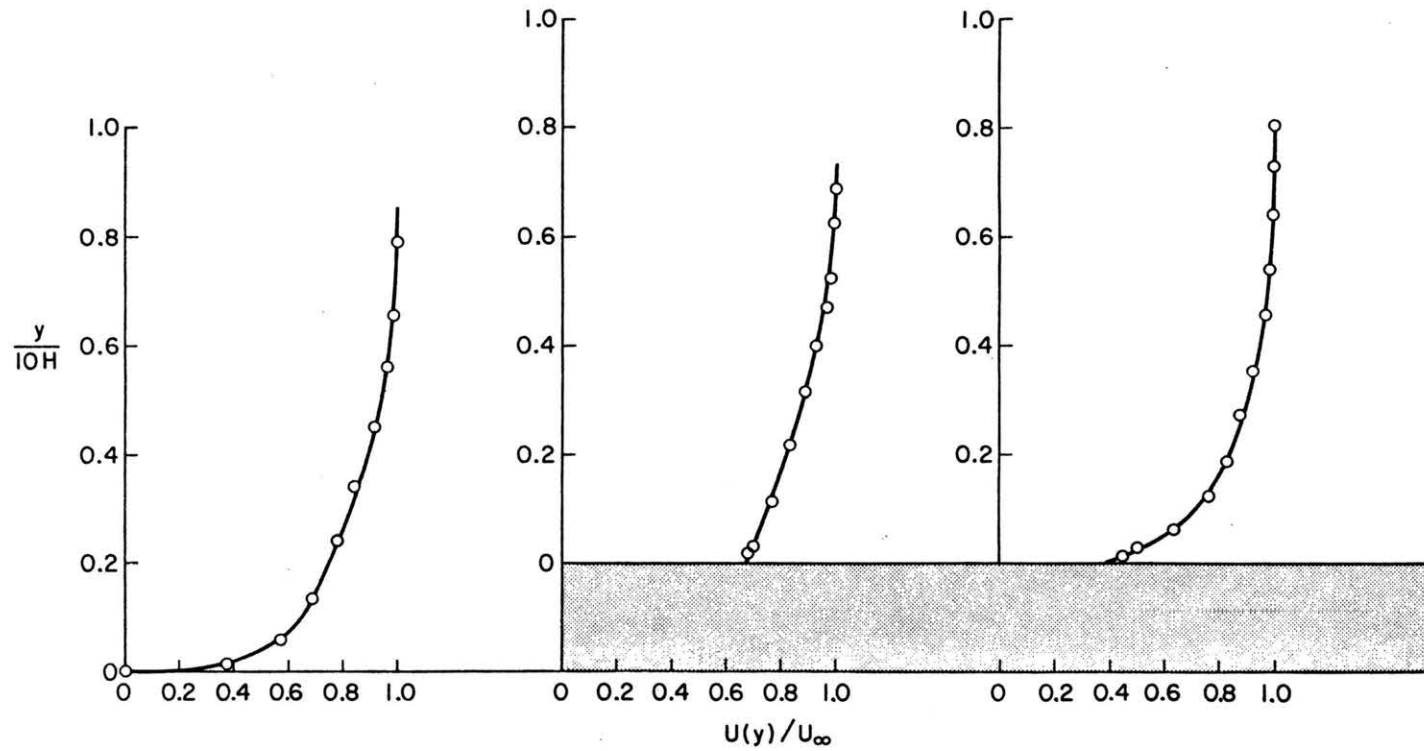
d) Trapezoidal

Figure A5 (continued) Velocity Profile for Hill Models



e) Ramp

Figure A5 (continued) Velocity Profile for Hill Models



f) Box

Figure A5 (concluded) velocity Profile for Hill Models

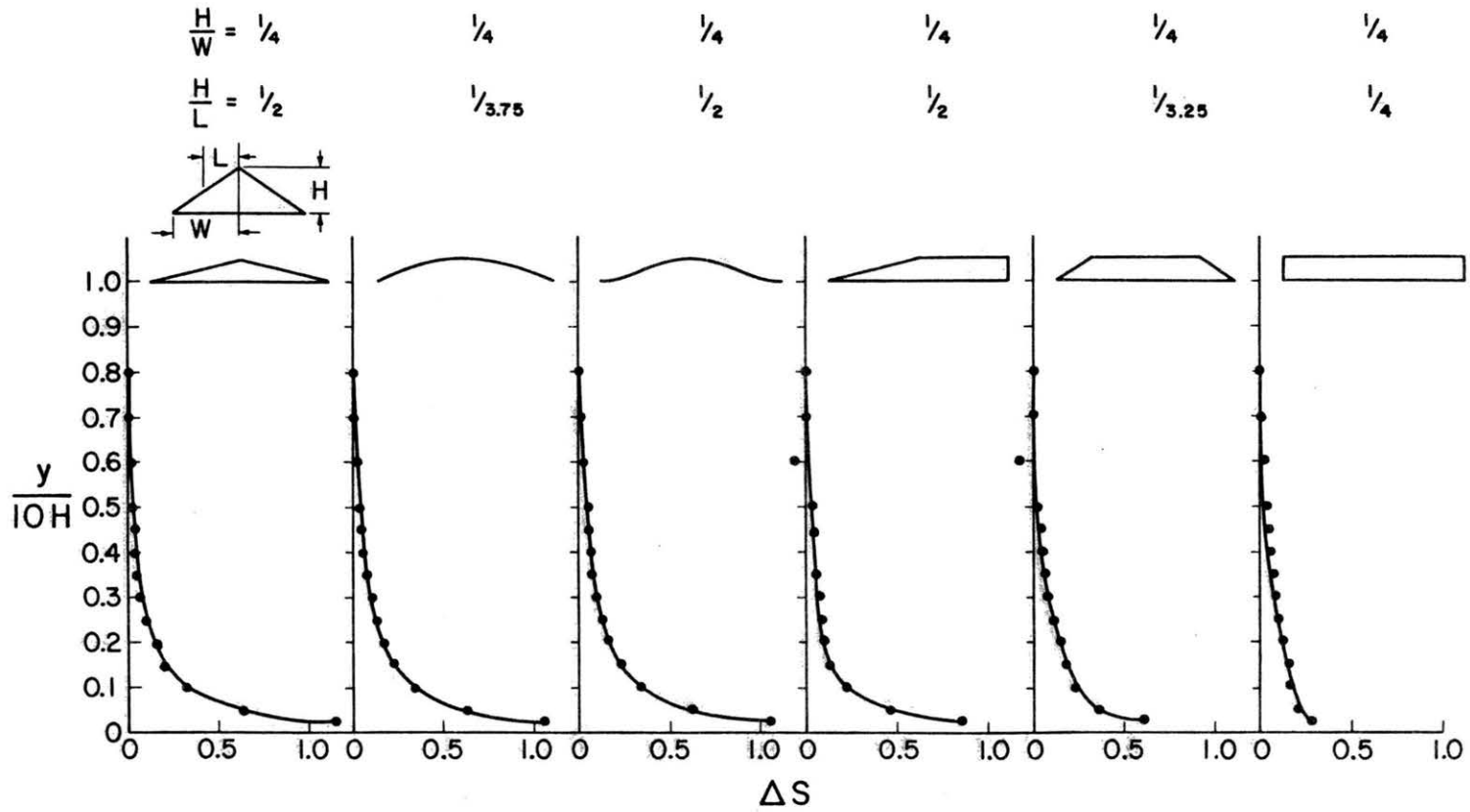
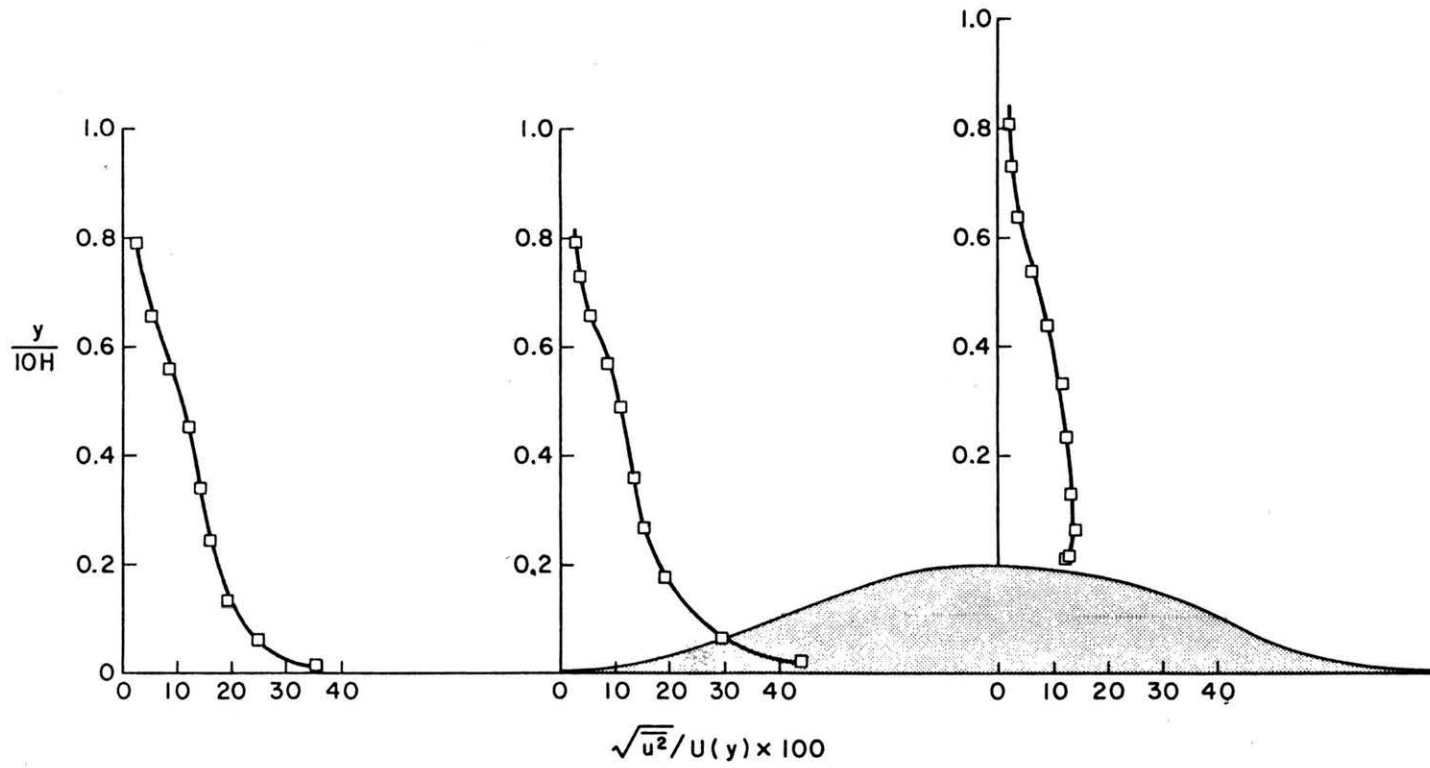
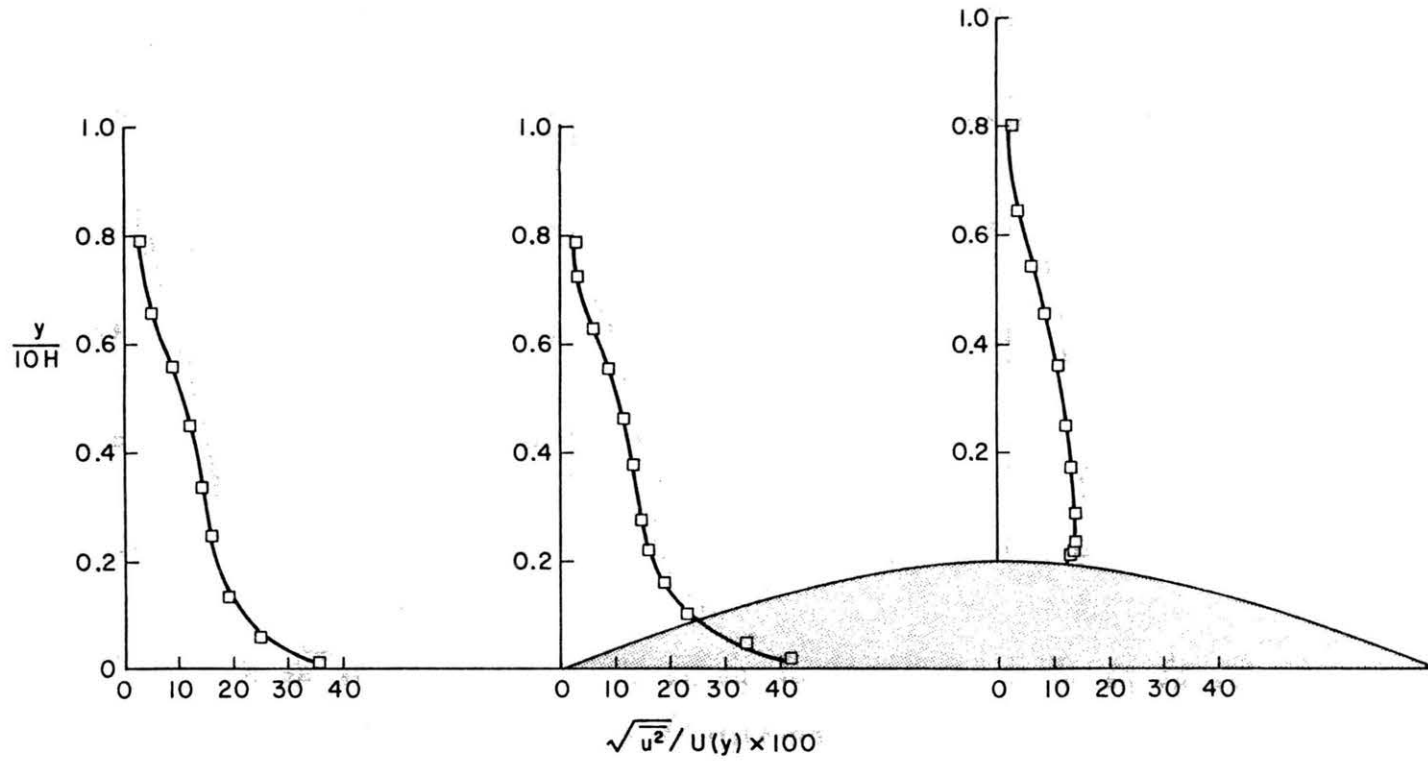


Figure A6 Velocity Speedup Between Approach Flow and Crest



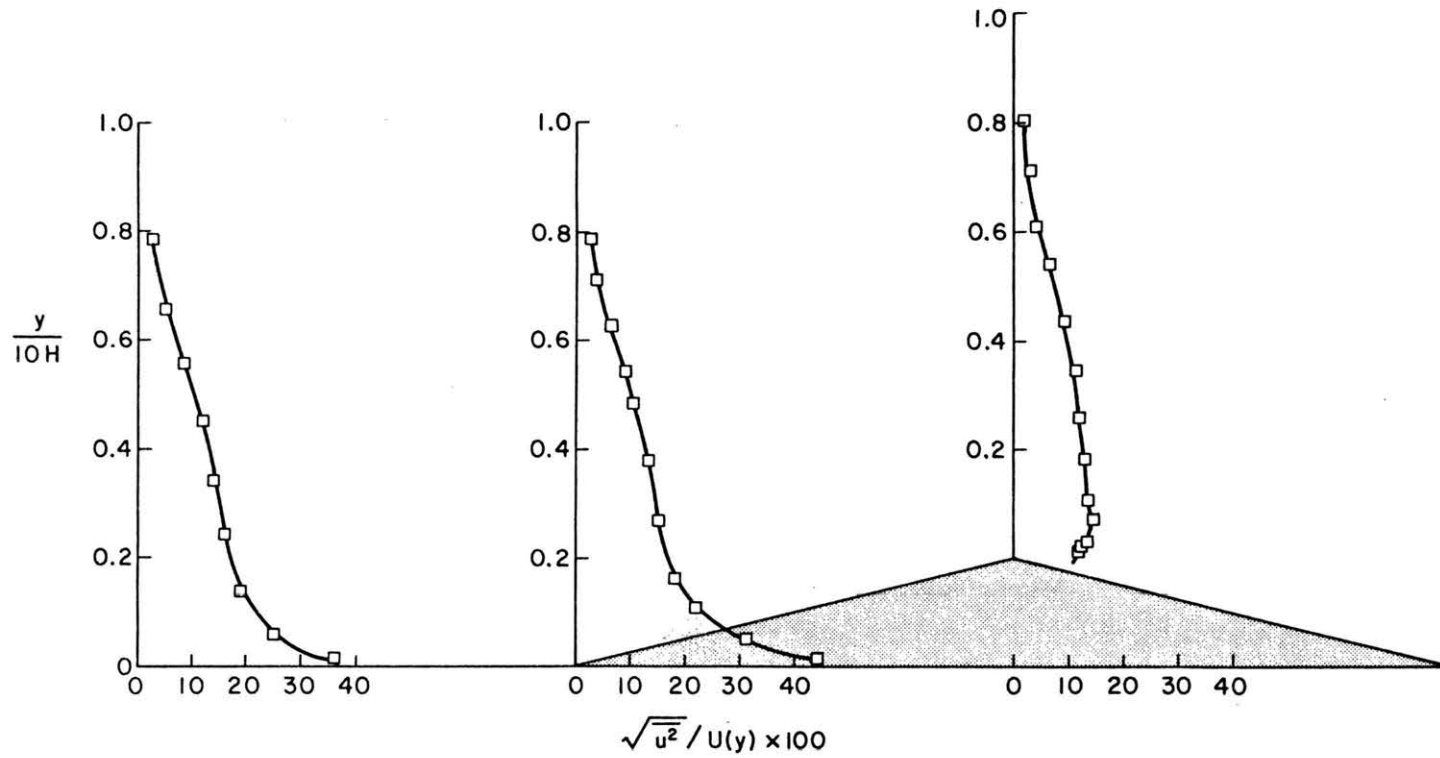
a) Full Sine Wave

Figure A7 Longitudinal Turbulent Component Hill Model



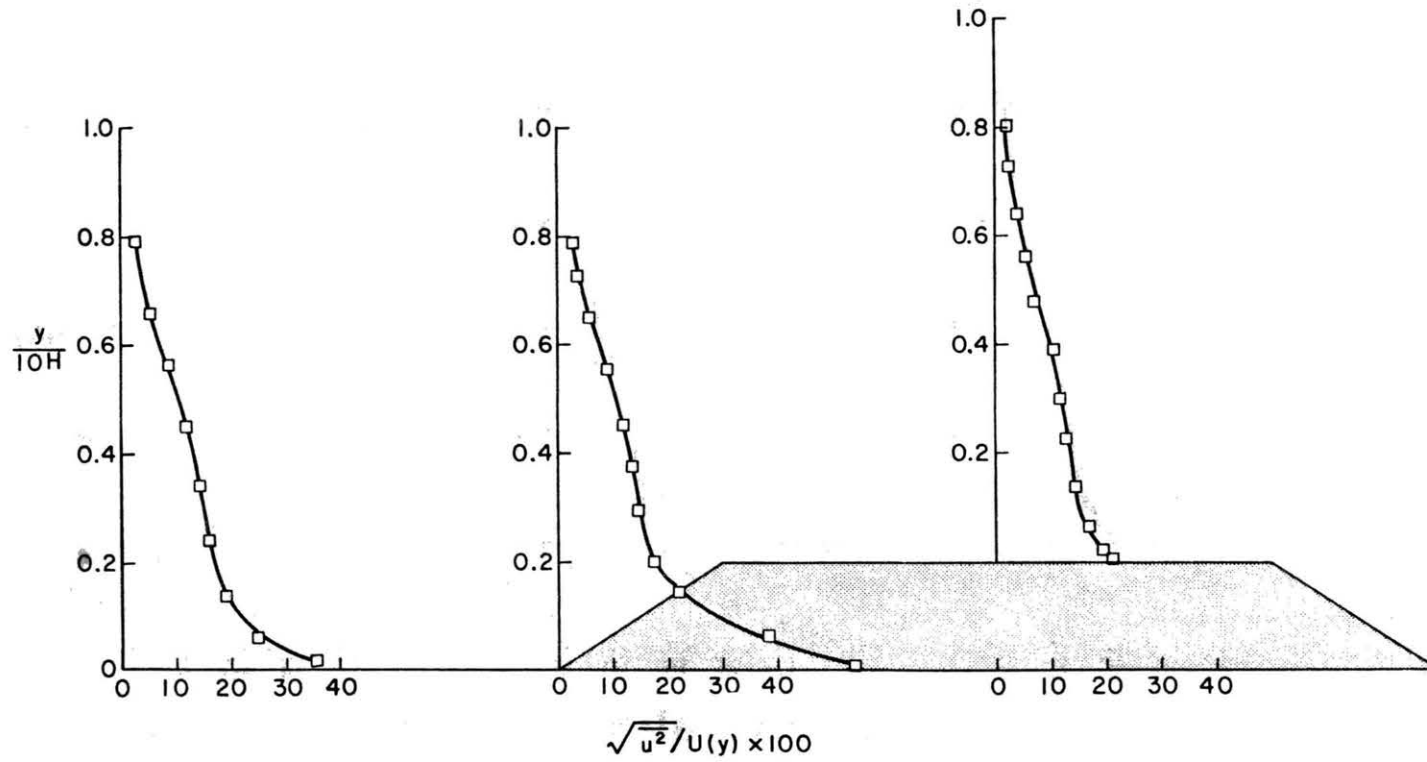
b) Half Sine Wave

Figure A7 (continued) Longitudinal Turbulent Component Hill Model



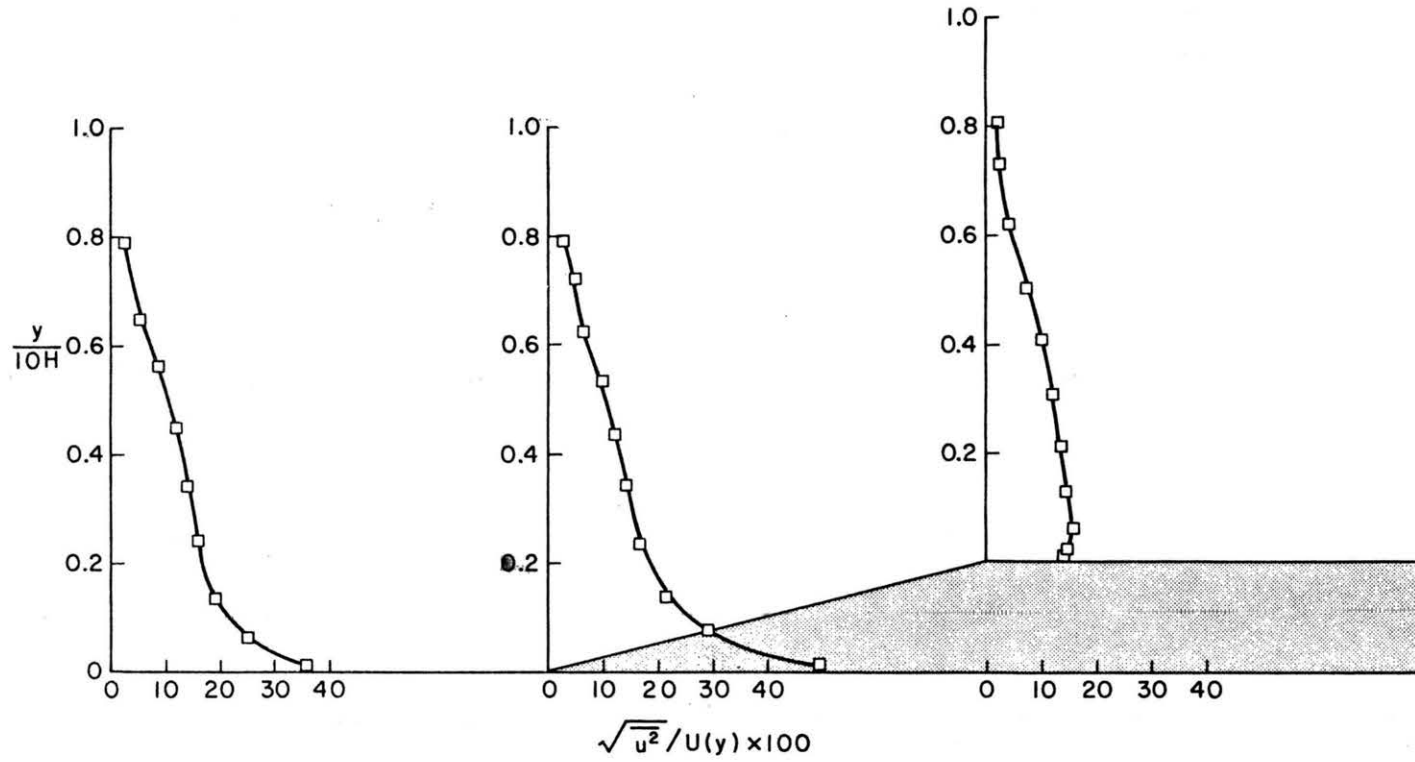
c) Triangular

Figure A7 (continued) Longitudinal Turbulent Component Hill Model



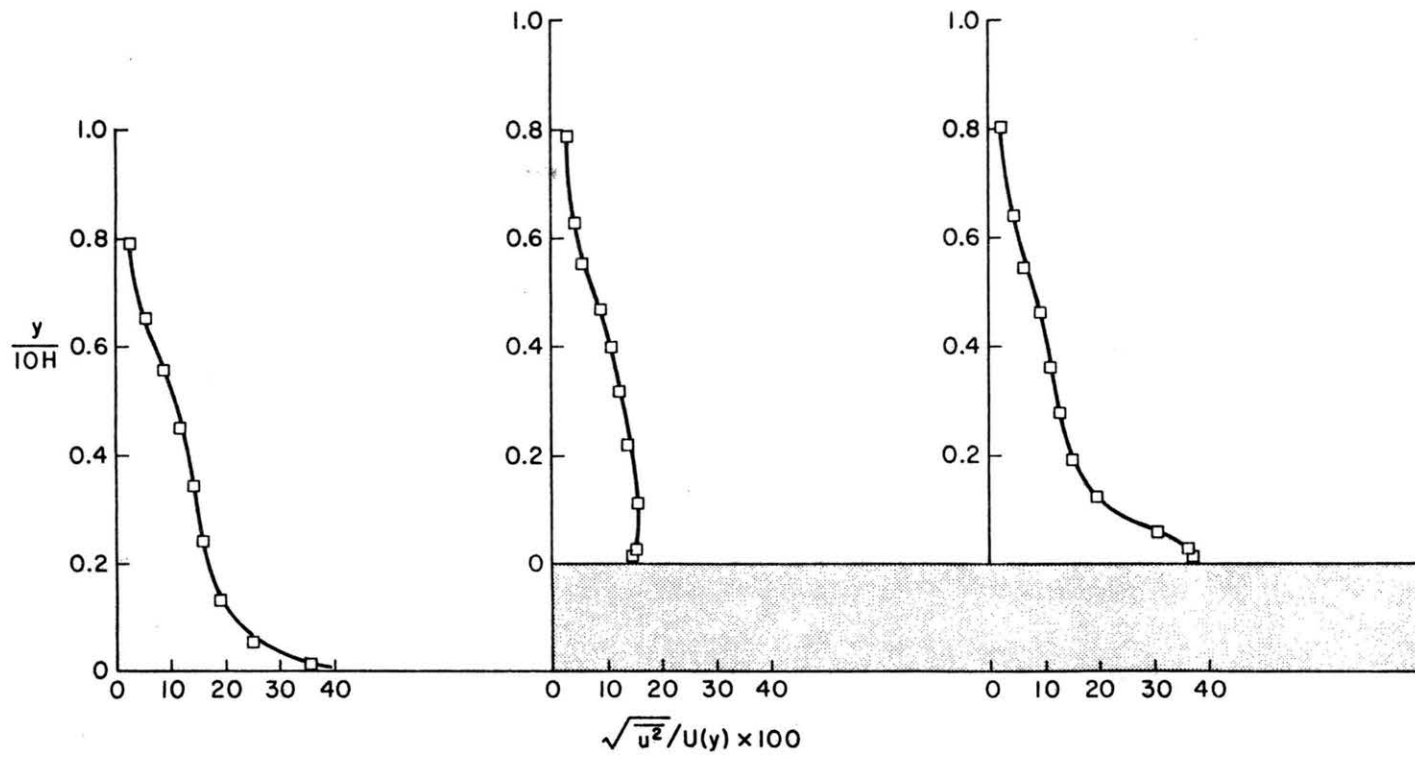
d) Trapezoidal

Figure A7 (continued) Longitudinal Turbulent Component Hill Model



e) Ramp

Figure A7 (continued) Longitudinal Turbulent Component Hill Model



f) Box

Figure A7 (concluded) Longitudinal Turbulent Component Hill Model

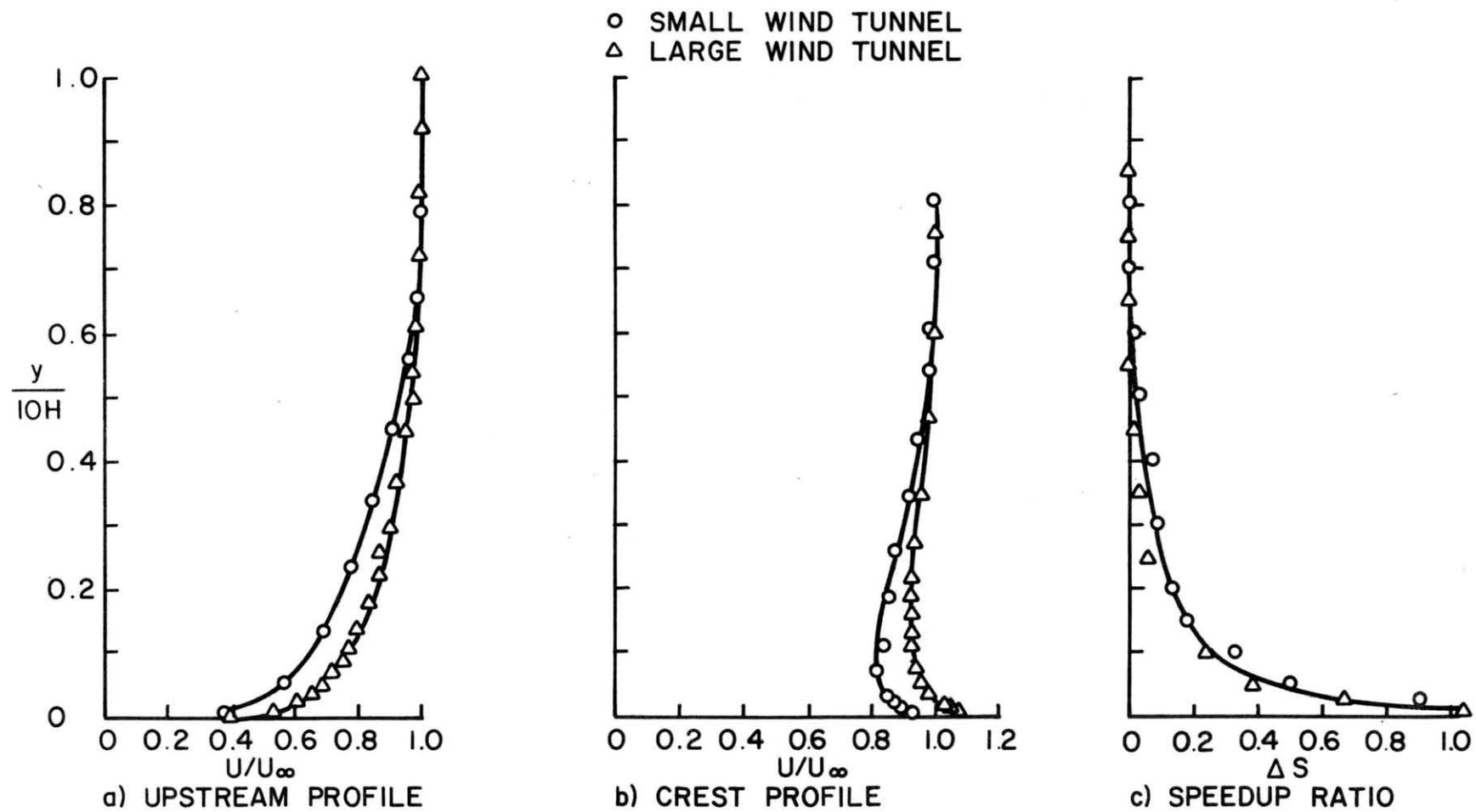


Figure A8 Comparison of Data From Two Similar Triangular Hills

APPENDIX B

BOUNDARY-LAYER TURBULENCE OVER TWO-DIMENSIONAL HILLS

by

Michael A. Rider

and

V. A. Sandborn

SUMMARY

Measurements of the mean and turbulent velocities for turbulent boundary layers over two-dimensional hills have been made. Triangular hills, with aspect ratios (height to vertical distance to crest) of 1:2, 1:4, and 1:6, were subjected to two different approach turbulent, boundary-layer flows. Mean velocities, longitudinal and vertical turbulent velocities, Reynolds stress and the wall, static pressure distributions are reported for a number of positions upstream, along, and at the crest of the hills.

As the flow advances up the hills, systematic changes in the mean and turbulent velocities occurred in the region near the hill surface. The flows in the outer region of the boundary layers above the hills were found to remain similar to the flow upstream of the hills. As the flow passes from the base of the hill to the crest, mean velocity, shear stress, and vertical turbulent velocity near the surface increased. The longitudinal turbulent velocity was found to decrease in magnitude as the flow progressed from the base to the crest of the hill.

INTRODUCTION

Annual mean and peak wind velocities are available for general areas throughout the United States and the world. This information is critical for the development of wind. It would be beneficial to the wind-power engineer to be able to predict from general wind data the flow characteristics at a specific location. However, rarely will the data be recorded at a proposed wind-power site. Reliable estimates of the local flow properties are needed. If the available wind data for the general area is at a station some distance from the site a means of extrapolating the desired information would be required.

In general, the approach terrain will affect the mean and turbulent flow properties. Moreover, to use the speedup effect of a hill, the predicted change in the airstream properties would be required. There are literally endless combinations of approach flow conditions and hill configurations. This study was limited to investigating two approach flow conditions and three two-dimensional triangular-shaped model hills.

The flow starts with a turbulent boundary layer developed over a flat plate with a zero pressure gradient. The turbulent boundary layer then flows over one of three triangular-shaped hills. Aspect ratios of the hills were (rise over run) 1:2, 1:4, and 1:6. Surveys were made of the mean velocity, the longitudinal and vertical turbulent velocities and the shear stress distributions. The measurements indicate how these different flow properties change in magnitude over a two-dimensional ridge. By adding upstream roughness a different approach turbulent boundary layer was formed. Measurements of the mean and the longitudinal turbulence velocity were made for the rough case.

The flat plate case represented a known point from which to evaluate the effect of the hills. In an effort to model atmospheric boundary layers in the wind tunnel, Zoric and Sandborn (1,2) have shown that similarity of turbulent boundary layers exist for large Reynolds numbers. Sandborn and Zoric have documented that for a flat plate turbulent boundary layer with a zero pressure gradient, similarity of the mean and turbulent velocities were present. When the turbulent quantities $\sqrt{u^2}$, $\sqrt{v^2}$ and \overline{uv} are normalized by dividing by the ratio of local wall shear to density, each of turbulent flow properties follows a similarity curve.

THEORETICAL BACKGROUND

To use wind power to the fullest in a particular area the local terrain effects must be known. Different hills or ridges will produce different degrees of speedup of the airstream as it approaches the summit. Thus, to take advantage of the speedup it is important to find the most advantageous location and to choose a proper wind system for the local conditions. The mean velocity distribution is of primary interest, but turbulent quantities must be known to insure structural stamina. The present study was directed toward evaluating the effect of a hill on a flow. The fundamental concerns were the mean velocity, the longitudinal and vertical turbulent velocity component distributions and the shear stress distributions.

Of specific interest was how far into the boundary layer would the impression of the hill be evident. Because of inertia of the flow, the outer reaches of the boundary layer were expected to remain similar to those upstream. The only portion of the flow expected to change was the region closest to the wall.

Prior to the test, it was known that a speedup of mean velocity would occur in the region nearest the hill. Furthermore, the increase in velocity gradient would produce an increase in surface shear stress. Not as obvious was the change in the turbulent components. Ribner and Tucker (3) considered turbulence in a contracting stream which gives an insight into the changes one may expect over a hill. Ribner and Tucker showed that when a flow was subjected to a contraction the longitudinal turbulent velocity component decreased and the lateral

component increased. Regarding the hill as a local contraction, it was anticipated that similar results would be found.

SURFACE SHEAR STRESS EVALUATION

Two methods were used to determine skin friction. The empirical Ludwig-Tillmann equation and the "law of the wall."

The Ludwig-Tillmann skin friction relation reads:

$$C_f \equiv \frac{\tau_w}{1/2 U_\infty^2} = .246 \times 10^{-.678H} \left(\frac{U_\infty \theta}{\nu}\right)^{-.268} \quad (B-1)$$

where the momentum thickness is,

$$\theta \equiv \int_0^\delta \frac{U}{U_\infty} \left(1 - \frac{U}{U_\infty}\right) dy$$

the form factor is,

$$H \equiv \frac{\delta^*}{\theta}$$

the displacement thickness is,

$$\delta^* \equiv \int_0^\delta \left(1 - \frac{U}{U_\infty}\right) dy$$

and δ is the boundary-layer thickness.

Justification for using this relation is based on earlier work reported by Tieleman (4). To check the reliability of the Ludwig-Tillmann equation, Tieleman compared direct measurements from a floating element shear plate and values determined from the Ludwig-Tillmann Equation (B-1) (see Figure B1). The agreement shown on Figure B1 demonstrated that the Ludwig-Tillmann equation was adequate for the present high Reynolds number flat plate, zero pressure gradient boundary layers.

The "law of the wall" credited to Prandtl (5) applies to the region nearest the wall where viscous effects are important. Nondimensionally the "law of the wall" reads:

$$\frac{U}{U_\tau} = f\left(\frac{U_\tau y}{\nu}\right) \quad (\text{B-2})$$

where

$$U_\tau^2 \equiv \frac{\tau_w}{\rho}$$

Patel (6) gives the following definitions of f for the given flow conditions:

(a) linear sublayer

$$U/U_\tau = U_\tau y/\nu \quad (\text{B-3a})$$

(b) fully turbulent region

$$U/U_\tau = A_1 \log_{10} \left(\frac{U_\tau y}{\nu} \right) + B_1 \quad (\text{B-3b})$$

(c) transition zone

$$U/U_\tau = A_1 \log_{10} \left[\left(\frac{U_\tau y}{\nu} \right) + C_1 \right] + B_1 \quad (\text{B-3c})$$

where the constants A_1 , B_1 and C_1 are assumed to be universal. From his work and other investigators, Patel assigns the following values for the fully turbulent region.

$$A_1 = 5.5 \quad \text{and} \quad B_1 = 5.45$$

The "law of the wall" is limited to zero and moderate pressure gradients. Patel suggests that the "law of the wall" may be used to determine the surface shear stress for pressure gradients in the range

$$0 > \frac{\nu}{(\rho U_\tau^3)} \frac{dp}{dx} > -0.007 \quad (\text{B-4})$$

within approximately 6% accuracy. For the zero and moderate pressure gradients, both the Ludwig-Tillmann and the "law of the wall" gives approximately the same value for the shear stress. Figure B2 gives values of C_f evaluated for the flat-plate flow of the present study.

SHEAR STRESS DISTRIBUTION EVALUATION

The following similarity method reported by Sandborn and Horstman (7), which was used to evaluate the turbulent, boundary-layer, shear stress distributions of the approach flow. This theoretical model accurately predicted the shear stress distributions for a flat plate, zero pressure gradient flow. Figure B3 is a comparison of the shear stress measured by Zoric and Sandborn and another by Klebanoff with similarity predictions. The solid line is the shear stress distribution evaluated directly from the mean velocity profile.

For a turbulent boundary layer the equation of motion in the x-direction is:

$$\rho U \frac{\partial U}{\partial x} + \rho V \frac{\partial U}{\partial y} = \frac{\partial p}{\partial x} + \frac{\partial \tau}{\partial y} \quad (\text{B-5})$$

where the shear stress (τ) is made up of the two parts--the mean and turbulent stress,

$$\tau \equiv \mu \frac{\partial U}{\partial y} + \overline{\rho uv} \quad (\text{B-6})$$

The boundary conditions require that at the wall

$$\tau = \tau_w \quad \text{and} \quad \frac{d\tau}{dy} = \frac{dp}{dx}$$

where p is the surface static pressure. Also at the outer limit of the turbulent boundary layer the shear stress approaches zero.

Sandborn assumed the following similarity for a compressible flow, although for the present study an incompressible flow is assumed.

$$\begin{aligned} \rho U &= \rho_e U_e f_{\rho U}(\eta) \\ U &= U_e f_U(\eta) \end{aligned} \quad (\text{B-7})$$

$$\tau = \tau_e \psi(\eta)$$

where $\rho_e U_e$ is a characteristic mass flow; U_e the characteristic velocity, and τ_e the characteristic shear stress. η is a non-dimensional variable resulting from dividing the vertical distance (y)

by the characteristic length (δ_e). Evaluating the differentials in terms of the similarity variables gives

$$\frac{\partial U}{\partial x} = f_U \frac{\partial U_e}{\partial x} + U_e \frac{\partial f_U}{\partial x} = f_U \frac{\partial U_e}{\partial x} - \frac{U_e}{\delta} \frac{d\delta_e}{dx} \eta f_U' U_e \quad (\text{B-8})$$

$$\frac{\partial U}{\partial y} = \frac{U_e}{\delta_e} f_U' \quad (\text{B-9})$$

and from continuity

$$\rho V = - \int_0^\eta \delta_e \frac{\partial \rho_e U_e}{\partial x} f_{\rho U} d\eta + \rho_e U_e \frac{d\delta_e}{dx} \int_0^\eta f'_{\rho U} \eta d\eta \quad (\text{B-10})$$

Substituting in the similarity values into the equation of motion yields

$$\begin{aligned} \rho_e U_e f_{\rho U} \left[f_U \frac{\partial U_e}{\partial x} - \frac{U_e}{\delta} \frac{d\delta_e}{dx} \eta f_U' \right] + \frac{U_e}{\delta} f_U' \left[- \delta \frac{\partial \rho_e U_e}{\partial x} \int_0^\eta f_{\rho U} d\eta \right. \\ \left. + \rho_e U_e \frac{d\delta_e}{dx} \int_0^\eta f'_{\rho U} \eta d\eta \right] = - \frac{\partial p}{\partial x} + \frac{\tau_e}{\delta} \psi' \quad (\text{B-11}) \end{aligned}$$

Solving for ψ' and integrating gives

$$\begin{aligned} \psi \equiv \frac{\tau}{\tau_e} = \frac{\rho_e \delta_e U_e}{\tau_e} \frac{dU_e}{dx} \left(\int_0^\eta f_{\rho U} f_U d\eta - \eta \right) \left(\frac{\delta_e U_e}{\tau_e} \frac{d\rho_e U_e}{dx} \right. \\ \left. + \frac{\rho_e U_e^2}{\tau_e} \frac{d\delta_e}{dx} \right) \int_0^\eta \left\{ f_U' \int_0^{\eta'} f_{\rho U} d\eta' \right\} d\eta + C \quad (\text{B-12}) \end{aligned}$$

For similarity it is required that the Equation (B-11) be independent of x , thus for compressible flow

$$\frac{\delta_e \rho_e U_e}{\tau_e} \frac{dU_e}{dx} = A_2 \quad (\text{a constant independent of } x) \quad (\text{B-13})$$

and

$$\frac{\delta_e U_e}{\tau_e} \frac{d\rho_e U_e}{dx} + \frac{\rho_e U_e^2}{\tau_e} \frac{d\delta_e}{dx} = B_2 \quad (\text{a constant independent of } x) \quad (\text{B-14})$$

For incompressible flow, $\frac{\delta \rho_e}{\delta x} = 0$, thus the similarity requirements are:

$$\rho \frac{\delta U_e}{\tau_e} \frac{dU_e}{dx} = A_2 \quad (\text{B-13a})$$

$$\rho \frac{U_e^2}{\tau_e} \frac{d\delta}{dx} = B_2 \quad (\text{B-14a})$$

To evaluate Equation (B-12) the following similarity characteristics were used: $U_e = U_\infty$, $\rho_e = \rho_\infty$, $\tau_e = \tau_w$, and δ_e , the characteristic length was equal to δ , where $\delta = y$ at $\tau = 0$. The final form of Equation (B-12) for an incompressible flat-plate flow with a zero pressure gradient is:

$$\psi \equiv \frac{\tau}{\tau_w} = 1 - \frac{U_\infty^2}{U_\tau^2} \frac{d\delta}{dx} \int_0^\eta \left\{ \frac{d(U/U_\infty)}{d\eta} \int_0^{\eta_1} \left(\frac{U}{U_\infty} \right) d\eta_1 \right\} d\eta \quad (\text{B-15})$$

where $U_\tau^2 \equiv \frac{\tau_w}{\rho}$. The boundary condition at $\eta = 0$ ($\frac{\tau}{\tau_w} = 1$) was used to evaluate the constant of integration.

TURBULENT VELOCITY COMPONENT SIMILARITY

Examination of measurements by different experimenters shows that similarity does exist for the total shear stress and the turbulent-velocity terms. Zero pressure gradient measurements by Zoric (2) at high Reynolds numbers and Klebanoff (8) at low Reynolds numbers demonstrate the validity of Equation (15) within experimental limits (10). Figures B3 and B4 show the agreement of the total shear-stress distribution when referenced to the wall shear stress and the boundary-layer thickness. The longitudinal shear components, $\sqrt{\frac{\rho u^2}{\tau_w}}$, also compare

well for $y/\delta \geq 0.05$ for the data of (2) and (8), as shown on Figure B5.

The vertical turbulent component, $\sqrt{\frac{\rho v^2}{\tau_w}}$, distributions do not agree as well as the total shear stress or the longitudinal turbulent component (see Figure B6). The measurements of Zoric do not show the drop in the $\sqrt{v^2}$ as did those of Klebanoff. An additional set of data recorded very close to the wall (4) reveals a very distinct maximum followed by a sharp decline in the vertical turbulent component.

The turbulent quantities $\sqrt{u^2}$, $\sqrt{v^2}$ and \overline{uv} will be presented, unless indicated, nondimensionalized by multiplying by the density and the farthest upstream estimations of the wall shear stress. The study of Sandborn and Horstman (7) suggests that the characteristic wall shear stress may be the upstream value when rapid pressure changes occur. Also, as the flow continued over the hills direct quantitative changes in the turbulence terms can easily be compared. In the derivation of the similarity relation between the shear stress and mean flow, the characteristic values are not defined. Thus, the characteristic shear stress and characteristic length need not be the local wall shear stress and the local boundary-layer thickness. For rapid distortion, the turbulent properties apparently cannot change quickly, so they will be convected along by the mean flow without undergoing major changes. As noted, the work of Sandborn and Horstman suggested that an upstream value of the surface shear stress may be a possible choice for the present flow cases. For the present evaluation a value of wall shear stress at a specific upstream location ($x = 55.8$ cm from the crest for smooth surface case, and $x = 50.8$ cm from the crest for the rough surface case) was used for the characteristic shear stress. The particular locations are somewhat arbitrary, but were selected to be upstream of where the flow is disturbed by the presence of the hill.

The characteristic length must reflect the distortion of the boundary layer coordinate system as the layer develops. If it is assumed that the hill models influence only the part of the boundary layer near the surface and not that of the outer part of the layer, then a characteristic length equivalent to the layer development without the hill might be employed. This assumption of neglecting the perturbation of the hill on the boundary-layer thickness length obviously would only be valid when the approach layer is thick compared to the hill height. For the present study it was found that the boundary-layer thickness develops nearly linear with x-distance (1). The present undisturbed boundary layers for both the smooth and rough surfaces appeared to grow at a rate of 1 cm for every 10 cm in the x-direction. Thus, the characteristic length (δ_e) was taken as the extrapolated boundary-layer thickness (in the

ratio of 1 to 10) from the measured approach profile thickness. Again this selection of a characteristic length is somewhat arbitrary. It is mainly justified in that it appears to produce a good correlation of the turbulence data over the hills in the outer part of the boundary layer. Other coordinate changes, such as following streamline paths, have been suggested; however for rapid distortions, the boundary-layer thickness appears to produce the most consistent correlation.

BOUNDARY CONDITIONS

In the atmosphere a wide spectrum of possible approach conditions might exist. In general the effect of a small hill in a deep boundary layer will depend on the energy distribution within the approach flow. The thicker the boundary layer the less the energy will be distributed in the region near the surface; thus, the lower the speedup effect of the hill will be. Local roughness of the approach surface will also act to remove more energy near the surface, which will also be seen in a thickening of the boundary layer. It is apparent that the higher the hill compared to the boundary-layer thickness the larger the speedup will be. Likewise for boundary layers of the same thickness, but different surface roughness, the layer over a smoother surface will produce the greater speedup. Two different approach turbulent boundary layers are considered in the present study. The first case is that of a smooth surface, while the second is produced by a long fetch of roughness.

Classical boundary-layer theory generally employs a coordinate system, which is perpendicular to the surface at all points along and near the surface (curvilinear coordinates). Over the hills this requirement of a curvilinear coordinate can also be expected to be valid. However, for engineering applications of velocity distributions for wind-power use, surveys and data in the vertical direction are desired. For the present study a simple rectangular coordinate system was employed, both for measurements and analysis. The x-distance coordinate originated at the crest of the hill and was measured positive in the upstream direction along the tunnel floor. The y-direction coordinate were measured positive from the local surface of the model at each x-location.

Evaluation of the local surface shear stress from Equations (B-1) or (B-2) requires the curvilinear-boundary layer coordinate system be employed. As a demonstration of the deviation from boundary-layer theory in the use of a vertical coordinate, an estimate of the surface shear from the law-of-the-wall concept was made for both a vertical and a curvilinear-coordinate evaluation (see Figure B7). The deviation shown in Figure B7 is mainly important in the lower portion of the hill.

EXPERIMENTAL SETUP

The measurements were taken in the Meteorological Wind Tunnel located in the Fluid Dynamics and Diffusion Laboratory at Colorado State University. The purpose of the experiment was to make surveys of flow characteristics over models of hills emersed in deep turbulent layers. The following sections will discuss the experimental facility equipment and technique.

WIND-TUNNEL FACILITY

As mentioned above the measurements were performed in the recirculating Meteorological Wind Tunnel shown in Figure B8. The flow rate in the tunnel is controlled by a variable-pitch, variable-speed propeller and can be set between 0.3 and 37 m/s with no more than one-half percent diviation from the desired velocity. The test section is approximately 1.8 m square, 27 m in length, and is preceded by a 9:1 contraction. A zero pressure gradient along the length of the test section was maintained with the adjustable ceiling. The ambient temperature was kept constant within $\pm 1/2^{\circ}\text{C}$ by the tunnel air-conditioning system.

The experiments were scheduled in two parts. The two parts had different upstream conditions; however, there were features, which were similar for both. At the entrance to the test section during both tests a 1.22 m long section of 1.27 cm gravel fastened to the floor followed by a 3.80 cm high sawtooth fence spanning the width of the tunnel was used to prompt the formation and growth of a large turbulent boundary layer.

In the initial test, a false floor was installed to which the models were secured (see Figure B9). The false floor was comprised of three sections: the approach ramp, horizontal test section, and the trailing down ramp. The floor originated 5.60 m from the sawtooth fence. The approach ramp, constructed from 0.32 cm masonite, was at an angle of 0.84° with the horizontal and had a length of 1.30 m. Following the upstream ramp was a 8.55 m long test section. This section was built from 1.91 cm plywood. The models tested were mounted directly on the plywood. Masonite, 0.32 cm thick, was then used in assembling the trailing ramp. This ramp was 0.90 m in length and formed an angle of -1.21° with the horizontal.

During the second test there was no false floor. However, a roughness beginning at 1.83 m from the sawtooth fence and ending at 11.43 m gave a different approach velocity profile (see Figure B10). The roughness was made up to aluminum sheets with ribs 0.16 cm in height. The ribs were randomly spaced normal and parallel to the flow. In this phase of the experimentation the models were mounted directly on the aluminum floor of the wind tunnel.

As mentioned above, a sawtooth boundary-layer trip was used to prompt the growth of turbulent boundary layer. A similarity velocity profile was attained within 6.1 m of the test section entrance. During the initial test the models were set 14.0 m from the entrance and during the second 18.6 m. For both flows the ceiling of the wind tunnel was adjusted to produce a near zero pressure gradient in the free streams of the test section. A slight acceleration occurred along the approach ramp.

MODEL DESCRIPTION

A series of triangular-shaped hills were designed and used for the tests (see Figure B11). The models were constructed using nine cross-section ribs made of 1.27 cm Plexiglas. The hill surface was placed over the ribs, and was made of 0.32 cm thick Plexiglas. The crest heights of each was 5.08 cm and with aspect ratios of 1:2, 1:4 and 1:6. All models were 183 cm in length. Each of the models were equipped with static pressure taps.

INSTRUMENTATION

The present study required both mean and turbulent velocities to be evaluated. The mean velocities and pressures were evaluated using special electronic transducers, while the turbulent terms were determined from hot wire anemometer measurements.

Actuator and Carriage

The measurements for this experiment required vertical surveys (y-direction) of the flow at particular longitudinal points (x-direction) along the center of the tunnel. To accomplish this the existing carriage of the wind tunnel was employed. The carriage had been constructed on a rail and wheel system. The rails 101.6 cm from the floor run the full length of the test section. This allows the carriage to be positioned at any desired point in the x-direction. A control unit outside the tunnel monitored the vertical movement of the probes as they traversed the boundary layer.

A stop rod mounted on the probe support was used to protect the probes from being driven into the floor. The stop rod also served as a means of determining the initial location of the probes above the surface, as noted on Figure 11. An electric indicator was triggered when the stop rod contacted the floor. During the second set of tests a 0.00254 cm dial indicator was employed to determine more accurately the y-locations of the probes above the surface.

STATIC PRESSURE MEASUREMENTS

Four different probes were used to measure the static pressure. The particular probe used depended on the location of the desired measurements. While making measurements of the mean velocity in the

boundary layer above the surface of the hill, two probes were used as static-pressure references. A commercial cylindrical pitot-static tube was used along with a commercial disk probe. In general, cylindrical probes are acceptable for free-stream and boundary-layer measurements. However, this type probe is accurate only when the flow is parallel to the probe. Near the hill surface the flow direction will not be parallel to the axis of the cylindrical probe. The disk probe was employed in the vicinity of the surface, since it was insensitive to flow direction.

The disk probe sampled the local static pressure through a small static tap drilled in the center of the 0.62 cm thin disk. The disk probe gives systematically lower static pressure readings, but was found to be insensitive to "pitch" angles of $+30^{\circ}$. The geometry of the disk probe restricted measurements near the surface. The cylindrical probe has a diameter of 0.18 cm with an elliptical nose. The static taps were located 2.22 cm from the support stem. This probe had a 0.040 cm hole for total pressure measurements.

Static-pressure measurements were also taken on the surface of the models and the floor of the tunnel. Each of the models contained a set of static pressure taps distributed over the centerline of the hill (see Figure B12). The static taps, sharp-edged and 0.064 cm in diameters, were drilled perpendicular to the model surface. On the upstream floor of the tunnel, static probes constructed from 0.079 cm i.d. and 0.139 cm o.d. brass tubing were used. The end of the tubes were soldered closed and a series of taps were drilled in a circle around the circumference of the tubing. The probes were secured to the wall of the tunnel.

When making static-pressure measurements, the reference was the static pressure in the free stream. A commercial pitot-static tube 0.318 cm diameter was used. It was a cylindrical probe with an elliptical nose. The total pressure tap in the tip of the nose was 0.079 cm in diameter. The static taps were 5.08 cm from the support stem. The only static pressures reported are wall static pressures upstream and on the hills. The purposes of the other static-pressure probes were to correct the measurements of the disk probe and their use as reference pressures.

VELOCITY MEASUREMENTS

Three different probes were used to measure the total pressure. Two of the probes were commercial pitot-static tubes described earlier and the third was a commercial Kiehl probe.

The two pitot-static probes were used mainly for control and calibration. The pitot-static tube used to survey the static pressure above the hill was also incorporated as a standard used to calibrate

the hot-wire probes. The second probe, which was maintained as a static-pressure reference, monitored the tunnel flow. This second probe was fixed in the freestream approximately 1 m ahead of the models.

The mean velocity measurements made during the surveys were sampled with the Kiehl probe. This probe has the capability of measuring total pressure even when the flow angles are $\pm 40^\circ$. The disk probe pressure was used to determine the local static pressure. For the range of velocities measured in the present study all three probes agreed with the laboratory standard pitot probe. No correction to the readings were made because of the total pressure probes.

TURBULENCE AND SHEAR STRESS MEASUREMENTS

Two types of hot-wire data were recorded. In the initial test a cross-wire system was used, while in the second a single horizontal wire fulfilled the requirement. The cross wire employed was not of the usual x-wire type, but had one wire normal and one wire yawed to the flow. Both probes were constructed in the Fluid Dynamics and Diffusion Laboratory at Colorado State University. The wire in both cases was 80% platinum and 20% iridium and 1.02×10^{-3} cm in diameter. The length of the wires varied but all were approximately 0.16 cm. The wires were soldered at each end to a support, which was protruding from a ceramic probe shielded by brass tubing. The sensor was then secured to the actuator system. A detailed discussion of the evaluation of the hot-wire output is given by Sandborn (13).

The hot wires were operated with commercial constant temperature anemometers. The output of the anemometers was amplified and read with mean d.c., and true r.m.s voltmeters. The voltmeters were equipped with R-C time constants to allow long time averages of the signals. An analog multiplier was employed to obtain the produce of the fluctuating output of the cross wires. The multiplier circuit was checked using a sine-wave generator.

Two capacitance pressure transducers were used for pressure measurements. The transducers were calibrated using a standard water micromanometer. These transducers are equipped with self-environmental control to maintain a constant operating temperature. Figure B13 is a schematic of the equipment setup.

RESULTS AND DISCUSSION

The major effect of a hill is to increase the local velocity near the surface. This effect is of great importance in wind-power application. The alteration of the mean wind profile will also be expected to alter the turbulence near the surface. Thus, the present study was directed at evaluating the effect of the hill on the mean and turbulent properties.

MEAN VELOCITY

Primary consideration for wind power is the change in the mean velocity distribution. It was found as the flow proceeded down the tunnel that similarity of the approach flow was maintained (see Figure B14). At the windward foot or base of the model hills, a slowdown of the airstream near the surface was evident. Once the flow passes over the base of the hill, there was a continuous increase of the velocity near the surface. The greatest speedup for all models tested was recorded at the crests. The similarity of the outer region of the flow was maintained over the hill (see Figure B15). It is important to note that the outer flow pressure was fixed approximately constant, which would help the flow to remain similar in the outer region. The largest increase in velocity for the first flow case was recorded with the 1:4 hill followed by the 1:6 and finally the 1:2 hill (see Figure B16).

Flow Case II with increased upstream roughness produced the same results for the two models, 1:2 and 1:6, tested (see Figure B17).

The 1:2 and 1:6 model hills caused a greater mean velocity speedup for Flow Case I than for Flow Case II. Flow Case I, with a 0.17 power law profile, produced a maximum speedup, ΔS , of 0.62 for the 1:6 model hill and 0.33 for the 1:2 model hill where

$$\Delta S = \frac{U_{\text{crest}}(\eta) - U_{\text{upstream}}(\eta)}{U_{\infty}} \quad (\text{B-16})$$

and $\eta_{\text{crest}} = \eta_{\text{upstream}} \approx 0.5$. The 1:4 model hill gave the maximum speedup of 0.68 for the same flow case. Flow Case II, representing a 0.26 power-law profile, was subjected to maximum speedups of 0.43 and 0.26 for the 1:6 and 1:2 model hills respectively.

Note that the turbulence terms are nondimensionalized by dividing by τ_w or τ_{ref} . As described earlier τ_w are values calculated for upstream profiles. The values used were $\tau_w = 0.1074 \text{ n/m}^2$ for Flow Case I at $x = 5.88 \text{ cm}$ and 0.0952 n/m^2 at $x = 50.80 \text{ cm}$ for Flow Case II.

LONGITUDINAL TURBULENT VELOCITIES

The longitudinal turbulent velocities in both flow cases varied in the same manner. At the foot of the hill the greatest magnitudes were recorded. This was succeeded by a continuous decrease in $\sqrt{u^2}$ near the surface with the decrease being greatest at the crest. A greater decrease in the longitudinal turbulent velocity component was noted for the second flow case with the larger values of approach turbulence. The alteration of the turbulence was restricted to that region near the wall (see Figures B18, B19, B20, B21).

The longitudinal turbulent velocity component, $\sqrt{u^2}$, compared closely with that found by Zoric (2) for the first test (see Figure B22).

As expected for the second flow case the $\sqrt{u^2}$ component was higher. In both cases the measurements of the longitudinal turbulent velocity component were reproducible (see Figure B23).

VERTICAL TURBULENT COMPONENT

The vertical turbulent component, $\sqrt{v^2}$, which was measured only in Flow Case I also varied as it passed over the hill. This turbulence component decreased up to the base of the hill, and then increased continuously to the crest. The change only involved the flow near the surface (see Figures B24 and B25). As discussed under Theoretical Background, the increase in $\sqrt{v^2}$ was expected from results for a contracting flow. When compared to Zoric's data in the outer region, the values obtained for $\sqrt{v^2}$ were close. However, when compared to Tieleman's data (4) near the wall the measurements appear to be somewhat lower (see Figure B26). (The data reported by Tieleman (4) were taken at a station almost 30 m downstream in the tunnel compared to the present data taken at a distance of 14 m.) The disagreement may in part be attributed to the strong velocity and turbulent gradients acting on the yawed wire in this region. Tieleman compensated for the gradients when he presented his results. A discussion of this is given by Sandborn (12). The first flow case may not be a true flat-plate flow since the false floor produced a change in the flow.

SHEAR STRESS DISTRIBUTION AND SURFACE STATIC PRESSURE

As the flow passes from the farthest upstream station toward the base of the hills, there was a decrease in surface shear stress and an increase in the surface static pressure. After passing the foot of the hill, the trend reversed and an increase in wall shear was present. The surface static pressure decreased along the reach of the hill. Figure B27 shows the change in surface shear stress and surface static pressure in terms of friction and pressure coefficients, where

$$C_f = \frac{\tau_{\text{wall local}}}{1/2 \rho U^2} \quad (\text{B-17})$$

and

$$C_p = \frac{P_{\text{static local}} - P_{\text{static F.S.}}}{1/2 \rho U^2} \quad (\text{B-18})$$

The surface shear stress at each station was estimated using the Ludwig-Tillmann equation and the "law of the wall." The values found using the "law of the wall" may be somewhat questionable for the pressure gradients obtained. Based on results of Patel (5), which was described earlier, the "law of the wall" applies within approximately 6% of the range given by Equation (B-4). For the present study the range was exceeded. For the 1:6 hill an average of about $\Delta \approx 0.032$ was computed. As a result, the values obtained for the wall shear stress on the surface of the hill would be expected to be consistently high. However, the numbers obtained do give approximate values. For the 1:6 and 1:2 hills the Ludwig-Tillmann equation gives lower values than the "law of the wall."

The affect of the hill on the shear-stress distribution was a local one. The shear-stress distribution remained unaffected in the outer region. Near the wall the distribution changed accordingly with the wall shear stress (see Figure B28). For Figures B28 (as noted on the figures) and B30, all points shown were calculated from the similarity Equation (B-15). For the other cases shown on Figure B28 the data points were evaluated from the cross-wire data. The curves through the cross-wire data were faired using the upstream similarity distribution and an approximate extrapolation to the known surface shear-stress value. The local slope of most of the shear stress curves at the wall ($\partial\tau/\partial y|_{y=0} = \partial p/\partial x$) are very steep, and as such were not shown on the fairings.

An explanation was given in the Theoretical Discussion for the method used to evaluate the upstream shear-stress distributions. Because the analysis depends on the mean velocity measurements and not the direct measure of the Reynolds stresses, it was possible to evaluate for both flow cases the upstream shear-stress distributions. When compared to Zoric's data, it was found that the shear-stress distribution of the first test was repeatedly lower (see Figure B29). Again this is attributed to the false floor. The second flow case yielded a similar result. However, these results were higher than that found in Flow Case I but still less than what Zoric found (see Figure B30).

The Reynolds stresses (\overline{uv}) were employed to evaluate the vertical turbulent velocity component $\sqrt{v^2}$. The cross correlation, \overline{uv} , was the most uncertain term to evaluate. It was believed that a multiplying circuit used in the measurements did not function as well as desired. The result was a greater scatter in the data for the \overline{uv} terms.

Determination of the $\sqrt{v^2}$ terms was also affected, but since it is presented as a square root the scatter does not appear as pronounced.

CONCLUSIONS

The present investigation studied two different approach flow cases and three different triangular hills. These two-dimensional model hills with aspect ratios of 1:2, 1:4 and 1:6 changed the mean and turbulent properties of the flow near the surface. From the experimental evidence the following conclusions can be drawn.

1. As the flow progressed from the upstream station to the crest there was no effect due to the hill on the flow properties in the outer region. The flow properties included are mean velocity and the longitudinal and vertical turbulent velocities along with the shear stress.

2. For the region near the wall there was a velocity speedup as the flow passed over the hill, with the maximum above the crest. The greatest speedup was for the 1:4 hill.

3. The longitudinal turbulent velocity, $\sqrt{u^2}$, increased up to the foot of the hill, then decreased as the flow passed over the hill. The decrease was greater for a turbulent boundary layer with larger turbulent velocities. The decrease was on the order of 12%.

4. The vertical turbulent velocity $\sqrt{v^2}$ decreased as the flow approached the base of the hill, then increased up to the summit. Both the increase in the vertical turbulent velocity and the decrease in the longitudinal turbulent velocity were consistent with theoretical results for a contracting flow.

5. The shear stress term (\overline{uv}) and the wall shear stress decreased from the upstream station to the base of the hill. Over the hill an increase of the shear stress was found.

6. A decrease in surface pressure and an increase in wall shear coincided with the increase in mean velocity. The opposite was true when the mean velocity decreased.

REFERENCES

1. Zoric, D. and Sandborn, V. A., Similarity of Large Reynolds Number Boundary Layers, Boundary Layer Meteorology, Vol. 2, No. 3, pp. 326-333, 1972.
2. Zoric, D. L., Approach of Turbulent Boundary Layer to Similarity, Ph.D. Dissertation, Colorado State University, Report CER68-69DLZ9, 1968.
3. Ribner, H. S. and Tucker, M., Spectrum of Turbulence in a Contracting Stream, National Advisory Committee for Aeronautics Rep. 1113, 1953.

REFERENCES (continued)

4. Tieleman, H. W., Viscous Region of Turbulent Boundary Layer, Ph.D. Dissertation, Colorado State University, Report No. CER67-67HWT21, 1967.
5. Prandtl, L., Recent Results of Turbulence Research NACA Tech. Memo. 720, 1933.
6. Patel, V. C., Calibration of the Preston Tube and Limitations on Its Use in Pressure Gradients, J. Fluid Mech., Vol. 23, Part 1, pp. 185-208, 1965.
7. Sandborn, V. A. and Horstman, C. C., Boundary Layer Shear Stress in Subsonic and Supersonic Flow, Symposium of Turbulent Shear Flow, Pennsylvania State University, 1977.
8. Klebanoff, P. S., Characteristics of Turbulence in a Boundary Layer With Zero Pressure Gradient, NACA TN 3178, 1954.
9. Sandborn, V. A., Class Notes for Experimental Methods in Fluid Mechanics, Civil Engineering Department, Colorado State University, CER71-72VAS40, 1972.
10. Sandborn, V. A., A Review of Turbulence Measurements in Compressible Flow, NACA Tech. Memo., X62, 337, March, 1974.
11. Schlichting, H., Boundary Layer Theory, McGraw-Hill Book Company, Inc., New York, 1960.
12. Sandborn, V. A., Effect of Velocity Gradients on Measurements of Turbulent Shear Stress, Colorado State University, AIAA J., Vol. 14, No. 3, pp. 400-402, March, 1976.
13. Sandborn, V. A., Resistance Temperature Transducers, Metrology Press, Fort Collins, Colorado, 1972.

Table BI Tabulated data for Flow Case I: 1:2 hill model

a) Position 30.99cm from crest. Free stream velocity 9.09m/s

Y/Delta	U(y)/U _∞	RMSU (ROE/T)**.5	RMSV (ROE/T)**.5	T(y)/T _{REF}
.005	.380	1.850	1.222	.792
.012	.519	2.223	1.323	.792
.029	.595	2.170	1.170	.790
.053	.641	2.105	1.237	.786
.084	.694	2.010	1.189	.775
.124	.728	1.881	1.245	.755
.196	.771	1.668	1.151	.699
.326	.842	1.606	1.144	.557
.480	.911	1.417	1.115	.359
.602	.949	1.240	.919	.208
.732	.979	.808	.639	.083
.875	.999	.443	.356	.006
1.017	1.000	.246	0.000	-.012

Table BI (continued) Tabulated data for Flow Case I: 1:2 hill model

b) Position 10.16cm from crest. Free stream velocity 9.61m/s

Y/Delta	U(y)/U _∞	RMSU (ROE/τ)**.5	RMSV (ROE/τ)**.5	τ(y)/τ REF
.021	.360	1.877	1.217	.550
.037	.469	2.082	1.260	.549
.070	.568	2.032	1.199	.545
.088	.607	2.026	1.170	.541
.123	.675	1.823	1.102	.531
.162	.738	1.838	1.167	.514
.201	.763	1.754	1.154	.493
.250	.795	1.650	1.133	.461
.314	.831	1.569	1.093	.412
.373	.874	1.519	1.113	.361
.458	.907	1.418	1.055	.282
.520	.931	1.378	.982	.226
.612	.947	1.221	.894	.147
.721	.977	.947	.696	.073
.824	.995	.629	.536	.025
.927	.998	.413	.350	.003
1.033	1.000	.284	.227	-.001

Table BI (continued) Tabulated data for Flow Case I: 1:2 hill model

c) Position 2.54cm from crest. Free stream velocity 9.53m/s

Y/DELTA	U(Y)/U _∞	RMSU (ROE/τ)**.5	RMSV (ROE/τ)**.5	T(Y)/T REF
.022	.707	2.086	1.375	1.198
.041	.728	2.004	1.278	1.076
.060	.758	2.007	1.262	1.104
.099	.805	2.002	1.183	1.181
.120	.823	1.899	1.163	1.061
.153	.841	1.817	1.159	.992
.177	.853	1.907	1.185	1.194
.215	.857	1.694	1.110	.845
.285	.881	1.614	1.096	.720
.356	.899	1.545	1.101	.656
.425	.916	1.471	1.035	.626
.505	.944	1.376	.939	.475
.568	.958	1.307	.846	.394
.653	.978	1.100	.705	.254
.746	.993	.926	.559	.200
.874	1.000	.492	.253	.003
.954	1.000	.369	.099	-.011
1.012	1.000	.275	0.000	-.029

Table BI (continued) Tabulated data for Flow Case I: 1:2 hill model

d) Position 5.08cm from crest. Free stream velocity 9.67m/s

Y/Delta	U(Y)/U _∞	RMSU (ROE/τ) ^{**0.5}	RMSV (ROE/τ) ^{**0.5}	τ(Y)/τ REF
.025	.595	1.936	1.256	.878
.038	.628	2.069	1.251	1.104
.057	.688	2.103	1.196	1.159
.082	.721	1.982	1.196	1.177
.102	.752	1.884	1.153	.979
.143	.789	1.655	1.125	.719
.181	.808	1.808	1.162	.960
.237	.851	1.689	1.141	.839
.333	.883	1.631	1.150	.805
.410	.912	1.521	1.031	.621
.507	.942	1.381	.954	.504
.636	.975	1.162	.781	.355
.775	.990	.866	.508	.171
.924	1.000	.453	.243	.033
1.034	1.000	.292	.090	-.002

Table BI. (concluded) Tabulated data for Flow Case I: 1:2 hill model

e) Position 0.00cm from crest. Free stream velocity 9.68m/s

Y/Delta	U(y)/U _∞	RMSU (ROE/τ) **.5	RMSV (ROE/τ) **.5	τ(y)/τ REF
.005	.723	1.819	1.479	.791
.026	.714	1.980	1.419	1.283
.056	.825	1.997	1.359	1.766
.095	.845	1.882	1.333	1.622
.136	.860	1.763	1.241	1.365
.198	.868	1.634	1.208	1.207
.277	.898	1.547	1.194	1.090
.363	.920	1.500	1.145	1.015
.460	.946	1.388	1.044	.837
.455	.959	1.289	.947	.731
.632	.979	1.108	.828	.554
.712	.993	.911	.737	.415
.783	.999	.696	.614	.269
.909	.999	.405	.391	.108
1.028	1.000	.217	.221	.031

Table BII Tabulated data for Flow Case I: 1:4 hill model

a) Position 22.86cm from crest. Free stream velocity 10.00m/s

Y/Delta	U(y)/U _∞	RMSU(ROE/τ)**.5	RMSV(ROE/τ)**.5	τ(y)/τ REF
.005	.428	1.770	1.166	.979
.010	.484	1.899	1.122	.979
.019	.540	2.003	1.331	.979
.028	.570	2.018	1.358	.978
.039	.610	2.046	1.351	.976
.046	.622	2.049	1.343	.974
.054	.644	2.058	1.357	.972
.062	.640	1.984	1.331	.969
.071	.652	1.972	1.323	.966
.080	.660	1.945	1.323	.962
.096	.676	1.925	1.314	.953
.113	.692	1.879	1.292	.943
.147	.745	1.850	1.276	.916
.181	.777	1.829	1.277	.884
.215	.795	1.771	1.267	.848
.300	.836	1.659	1.215	.735
.395	.865	1.452	1.055	.591
.473	.932	1.353	.959	.465
.558	.955	1.099	.901	.334
.641	.995	.922	.782	.220
.729	1.000	.773	.679	.121
.828	.997	.462	.442	.047
.999	1.000	.214	.100	-.000
1.168	.995	.141	.105	-.000
1.280	.990	.140	.056	-.000

Table BII. (continued) Tabulated data for Flow Case I: 1:4 hill model

b) Position 15.24cm from crest. Free stream velocity 10.05m/s

Y/Delta	U(y)/U _∞	RMSU (ROE/τ)**.5	RMSV (ROE/τ)**.5	τ(y)/τ REF
.007	.537	1.870	1.421	.708
.011	.542	1.901	1.479	.911
.020	.572	2.010	1.503	1.173
.031	.614	2.067	1.477	1.299
.039	.647	2.049	1.458	1.328
.049	.662	2.008	1.438	1.260
.057	.669	2.031	1.440	1.378
.071	.685	1.976	1.402	1.302
.093	.709	1.920	1.378	1.300
.109	.711	1.850	1.335	1.198
.129	.730	1.838	1.333	1.236
.145	.738	1.781	1.302	1.171
.181	.801	1.769	1.260	1.184
.221	.829	1.739	1.268	1.141
.295	.859	1.612	1.206	.973
.385	.927	1.453	1.032	.752
.472	.960	1.352	.941	.596
.561	.965	1.147	.945	.588
.649	1.005	.857	.750	.324
.823	1.000	.521	.480	.086
1.066	1.000	.164	0.000	-.038
1.289	.995	.136	0.000	-.035

Table BII (continued) Tabulated data for Flow Case I: 1:4 hill model

c) Position 0.00cm from crest. Free stream velocity 9.70m/s

Y/Delta	U(y)/U _∞	RMSU(ROE/τ)**.5	RMSV(ROE/τ)**.5	T(y)/T REF
.005	1.072	1.920	.862	.109
.001	1.070	1.765	1.200	.434
.016	1.052	1.778	1.374	.737
.025	1.014	1.821	1.496	1.044
.045	.977	1.762	1.456	1.055
.072	.957	1.737	1.453	1.105
.104	.941	1.671	1.414	1.046
.148	.934	1.599	1.376	.984
.182	.934	1.531	1.316	.834
.221	.934	1.494	1.310	.861
.260	.932	1.458	1.267	.806
.297	.934	1.426	1.239	.775
.370	.938	1.344	1.182	.685
.477	.954	1.241	1.056	.551
.637	.977	1.035	.815	.291
.822	.994	.643	.311	-.078
1.033	1.000	.220	.148	-.272

Table BII (concluded) Tabulated data for Flow Case I: 1:4 hill model

d) Position 7.62cm from crest. Free stream velocity 9.95m/s

Y/Delta	U(y)/U _∞	RMSU (ROE/τ)**.5	RMSV (ROE/τ)**.5	τ(y)/τ REF
.005	.529	1.341	1.289	-.061
.014	.538	1.368	1.368	.114
.021	.553	1.455	1.462	.388
.032	.567	1.509	1.481	.565
.042	.709	1.921	1.567	1.266
.067	.738	1.861	1.497	1.244
.095	.772	1.766	1.460	1.216
.122	.799	1.733	1.421	1.146
.163	.878	1.662	1.366	1.112
.212	.899	1.611	1.333	1.048
.294	.930	1.500	1.229	.875
.421	.953	1.268	.990	.495
.505	.965	1.114	.859	.351
.671	.989	.822	.558	.039
.842	1.000	.333	0.000	-.236
1.001	.993	.129	0.000	-.292

Table BIII Tabulated data for Flow Case I: 1:6 hill model

a) Position 55.88cm from crest. Free stream velocity 9.48m/s

Y/Delta	U(y)/U _∞	RMSU (ROE/τ)**.5	RMSV (ROE/τ)**.5	τ(y)/τ REF
.004	.396	2.395	.916	1.000
.010	.530	2.332	1.150	1.000
.027	.608	2.182	1.138	.998
.043	.655	2.110	1.208	.995
.057	.688	2.143	1.209	.991
.075	.730	1.992	1.183	.984
.100	.760	1.907	1.186	.971
.122	.788	1.835	1.228	.956
.153	.814	1.784	1.252	.930
.196	.825	1.624	1.202	.887
.248	.869	1.569	1.206	.823
.285	.869	1.510	1.205	.773
.333	.899	1.444	1.174	.701
.409	.923	1.366	1.144	.580
.500	.950	1.196	1.000	.436
.599	.975	1.033	.875	.289
.682	.988	.802	.643	.187
.799	.997	.585	.441	.083
.908	.999	.394	.150	.035
1.020	1.000	.123	0.000	.025
1.178	1.000	.075	0.000	.025

Table BIII (continued) Tabulated data for Flow Case I: 1:6 hill model

b) Position 30.48cm from crest. Free stream velocity 9.50m/s

Y/Delta	$U(y)/U_{\infty}$	RMSU (ROE/ τ) ^{**} .5	RMSV (ROE/ τ) ^{**} .5	$\tau(y)/\tau_{REF}$
.004	.321	2.342	.964	.867
.017	.500	2.015	1.121	.866
.026	.556	2.138	1.139	.865
.041	.594	2.097	1.169	.863
.053	.630	2.074	1.135	.861
.065	.653	2.011	1.220	.857
.084	.697	1.957	1.186	.850
.099	.707	1.941	1.218	.843
.134	.748	1.867	1.267	.822
.204	.813	1.751	1.302	.764
.324	.883	1.510	1.225	.622
.432	.931	1.326	1.150	.472
.585	.976	1.052	.894	.264
.740	.999	.671	.537	.102
.948	1.000	.202	0.000	.009
1.149	1.000	.080	0.000	.006

Table BIII (continued) Tabulated data for Flow Case I: 1:6 hill model

c) Position 12.70cm from crest. Free stream velocity 9.59m/s

Y/Delta	U(y)/U _∞	RMSU (ROE/T) **.5	RMSV (ROE/T) **.5	T(y)/T REF
.010	.680	2.052	.915	.080
.018	.711	2.002	1.163	.443
.031	.741	2.040	1.342	.853
.047	.779	2.008	1.343	.972
.063	.788	1.950	1.359	.961
.082	.806	1.885	1.394	1.008
.111	.842	1.765	1.371	.939
.147	.867	1.728	1.378	.976
.176	.875	1.638	1.376	.943
.233	.900	1.530	1.313	.857
.318	.923	1.444	1.279	.828
.405	.962	1.235	1.097	.570
.566	.996	.980	.852	.283
.709	1.000	.650	.583	.068
.872	1.000	.253	0.000	-.134
1.022	1.000	.140	0.000	-.136
1.159	1.000	.081	0.000	-.143

Table BIII (continued) Tabulated data for Flow Case I: 1:6 hill model

d) Position 22.86cm from crest. Free stream velocity 9.58m/s

Y/DELTA	U(y)/U _∞	RMSU (ROE/τ)**.5	RMSV (ROE/ν)**.5	τ(y)/τ REF
.005	.589	1.975	1.263	-.186
.013	.602	2.075	1.440	.377
.020	.637	2.146	1.454	.664
.031	.670	2.085	1.441	.749
.045	.681	2.018	1.369	.803
.059	.702	1.948	1.348	.857
.097	.752	1.902	1.347	1.042
.133	.789	1.738	1.268	.973
.164	.825	1.726	1.260	1.024
.259	.876	1.619	1.217	1.022
.342	.909	1.442	1.085	.829
.421	.933	1.254	.974	.651
.527	.966	1.146	.887	.541
.675	.991	.756	.541	.169
.845	.999	.358	0.000	-.053
.991	.997	.144	0.000	-.106
1.144	1.000	.080	0.000	-.115

Table BIII (continued) Tabulated data for Flow Case I: 1:6 hill model.

e) Position 0.00cm from crest. Free stream velocity 9.68m/s

Y/Delta	U(y)/U _∞	RMSU(ROE/T)**.5	RMSV(ROE/T)**.5	τ(y)/τ REF
.006	1.021	2.590	.916	.558
.014	.943	2.318	1.018	.514
.023	.986	2.076	1.262	.712
.033	.964	1.901	1.349	.747
.046	.949	2.063	1.507	1.190
.058	.949	2.021	1.479	1.168
.067	.927	1.903	1.453	1.054
.095	.934	1.826	1.458	1.033
.114	.942	1.787	1.453	1.035
.134	.919	1.715	1.392	1.051
.173	.912	1.611	1.398	.959
.236	.919	1.524	1.351	.891
.337	.934	1.396	1.253	.747
.440	.964	1.144	1.002	.449
.645	.964	.880	.782	.254
.772	.986	.626	.521	.027
.938	.996	.345	0.000	-.105
1.153	1.000	.198	0.000	-.113
1.405	1.000	.144	0.000	-.110

Table BIII (concluded) Tabulated data for Flow Case I: 1:6 hill model

f) Position 5.08cm from crest. Free stream velocity 9.66m/s

Y/Delta	U(y)/U _∞	RMSU (ROE/τ)**.5	RMSV (ROE/τ)**.5	τ(y)/τ REF
.009	.801	2.030	.981	.232
.017	.827	2.027	1.218	.651
.023	.844	2.020	1.320	.824
.039	.861	2.024	1.399	1.082
.057	.885	2.029	1.476	1.312
.073	.893	1.969	1.467	1.293
.105	.901	1.876	1.437	1.232
.145	.909	1.717	1.504	1.121
.179	.917	1.637	1.375	1.026
.206	.924	1.633	1.376	1.099
.298	.947	1.501	1.257	.869
.380	.967	1.388	1.173	.742
.458	.977	1.254	1.059	.594
.538	.990	1.106	.929	.422
.708	1.000	.741	.571	.101
.883	1.000	.296	0.000	-.136
1.006	1.000	.136	0.000	-.162
1.154	1.000	.101	0.000	-1.276

Table BIV Tabulated data for Flow Case II: 1:2 hill model.

a) Position 50.80cm from crest. Free stream velocity 9.48m/s

Y/Delta	U(y)/U _∞	RMSU(ROE/τ)**.5	τ(y)/τ REF
.001	.351	2.435	.956
.003	.438	2.334	.956
.006	.485	2.365	.956
.008	.512	2.390	.956
.012	.540	2.447	.956
.016	.566	2.511	.955
.028	.614	2.607	.954
.062	.671	2.460	.948
.128	.718	2.376	.918
.192	.748	2.203	.871
.257	.776	2.200	.808
.354	.822	2.118	.691
.453	.877	1.968	.552
.582	.934	1.597	.361
.776	.989	.761	.117
.983	1.000	.269	.000

b) Position 30.48cm from crest. Free stream velocity 9.74m/s

Y/Delta	U(y)/U _∞	RMSU(ROE/τ)**.5	τ(y)/τ REF
.001	.294	2.297	.850
.003	.390	2.518	.850
.005	.429	2.497	.850
.008	.432	2.409	.850
.019	.490	2.578	.849
.036	.540	2.641	.847
.064	.612	2.664	.842
.093	.645	2.555	.832
.124	.655	2.413	.818
.188	.707	2.327	.777
.250	.737	2.234	.722
.345	.778	2.120	.616
.457	.837	2.004	.469
.563	.885	1.787	.320
.752	.957	.963	.085
.953	1.000	.340	0.000

Table BIV (continued) Tabulated data for Flow Case II: 1:2 hill model

c) Position 15.24cm from crest. Free stream velocity 9.69m/s.

Y/Delta	$U(y)/U_{\infty}$	$RMSU(ROE/\tau)^{*.5}$	$\tau(y)/\tau_{REF}$
.001	.193	2.044	.702
.003	.277	2.561	.702
.005	.296	2.622	.702
.007	.313	2.590	.702
.012	.340	2.646	.702
.028	.418	2.862	.701
.059	.497	2.730	.698
.089	.538	2.602	.692
.119	.597	2.419	.683
.181	.657	2.332	.656
.270	.739	2.250	.597
.364	.799	2.131	.515
.486	.872	1.948	.388
.646	.939	1.485	.214
.777	.934	.671	.091
.927	1.000	.268	.009

d) Position 10.16cm from crest. Free stream velocity 9.71m/s.

Y/Delta	$U(y)/U_{\infty}$	$RMSU(ROE/\tau)^{*.5}$	$\tau(y)/\tau_{REF}$
.001	.050	.548	.607
.003	.105	1.343	.607
.005	.136	1.673	.607
.007	.168	1.953	.607
.012	.213	2.254	.607
.022	.284	2.500	.606
.055	.466	2.814	.604
.085	.532	2.022	.600
.117	.592	2.293	.593
.187	.677	2.124	.569
.266	.730	1.382	.526
.358	.820	.546	.459
.480	.878	1.720	.352
.625	.947	1.395	.216
.761	.985	.788	.102
.918	1.000	.286	.023

Table BIV (continued) Tabulated data for Flow Case II: 1:2 hill model.

e) Position 7.62 cm from crest. Free stream velocity 9.70m/s.

Y/ZDELTA	U(y)/U _∞	RMSU (ROE/τ) **.5
.001	.824	3.607
.003	.277	1.709
.005	.298	1.772
.007	.308	1.918
.014	.360	2.124
.034	.428	2.462
.064	.520	2.552
.094	.589	2.386
.155	.671	2.212
.218	.734	2.118
.307	.790	2.063
.398	.844	2.000
.520	.905	1.759
.703	.976	.976
.897	1.000	.295

f) Position 2.54cm from crest. Free stream velocity 9.70m/s.

Y/ZDELTA	U(y)/U _∞	RMSU (ROE/τ) **.5
.001	.440	2.032
.003	.482	1.809
.005	.492	1.724
.012	.507	1.760
.020	.542	1.915
.033	.576	2.117
.060	.650	2.204
.092	.690	2.211
.154	.734	2.158
.217	.780	2.077
.314	.831	2.052
.415	.873	1.994
.504	.913	1.783
.695	.963	1.096
.900	.999	.036

Table BIV (concluded) Tabulated data for Flow Case II: 1:2 hill model

g) Position 0.00cm from crest. Free stream velocity 9.71m/s

Y/DELTA	U(y)/U _∞	RMSU(ROE/T)**.5
.001	.602	2.011
.003	.635	1.748
.006	.640	1.670
.008	.643	1.750
.021	.681	2.006
.046	.691	2.145
.087	.729	2.161
.130	.753	2.094
.164	.772	2.073
.228	.802	2.047
.294	.836	2.039
.390	.876	1.946
.489	.912	1.792
.653	.966	1.222
.748	.985	.815
.892	1.000	.327

Table BV. Tabulated data for Flow Case 11: 1:6 hill model

a) Position 50.80cm from crest. Free stream velocity 9.57m/s.

Y/DELTA	u(y)/u _∞	RMSU (ROE/T)**.5	(y)/T REF
.001	.340	2.350	1.000
.003	.452	2.367	1.000
.005	.483	2.410	1.000
.008	.501	2.366	1.000
.014	.545	2.449	1.000
.024	.579	2.518	.999
.036	.620	2.521	.997
.061	.648	2.440	.992
.093	.690	2.332	.980
.123	.787	2.404	.964
.185	.763	2.201	.918
.248	.790	2.168	.855
.341	.845	2.080	.737
.434	.889	1.964	.601
.558	.929	1.713	.405
.705	.975	1.168	.191
.821	.987	.452	.059
.946	1.000	.221	0.000

b) Position 35.56cm from crest. Free stream velocity 9.40m/s

Y/DELTA	U(y)/U _∞	RMSU (ROE/T)**.5	T (y) / T REF
.001	.304	2.294	.925
.003	.411	2.443	.925
.005	.450	2.442	.925
.007	.472	2.450	.925
.012	.501	2.472	.925
.028	.591	2.604	.924
.059	.649	2.538	.918
.100	.696	2.403	.905
.140	.728	2.282	.884
.184	.760	2.195	.854
.244	.794	2.143	.803
.304	.832	2.076	.739
.394	.871	2.031	.627
.486	.918	1.841	.501
.608	.960	1.286	.331
.731	.987	.880	.177
.921	1.000	.314	.032

Table BV (continued) Tabulated data for Flow Case II: 1:6 hill model

c) Position 20.32cm from crest. Free stream velocity 10.21m/s.

Y/DELTA	U(y)/U _∞	RMSU(ROE/T)**.5
.001	.356	2.432
.003	.456	2.497
.005	.494	2.341
.008	.503	2.346
.014	.523	2.489
.027	.559	2.626
.052	.608	2.637
.088	.655	2.594
.157	.698	2.464
.220	.761	2.421
.284	.797	2.356
.376	.884	2.308
.473	.927	2.087
.594	.972	1.665
.720	.992	1.110
.919	1.000	.266

d) Position 12.70cm from crest. Free stream velocity 10.78m/s

Y/DELTA	U(y)/U _∞	RMSU(ROE/T)**.5
.001	.407	2.589
.003	.520	2.542
.005	.549	2.307
.008	.570	2.225
.013	.591	2.214
.026	.633	2.394
.052	.677	2.414
.080	.708	2.368
.116	.748	2.327
.181	.811	2.315
.235	.832	2.269
.332	.881	2.202
.460	.923	1.955
.639	.979	1.344
.758	.995	.912
.919	1.000	.350

Table BV (concluded) Tabulated data for Flow Case II: 1:6 hill model

e) Position 7.62cm from crest. Free stream velocity 9.54m/s.

Y/DELTA	U(y)/U _∞	RMSU(ROE/τ)**.5
.001	.500	2.568
.003	.613	2.428
.006	.643	2.196
.008	.650	2.091
.015	.685	2.176
.027	.696	2.270
.063	.741	2.287
.127	.793	2.209
.209	.826	2.138
.289	.859	2.146
.387	.892	2.037
.517	.938	1.791
.645	.994	1.306
.777	1.000	.751
.919	1.000	.320

f) Position 0.00cm from crest. Free stream velocity 9.26m/s.

Y/DELTA	U(y)/U _∞	RMSU(ROE/τ)**.5
.001	.767	2.462
.003	.860	2.264
.006	.883	2.036
.008	.880	2.040
.014	.872	2.003
.021	.877	2.109
.033	.886	2.195
.067	.874	2.168
.107	.860	2.107
.174	.860	2.062
.275	.870	2.032
.375	.889	1.911
.524	.951	1.572
.654	.980	1.246
.781	.995	.822
.917	1.000	.402

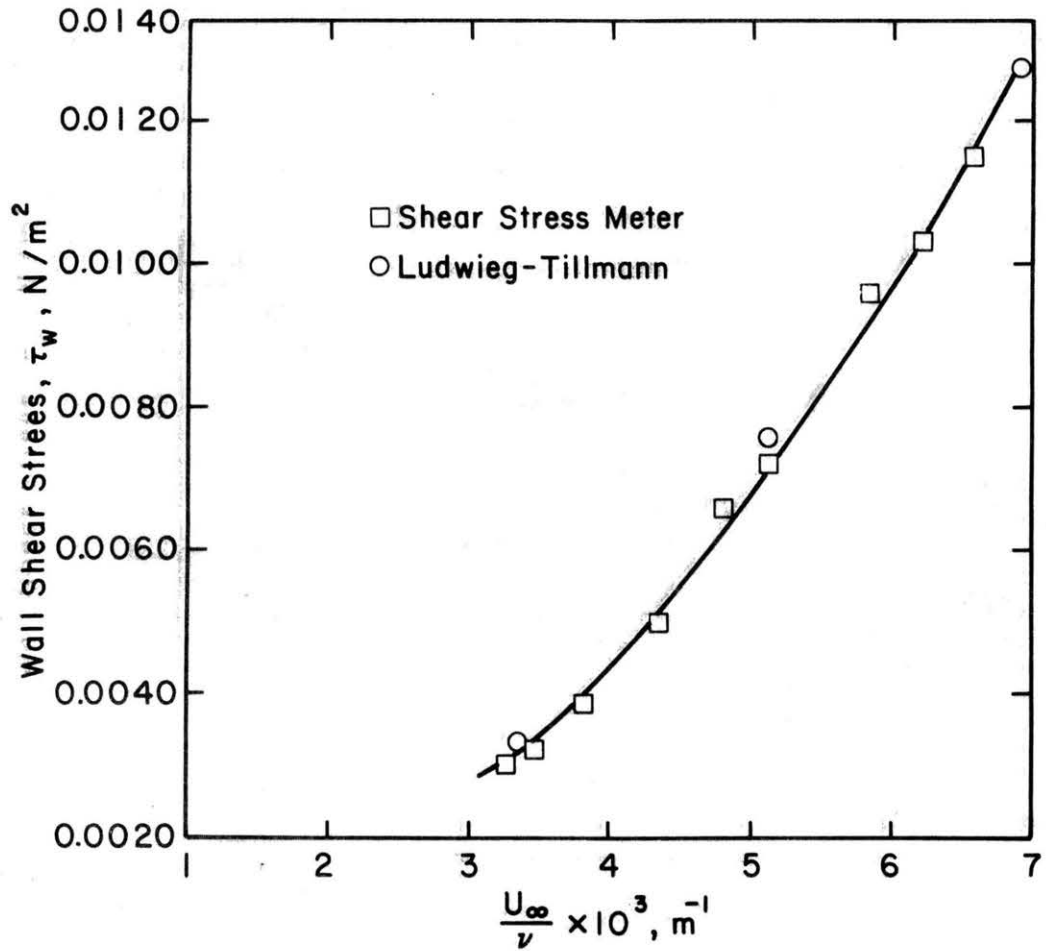


Figure B1 Comparison of Ludwig-Tillmann equation and shear-stress meter (4)

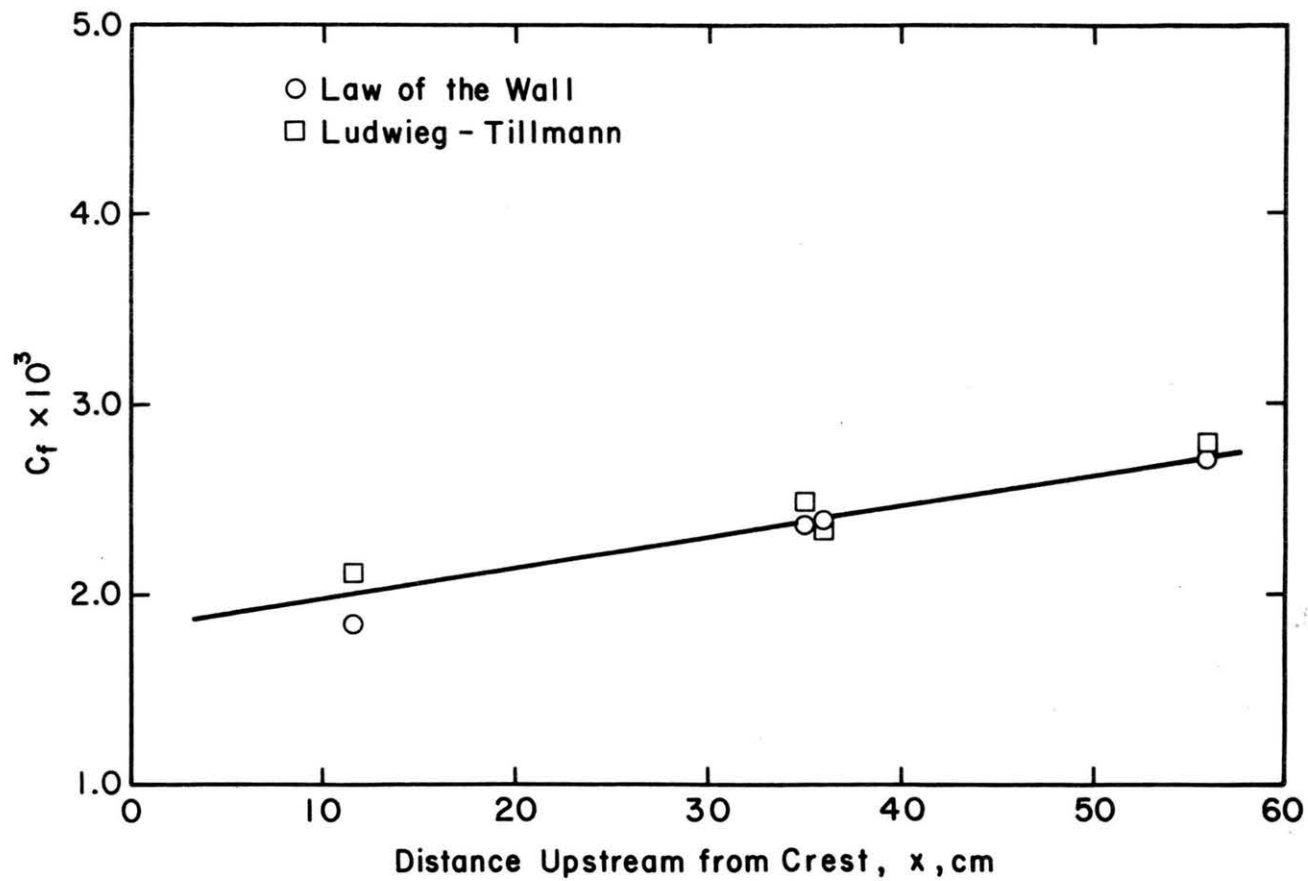


Figure B2 Comparison of shear stress evaluated by Ludwig-Tillmann equation and "law of the wall" on flat plate

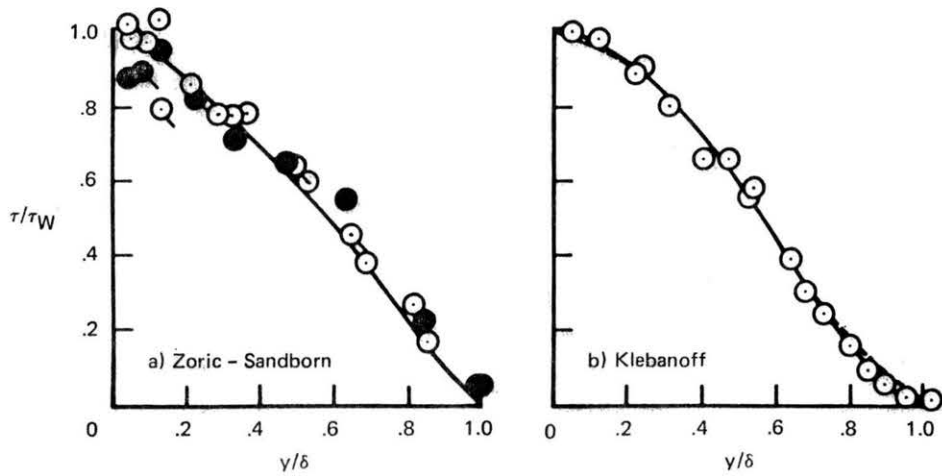


Figure B3 Comparison of shear-stress distribution, for zero pressure gradient flow, with values determined from equation (A-15) (7)

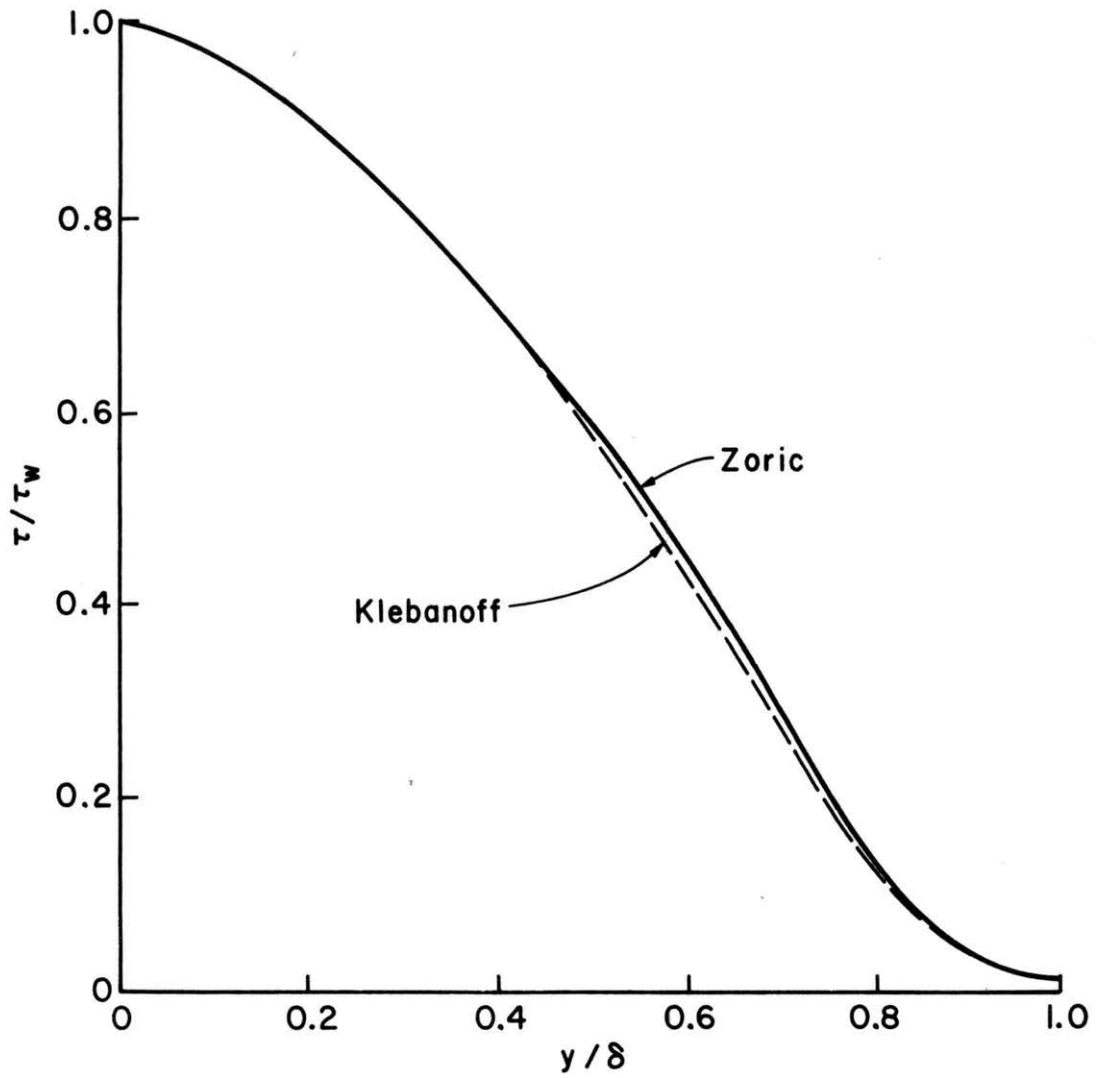


Figure B4 Comparison of shear stress measurements by Klebanoff and Zoric (10)

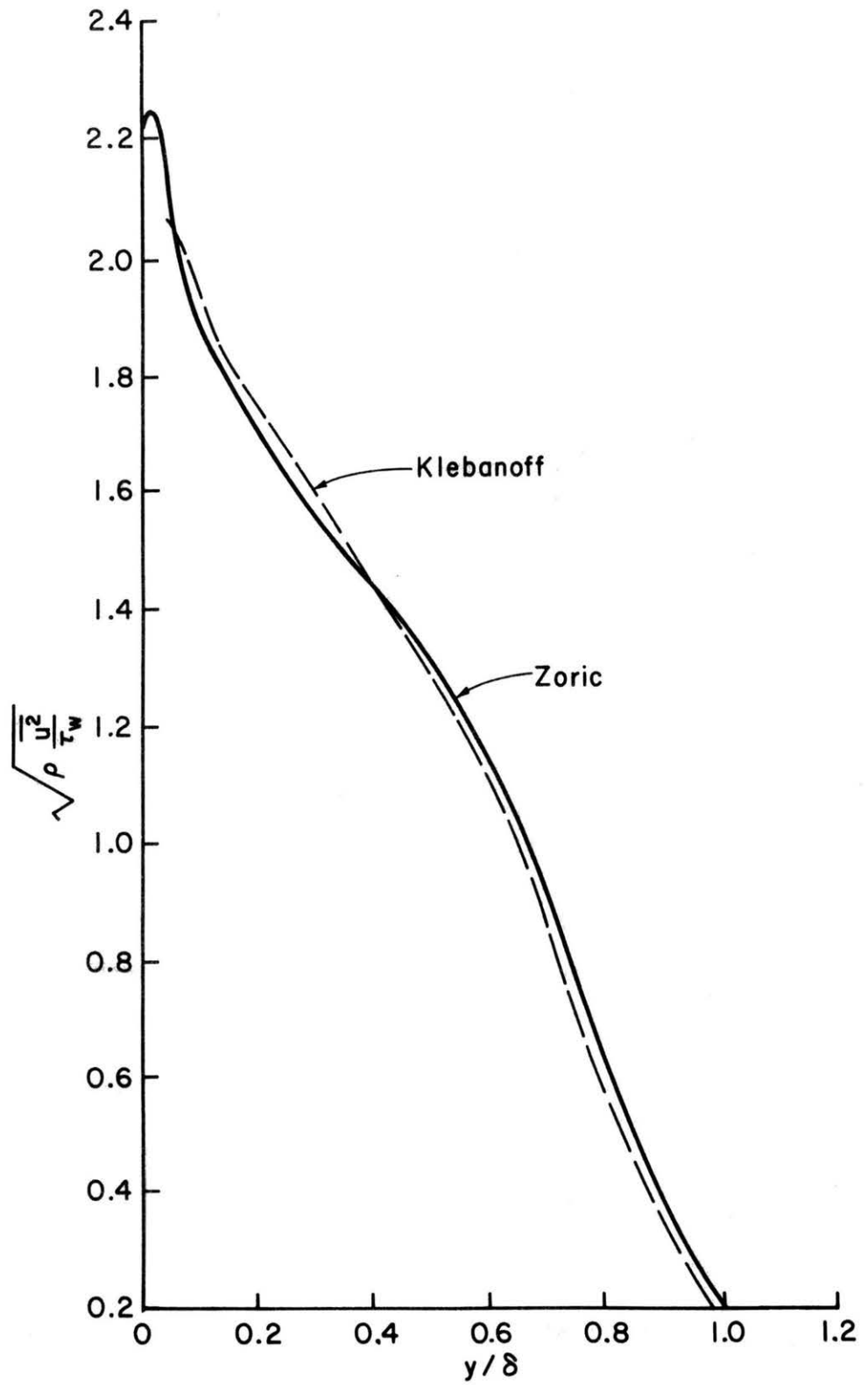


Figure B5 Comparison of flat plate longitudinal turbulent velocity distribution of Klebanoff and Zoric (10)

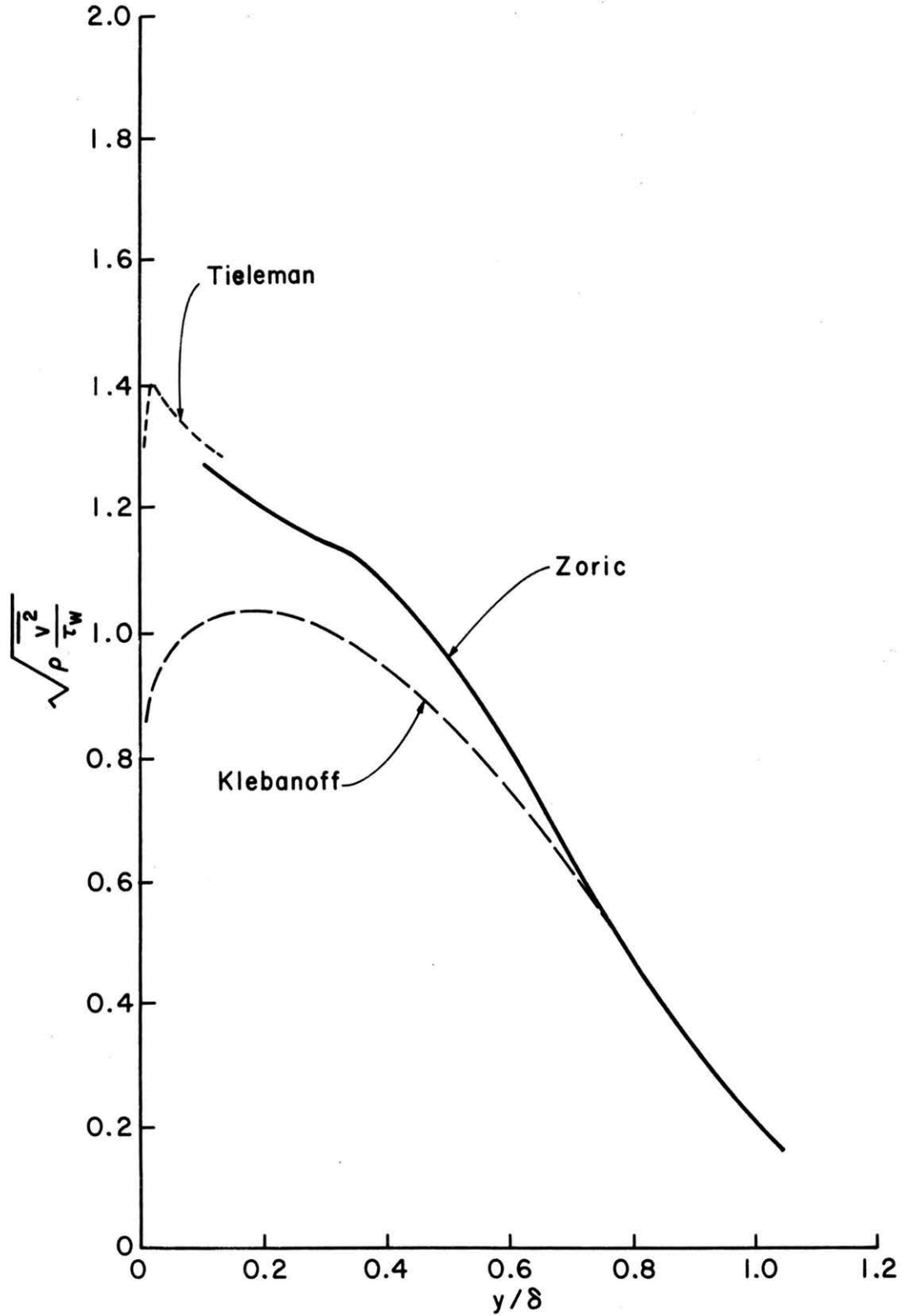


Figure B6 Comparison of flat plate vertical turbulent velocity distribution of Klebanoff, Zoric and Tieleman (10)

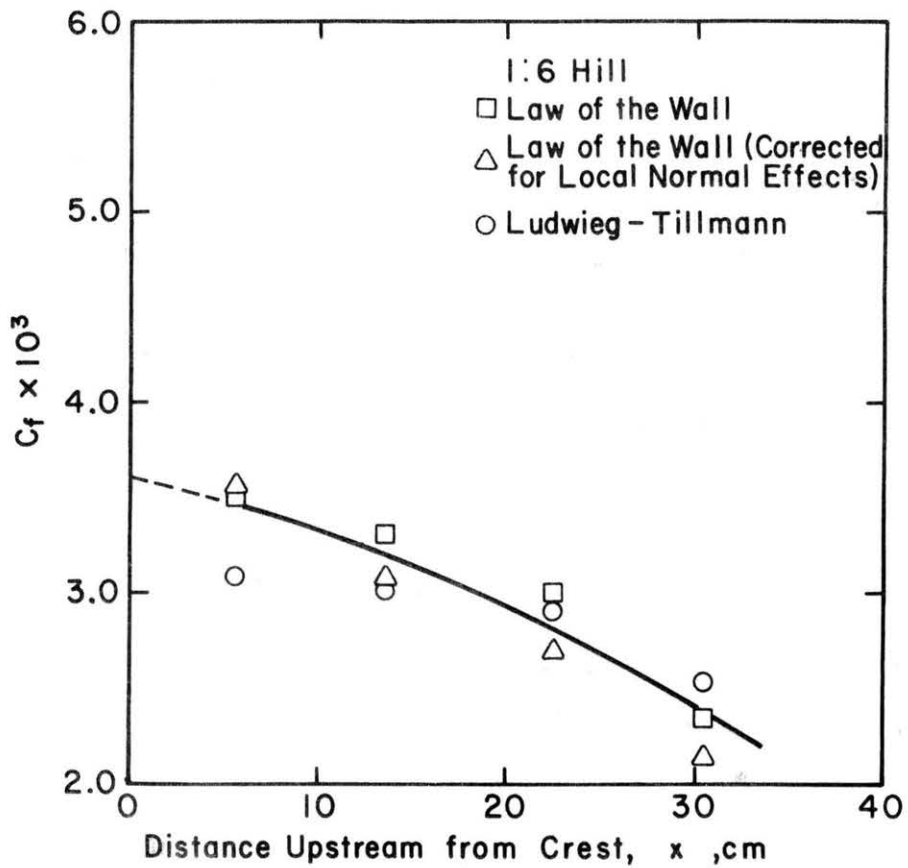
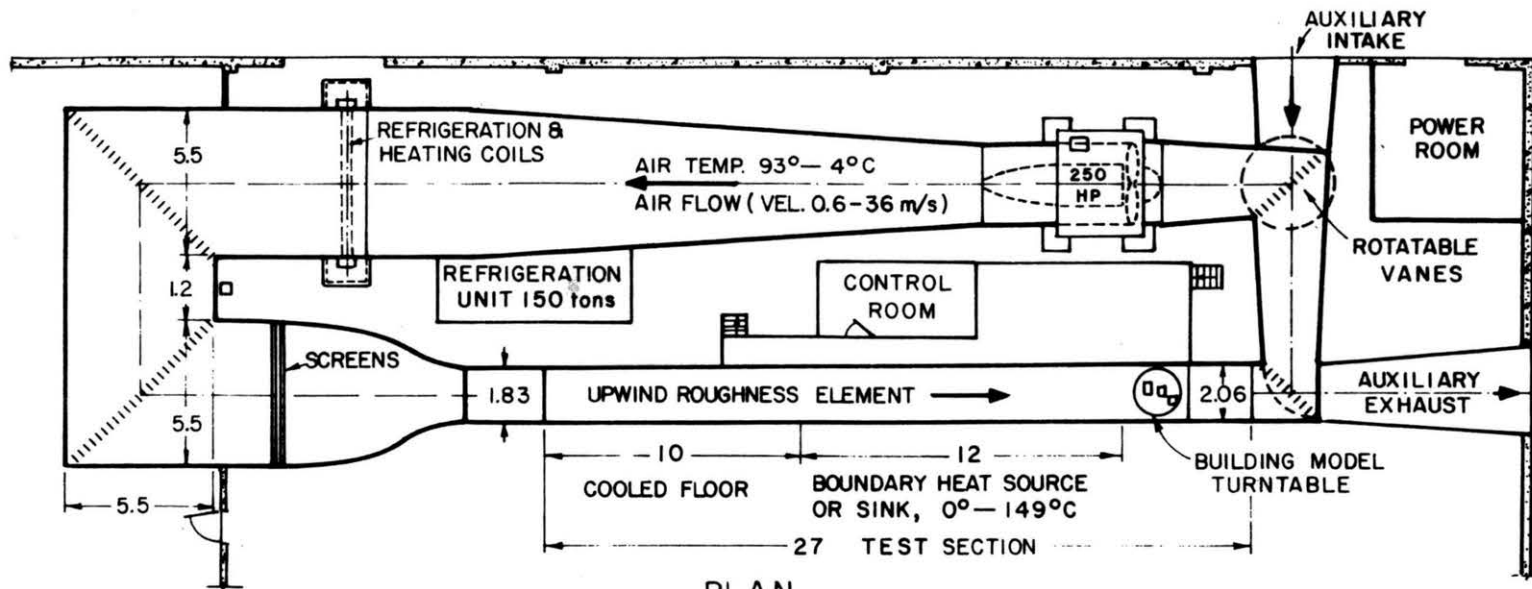
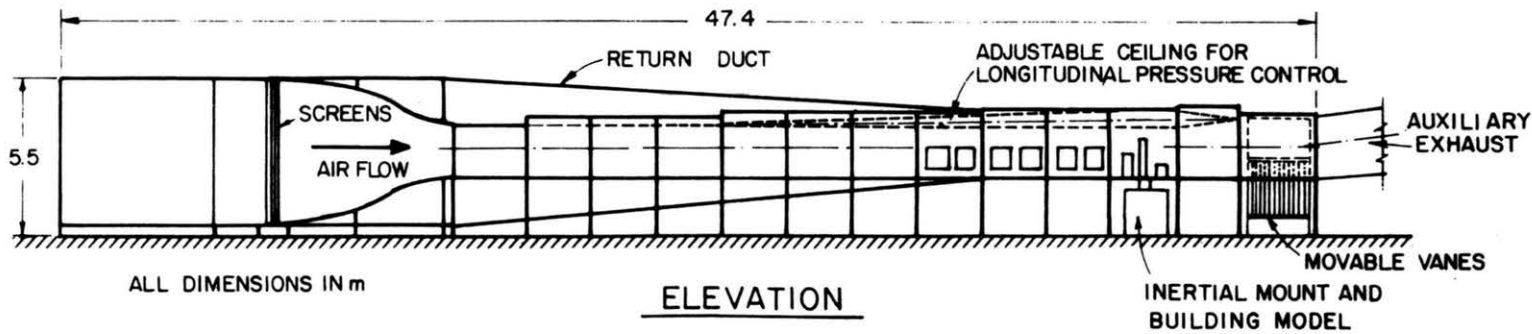


Figure B7 Shear stress evaluated by the "law of the wall" for standard coordinates and curvilinear coordinates



PLAN



ELEVATION

Figure B8 METEOROLOGICAL WIND TUNNEL

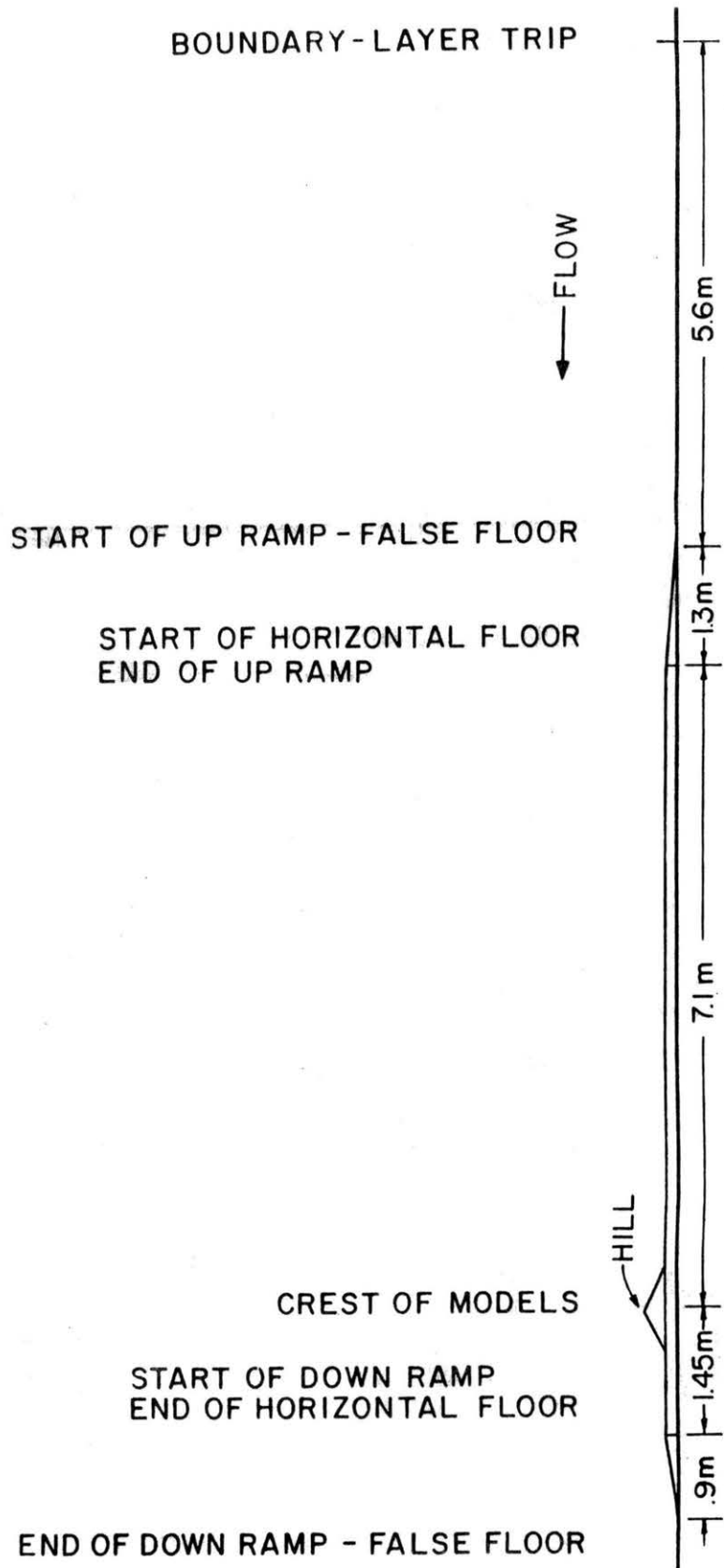


Figure B9 Tunnel setup for Flow Case I

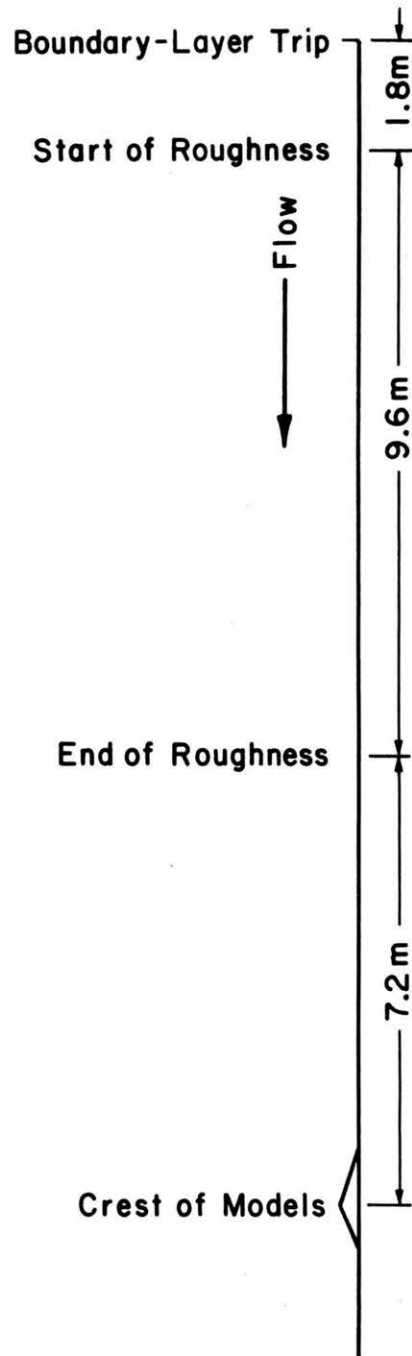


Figure B10 Tunnel setup for Flow Case II

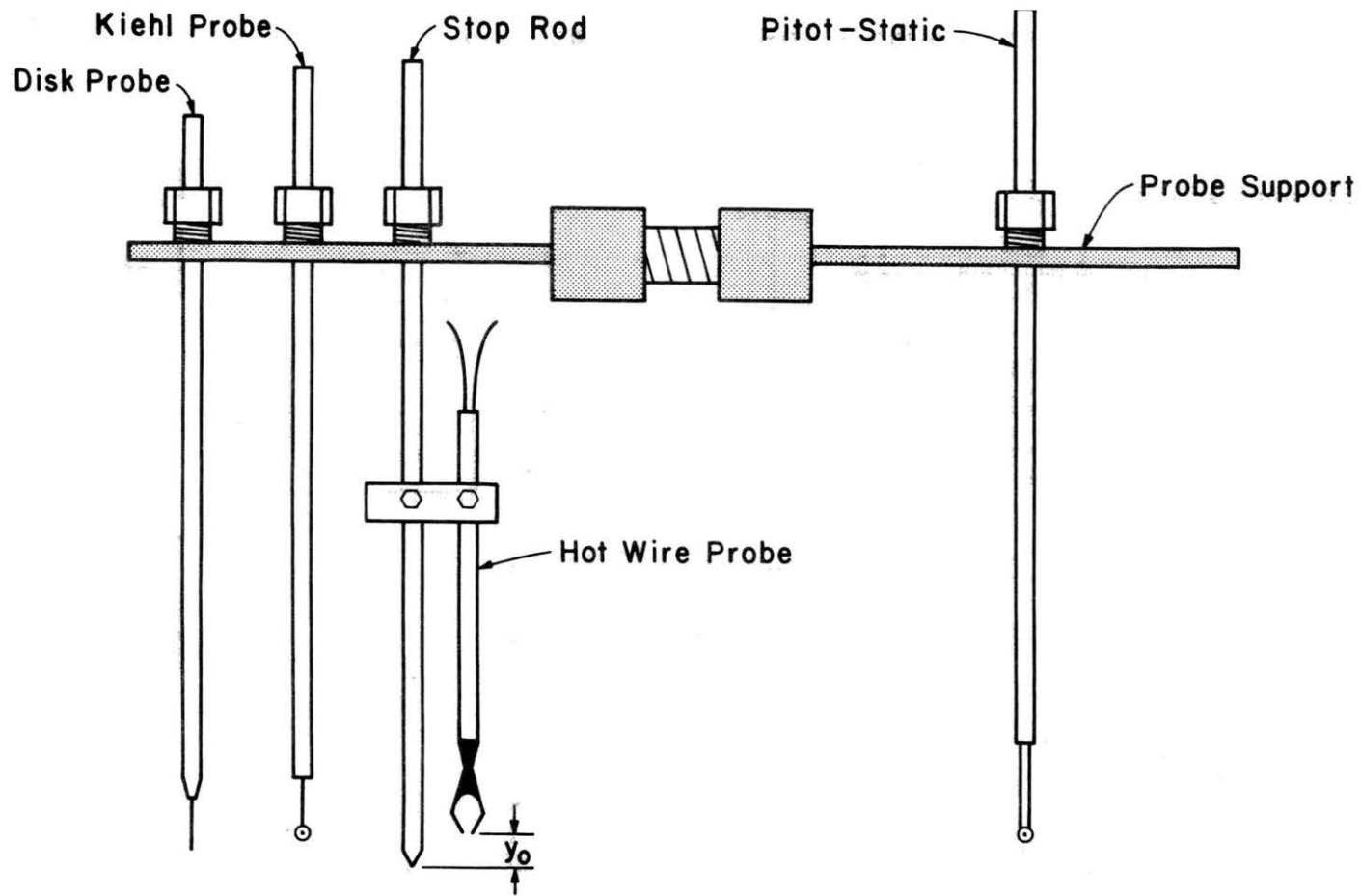

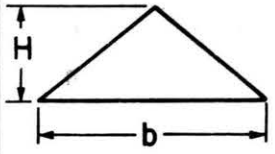


Figure B11 Schematic of probes.

Hill Shape	Height-Length Ratio	Location of Static Pressure Taps along Surface of Hill 
	H= 5.08 1 : 2 b=20.32	<div style="display: flex; justify-content: space-between; width: 100%;"> <div style="width: 45%; text-align: right;"> 1.91 2.54 1.27 1.27 1.27 1.27 </div> <div style="width: 10%; text-align: center;"> ● </div> <div style="width: 45%; text-align: left;"> 0.64 0.64 0.64 0.64 1.27 1.27 1.27 1.27 </div> </div>
	H= 5.08 1 : 4 b=40.04	<div style="display: flex; justify-content: space-between; width: 100%;"> <div style="width: 45%; text-align: right;"> 2.54 2.54 2.54 2.54 2.54 1.27 1.27 </div> <div style="width: 10%; text-align: center;"> ● </div> <div style="width: 45%; text-align: left;"> 1.27 1.27 1.27 1.27 2.54 2.54 2.54 2.54 </div> </div>
	H= 5.08 1 : 6 b=60.96	<div style="display: flex; justify-content: space-between; width: 100%;"> <div style="width: 45%; text-align: right;"> 5.08 5.08 5.08 2.54 2.54 </div> <div style="width: 10%; text-align: center;"> ● </div> <div style="width: 45%; text-align: left;"> 1.27 1.27 2.54 2.54 2.54 2.54 2.54 2.54 2.54 </div> </div>

Crest

Figure B12 Model description and instrumentation location, dimension listed in cm

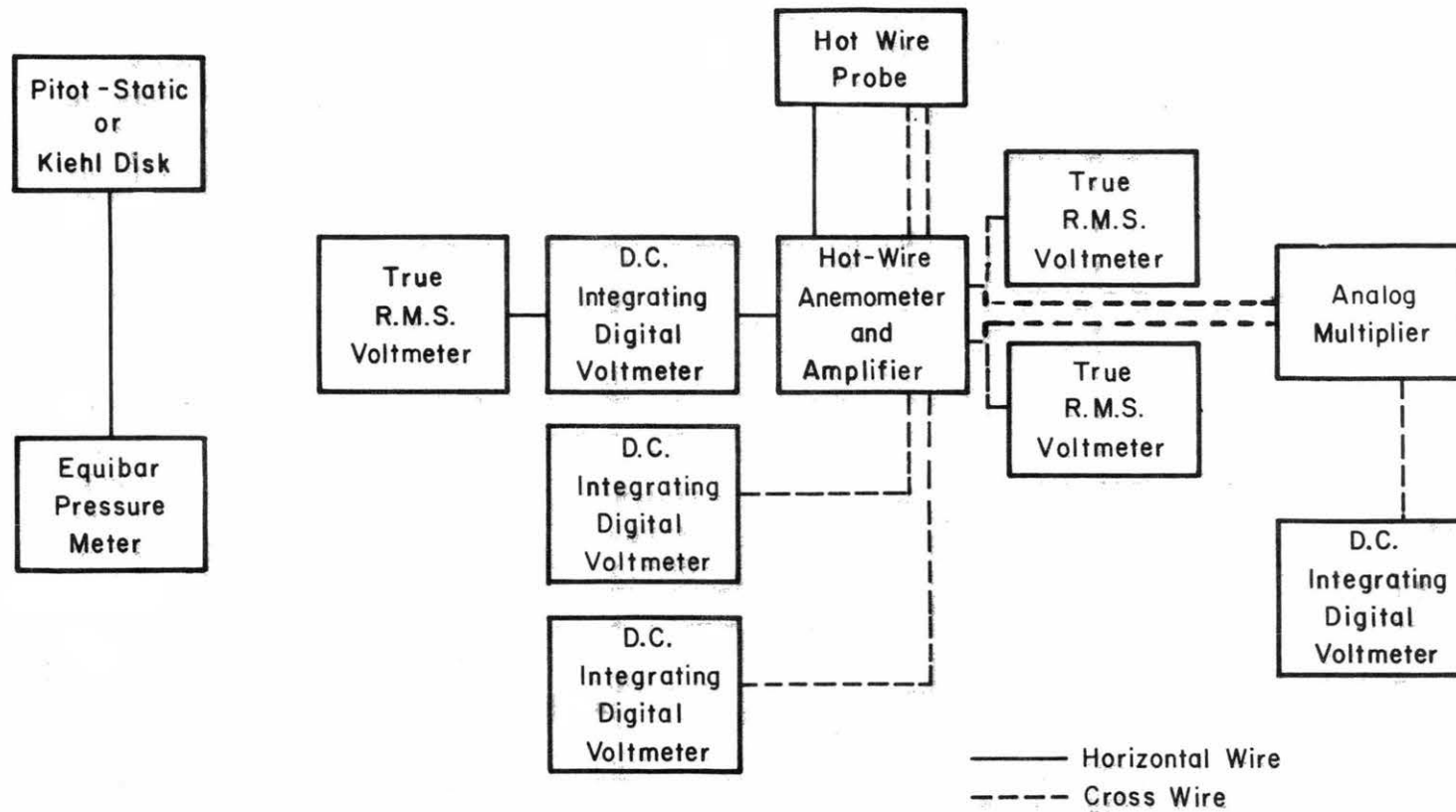


Figure B13 Schematic of equipment setup

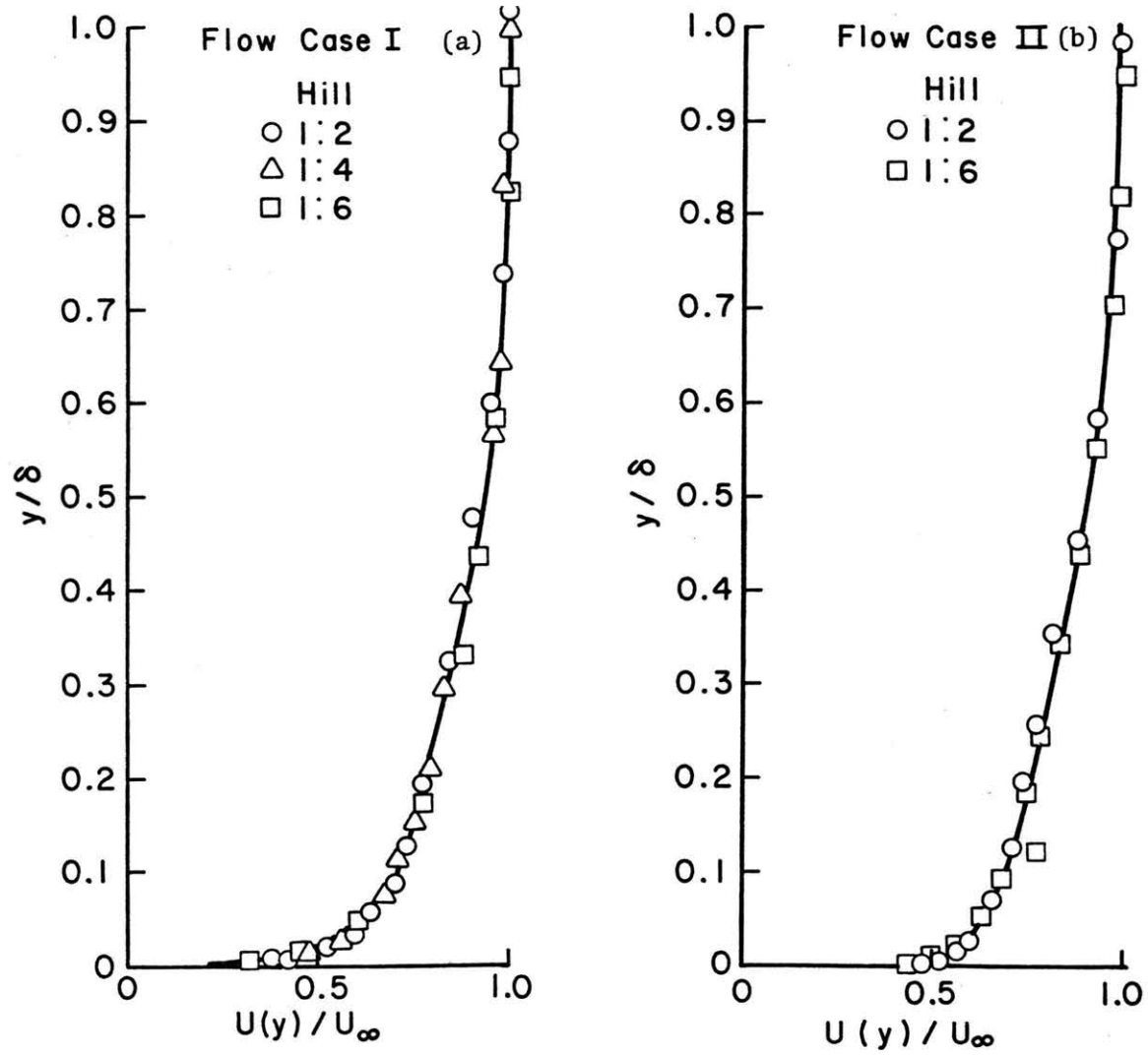
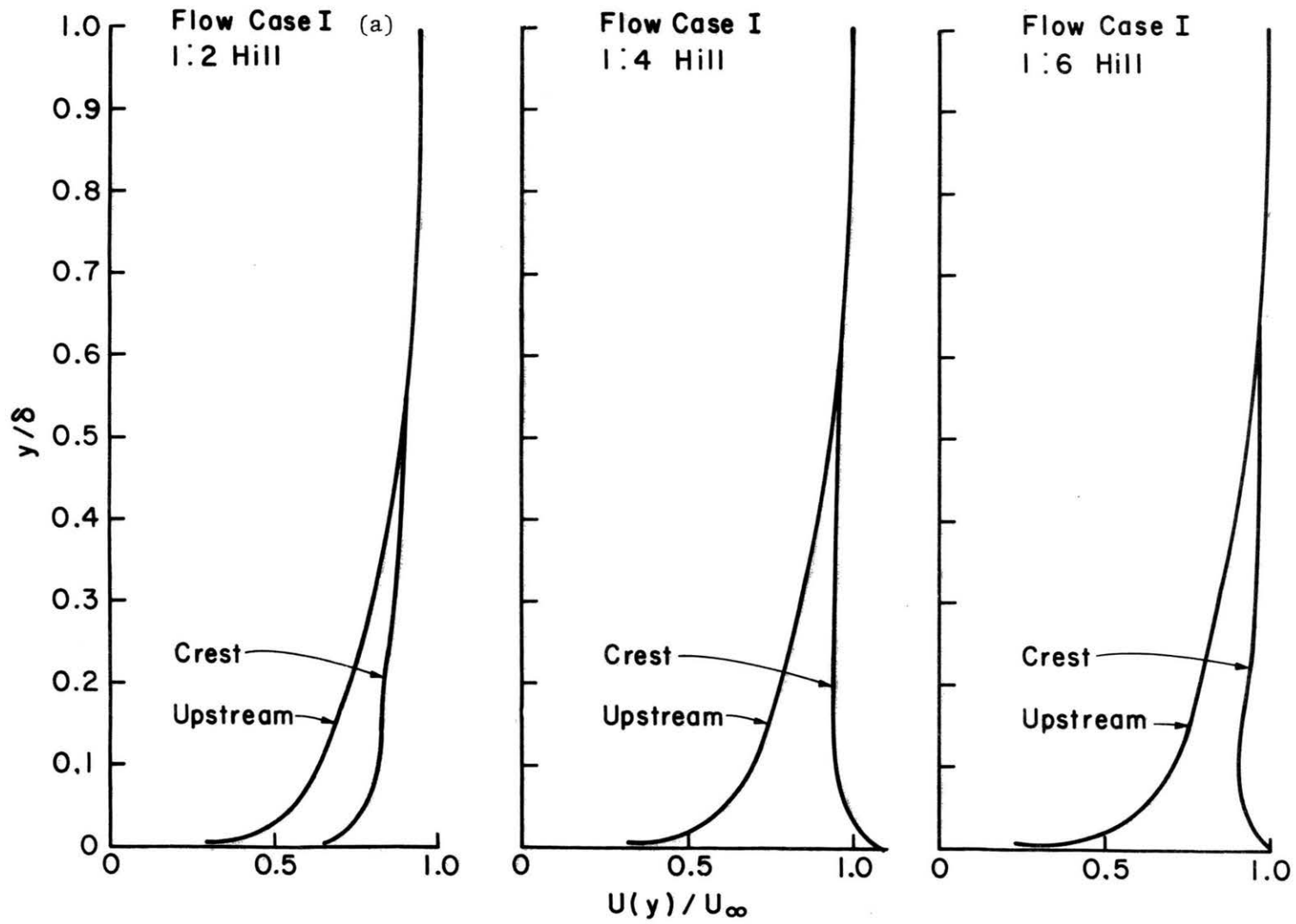
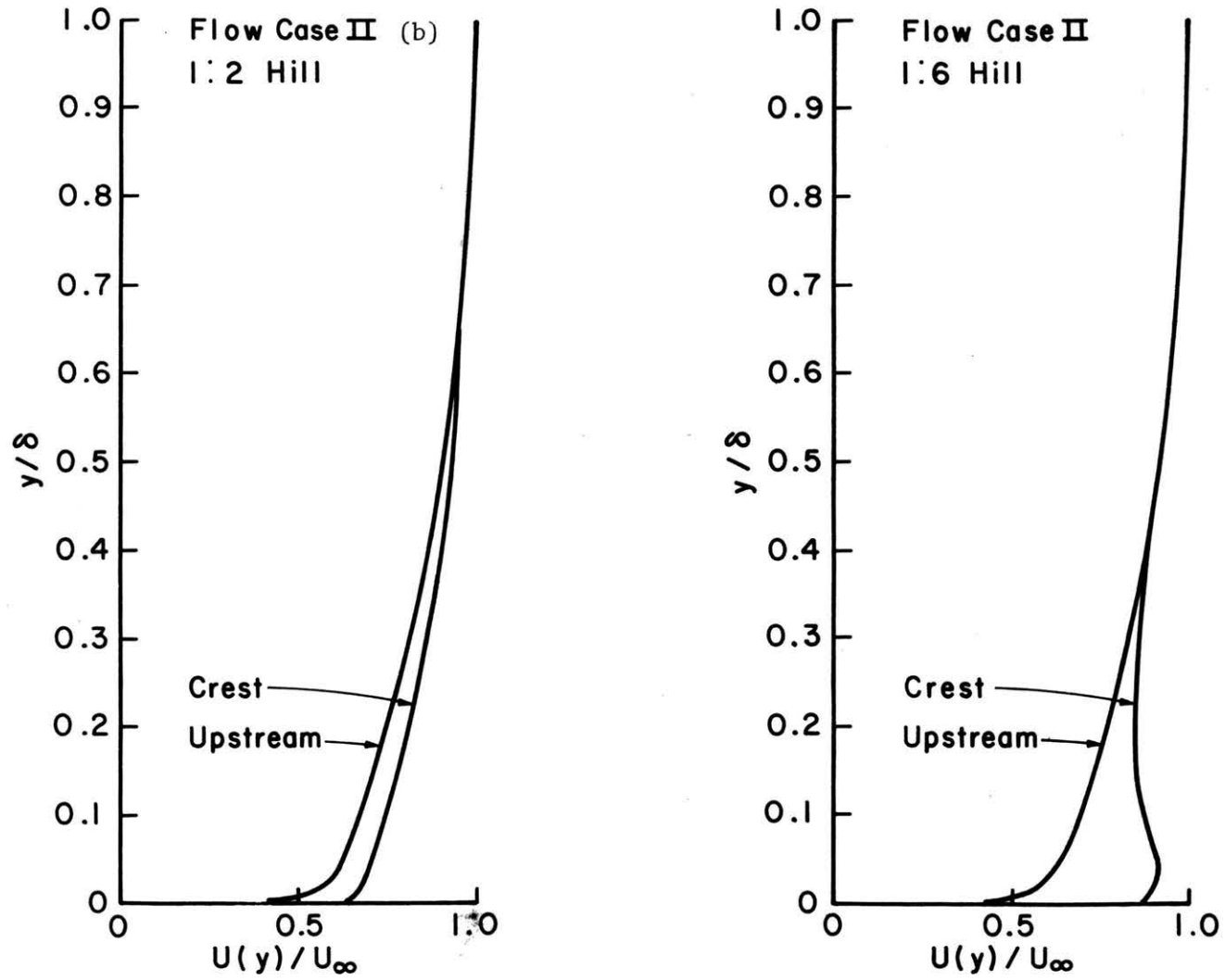


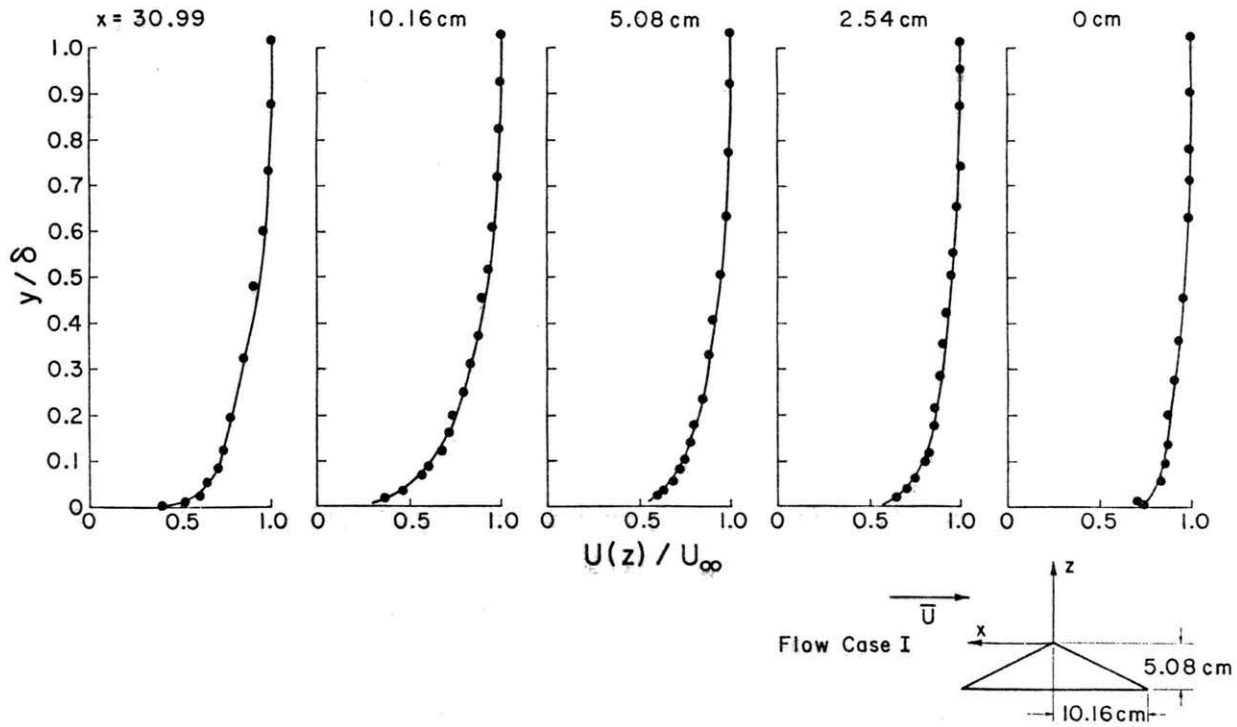
Figure B14 Velocity similarity profiles for both flow cases



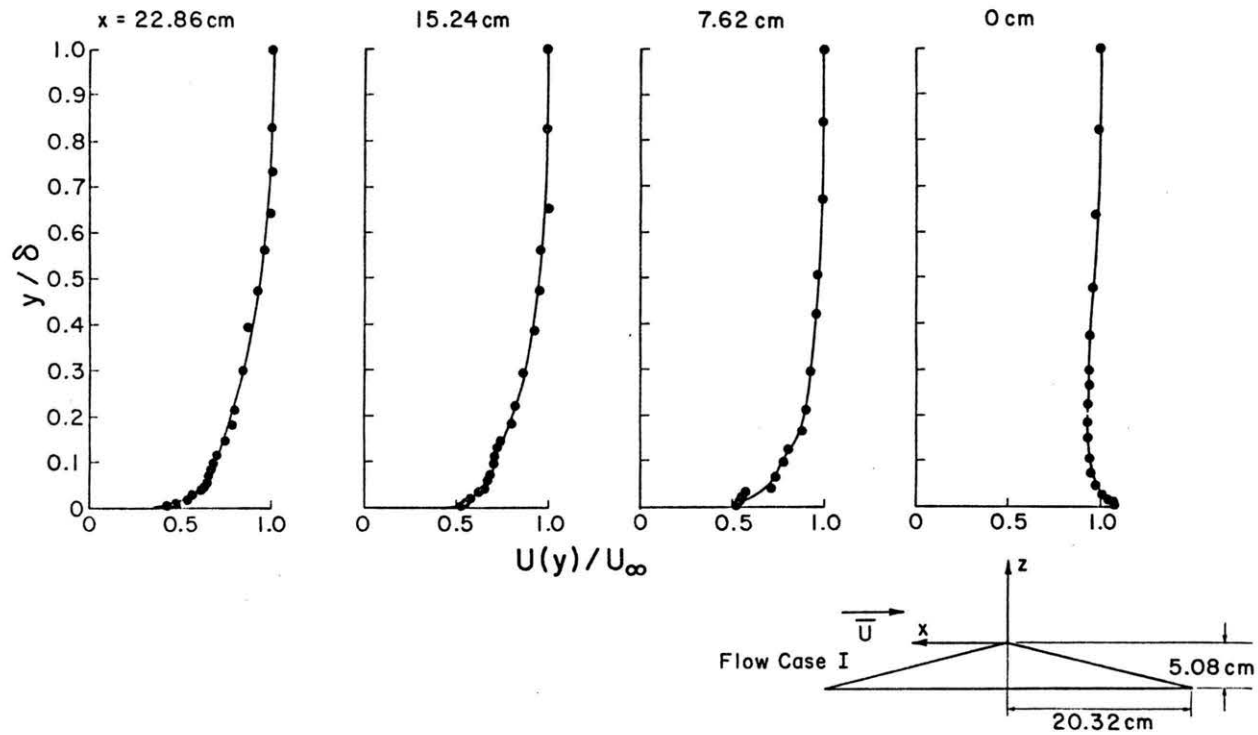
a) Flow Case I.
 Figure B15 Upstream similarity velocity profiles and velocity profiles at the crest.



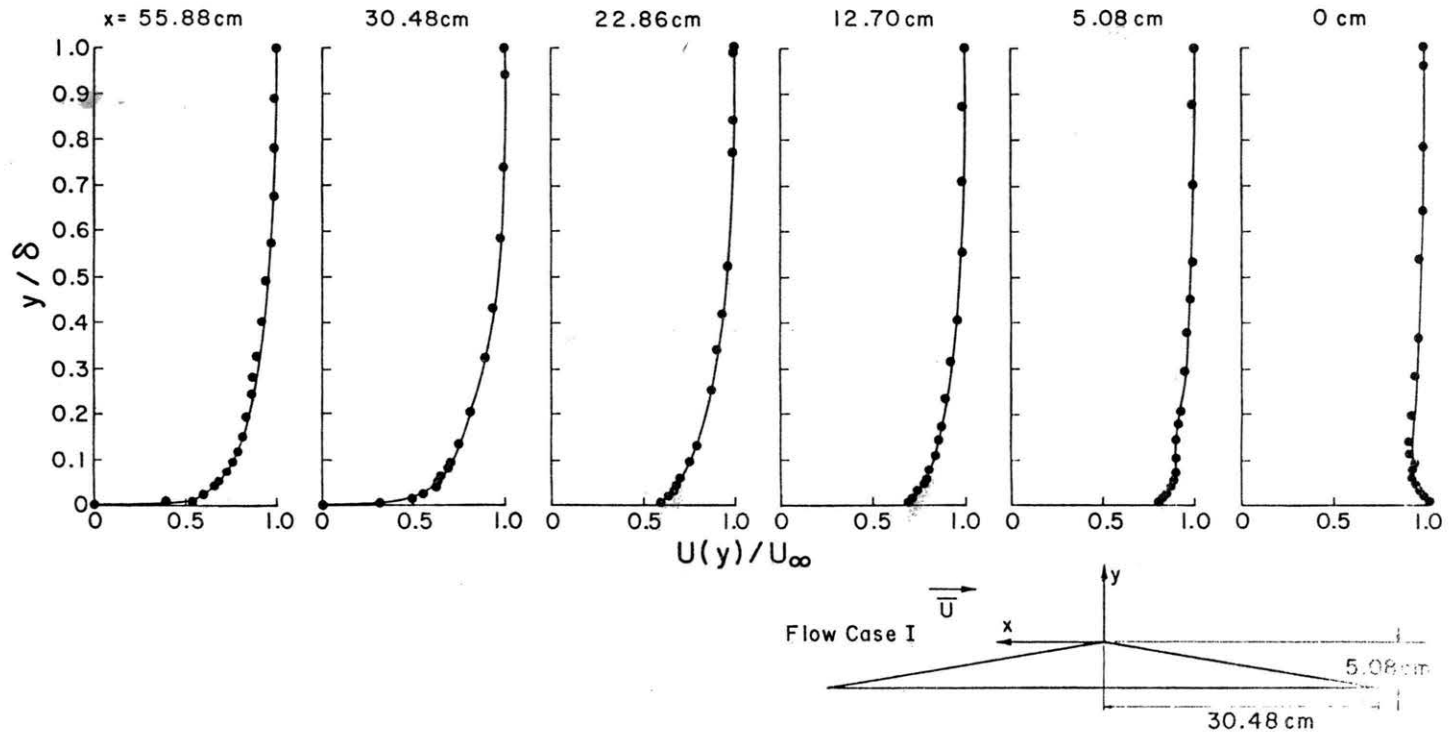
b) Flow Case II
 Figure B15 (concluded) Upstream similarity velocity profiles and velocity profiles at the crest



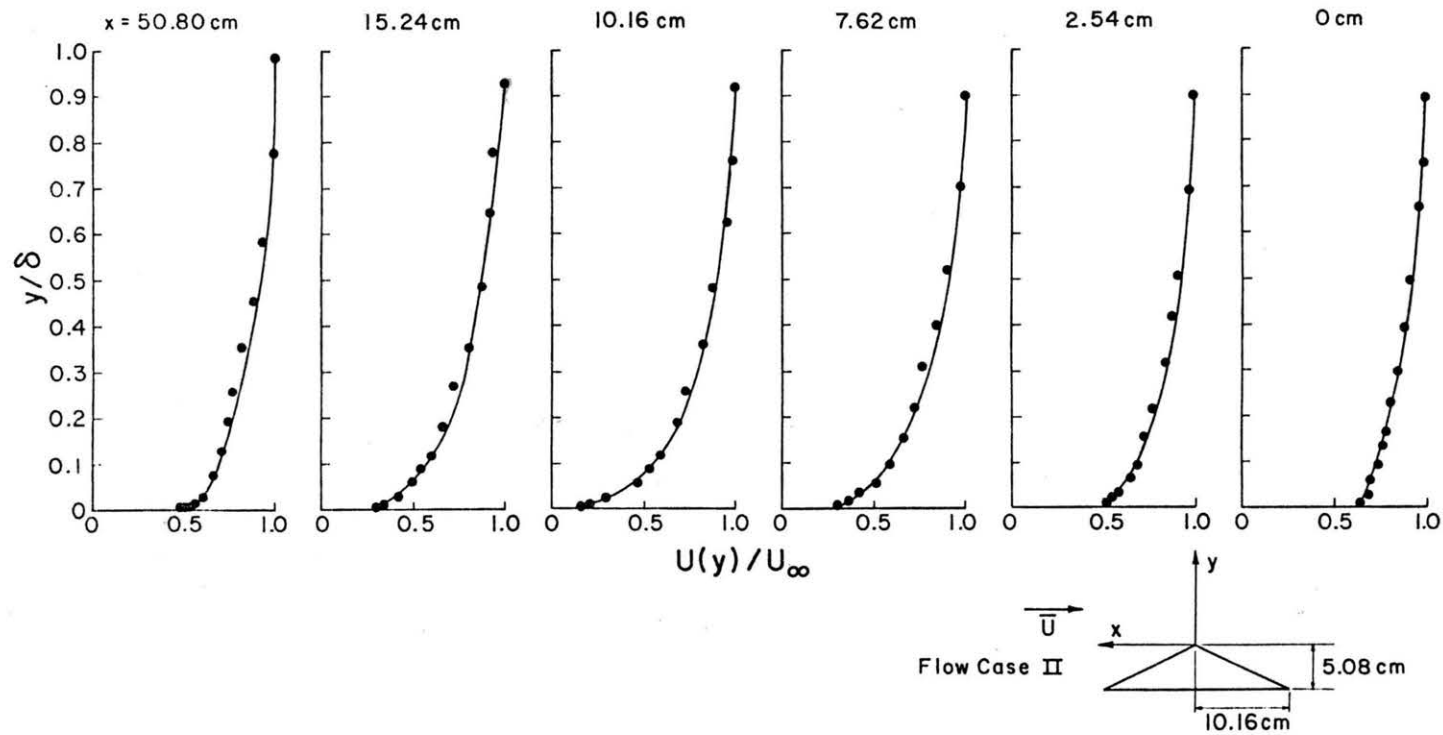
a) 1:2 hill.
 Figure B16 Velocity profiles Flow Case I



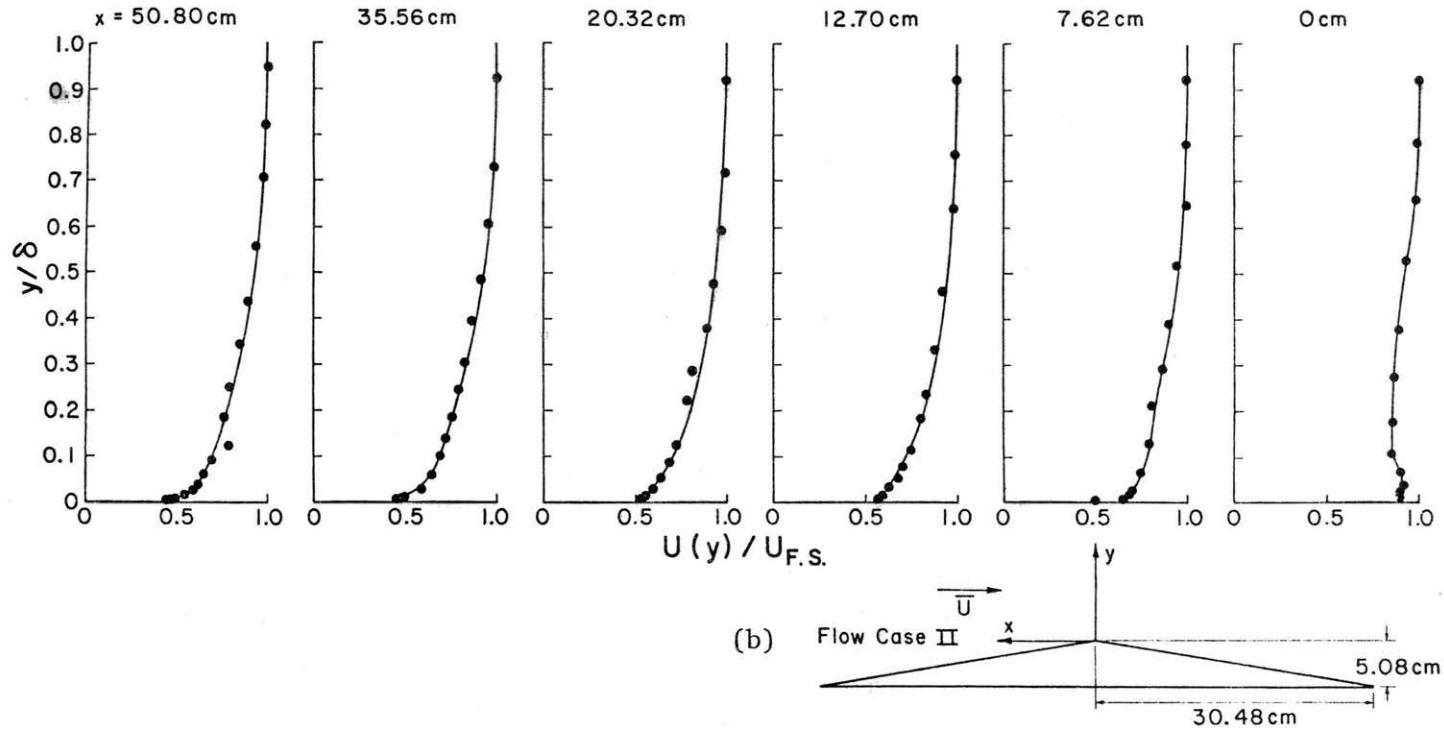
b) 1:4 hill
 Figure B16 (continued) Velocity profiles Flow Case I



c) 1:6 hill
 Figure B16 (concluded) Velocity profiles Flow Case I



a) 1:6 hill
Figure B17 Velocity profiles Flow Case II



b) 1:6 hill
 Figure B17 (concluded) Velocity profiles Flow Case II

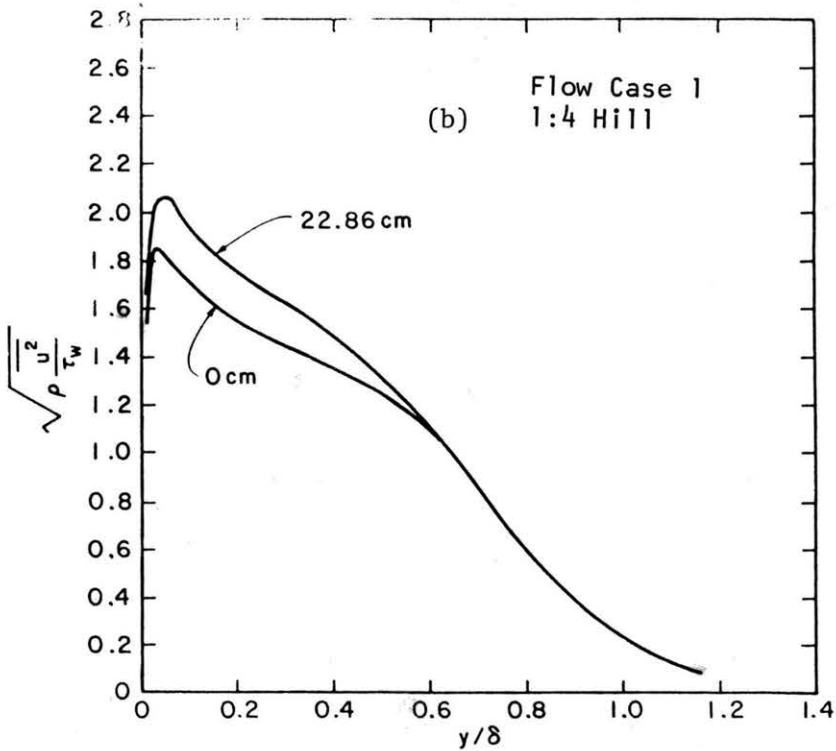
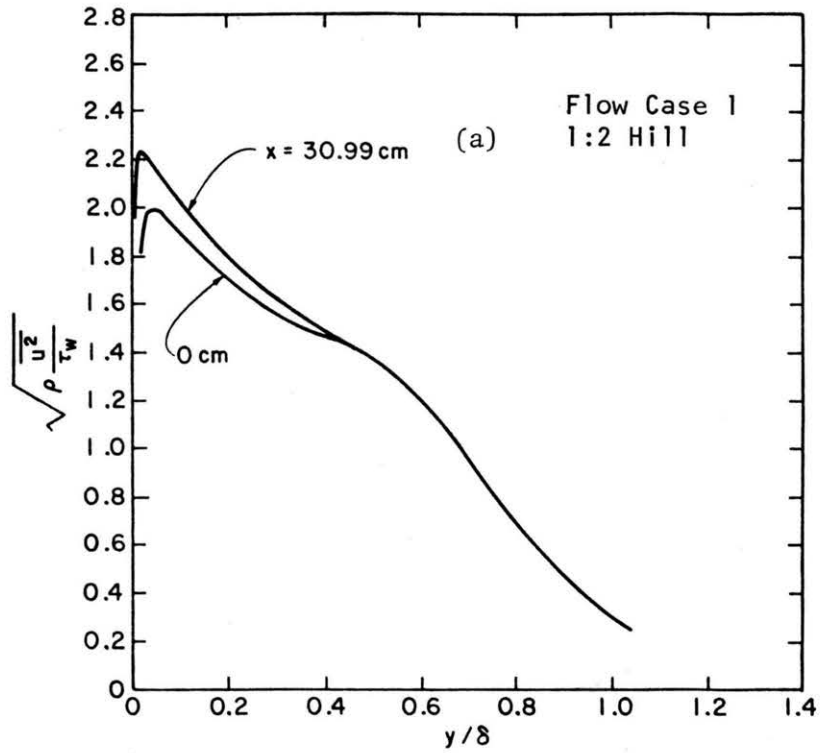


Figure B18 Upstream $\sqrt{\rho \frac{u^2}{\tau_w}}$ measurements compared to
 $\sqrt{\rho \frac{u^2}{\tau_w}}$ measurements at crest (Flow Case I)

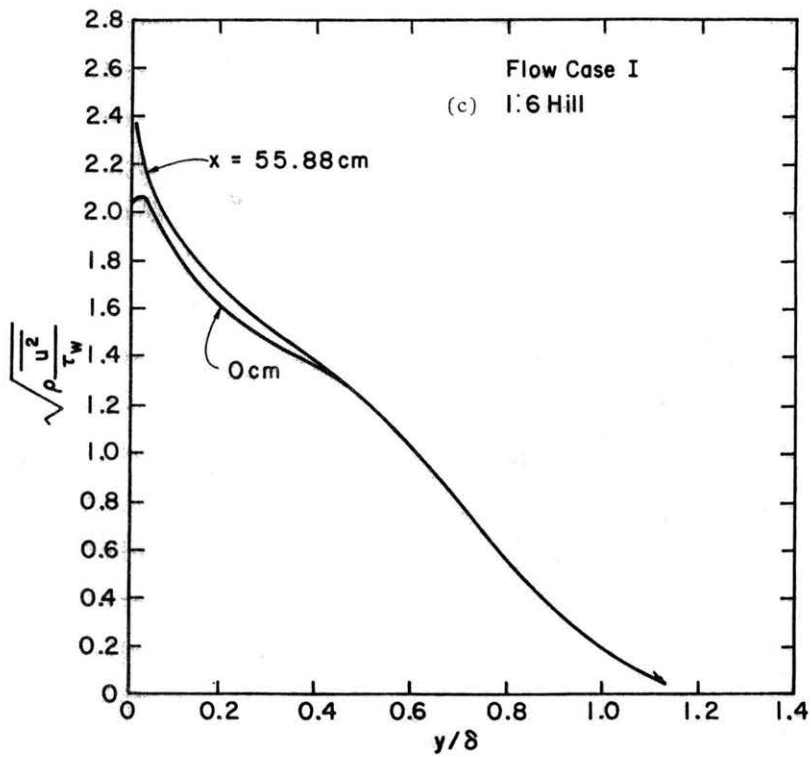


Figure B18 (concluded) Upstream $\sqrt{\rho \frac{u^2}{\tau_w}}$ measurements compared to $\sqrt{\rho \frac{u^2}{\tau_w}}$ measurements at crest (Flow Case I)

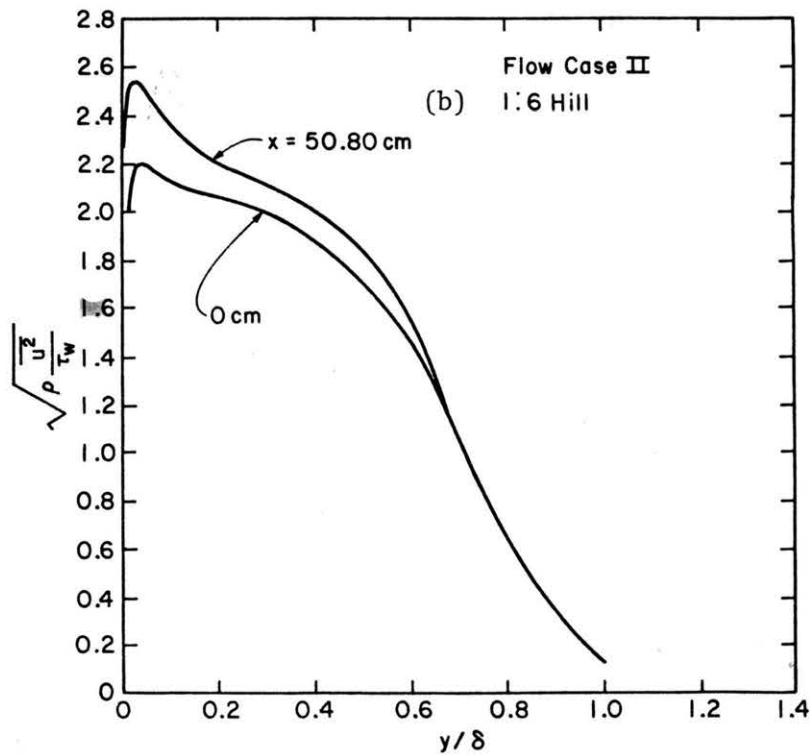
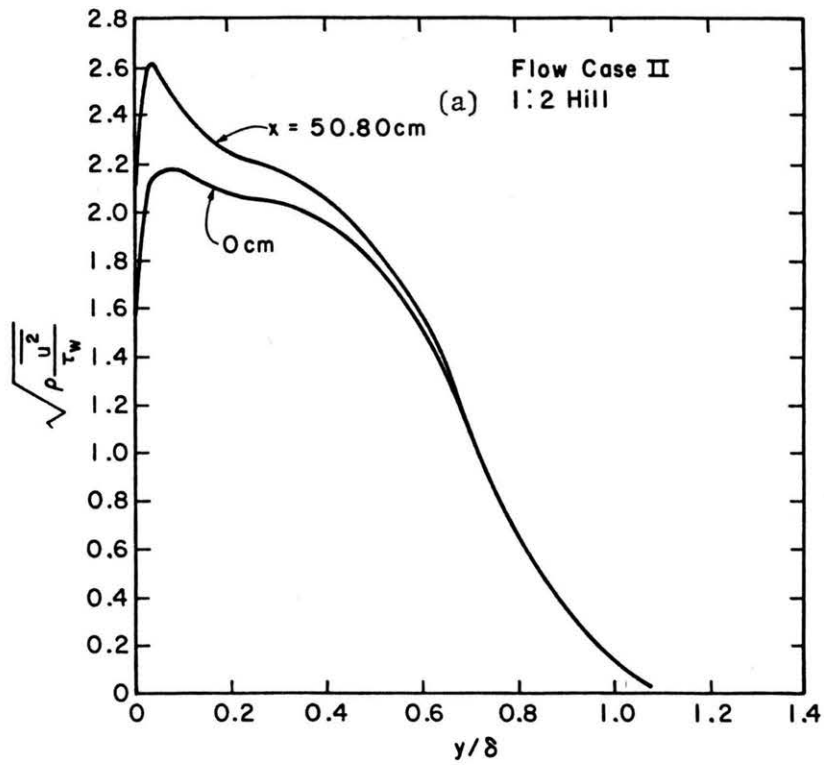


Figure B19 Upstream $\sqrt{\rho \frac{u^2}{\tau_w}}$ measurements compared to $\sqrt{\rho \frac{u^2}{\tau_w}}$ measurements at crest. (Flow Case II)

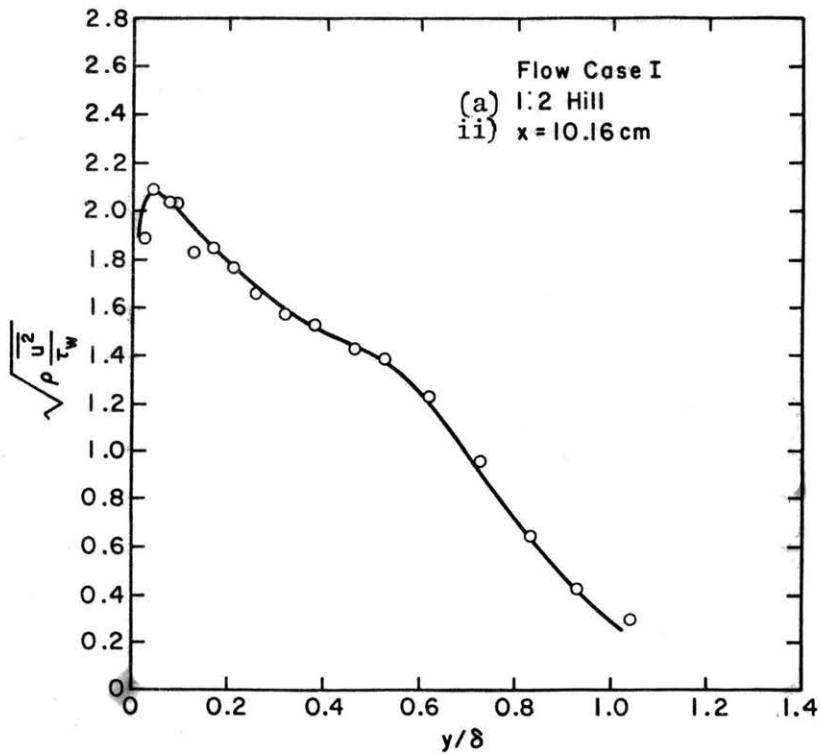
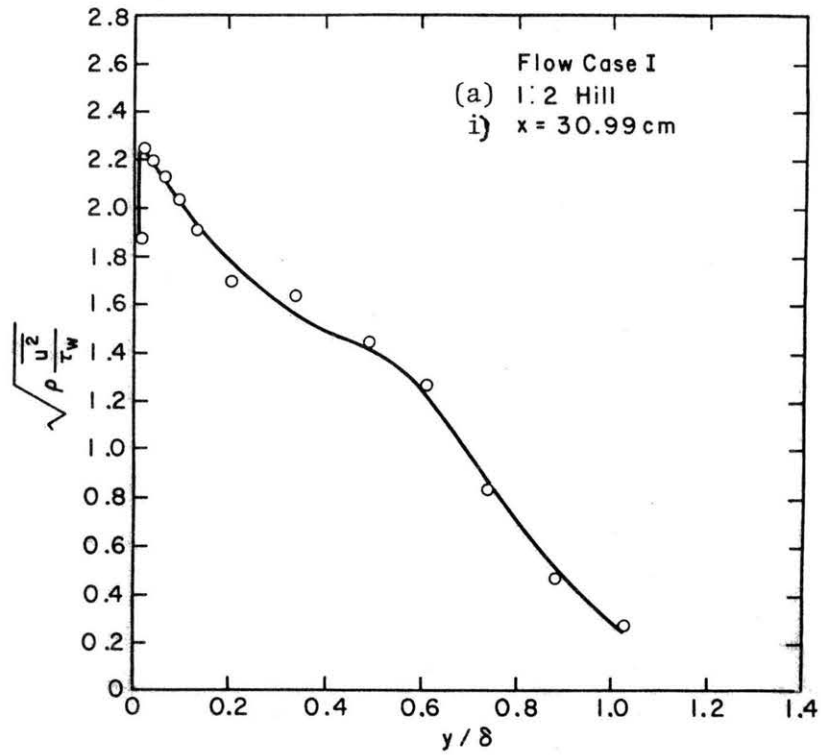


Figure B20 $\sqrt{\rho \frac{u^2}{\tau_w}}$ profiles Flow Case I

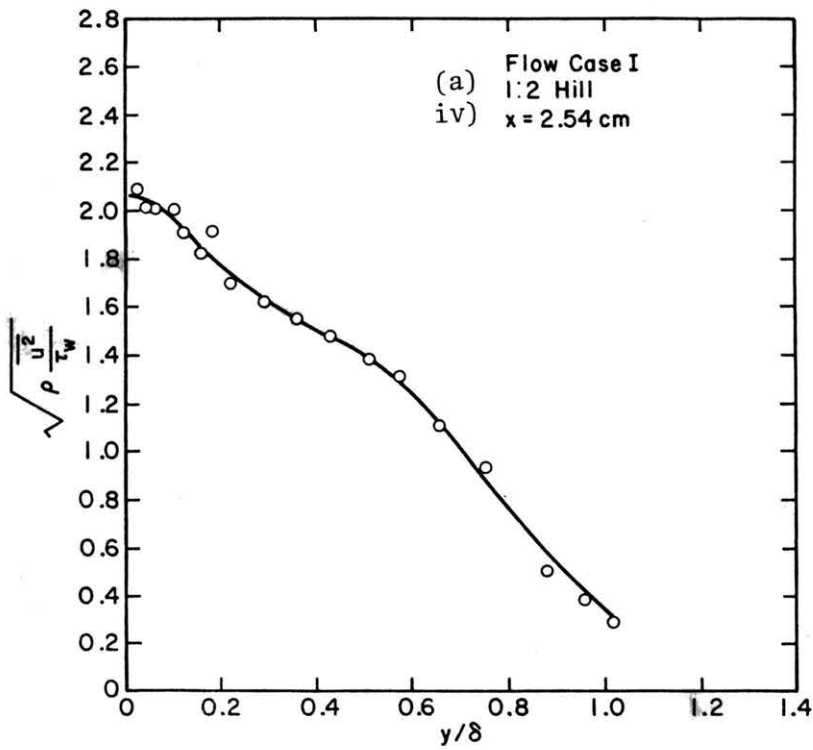
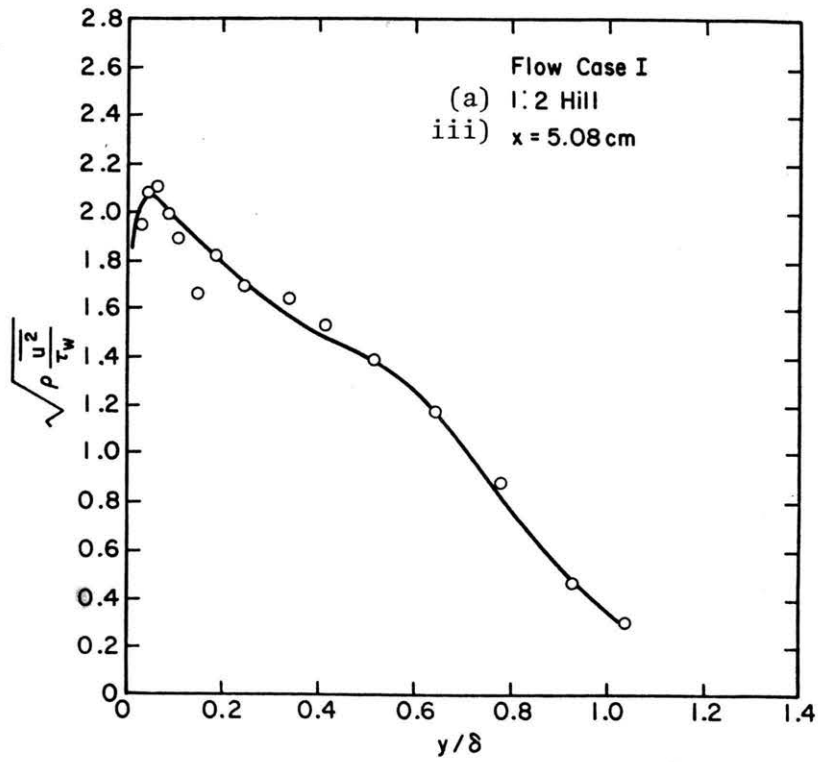


Figure B20 (continued) $\sqrt{\rho \frac{u^2}{\tau_w}}$ profiles Flow Case I

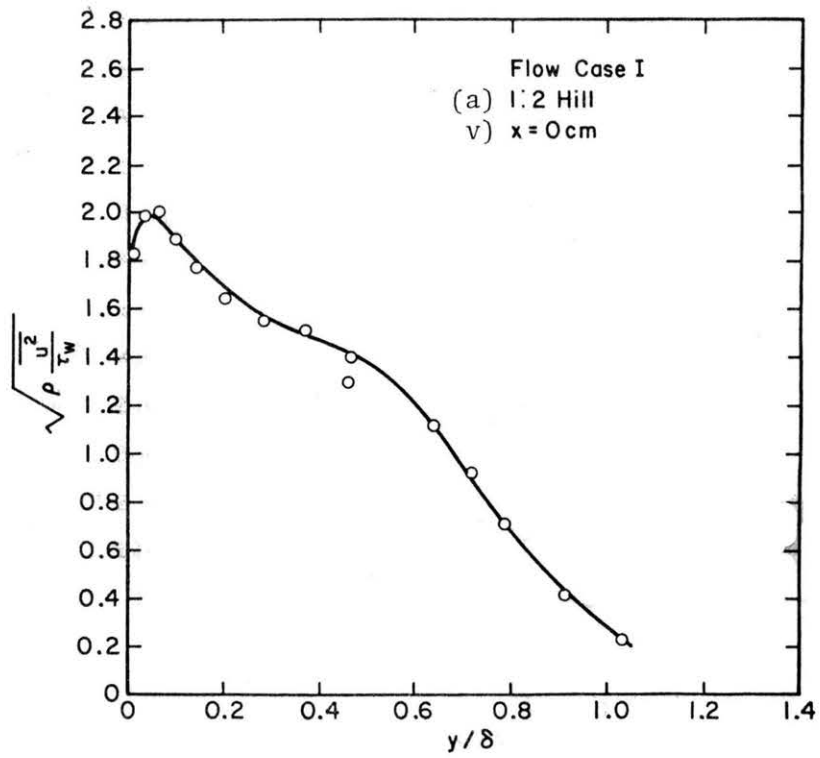


Figure B20 (continued) $\sqrt{\rho \frac{u^2}{\tau_w}}$ profiles Flow Case I

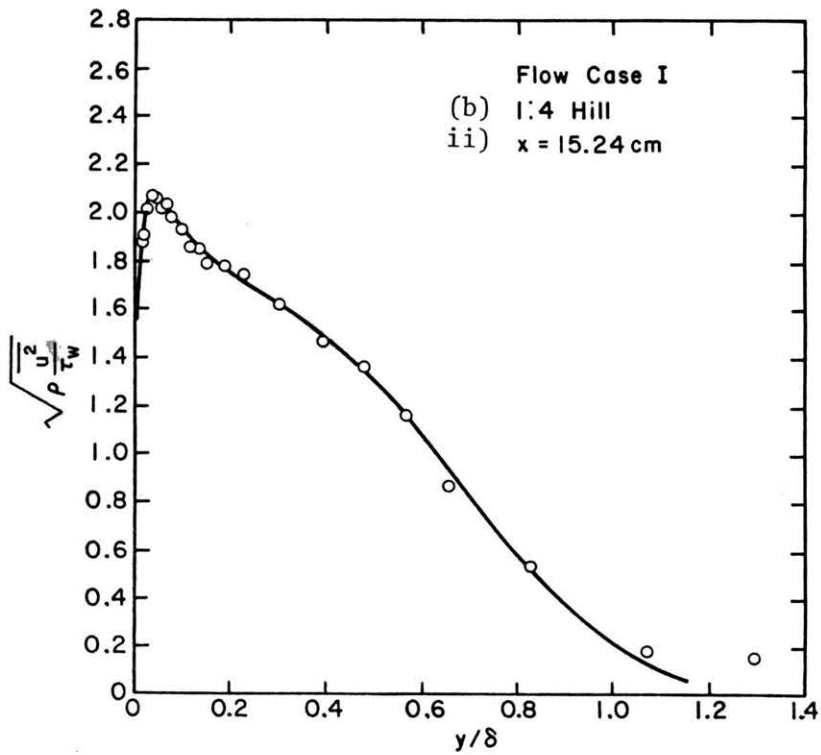
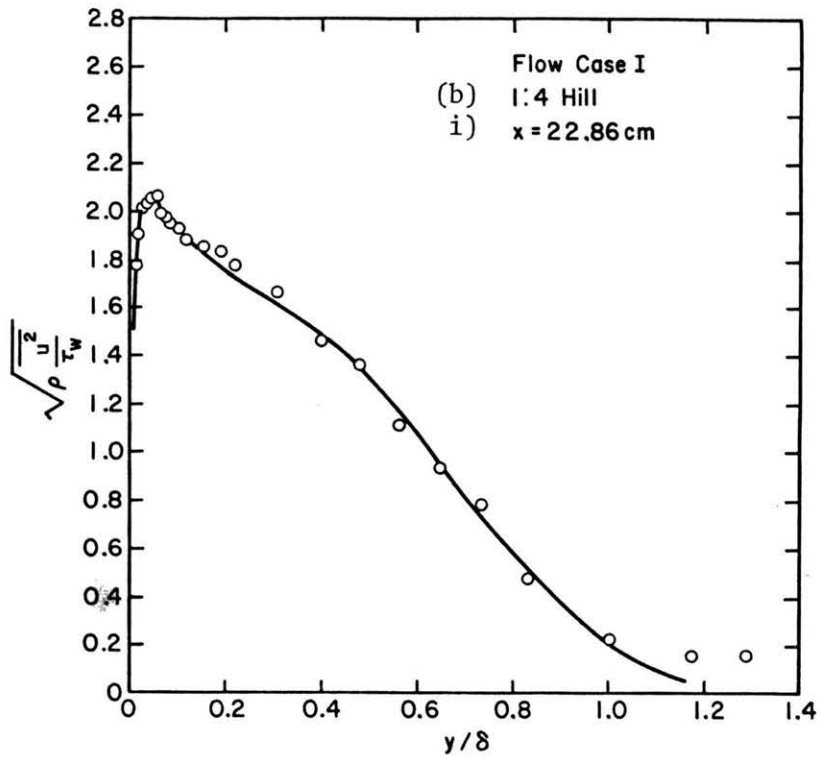


Figure B20 (continued) $\sqrt{\rho \frac{u^2}{\tau_w}}$ profiles Flow Case I

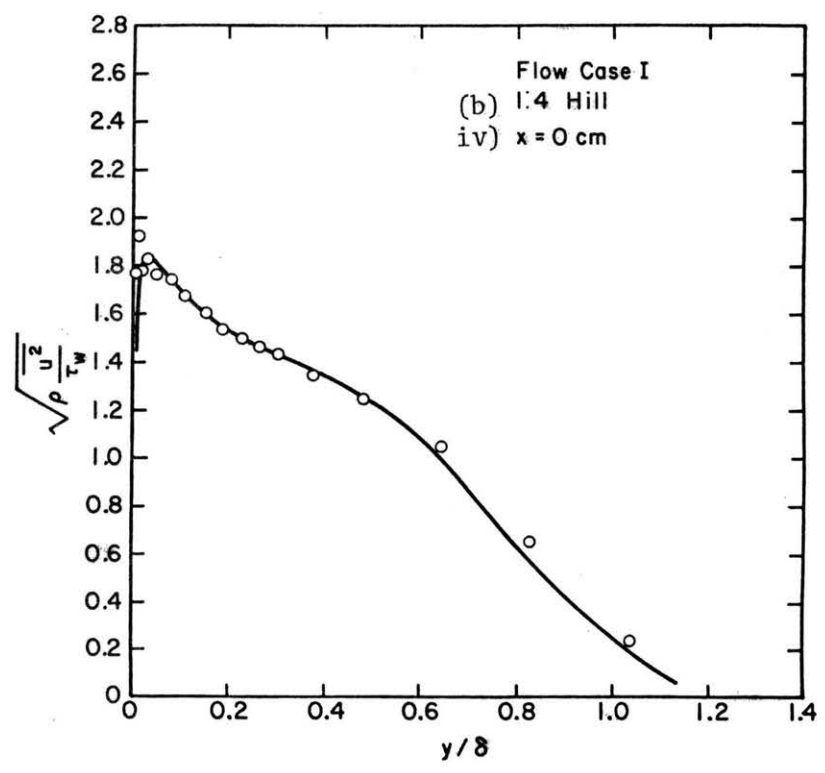
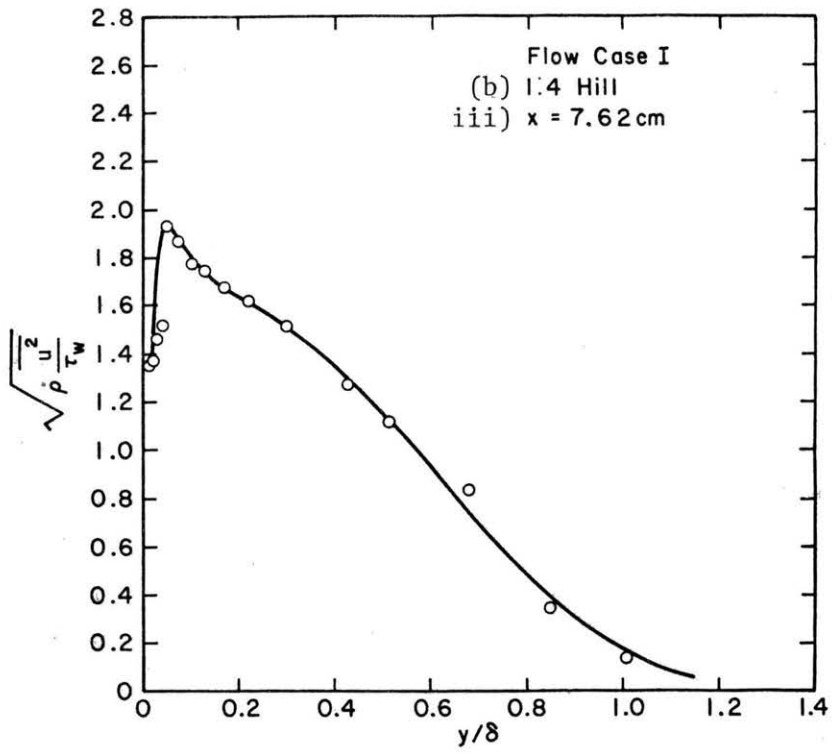


Figure B20 (continued) $\sqrt{\rho \frac{u^2}{\tau_w}}$ profiles Flow Case I

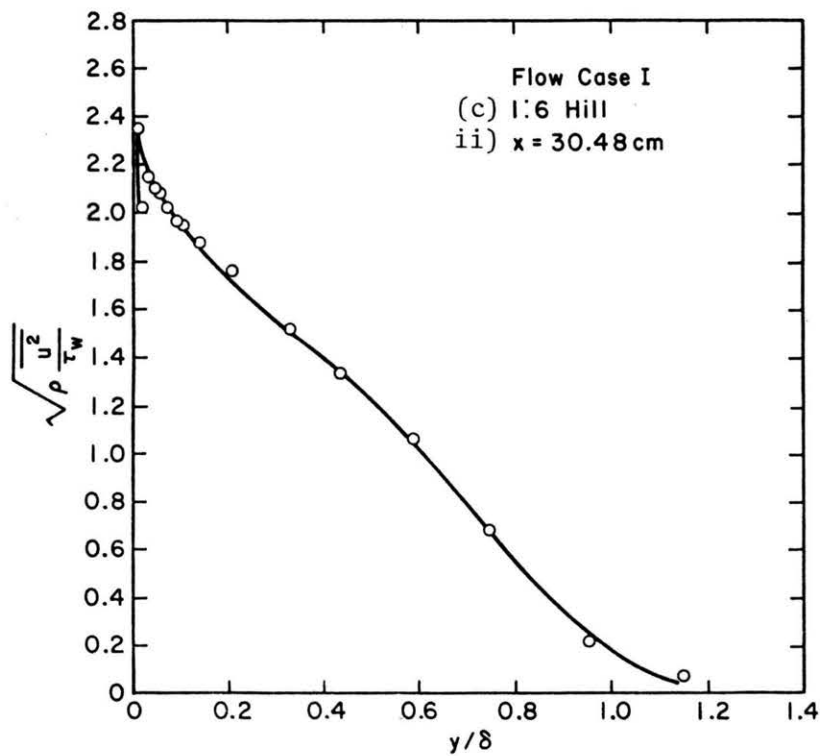
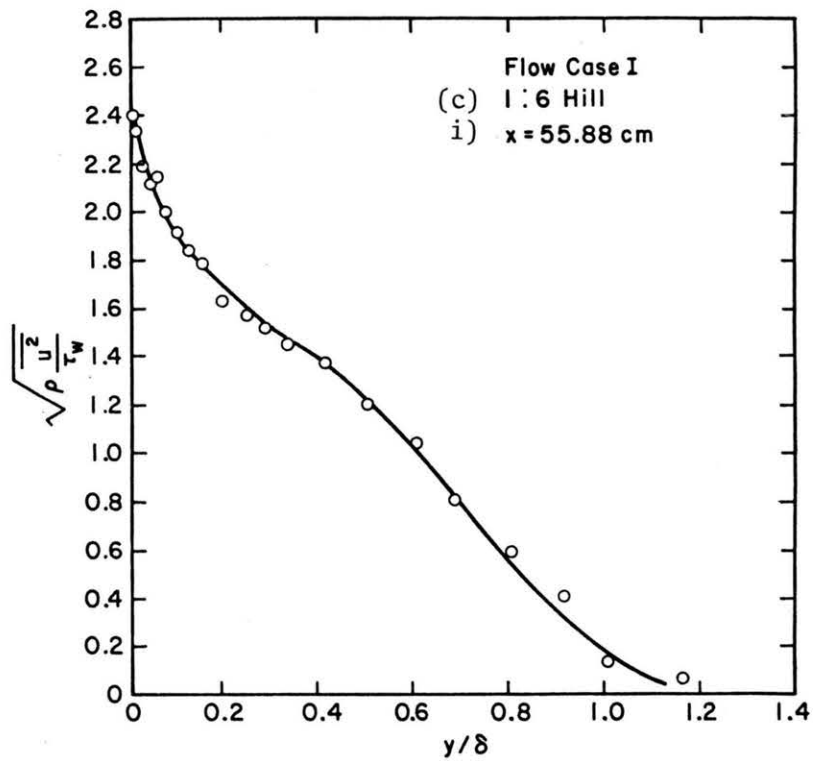


Figure B20 (continued) $\sqrt{\rho \frac{u^2}{\tau_w}}$ profiles Flow Case I

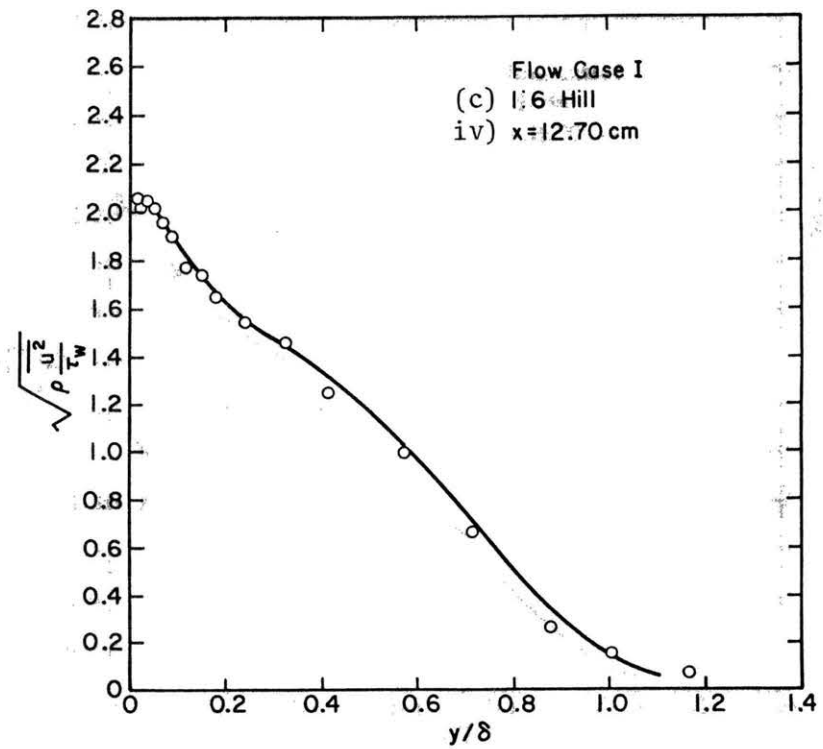
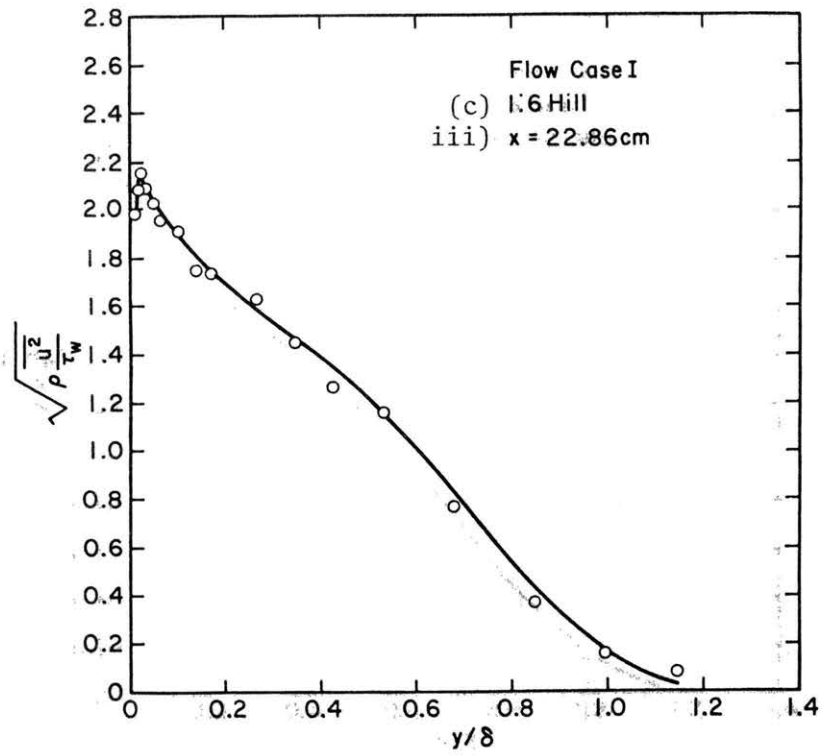


Figure B20 (continued) $\sqrt{\rho \frac{u^2}{\tau_w}}$ profiles Flow Case I

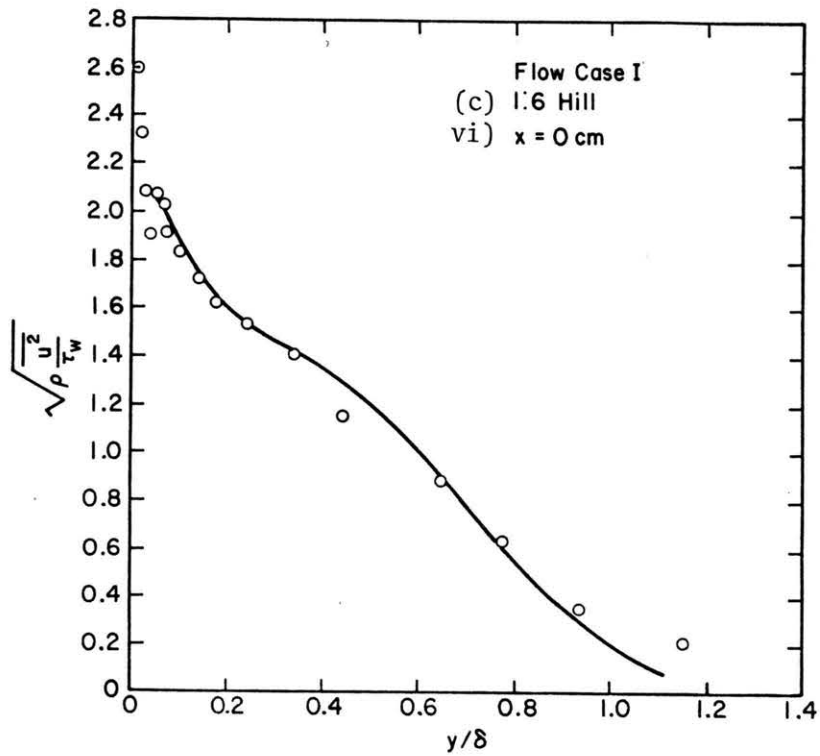
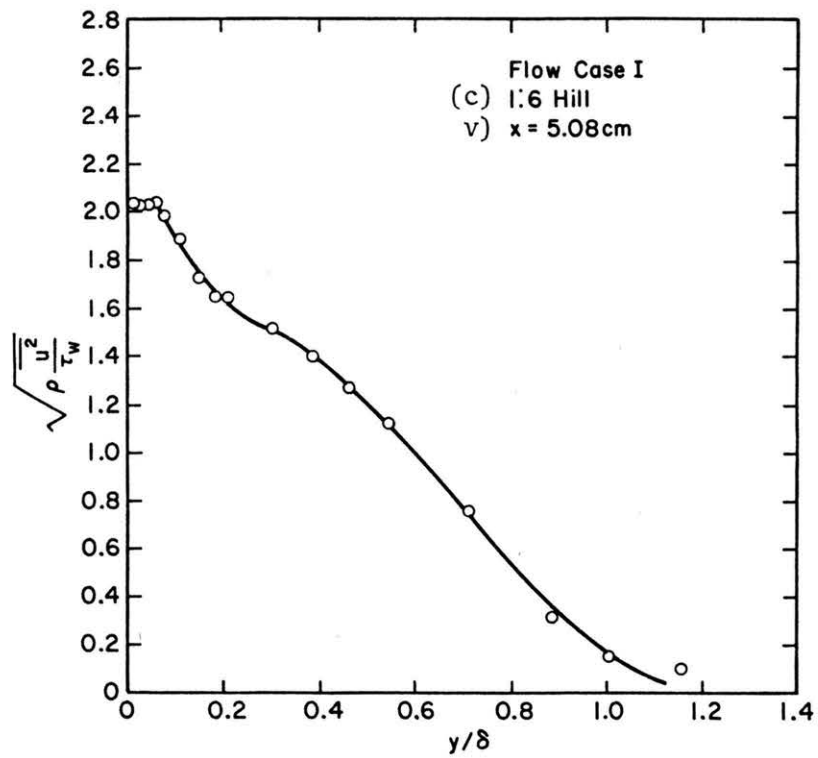


Figure B20 (concluded) $\sqrt{\rho \frac{u^2}{\tau_w}}$ profiles Flow Case I

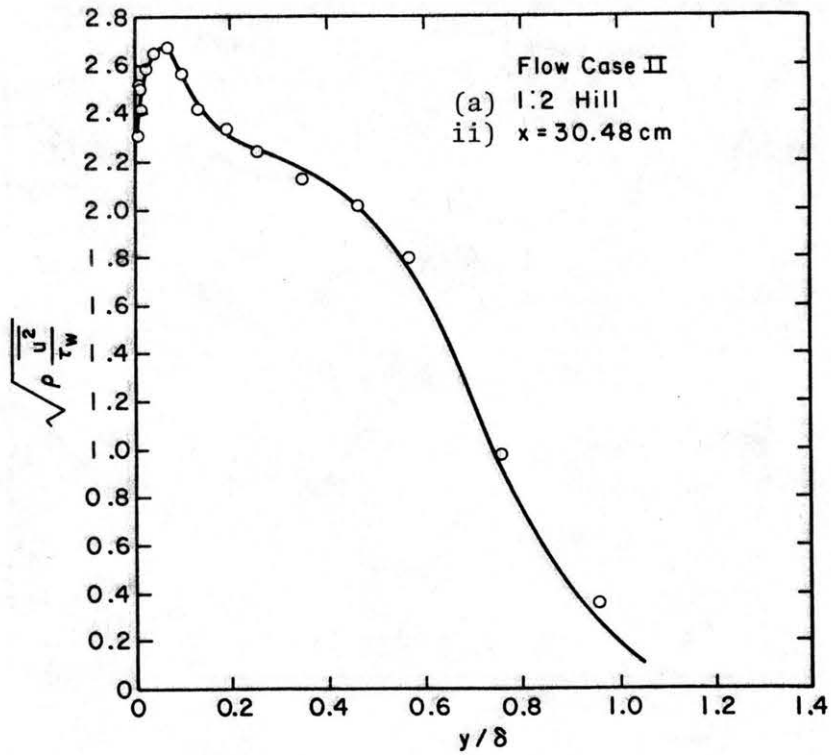
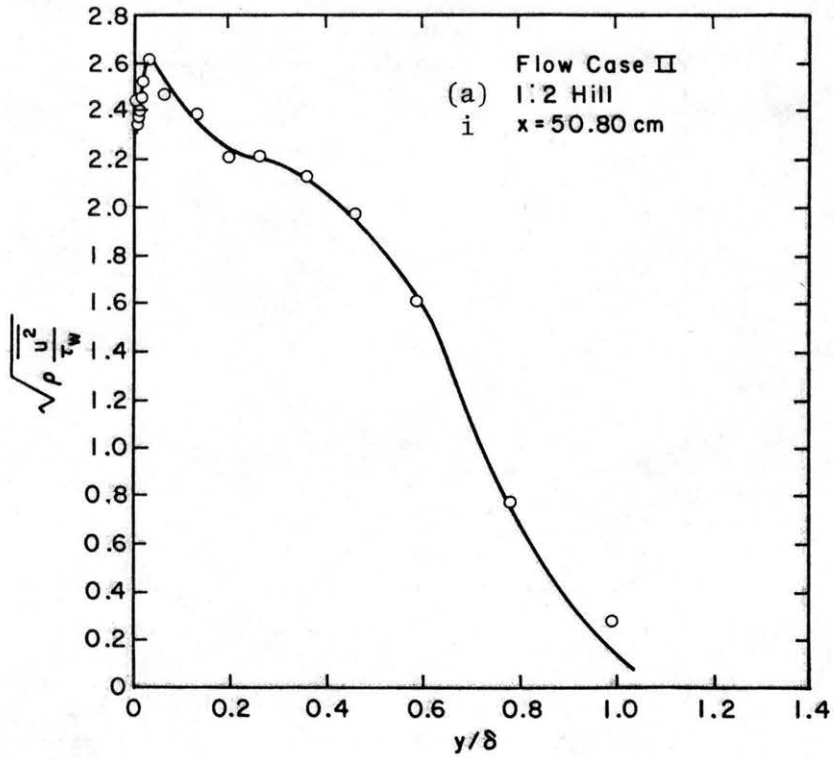


Figure B21. $\sqrt{\frac{\rho u^2}{\tau_w}}$ profiles Flow Case II

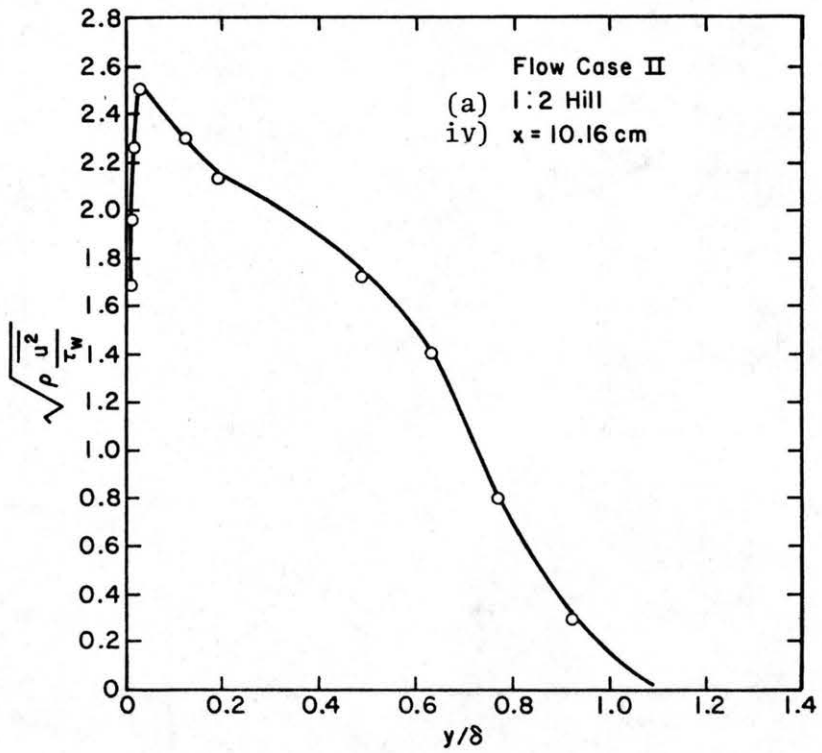
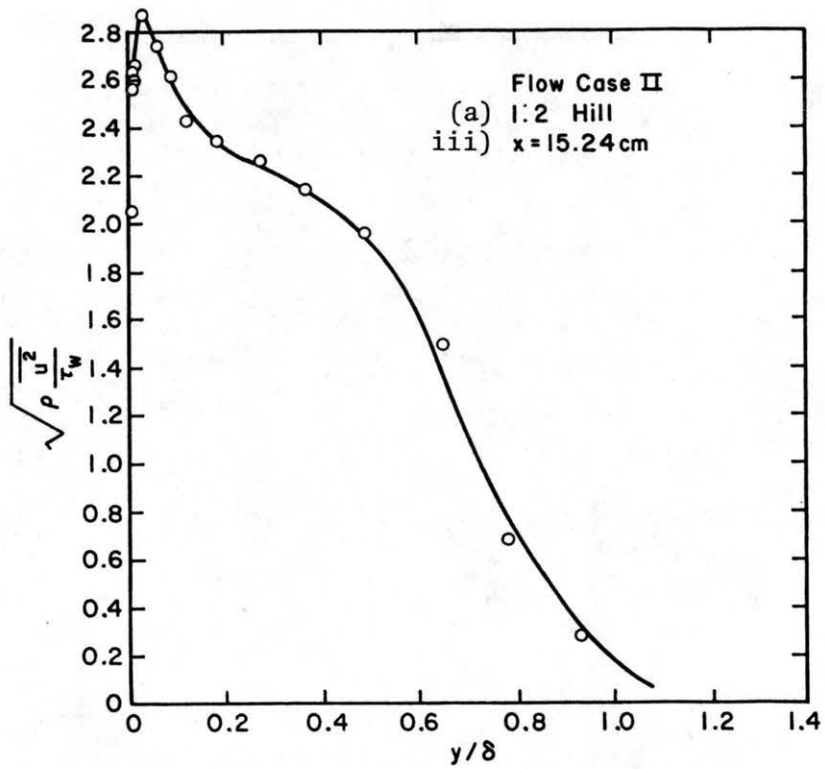


Figure B21. (continued) $\sqrt{\rho \frac{u^2}{\tau_w}}$ profiles Flow Case II

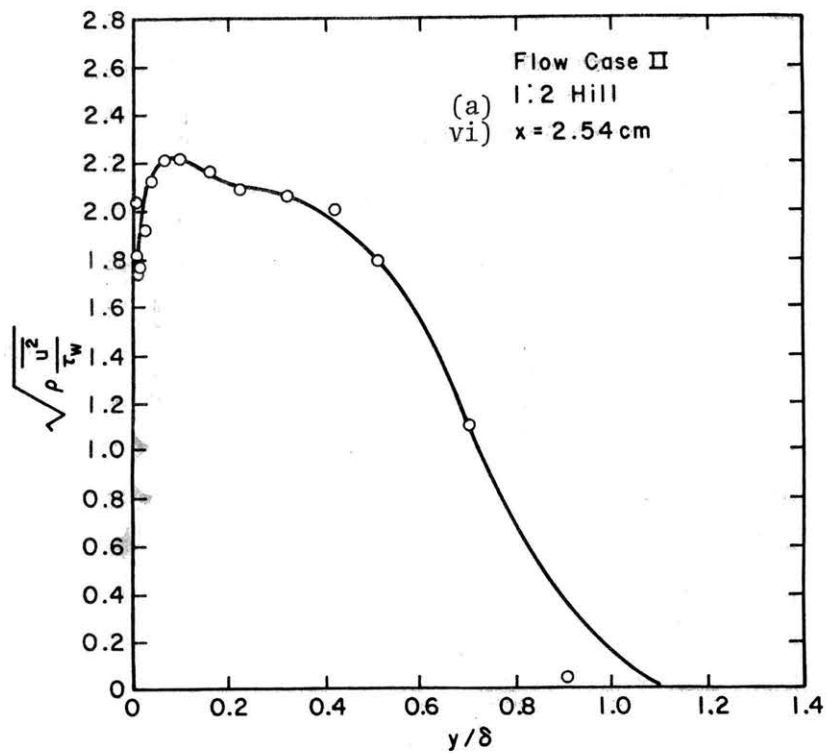
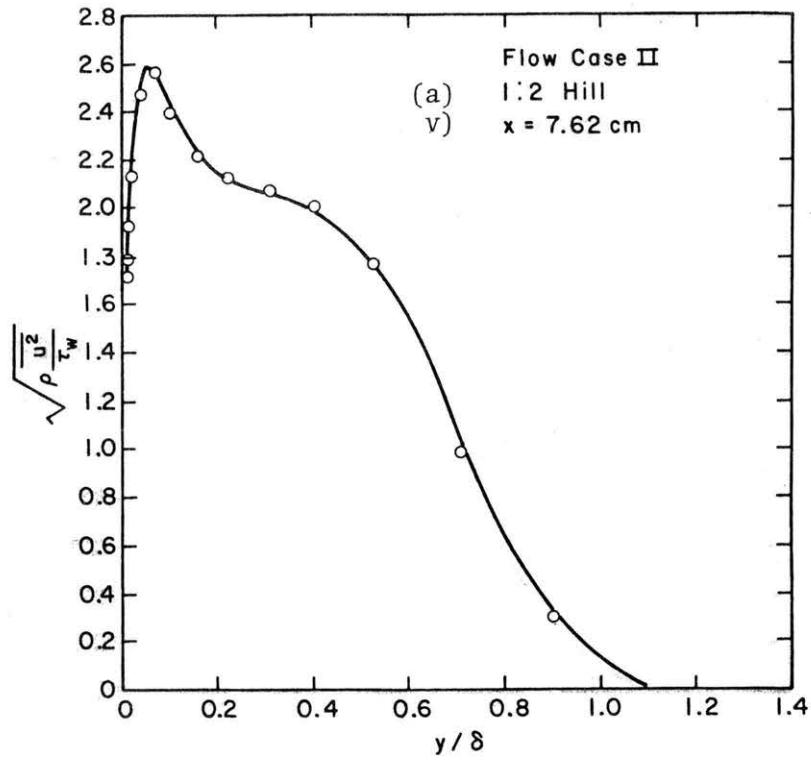


Figure B21. (continued) $\sqrt{\rho \frac{u^2}{\tau_w}}$ profiles Flow Case II

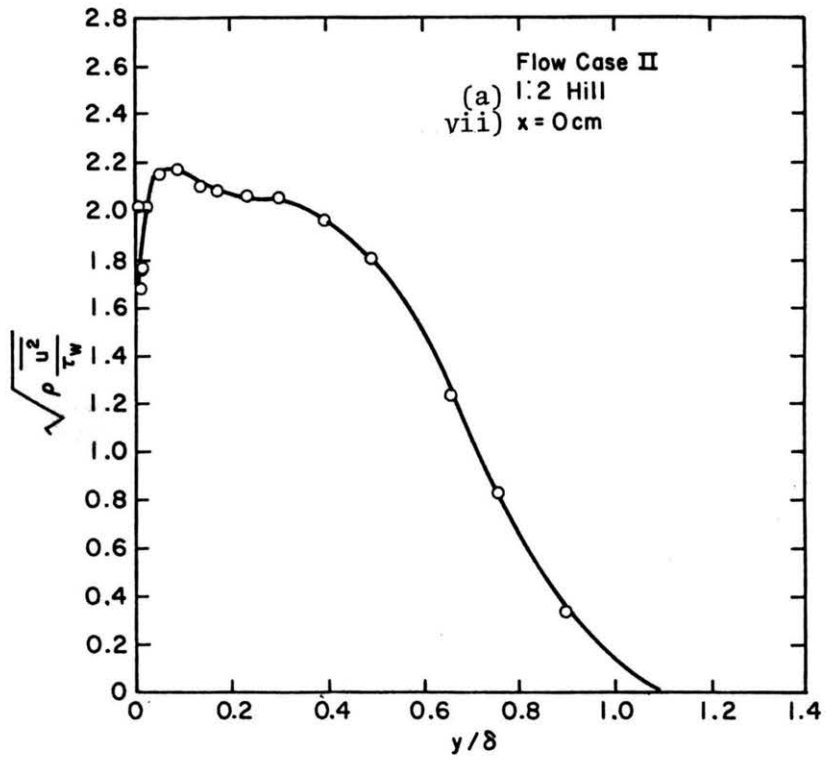


Figure B21. (continued) $\sqrt{\rho \frac{u^2}{\tau_w}}$ profiles Flow Case II

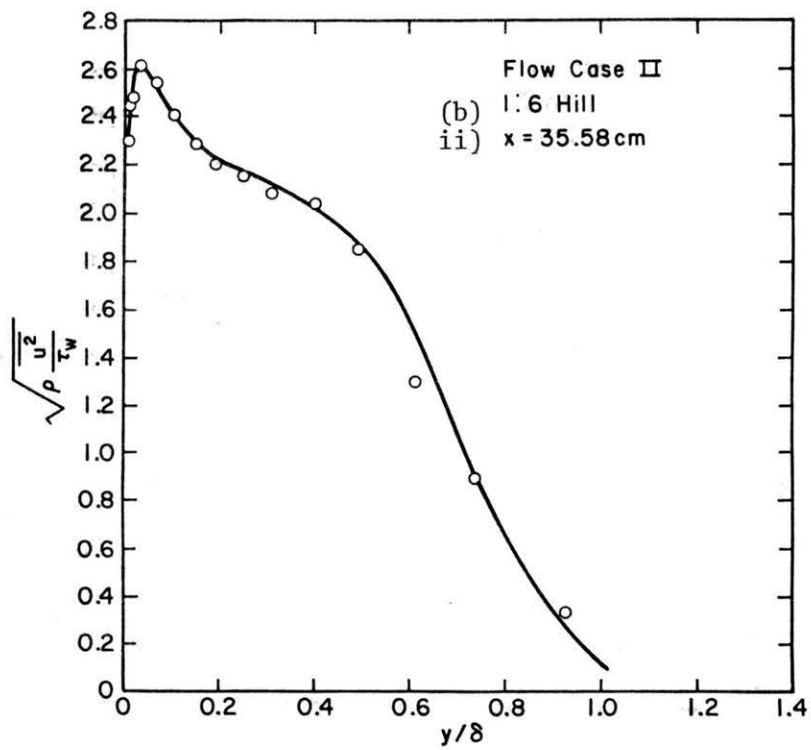
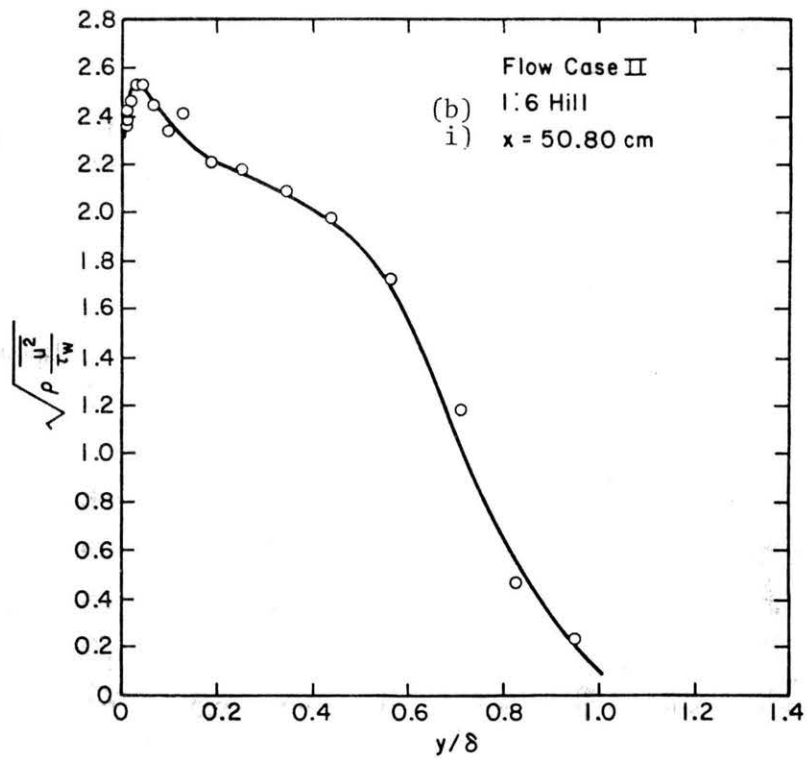


Figure B21. (continued) $\sqrt{\rho \frac{u^2}{\tau_w}}$ profiles Flow Case II

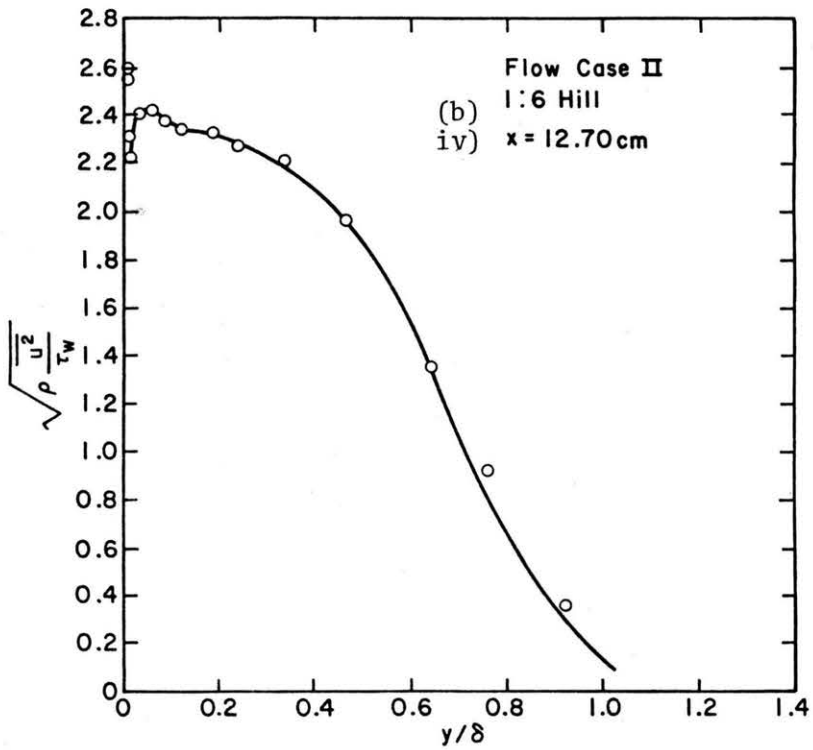
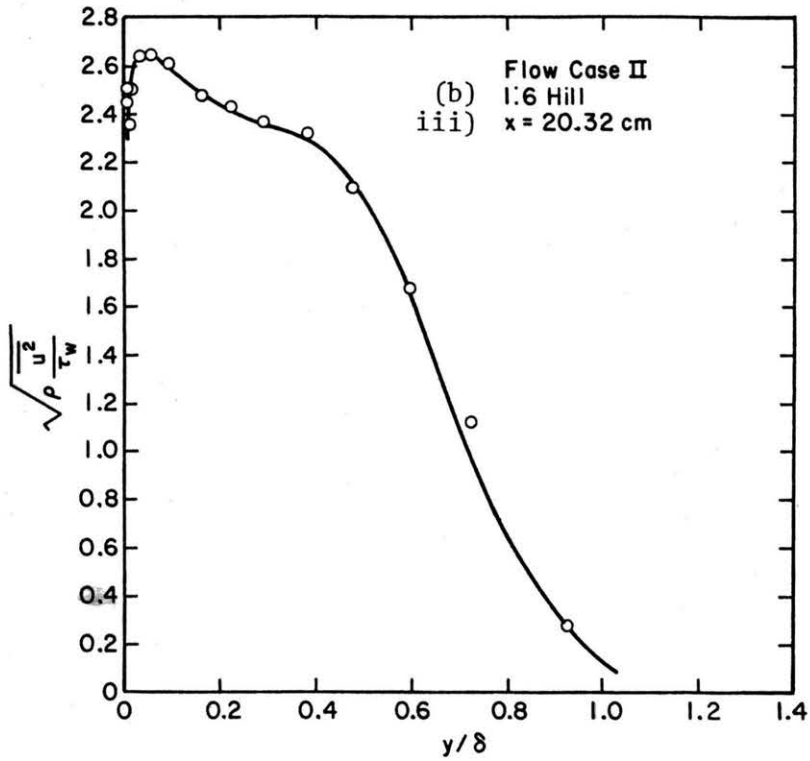


Figure B21. (continued) $\sqrt{\rho \frac{u^2}{\tau_w}}$ profiles Flow Case II

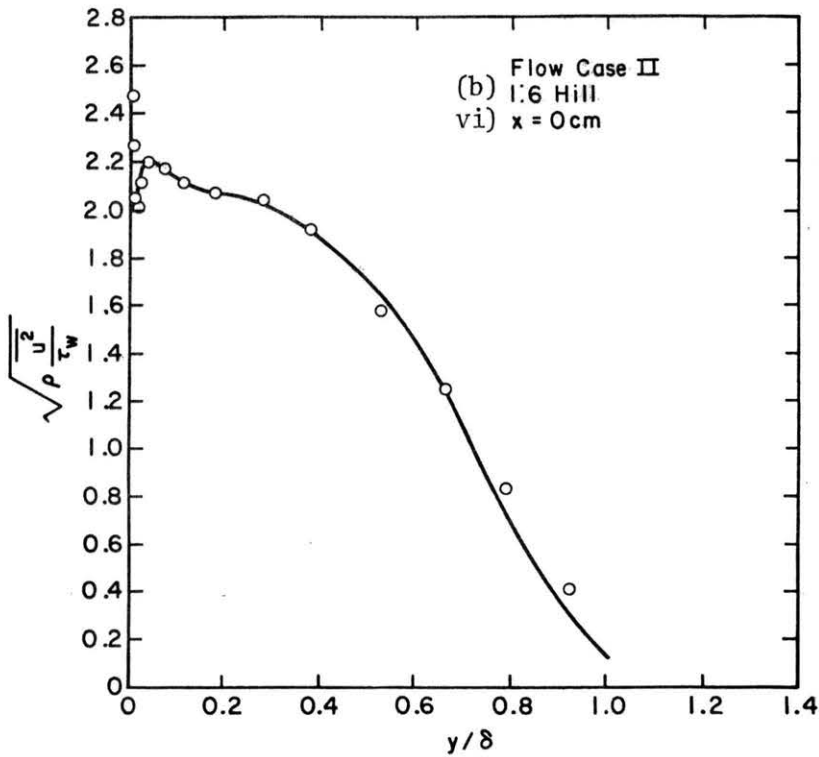
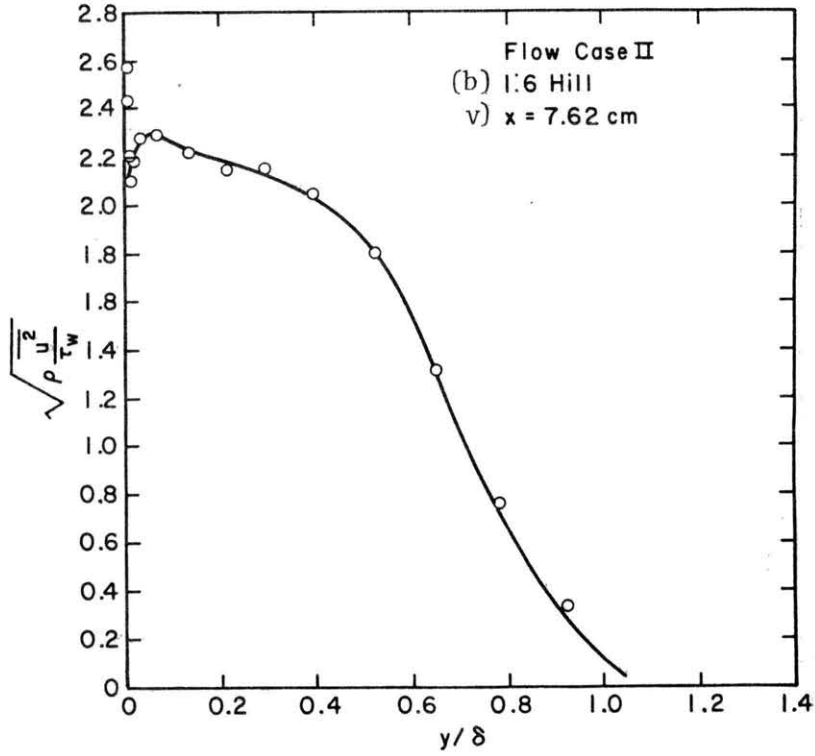


Figure B21. (concluded) $\sqrt{\rho \frac{u^2}{\tau_w}}$ profiles Flow Case II

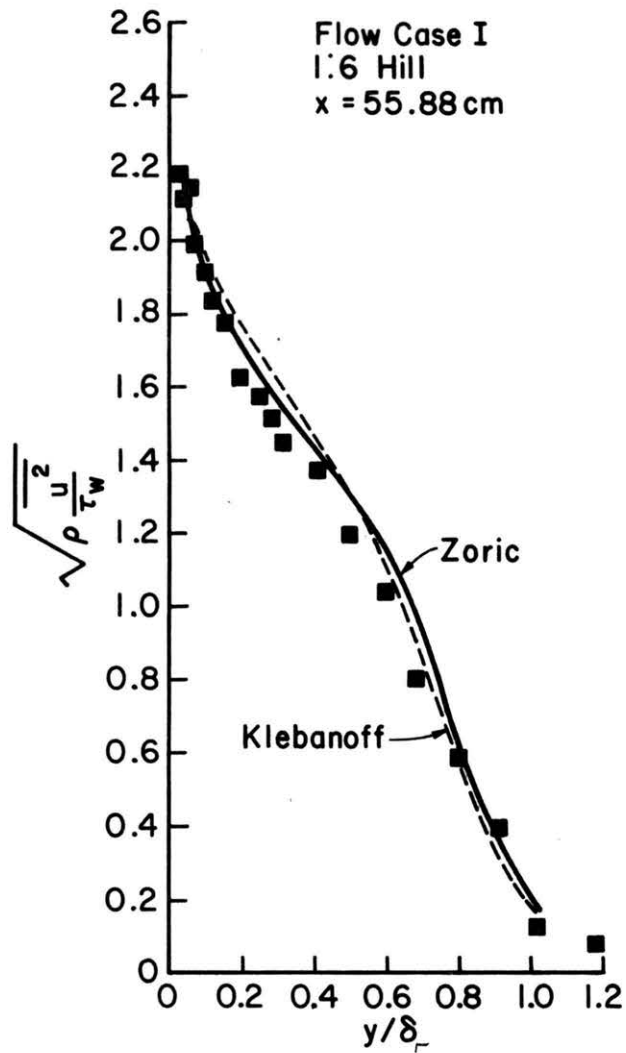


Figure B22. Comparison of upstream $\sqrt{\rho \frac{u^2}{\tau_w}}$ measurements to those of Zoric and Klebanoff. Flow Case I

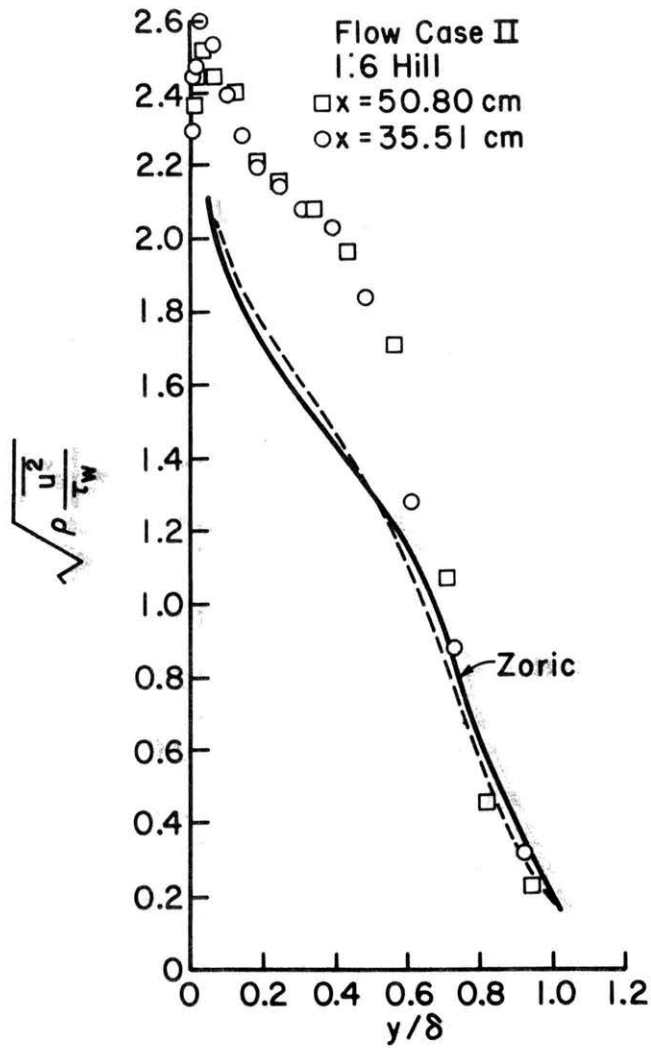


Figure B23. Comparison of upstream $\sqrt{\rho \frac{u^2}{\tau_w}}$ measurements to those of Zoric and Klebanoff. Flow Case II

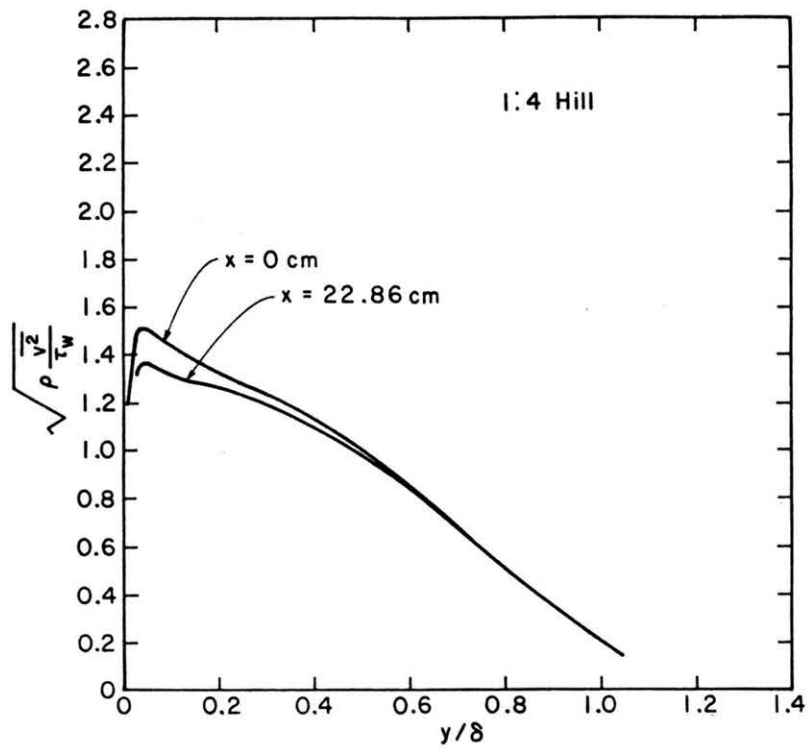
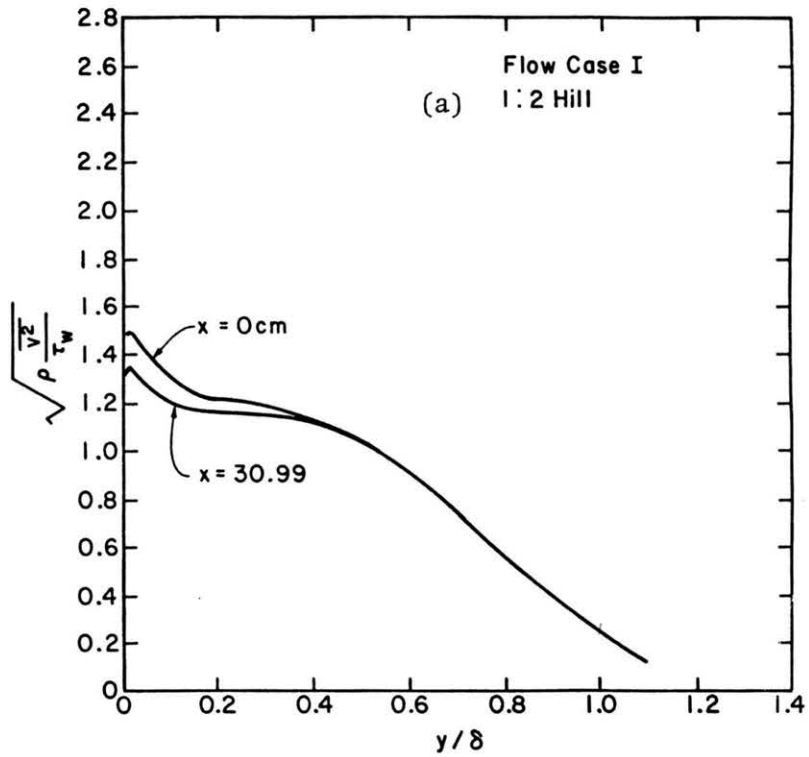


Figure B24. Upstream $\sqrt{\rho \frac{v^2}{\tau_w}}$ measurements compared to $\sqrt{\rho \frac{v^2}{\tau_w}}$ measurements at crest. Flow Case I

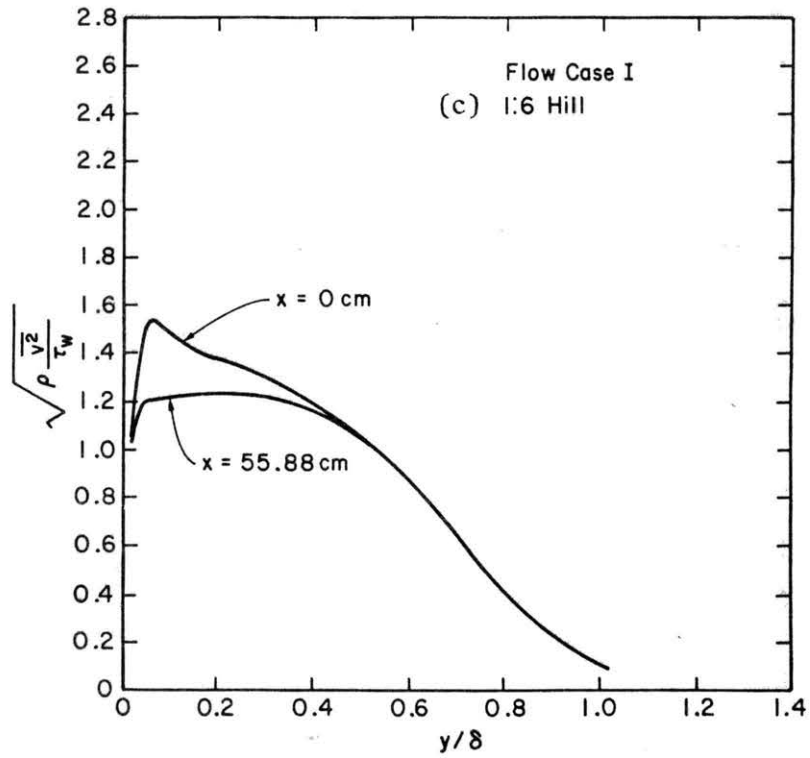


Figure B24. (concluded) Upstream $\sqrt{\rho \frac{v^2}{\tau_w}}$ measurements compared to $\sqrt{\rho \frac{v^2}{\tau_w}}$ measurements at crest. Flow Case I.

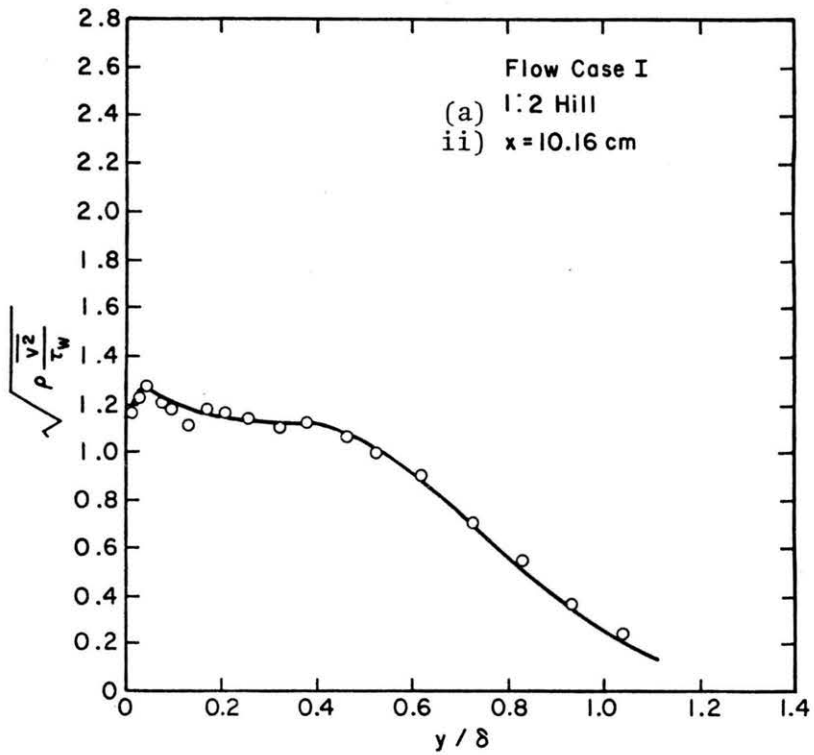
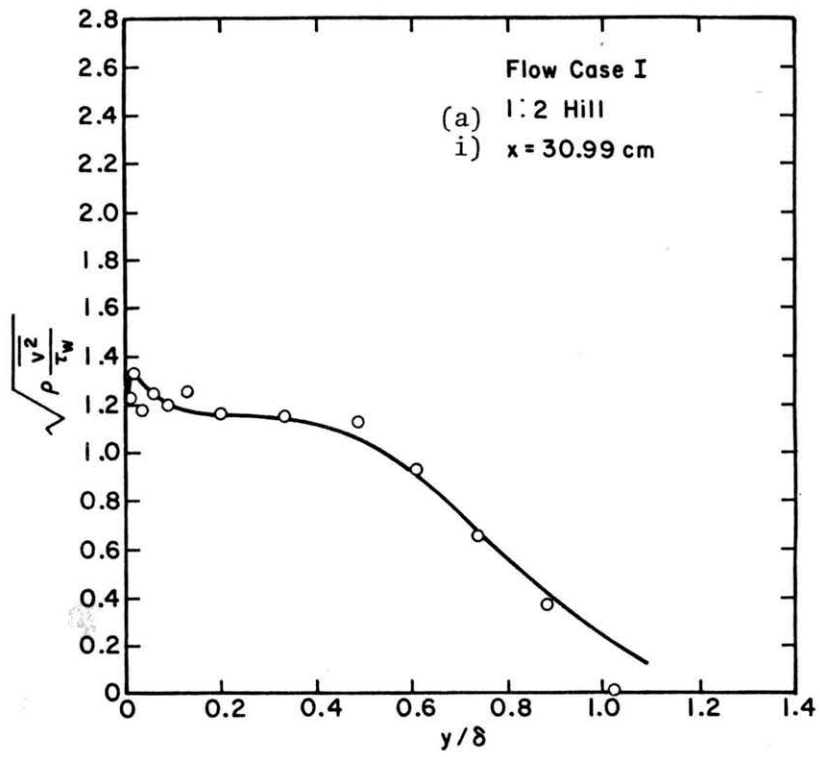


Figure B25. $\sqrt{\rho \frac{v^2}{\tau_w}}$ profiles Flow Case I

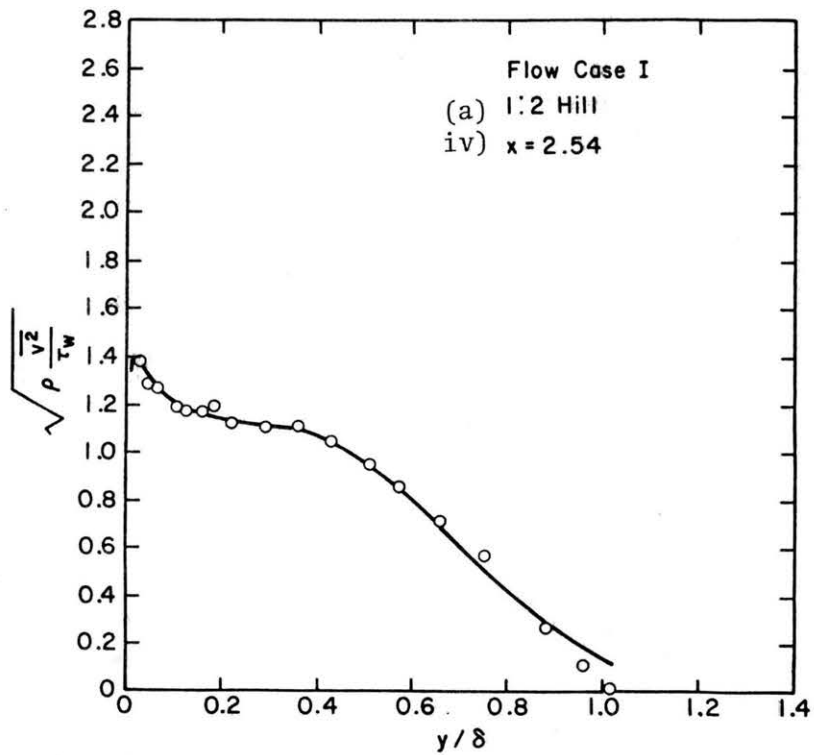
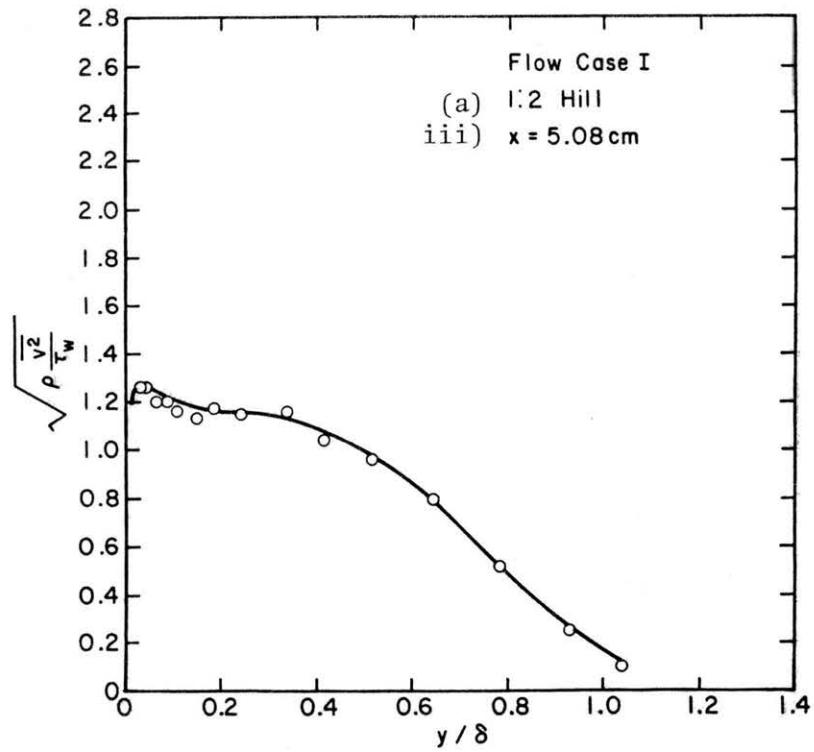


Figure B25. (continued) $\sqrt{\rho \frac{v^2}{\tau_w}}$ profiles Flow Case I

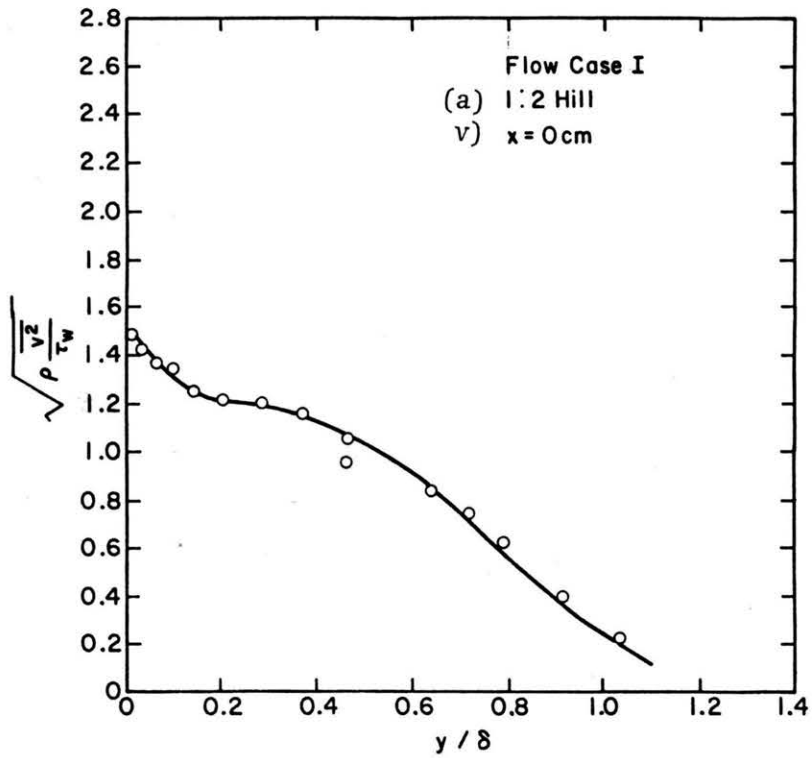


Figure B25. (continued) $\sqrt{\frac{\rho v^2}{\tau_w}}$ profiles Flow Case I.

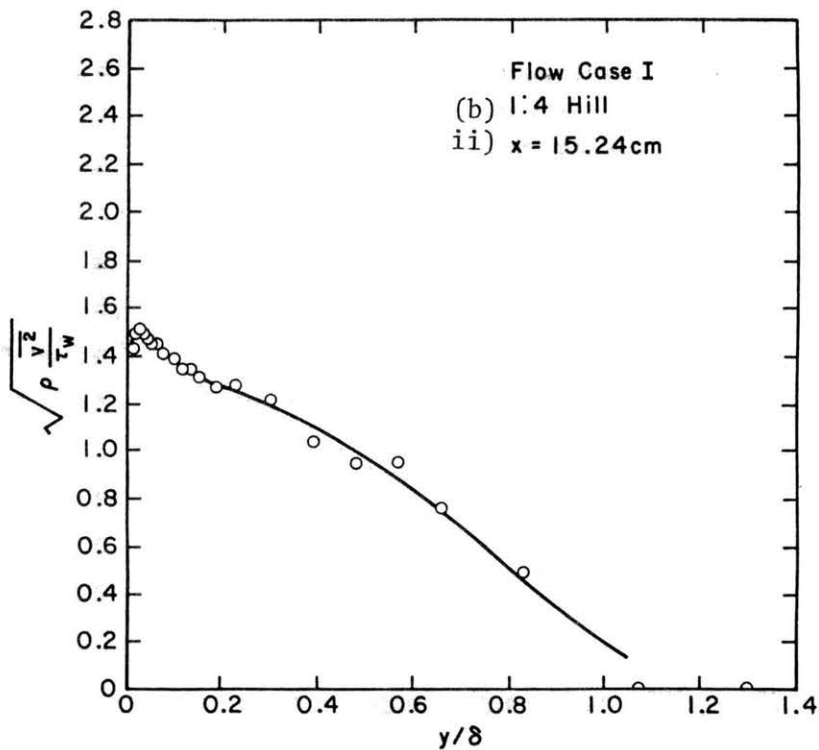
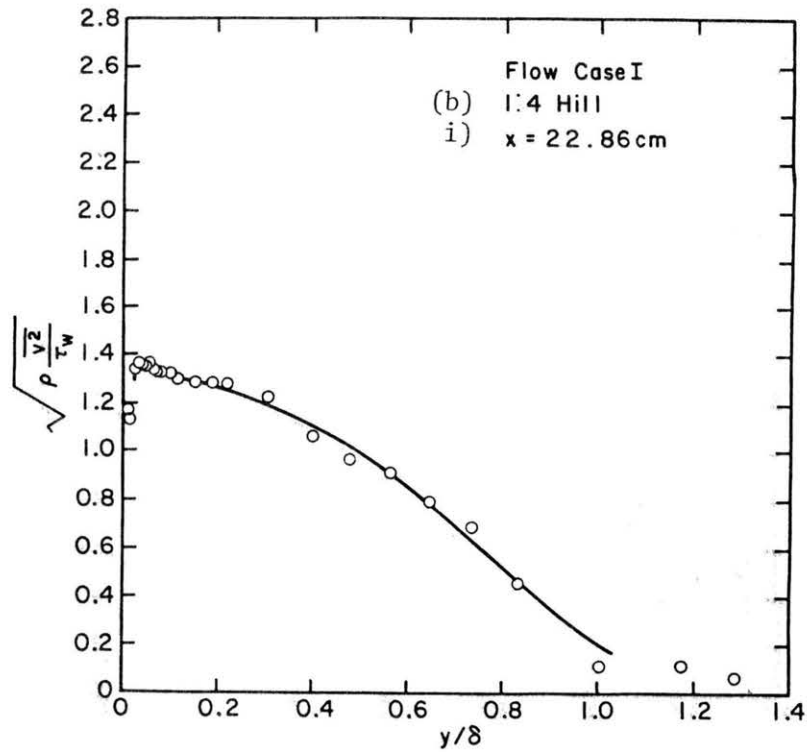


Figure B25. (continued) $\sqrt{\rho \frac{v^2}{\tau_w}}$ profiles Flow Case I.

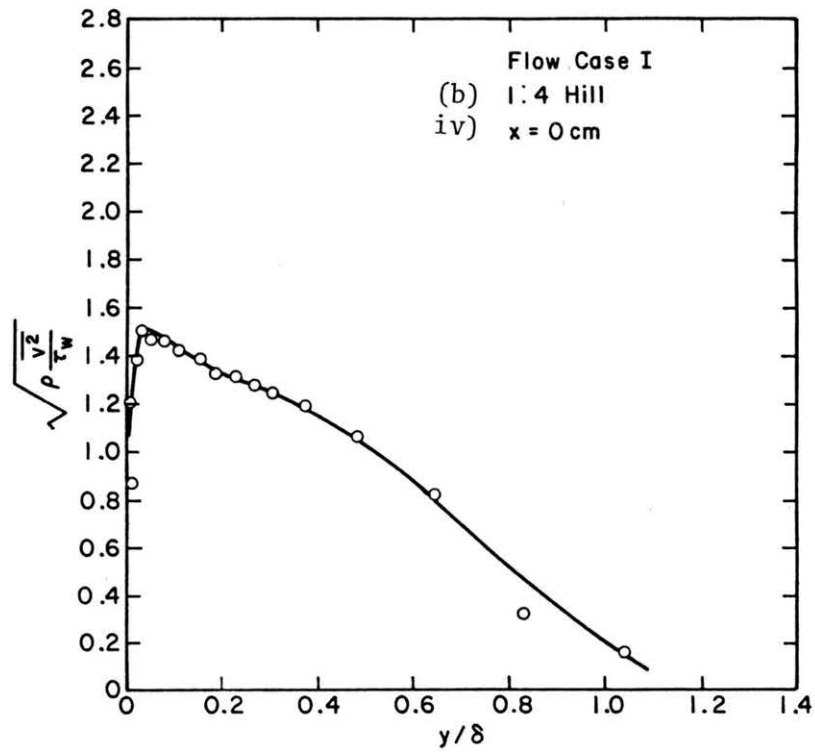
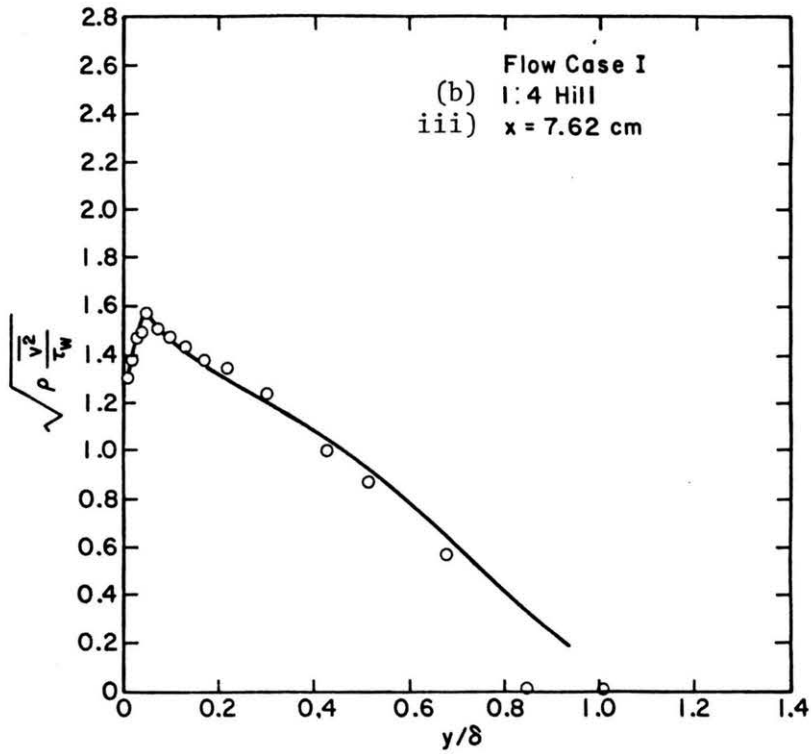


Figure B25. (continued) $\sqrt{\rho \frac{v^2}{\tau_w}}$ profiles Flow Case I

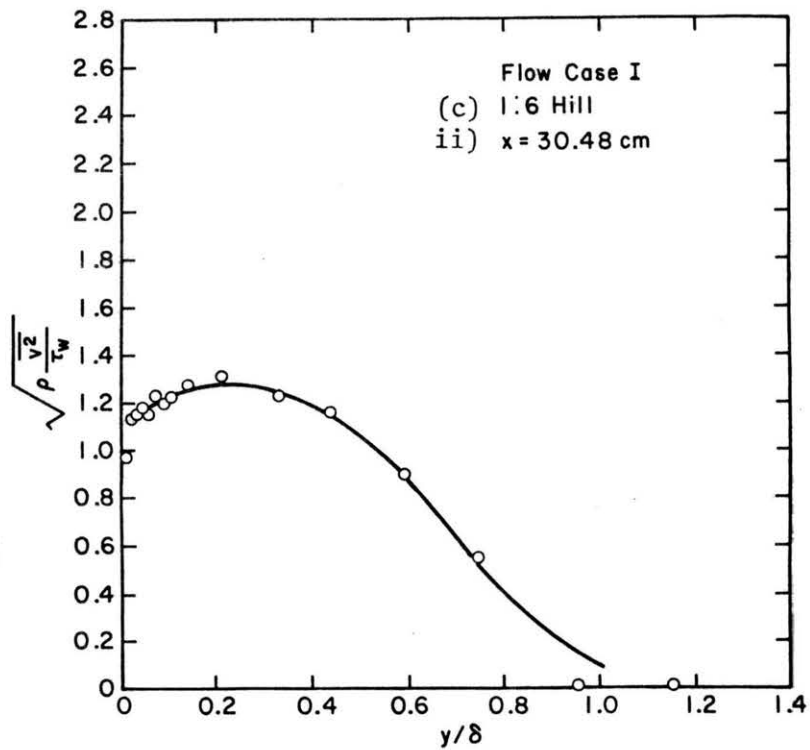
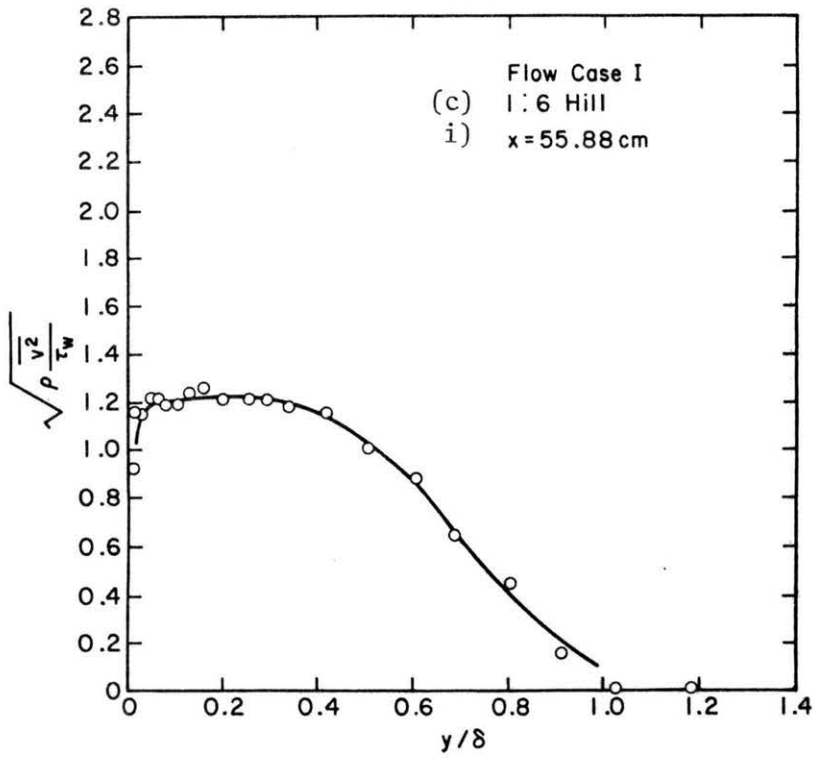


Figure B25. (continued) $\sqrt{\rho \frac{v^2}{\tau_w}}$ profiles Flow Case I

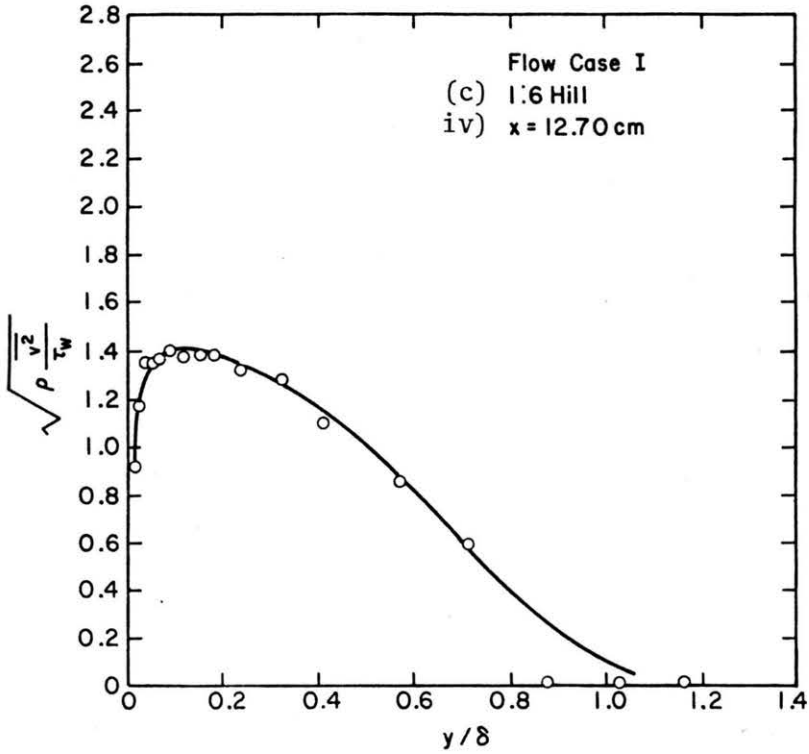
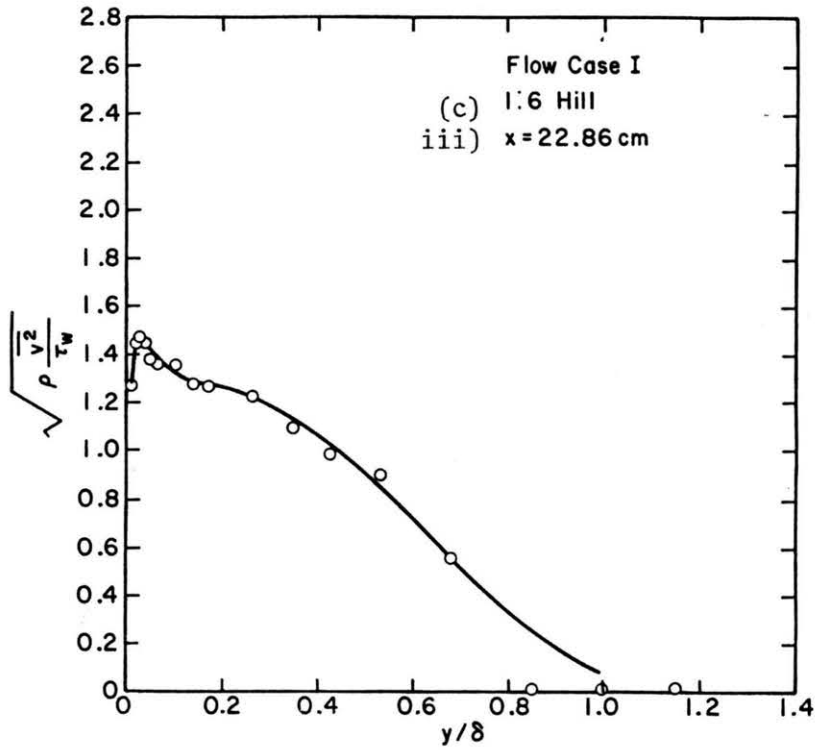


Figure B25. (continued) $\sqrt{\rho \frac{v^2}{\tau_w}}$ profiles Flow Case I

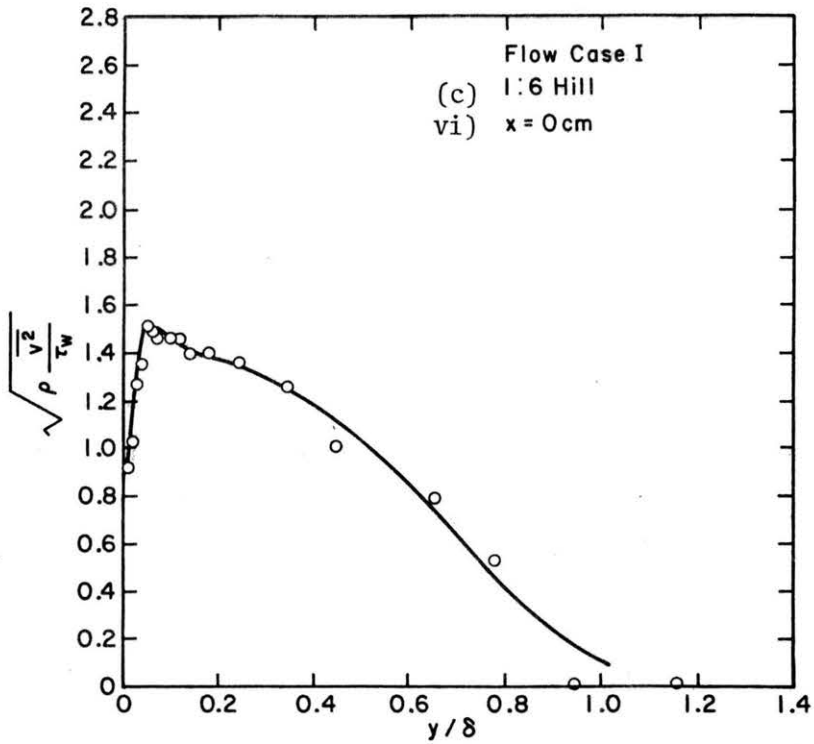
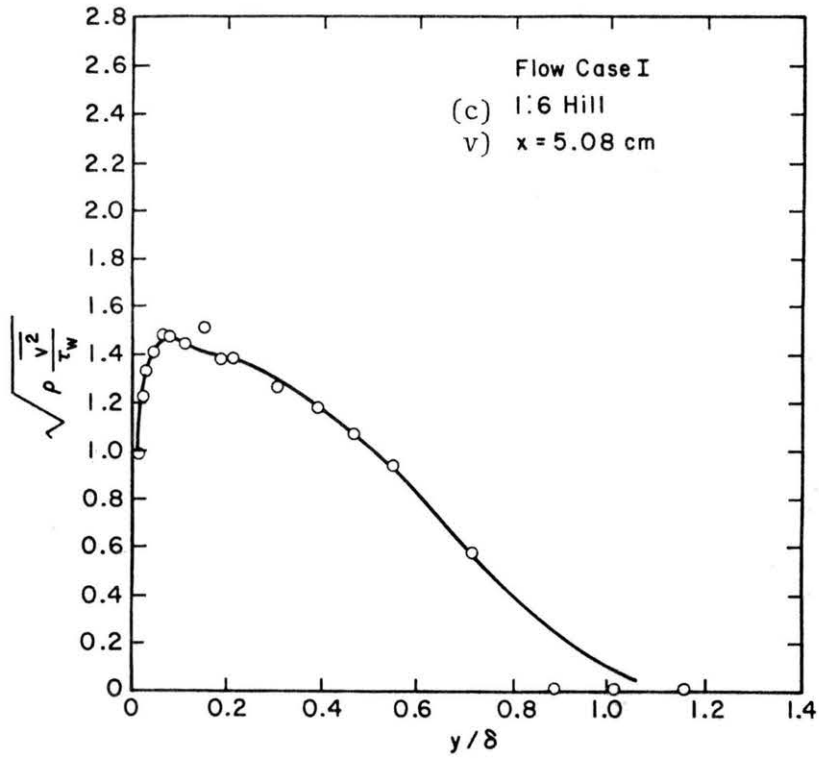


Figure B25. (concluded) $\sqrt{\rho} \frac{v^2}{\tau_w}$ profiles Flow Case I.

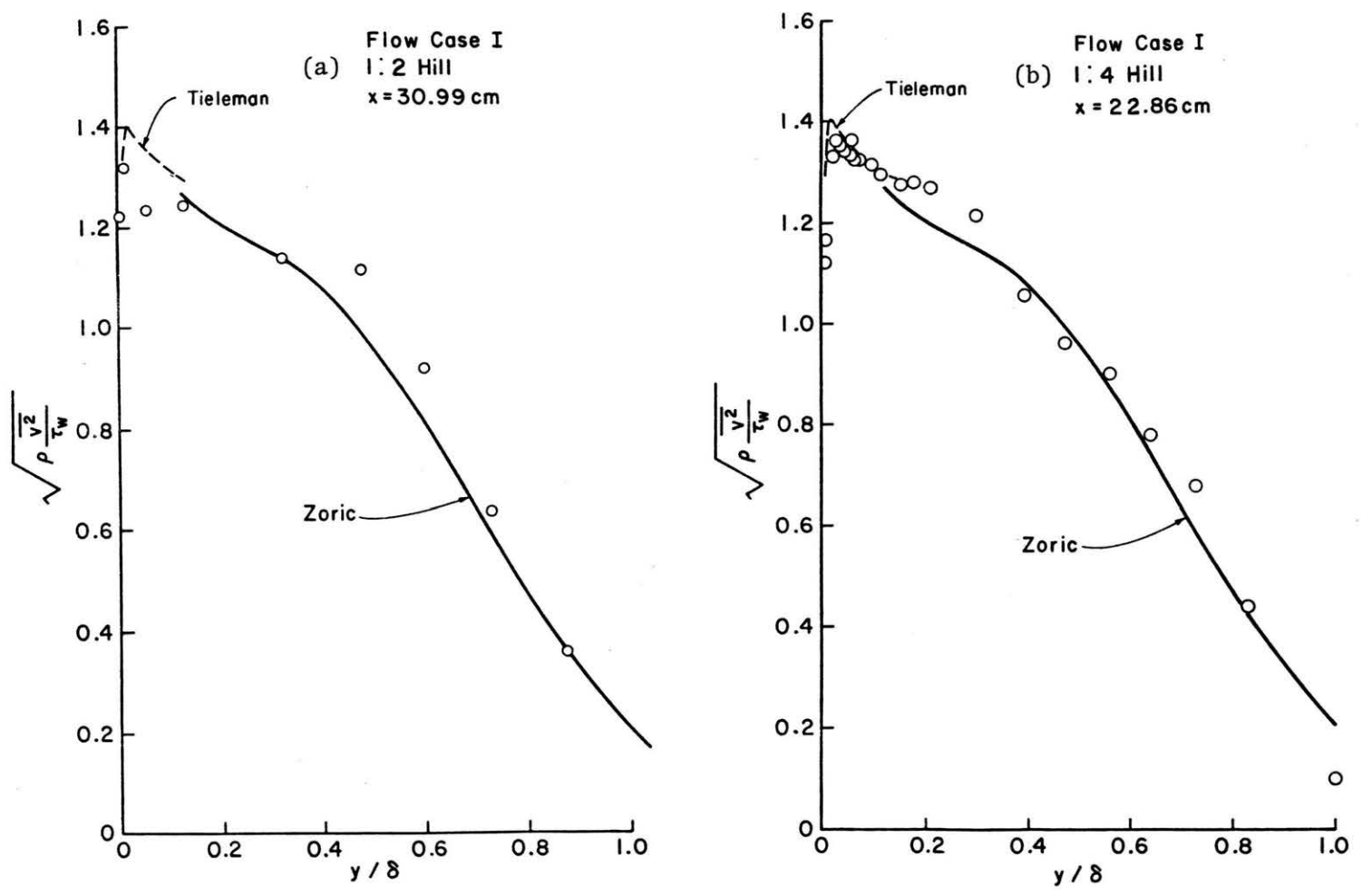


Figure B26. Comparison of $\sqrt{\rho \frac{v^2}{\tau_w}}$ measurements to those of Zoric and Tieleman. Flow Case I.

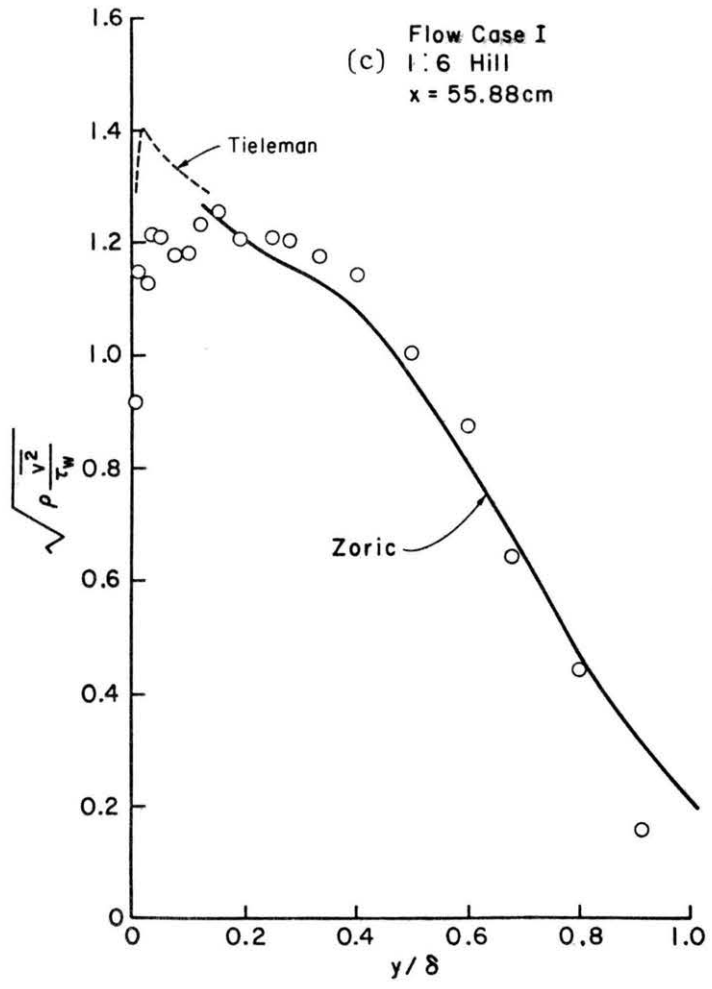


Figure B26. (concluded) Comparison of $\sqrt{\rho \frac{v^2}{\tau_w}}$ measurements to those of Zoric and Tieleman. Flow Case I

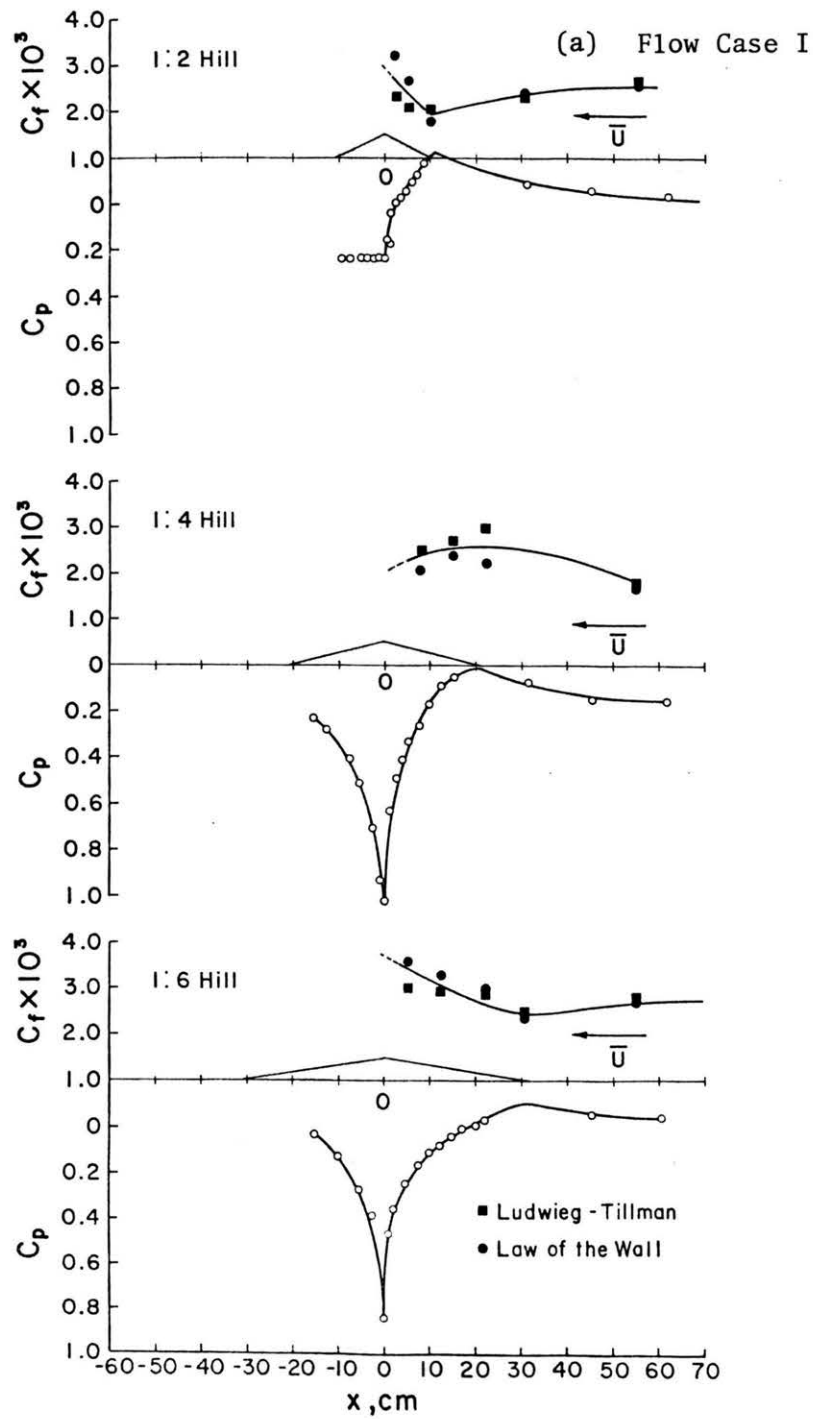


Figure B27. Wall, shear stress, and static pressure distribution

(b) Flow Case II

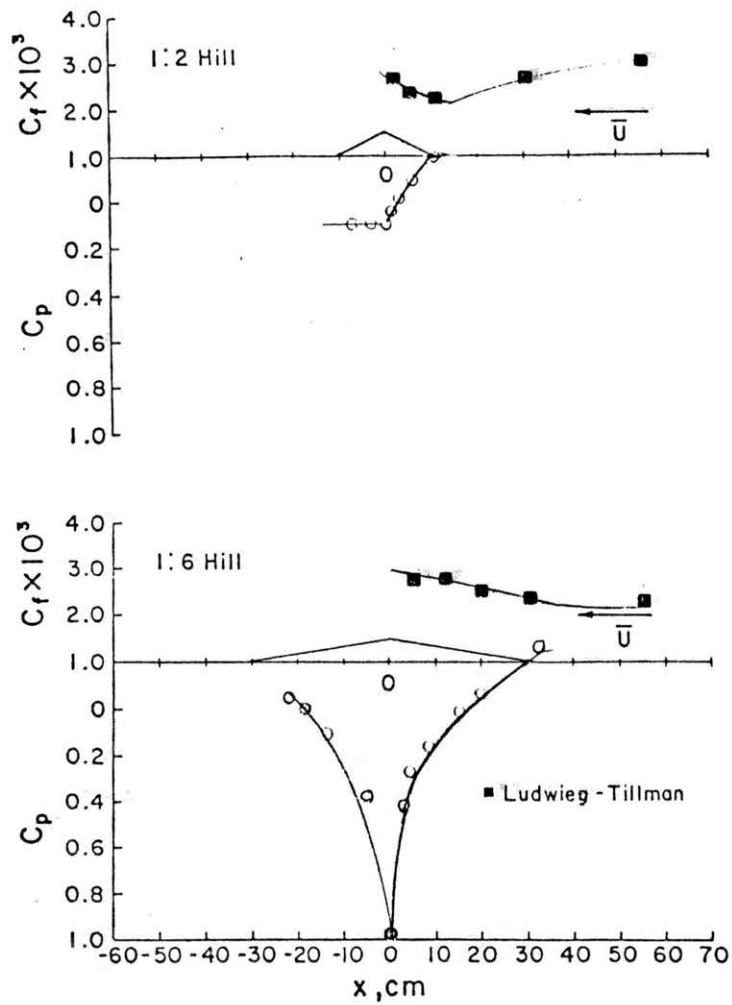


Figure B27. (concluded) Wall, shear stress, and static pressure distribution

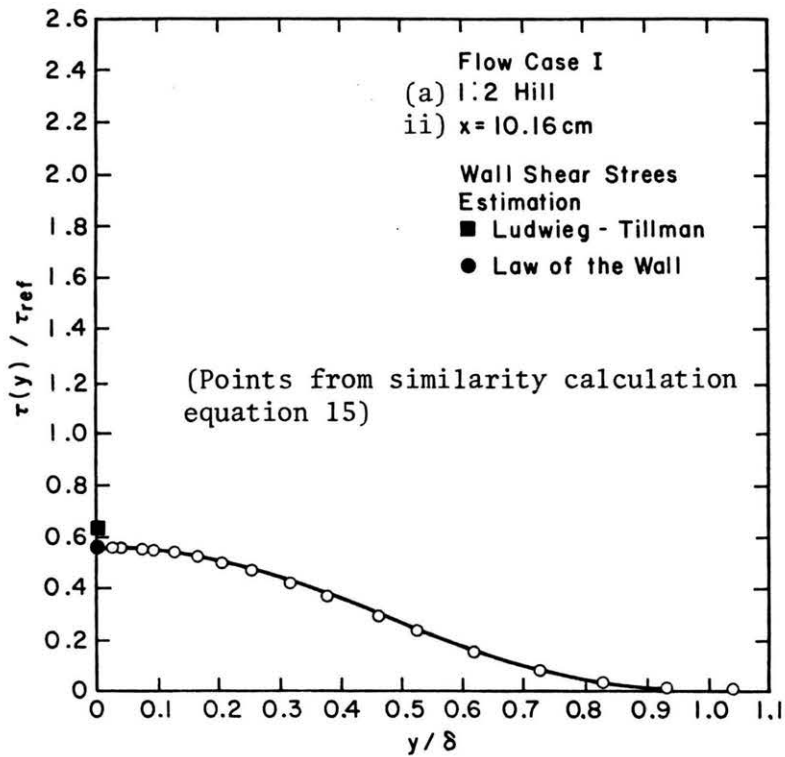
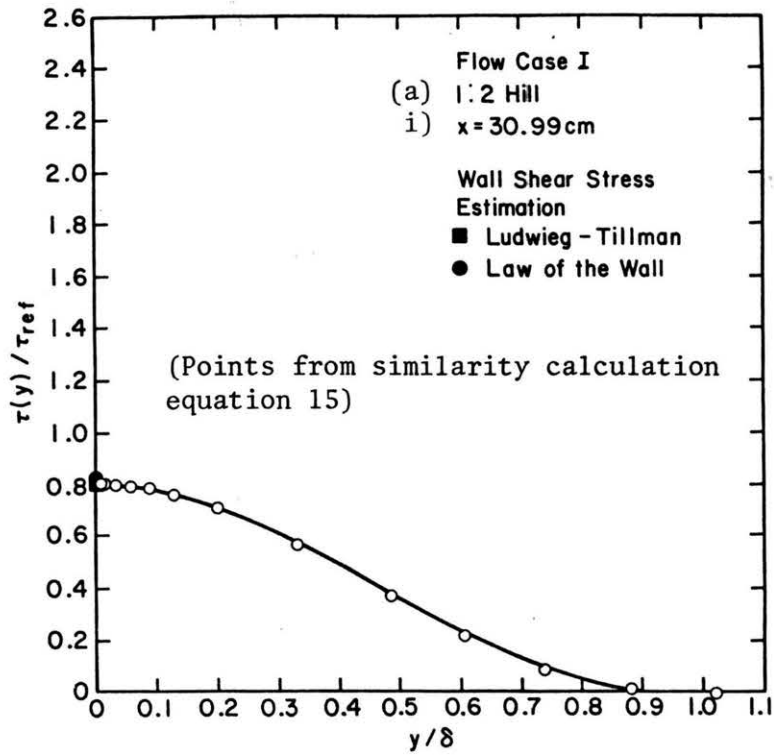


Figure B28. Shear stress distribution Flow Case I

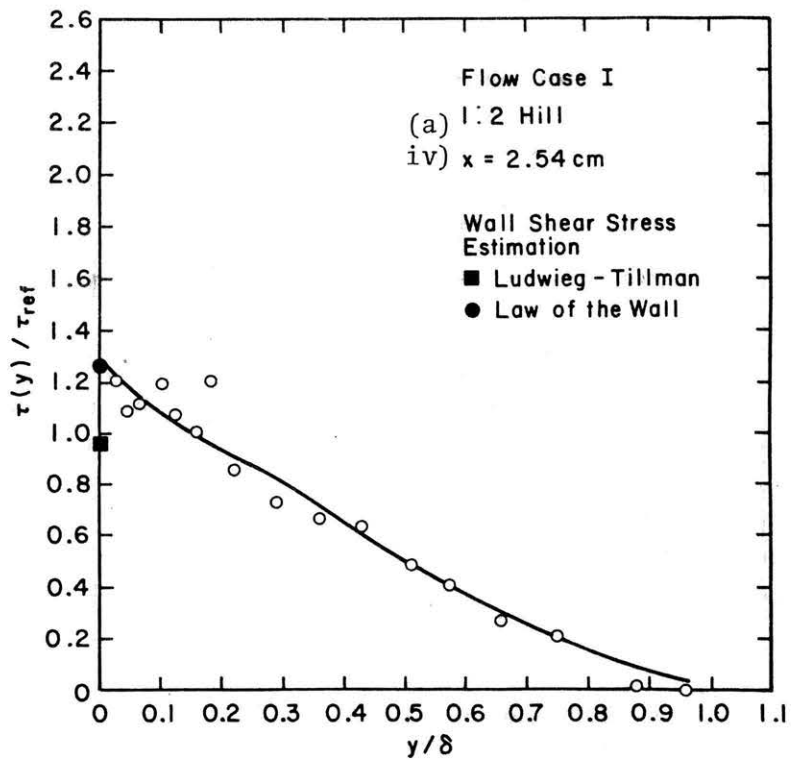
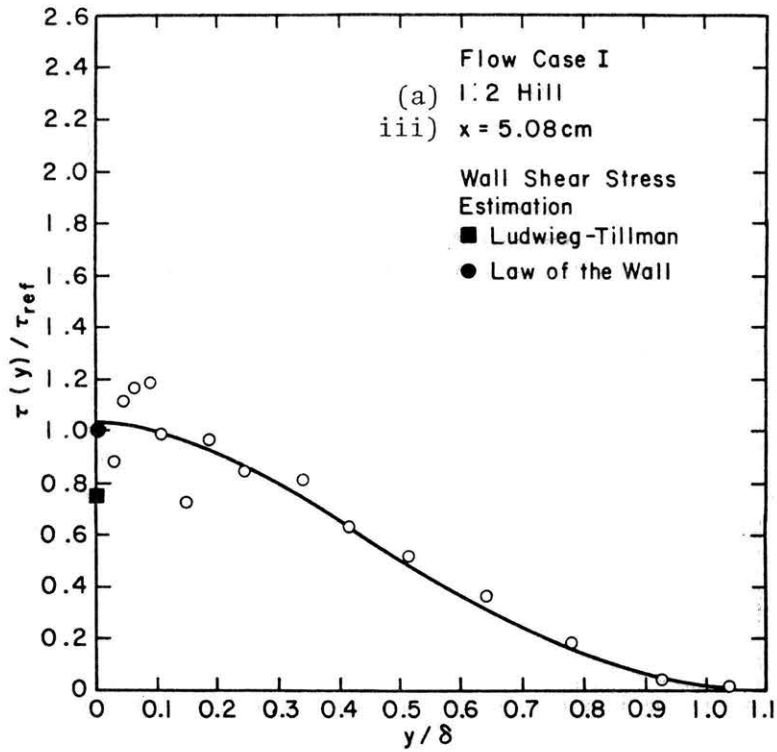


Figure B28. (continued) Shear stress distribution Flow Case I

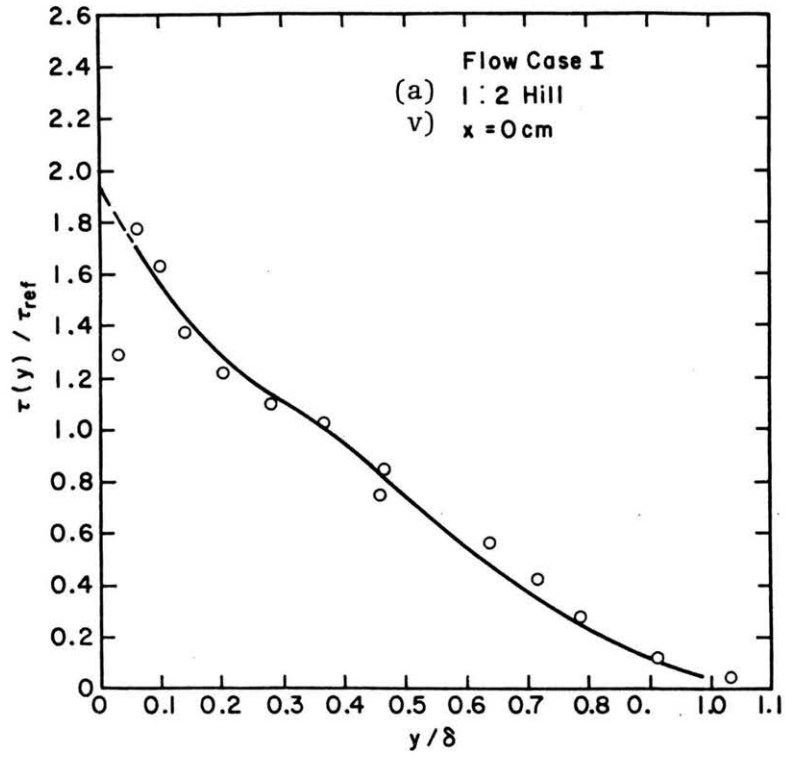


Figure B28. (continued) Shear stress distribution Flow Case I

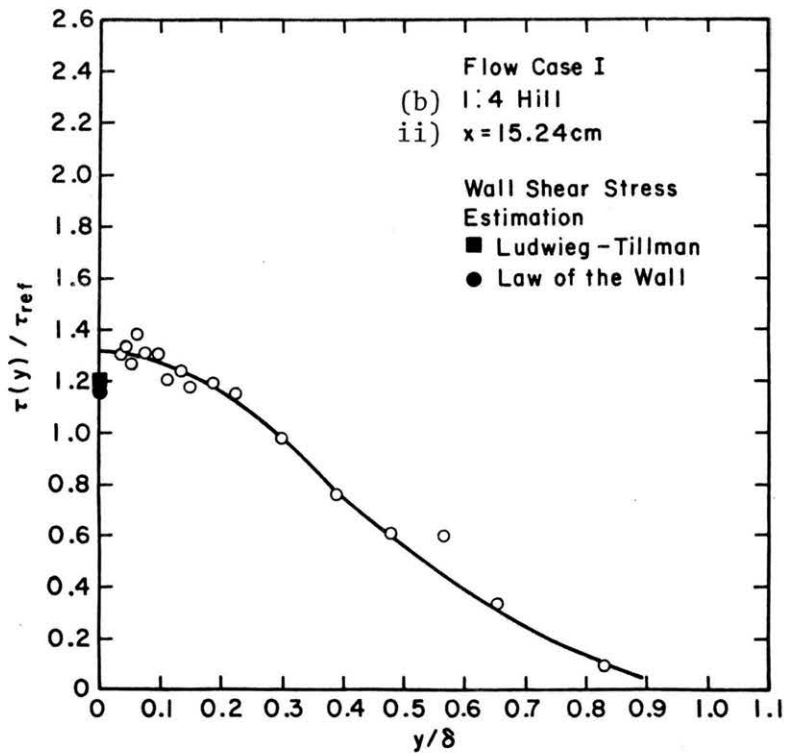
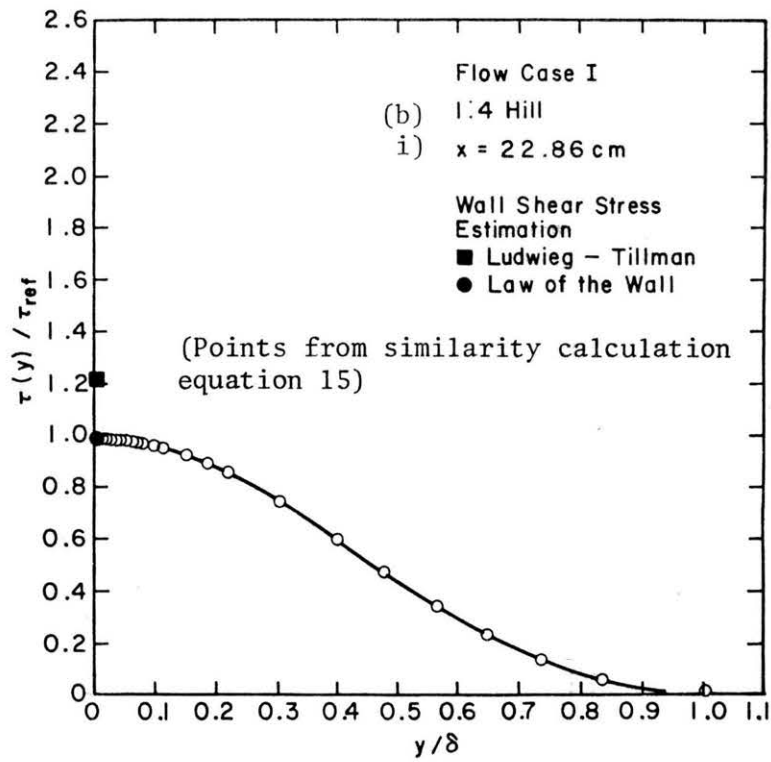


Figure B28. (continued) Shear stress distribution Flow Case I

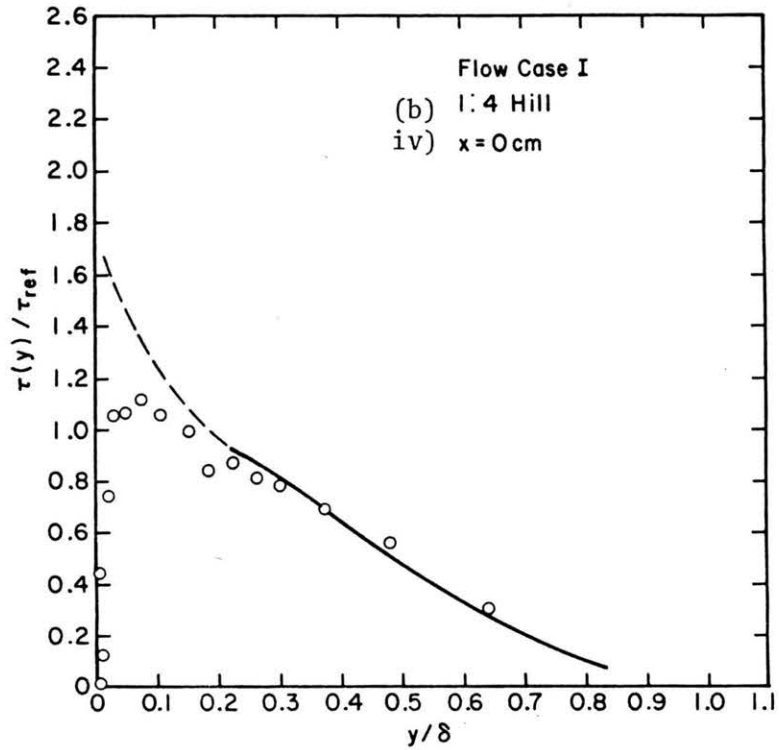
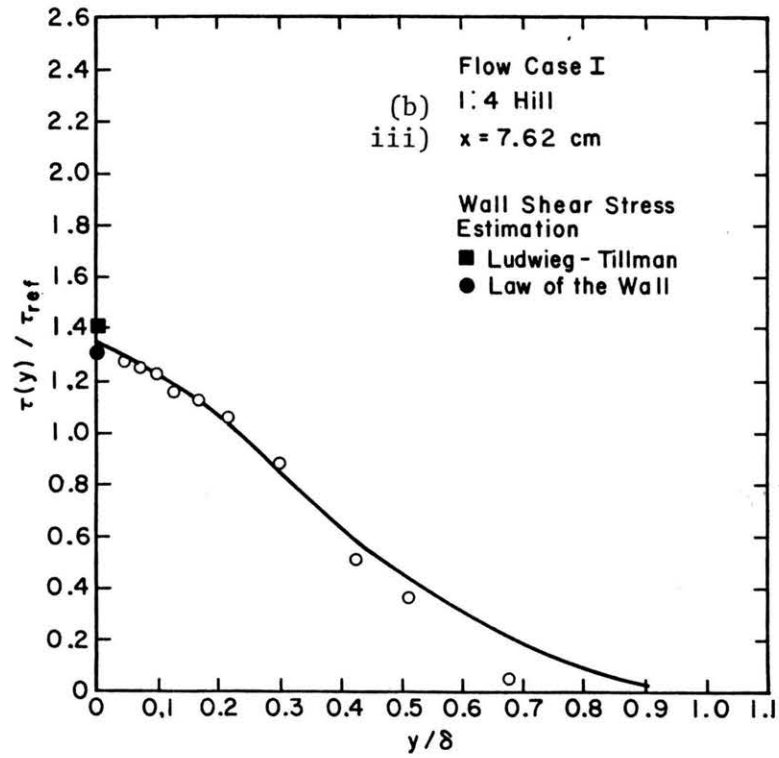


Figure B28. (continued) Shear stress distribution Flow Case I

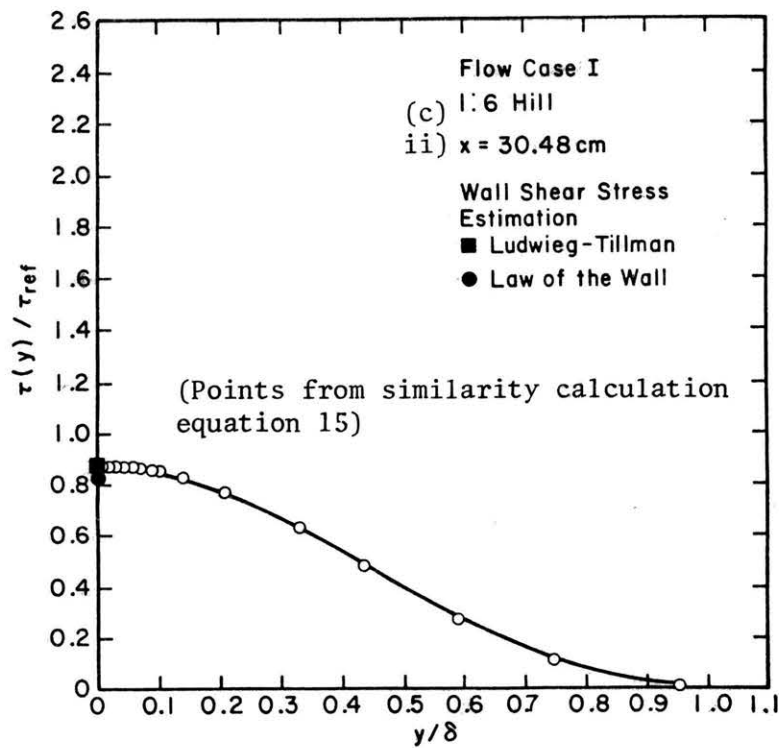
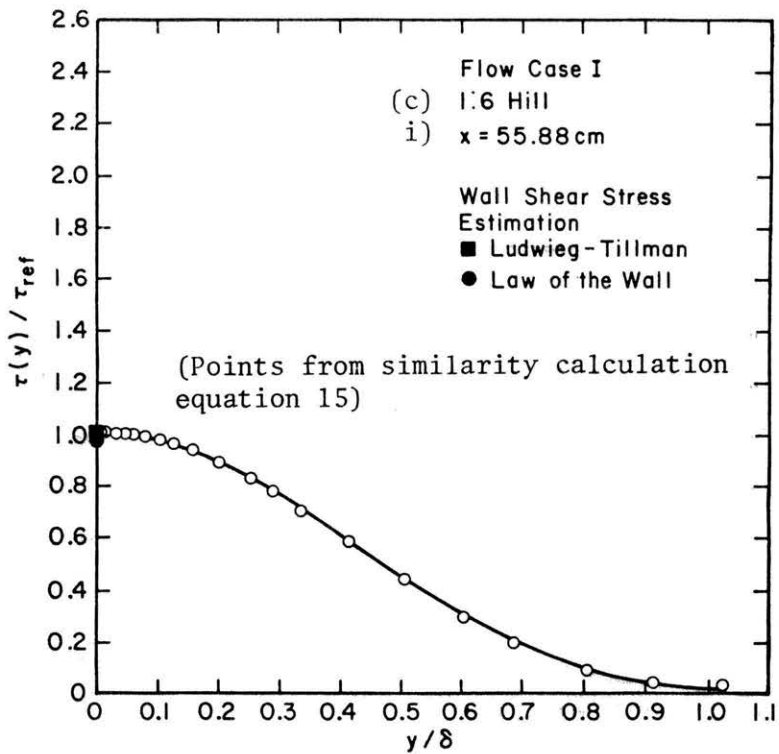


Figure B28. (continued) Shear stress distribution Flow Case I

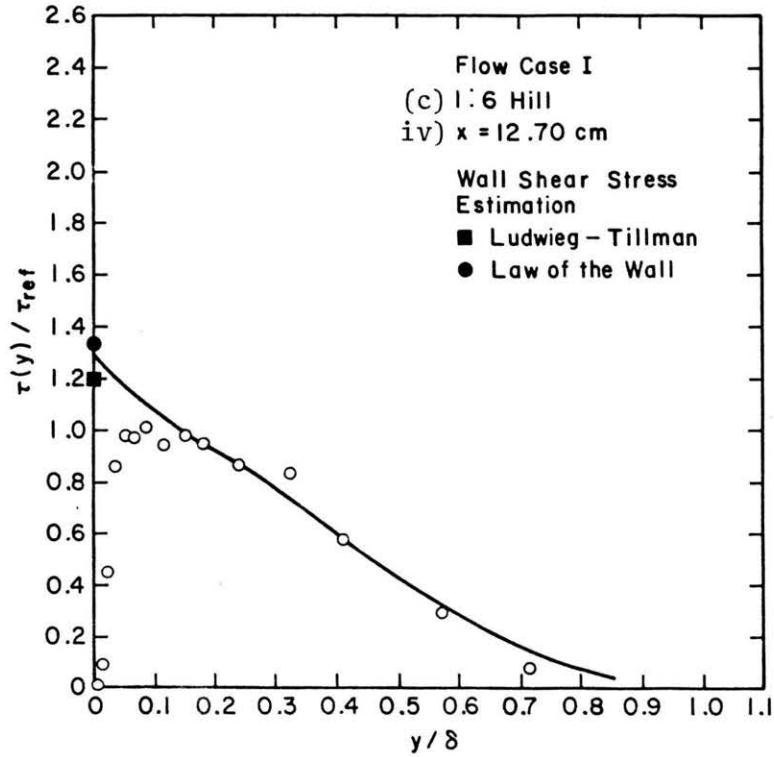
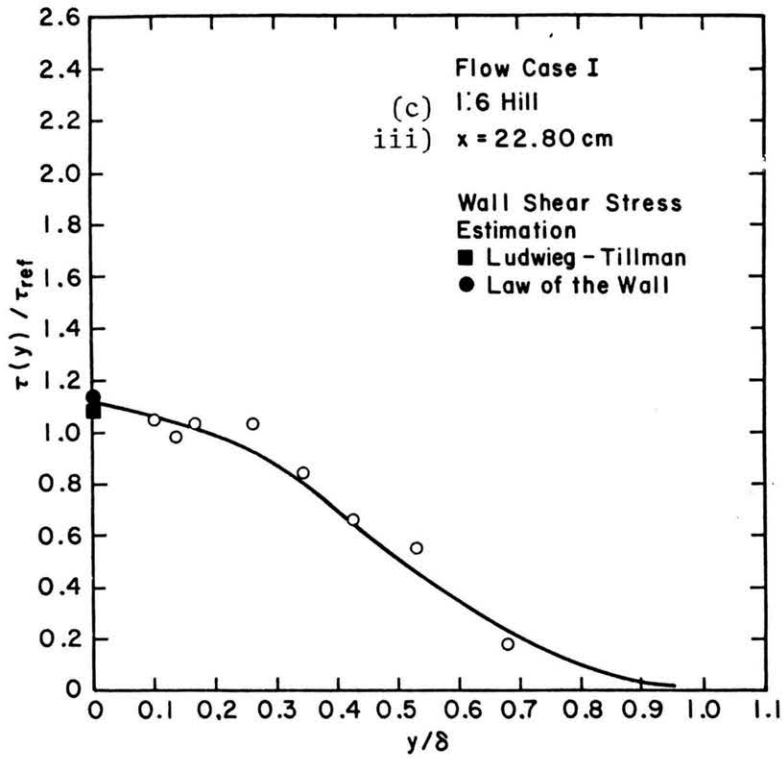


Figure B28. (continued) Shear stress distribution Flow Case I

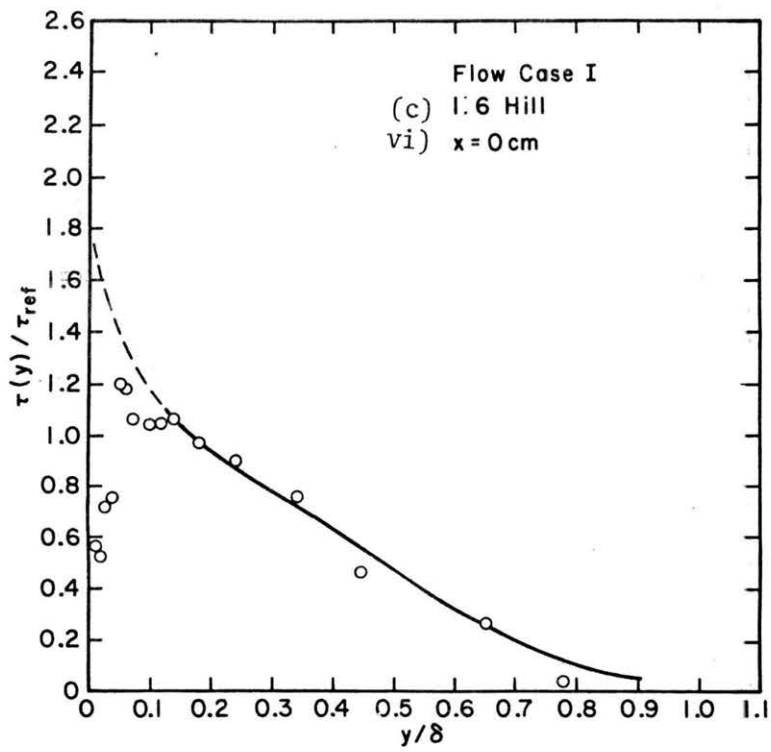
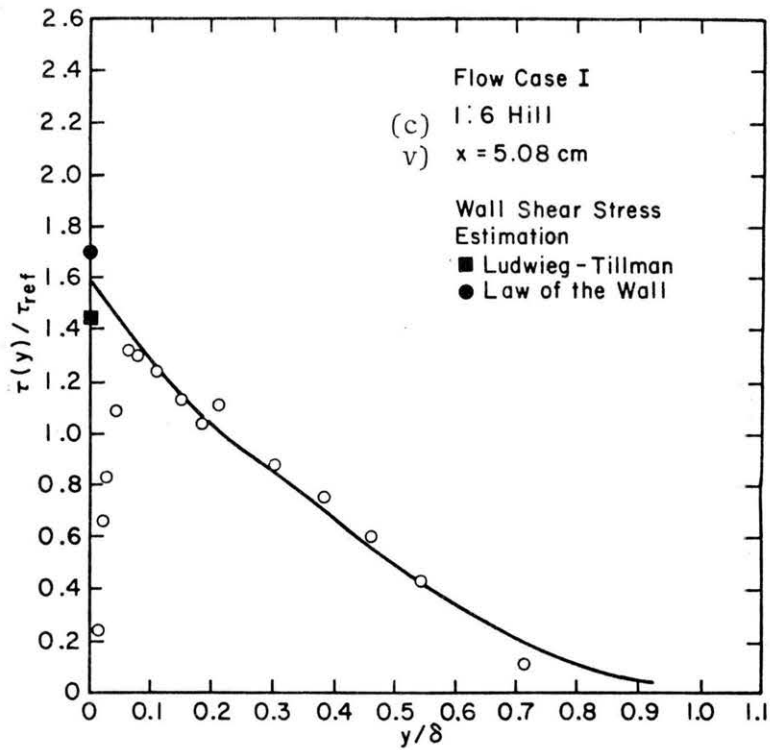


Figure B28. (concluded) Shear stress distribution Flow Case I.

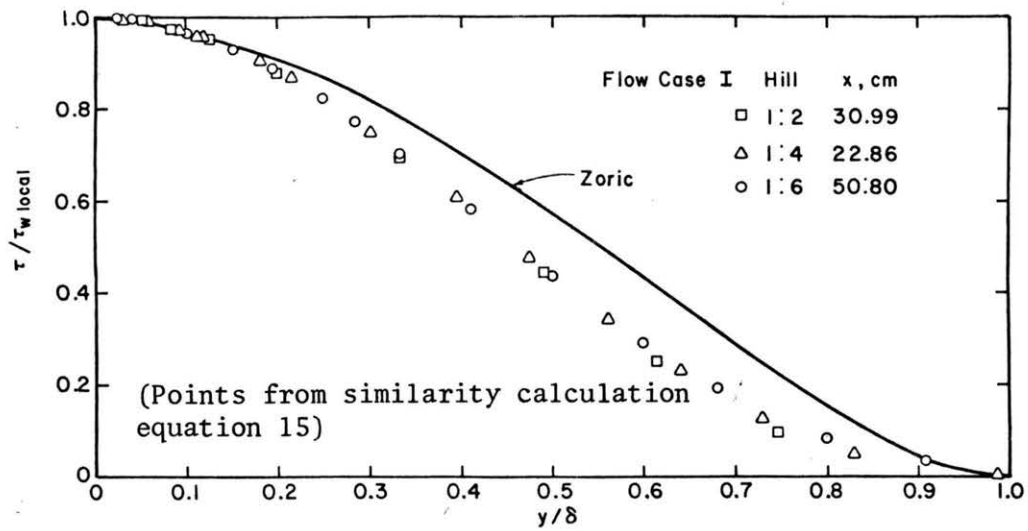


Figure B29. Comparison of upstream shear stress distribution to that of Zoric. Flow Case I.

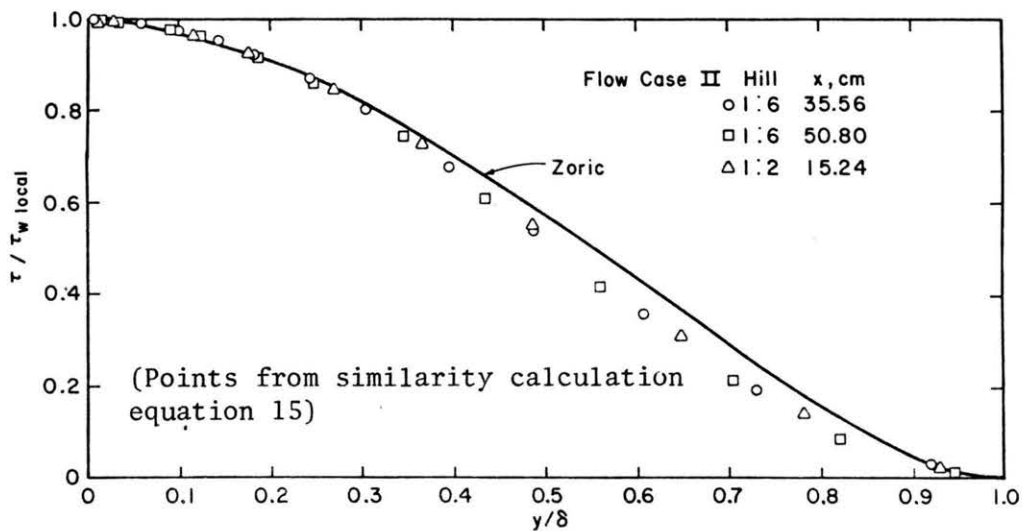


Figure B30. Comparison of upstream shear stress distribution to that of Zoric. Flow Case II

APPENDIX C

MEASUREMENTS OF MEAN AND TURBULENT VELOCITIES AND TEMPERATURE FOR THERMALLY STRATIFIED FLOWS

By M. A. Rider, R. J. B. Bouwmeester, V. A. Sandborn and R. N. Meroney

SUMMARY

A series of mean and turbulent velocity and temperature profiles were taken over the forward facing surface of two-dimensional, triangular ridges. The ridges have slopes of 1 to 4 and 1 to 6, with crest heights of 5 cm. The freestream velocity was varied from 2.8 to 8.9 c/sec with a corresponding variation in Richardson number from 8×10^{-2} to 4×10^{-3} . The freestream temperature was held constant at a nominal value of 38°C and the surface temperature was set at 0°C.

INTRODUCTION

Previous wind-tunnel studies at the speedup over two-dimensional ridges indicate that they are ideal shapes to employ as amplifiers of wind for wind-power sites. The present study was conducted as a part of this overall evaluation of two-dimensional ridges. It was intended as a check on the effect of thermal, stable, stratification on the airflow over two-dimensional ridges.

MEASUREMENTS

The measurements were made in the wind tunnel described in detail by Rider and Sandborn (see Appendix B, Figure B8). With the exception of the heated airstream and the cooled surface, the test setup was identical to the "Flow Case II" conditions of Rider and Sandborn. For the present study the plastic, triangular ridges are set directly on the metal floor of the wind tunnel. The floor is cooled by circulating brine through coils mounted in the floor. Thermocouples imbedded in the floor were used to adjust the brine flow to produce a uniform 0°C temperature along the surface upstream of the ridge. The freestream temperature was controlled by a heat exchanger in the return flow leg of the tunnel.

Measurements of the local dynamic pressure were made with a Kieh1 probe and the local static pressure were measured at the model surface. Both a small-diameter resistance thermometer and a thermistor probe were used to evaluate the turbulent velocity. Mean velocity profiles were evaluated from the dynamic pressure surveys and calculation of the local density from the temperature measurements. Values of the mean and turbulent velocities and temperatures are given in Table CI and CII and are plotted in Figures C1 through C4. For the low velocities of the present tests it was assumed that the recovery temperature of the

resistance thermometer and the thermistor was equal to the total temperature. The total temperature in turn was taken as the static temperature.

Temperature fluctuations were evaluated directly from the resistance thermometer. The detection current through the resistance wire was held constant. The temperature fluctuation was determined from the root mean square voltage fluctuation across the wire from the relation

$$\sqrt{\overline{t^2}} = \frac{dT}{dE} \sqrt{\overline{e^2}} = I/R_0 \alpha \sqrt{\overline{e^2}} \quad (C1)$$

where I is the wire current; R_0 is the wire resistance at temperature T_0 ; α is the thermal coefficient of resistance of the wire material. In actual use, the value of $I/R_0 \alpha$ was determined by calibrating the resistance thermometer in the freestream by varying the air temperature. The value of dT/dE was determined directly from the calibration curve. The resistance thermometer was a platinum - 10% rhodium wire, 5×10^{-5} cm in diameter wire. The bare wire without electronic compensation is able to follow temperature fluctuations of the order of 3000 hertz in still air. With the increased heat transfer because of the flow, the transient response of the resistance thermometer will be increased several times over that in still air. Thus, no external compensation for thermal inertia of the resistance thermometer was required in the present study. No corrections were applied for end effects as a result of wire supports.

The hot-wire anemometer was operated at several different overheat temperatures in order to vary the velocity and temperature sensitivity. The output of the hot wire is both a function of velocity and temperature, with fluctuation voltage given as:

$$e = \frac{dE}{dU} u + \frac{dE}{dT} t' \quad (C2)$$

where E is wire total voltage, U flow velocity, T total temperature, e the ac component of the wire voltage, u the fluctuation of velocity in the direction of the mean flow, and t' the fluctuation in temperature. The statistical measured root mean square, or for convenience, mean square voltage ($\overline{e^2}$) is:

$$\overline{e^2} = S_u^2 \overline{u^2} + 2S_u S_t \overline{ut'} + S_t^2 \overline{t'^2} \quad (C3)$$

By varying the hot-wire temperature the transducer sensitivity to velocity, $S_u (\equiv \frac{dE}{dU})$ varies while the temperature sensitivity $S_t (\equiv \frac{dE}{dT})$ changes only slightly. Operation at three different overheats allow the three turbulent quantities to be evaluated. For the present measurements, the temperature fluctuations $\sqrt{t'^2}$ were determined directly from the resistance thermometer, so only two overheats were required to evaluate $\sqrt{u'^2}$ and $\overline{ut'}$. At large values of overheat, the wire is more sensitive to velocity than to temperature, so that accurate values of $\sqrt{u'^2}$ are obtained. For the present data the values of $\overline{ut'}$ obtained were not as consistent as would be desired; thus, only the velocity component was evaluated in detail. At the present it does not appear that the cross-correlation ($\overline{ut'}$) is of major interest in wind-power applications, so accurate evaluation of this term was not pursued. Only values of $\sqrt{t'^2}$ are given.

RESULTS

The mean velocity distributions measured over the two ridges are shown in Figures C1 and C2. The profiles are similar to those measured in the neutral flow studies. Although the speedup ratios are nearly the same for the different approach velocities, the shape of the profile at the crest is different (see Figures C1a, b and c). The desirable, near constant, velocity variation at the crest for a freestream velocity of 8.9 m/sec is not present at the lower velocities. For wind-power applications, it is desirable to have a constant velocity over the vertical distance of the propeller blade. Obviously it is more desirable to have the constant velocity profile at the higher velocities as this will produce less of a strain on the bearings.

The mean temperature profiles are shown in Figures C3 and C4. The ridges compared to a level surface increase the temperature near the crest much as they do with the velocity. The increase in temperature near the surface does not appear to be as pronounced as the wind effect. The increased temperature will produce a decrease in the local density, which will reduce the overall power available from a wind turbine. This reduction in power as a result of the decrease in density would appear to be very small compared to the increase in power as a result of the amplification of the flow velocity over two-dimensional ridges. The data indicate that the thermal stratification may have a slightly more pronounced effect on the 1-to-6 triangular ridge than on the 1-to-4 ridge.

Figures C5 and C6 show the variation of the longitudinal turbulent velocity above the ridges. Details of the turbulent velocity variations for the neutral case were given in Appendix B. It was noted that the fluctuating longitudinal velocity decreased as the crest was approached

much as would be predicted for a contraction. The stably stratified data show the same effect. Near the surface the velocity fluctuations are found to decrease at the crest. The effect is much more pronounced for the larger Richardson numbers. The "damping" of the turbulence first by the contraction effect of the ridge and secondly by the stratification is a desirable feature for the design of wind-power systems.

Figures C7 and C8 show the variations of the temperature fluctuations. The magnitude of the temperature fluctuations appears to remain nearly constant across the flow independent of the location on the ridge.

Obviously the turbulent temperature "intensity" $\sqrt{t'^2}/T$ will decrease at the crest of the ridges. In general the temperature fluctuations are a passive scalar quantity which is unaffected by the contraction effect of the ridges.

TABLE CI 1 TO 4 RIDGE DATA

a) U AT INFINITY = 8.90 M/S
 RICHARDSON NO. = .440E-02

UPSTREAM AT X = 61 CM

y (CM)	U (M/S)	T (C)	URMS (M/S)	TRMS (C)
.20	4.40	20.00	.94	3.46
.99	5.17	26.26	.71	2.93
2.46	5.90	30.19	.66	2.67
4.17	6.35	32.11	.84	2.43
5.99	6.64	33.50	.73	2.22
9.60	6.99	35.10	.72	1.94
16.56	7.47	37.26	.70	1.61
27.20	8.29	39.40	.44	1.21
37.82	8.77	41.04	****	.78
53.47	8.90	42.26	.07	.23

FOOT AT X = 20 CM

y (CM)	U (M/S)	T (C)	URMS (M/S)	TRMS (C)
.20	3.03	19.95	1.03	3.12
.38	3.51	23.38	.83	3.00
.89	4.09	25.29	.77	2.81
1.27	4.45	26.08	.75	2.81
1.98	4.91	28.16	.67	2.78
3.73	5.53	30.26	.69	2.66
5.66	6.15	32.05	.75	2.42
9.00	6.60	33.62	.70	2.10
12.60	7.14	35.18	.68	1.90
16.08	7.46	36.27	.64	1.69
23.14	8.06	38.12	.62	1.44
31.98	8.60	39.68	.44	1.14
42.57	8.95	41.05	.24	.62
52.88	9.00	42.37	.04	.33

CREST AT X = 0.0 CM

y (CM)	U (M/S)	T (C)	URMS (M/S)	TRMS (C)
.23	8.23	27.76	.79	2.31
.38	8.44	27.81	.79	2.32
.64	8.35	28.30	.77	2.49
1.19	8.34	29.61	.80	2.70
1.91	8.27	30.60	.71	2.64
2.77	8.16	31.95	.72	2.37
4.22	8.11	32.92	.72	2.21
7.70	8.03	34.79	.68	1.92
11.20	8.13	36.02	.63	1.67
18.34	8.54	37.92	.54	1.37
25.40	8.83	39.09	.46	1.19
32.44	9.03	40.17	.33	.86
42.77	9.06	41.47	.10	.56
49.68	9.03	41.89	.07	.24

TABLE CI 1 TO 4 RIDGE DATA

b) U AT INFINITY = 5.80 M/S
 RICHARDSON NO. = .850E-02

UPSTREAM AT X = 61 CM

Y (CM)	U (M/S)	T (C)	URMS (M/S)	TRMS (C)
.20	2.75	19.32	.89	.14
.29	2.86	20.37	.81	.08
.42	2.97	21.51	.74	.04
.67	3.05	22.63	.69	.03
1.18	3.28	24.13	.62	.02
2.20	3.57	26.15	.66	.02
3.29	3.77	27.39	.60	.02
4.34	3.95	29.09	.46	.02
5.39	4.30	31.11	.47	.02
6.40	4.62	33.05	.38	.02
7.43	4.97	34.69	.35	.02
8.48	5.26	36.50	.33	.02
9.53	5.51	37.73	.31	.02
10.57	5.67	38.37	.30	.02
11.61	5.71	38.93	.30	.02

FOOT AT X = 20 CM

y (CM)	U (M/S)	T (C)	URMS (M/S)	TRMS (C)
.20	1.94	15.39	.72	.81
.28	2.04	15.51	.66	.79
.43	2.05	15.70	.78	.86
.66	2.25	18.39	.61	.85
1.17	2.60	20.81	.51	.65
2.18	3.01	23.12	.46	.50
3.28	3.22	24.72	.39	.40
4.36	3.60	26.46	***	.23
5.43	3.99	28.48	.33	.02
6.48	4.55	30.77	.30	.81
7.53	4.97	32.51	.25	.56
8.57	5.37	34.25	.22	.37
9.66	5.70	35.55	.19	.00
10.76	5.87	36.55	.07	.65
11.81	5.89	36.94	.03	.26

TABLE CI 1 TO 4 RIDGE DATA

b) (concluded) U AT INFINITY = 5.80 M/S
 RICHARDSON NO. = .850E-02

CENTER AT X = 10 CM

y (CM)	U (M/S)	T (C)	URMS (M/S)	TRMS (C)
.41	3.10	21.14	.39	2.42
.48	3.14	21.32	.37	2.48
.74	3.28	21.85	.42	2.59
1.02	3.37	22.38	.38	2.62
1.45	3.52	23.57	.34	2.67
2.18	3.78	24.61	.42	2.59
3.35	3.90	26.03	.35	2.77
5.79	4.09	28.00	.37	2.19
10.31	4.55	30.02	.30	1.91
15.60	4.88	31.94	.38	1.69
20.88	5.15	33.63	.29	1.50
27.94	5.42	35.06	.24	1.23
38.53	5.71	36.86	.22	.75
51.94	5.77	37.82	*.22	.23

CREST AT X = 0.0 CM

y (CM)	U (M/S)	T (C)	URMS (M/S)	TRMS (C)
.20	4.76	23.16	.32	2.26
.28	4.81	23.43	.34	2.34
.38	4.72	23.69	.33	2.49
.79	4.74	24.44	.33	2.56
1.14	4.76	24.87	.35	2.55
1.68	4.68	25.55	.36	2.49
2.21	4.88	26.64	.34	2.44
3.33	4.83	27.58	.35	2.46
5.36	4.86	29.14	.30	1.98
7.65	4.94	30.33	.30	1.88
11.02	5.03	31.94	.28	1.50
18.14	5.22	33.35	.26	1.25
25.12	5.54	35.35	.25	.75
35.74	5.80	36.90	.12	.76

TABLE CI 1 TO 4 RIDGE DATA

c) U AT INFINITY = 2.80 M/S
 RICHARDSON NO. = .800E-01

UPSTREAM AT X = 61 CM

y (CM)	U (M/S)	T (C)	URMS (M/S)	TRMS (C)
.20	1.03	12.02	.50	1.68
.33	1.10	12.65	.67	1.98
.66	1.24	15.62	.37	2.32
1.04	1.33	17.17	.38	2.25
1.78	1.42	18.52	.35	2.04
3.48	1.52	21.08	.31	1.94
5.97	1.75	23.54	.26	1.79
9.50	1.87	25.98	.24	1.64
13.03	2.08	27.93	.22	1.52
16.54	2.21	29.44	.20	1.42
20.06	2.42	31.87	.15	1.25
23.57	2.57	33.80	.17	.97
27.08	2.74	35.31	.05	.47
30.59	2.82	36.11	.04	.33

FOOT AT X = 20 CM

y (CM)	U (M/S)	T (C)	URMS (M/S)	TRMS (C)
.20	.69	18.46	.35	4.11
.28	.68	17.14	***	2.82
.64	.84	16.21	.47	2.02
1.09	.97	17.19	.55	2.01
1.70	1.03	17.36	.45	1.84
2.41	1.17	18.35	.34	1.90
3.12	1.34	19.33	.38	1.31
4.19	1.44	20.41	.35	1.80
5.61	1.49	21.79	.33	1.81
9.09	1.69	24.44	.18	1.69
16.23	2.07	28.07	.19	1.42
23.29	2.30	30.60	.17	1.27
30.33	2.51	32.66	.15	1.11
39.14	2.74	34.38	.09	.64
53.01	2.83	35.37	.02	.20

TABLE CI 1 TO 4 RIDGE DATA

c) (concluded) U AT INFINITY = 2.80 M/S
 RICHARDSON NO. = .800E-01

CENTER AT X = 10 CM

y (CM)	U (M/S)	T (C)	URMS (M/S)	TRMS (C)
.41	1.11	16.05	.35	1.86
.53	1.21	16.49	.34	1.96
.89	1.29	16.73	.35	2.08
1.42	1.36	17.84	.34	2.05
2.54	1.53	19.57	.36	1.97
4.65	1.64	21.76	.27	1.88
6.76	1.79	23.79	.25	1.74
10.29	2.02	26.16	.21	1.61
13.82	2.12	27.89	.18	1.47
20.93	2.38	30.70	.18	1.31
27.91	2.59	32.68	.13	1.11
34.95	2.75	34.07	.11	.77
42.04	2.83	34.92	.05	.43
51.74	2.86	35.55	.04	.36

CREST AT X = 0.0 CM

y (CM)	U (M/S)	T (C)	URMS (M/S)	TRMS (C)
.23	1.88	19.44	.30	1.79
.36	1.89	19.68	.28	1.97
.48	1.83	19.88	.31	2.07
.84	1.94	20.56	.26	2.19
1.32	1.99	21.70	.29	2.43
2.08	2.07	22.69	.29	2.37
4.17	2.08	25.60	.25	2.04
5.97	2.16	27.36	.25	1.90
7.70	2.26	28.84	.22	1.77
11.23	2.42	31.02	.20	1.60
18.29	2.56	34.10	.18	1.38
25.37	2.85	36.21	.15	1.10
33.99	2.92	37.83	.12	.62
48.62	2.92	39.19	.25	.40

TABLE CII 1 TO 6 RIDGE DATA

U AT INFINITY = 5.70 M/S
 RICHARDSON NO. = .160E-01

UPSTREAM AT X = 61 CM

Y (CM)	U (M/S)	T (C)	URMS (M/S)	TRMS (C)
.20	2.17	15.79	1.11	2.82
.30	2.29	15.57	1.16	2.82
.66	2.74	22.05	.74	2.91
1.22	2.95	24.30	.44	2.66
1.75	3.21	26.00	.44	2.57
4.19	3.55	28.88	.33	2.23
6.02	3.82	30.51	.49	2.12
9.50	4.17	32.41	.43	1.91
13.44	4.32	33.47	.34	1.78
16.56	4.59	35.05	.32	1.63
20.62	4.97	37.00	.29	1.40
24.46	5.30	38.64	.19	1.09
29.10	5.66	40.04	.14	.64
34.10	5.71	41.24	***	.37

FOOT AT X = 20 CM

Y (CM)	U (M/S)	T (C)	URMS (M/S)	TRMS (C)
.20	1.76	16.70	1.05	2.92
.30	2.09	19.23	.86	3.12
.66	2.52	22.89	.68	2.84
1.35	2.88	24.84	.60	2.54
2.79	3.28	26.56	.57	2.39
4.90	3.65	29.21	.29	2.18
7.70	3.87	30.41	.42	2.01
11.23	4.26	32.52	.44	1.85
14.96	4.38	32.98	***	1.67
18.39	4.71	34.96	.19	1.57
23.24	4.96	36.27	.38	1.47
30.33	5.31	37.97	.25	1.17
37.49	5.56	38.80	.13	.87
44.17	5.69	39.55	.09	.65
51.21	5.73	40.28	***	.37

TABLE CII 1 10 6 RIDGE DATA

U AT INFINITY = 5.70 M/S
 RICHARDSON NO. = .160E-01

CENTER AT X = 10 CM

y (CM)	U (M/S)	T (C)	URMS (M/S)	TRMS (C)
.32	3.03	22.23	.66	2.30
.51	3.18	23.00	.45	2.52
.69	3.16	23.27	.46	2.57
1.07	3.24	24.08	.41	2.66
1.57	3.38	24.91	.40	2.66
2.62	3.55	26.62	.47	2.60
3.71	3.78	27.82	.41	2.37
6.53	4.09	29.86	.36	2.15
10.08	4.32	32.01	.36	1.91
13.56	4.43	33.25	.36	1.81
20.62	4.83	35.59	.36	1.82
29.44	5.28	37.59	.32	1.82
39.73	5.45	39.01	.22	1.79
51.13	5.71	40.14	.05	.39

CHEST AT X = 0.0 CM

y (CM)	U (M/S)	T (C)	URMS (M/S)	TRMS (C)
.15	4.54	23.17	.53	1.69
.38	4.74	24.14	.34	2.40
.56	4.81	24.44	.37	2.51
.71	4.78	24.78	.35	2.52
1.09	4.71	25.07	.48	2.59
1.60	4.82	25.90	.40	2.69
2.31	4.72	27.21	.34	2.61
3.63	4.62	28.66	.40	2.43
5.66	4.67	29.86	.37	2.00
11.00	4.77	32.88	.34	1.87
18.06	5.10	35.22	.27	1.53
26.85	5.39	36.95	.27	1.23
37.62	5.70	38.78	.25	.81
49.20	0.00	39.92	.09	.39

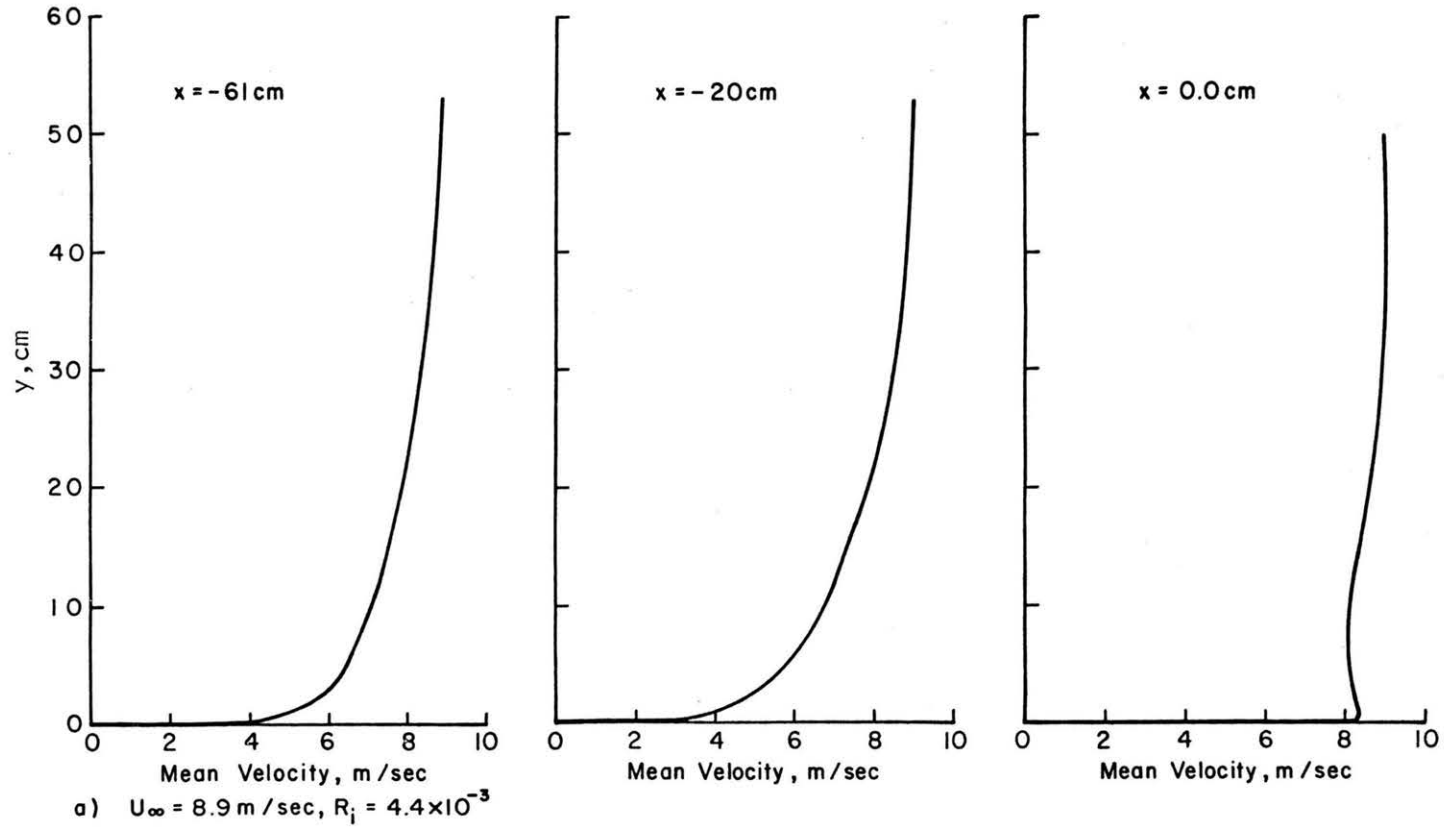


Figure C1 Velocity distributions over the 1 to 4 slope ridge

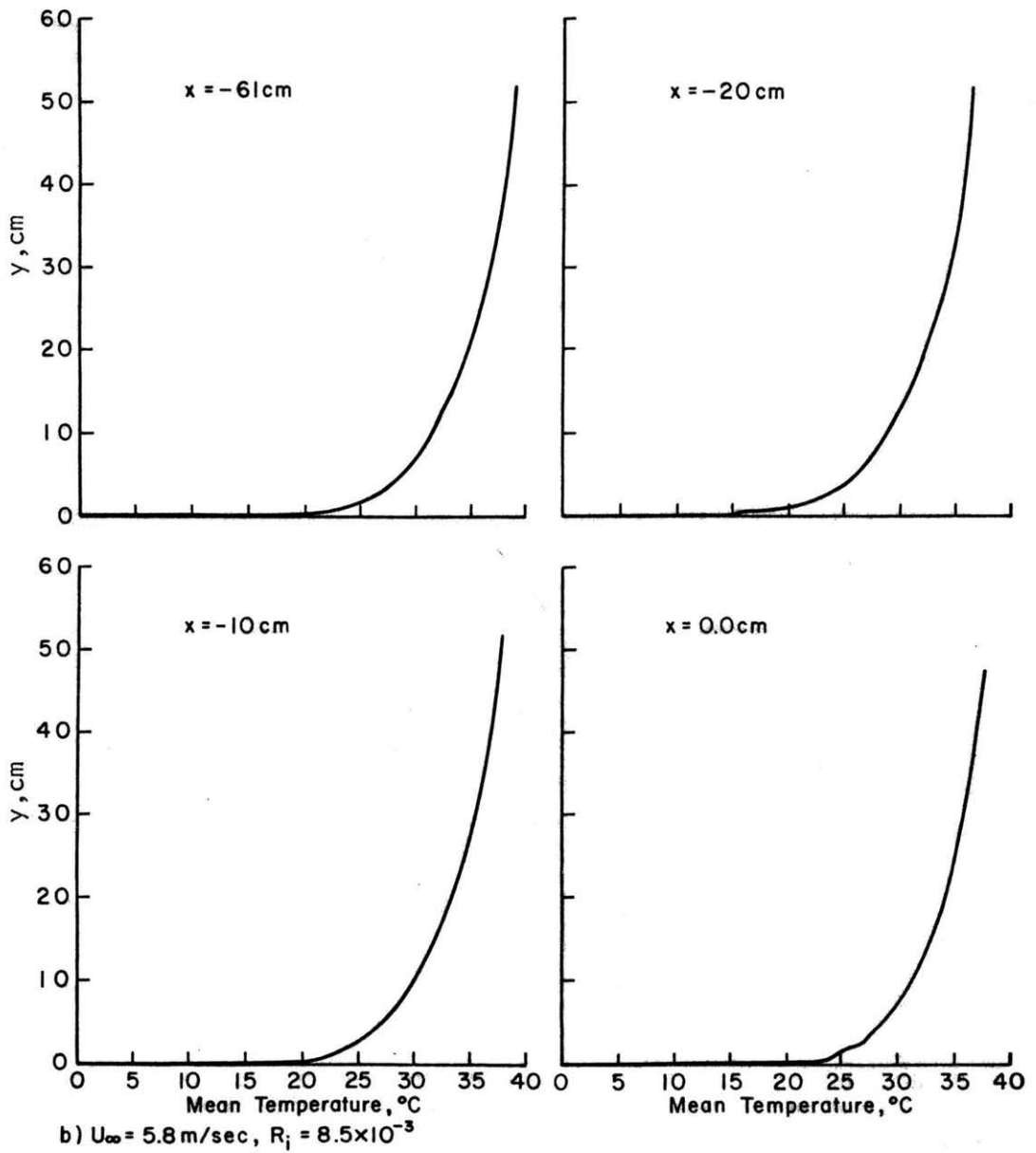


Figure C1 (continued) Velocity distributions over the 1 to 4 slope ridge

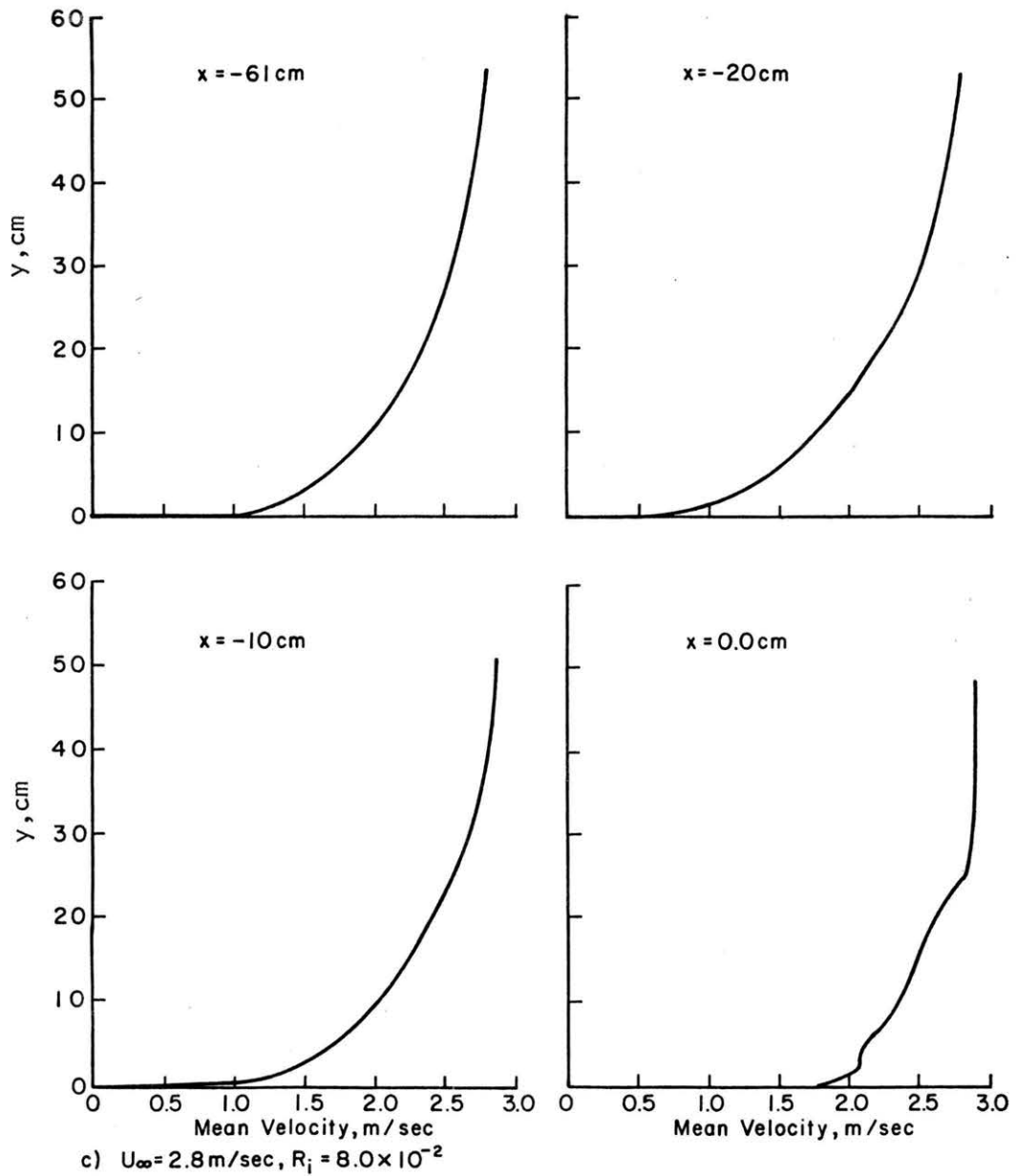


Figure C1 (concluded) Velocity distributions over the 1 to 4 slope ridge.

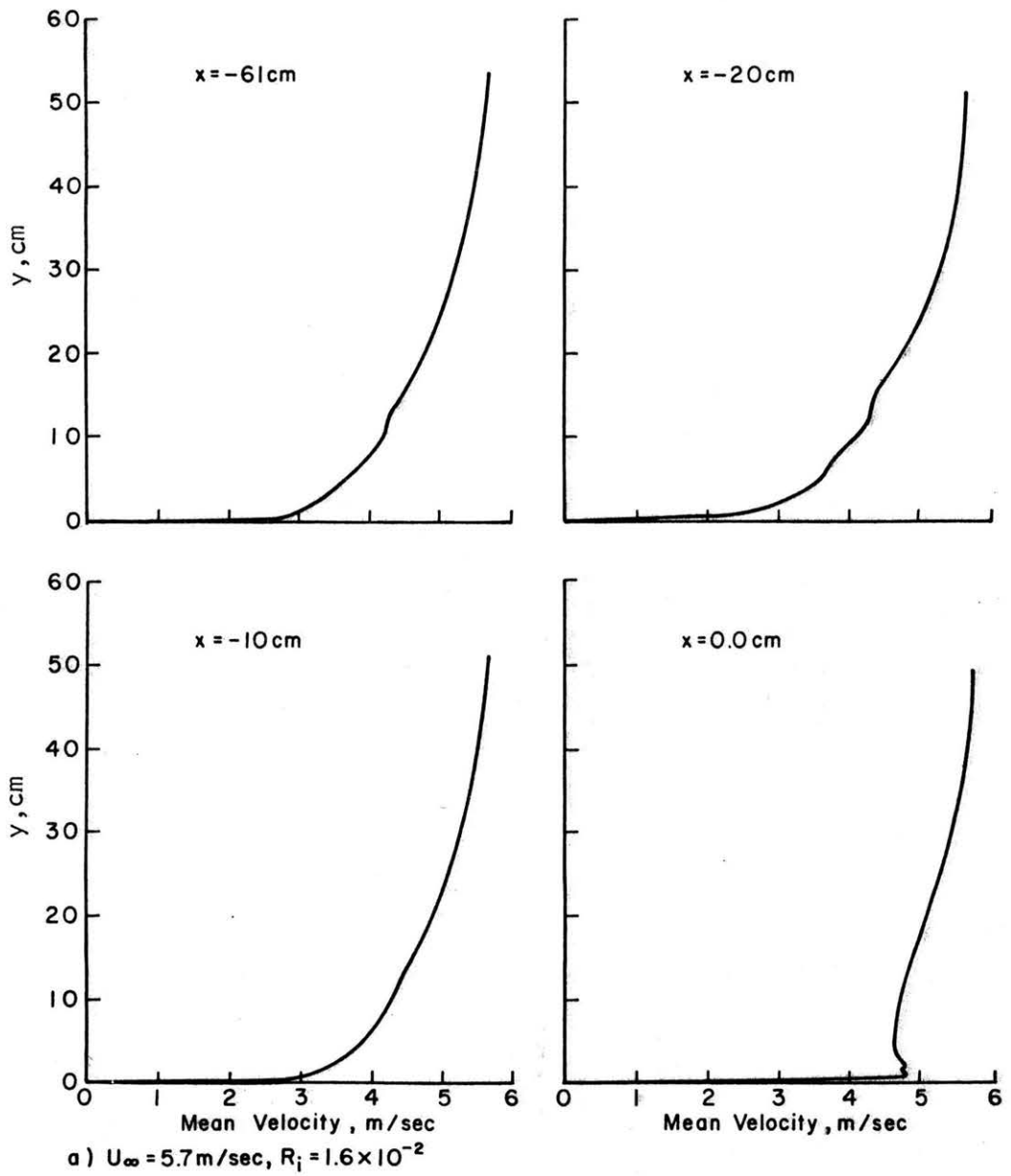


Figure C2 Velocity distribution over the 1 to 6 slope ridge.

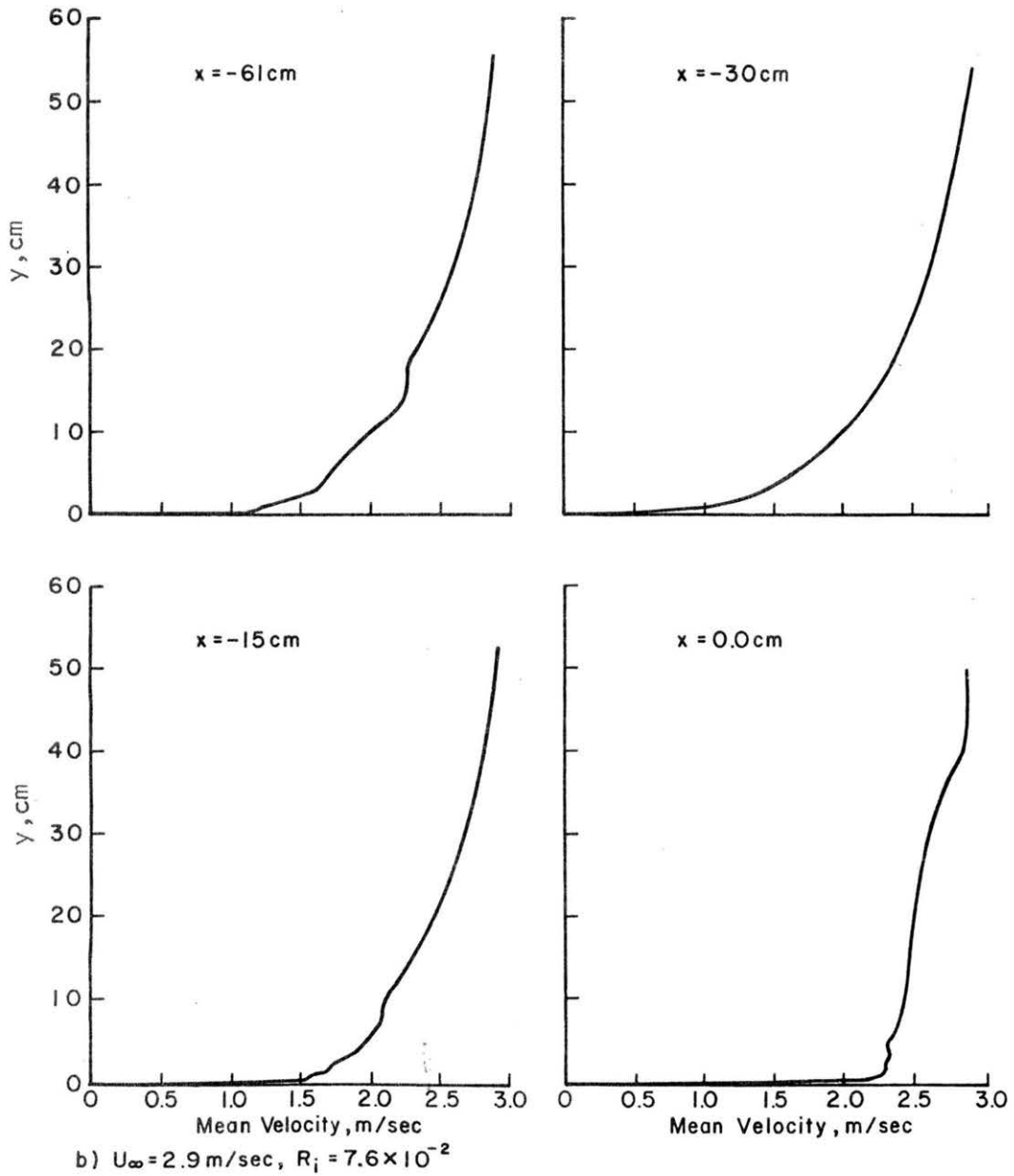


Figure C2 (concluded) Velocity distribution over the 1 to 6 slope ridge

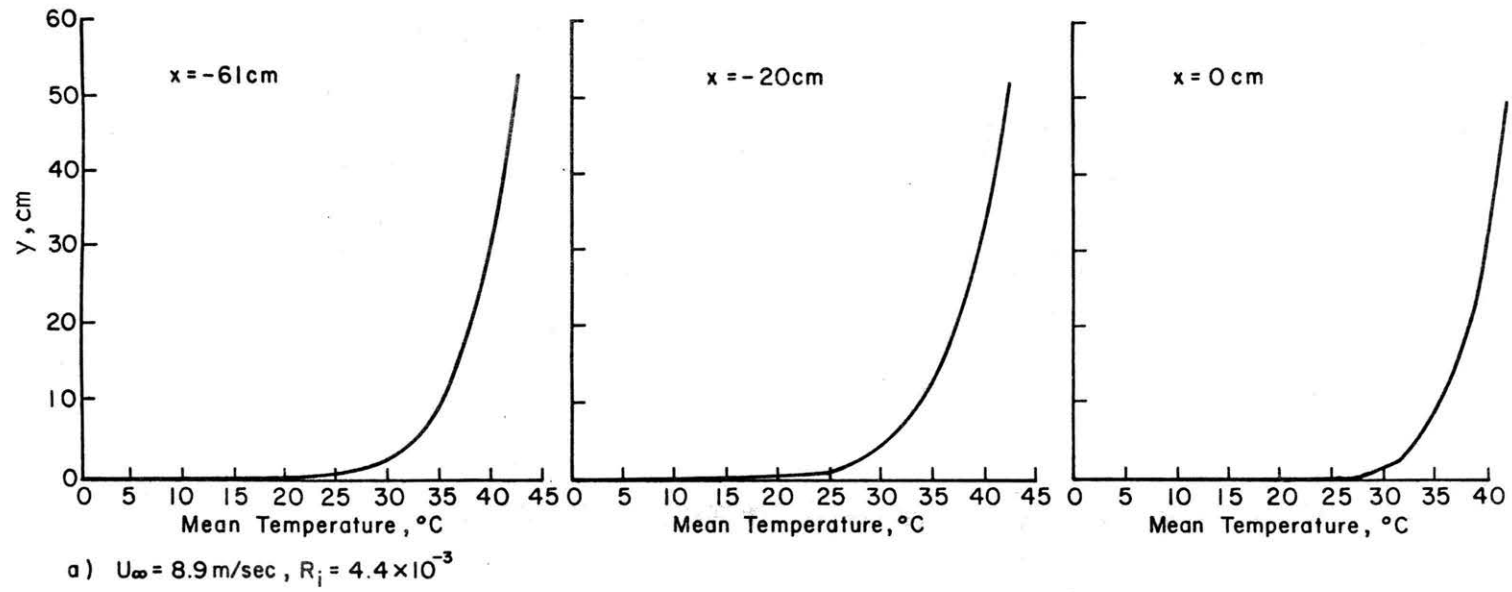


Figure C3 Temperature distribution over the 1 to 4 slope ridge

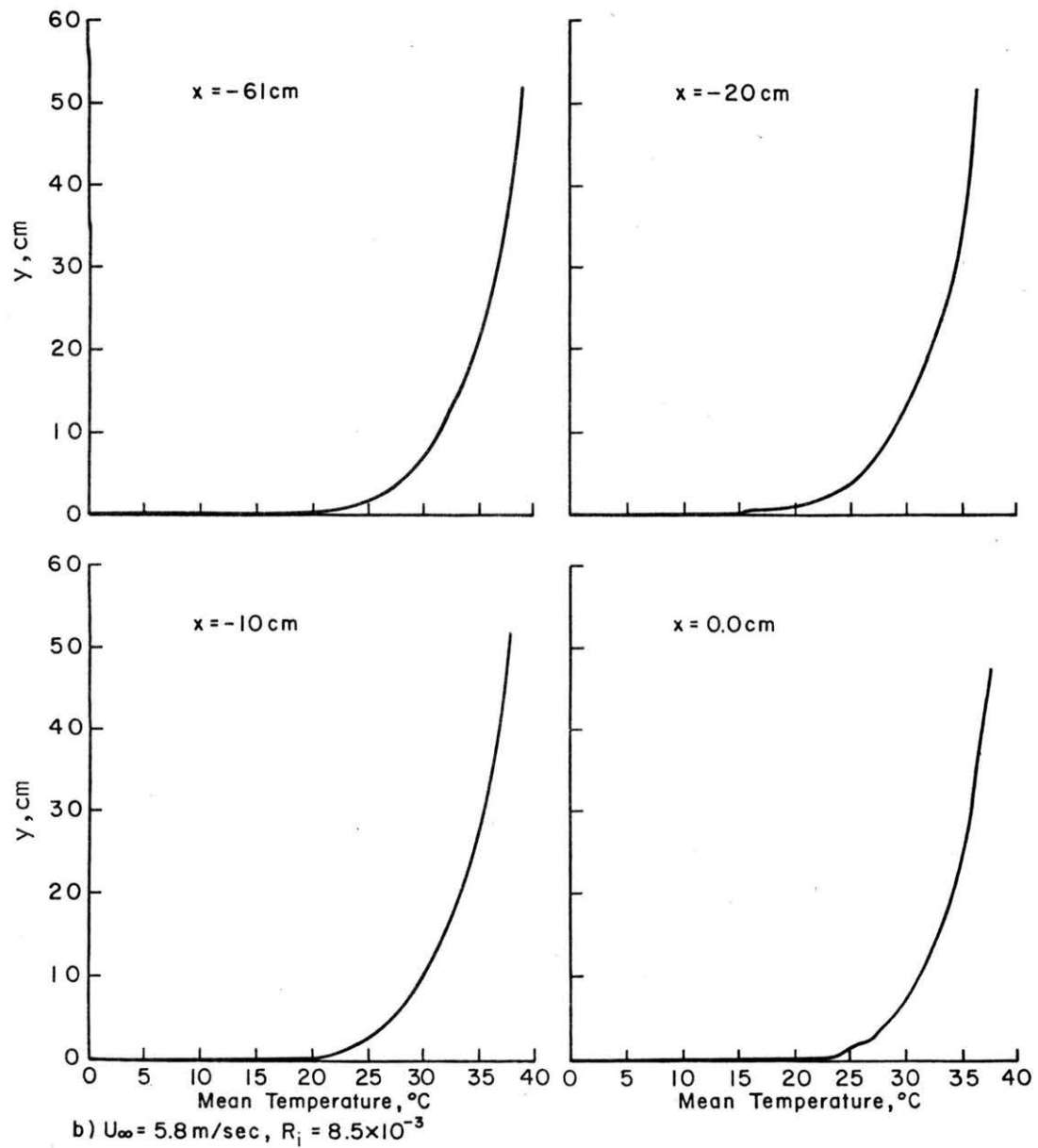


Figure C3 (continued) Temperature distribution over the 1 to 4 slope ridge.

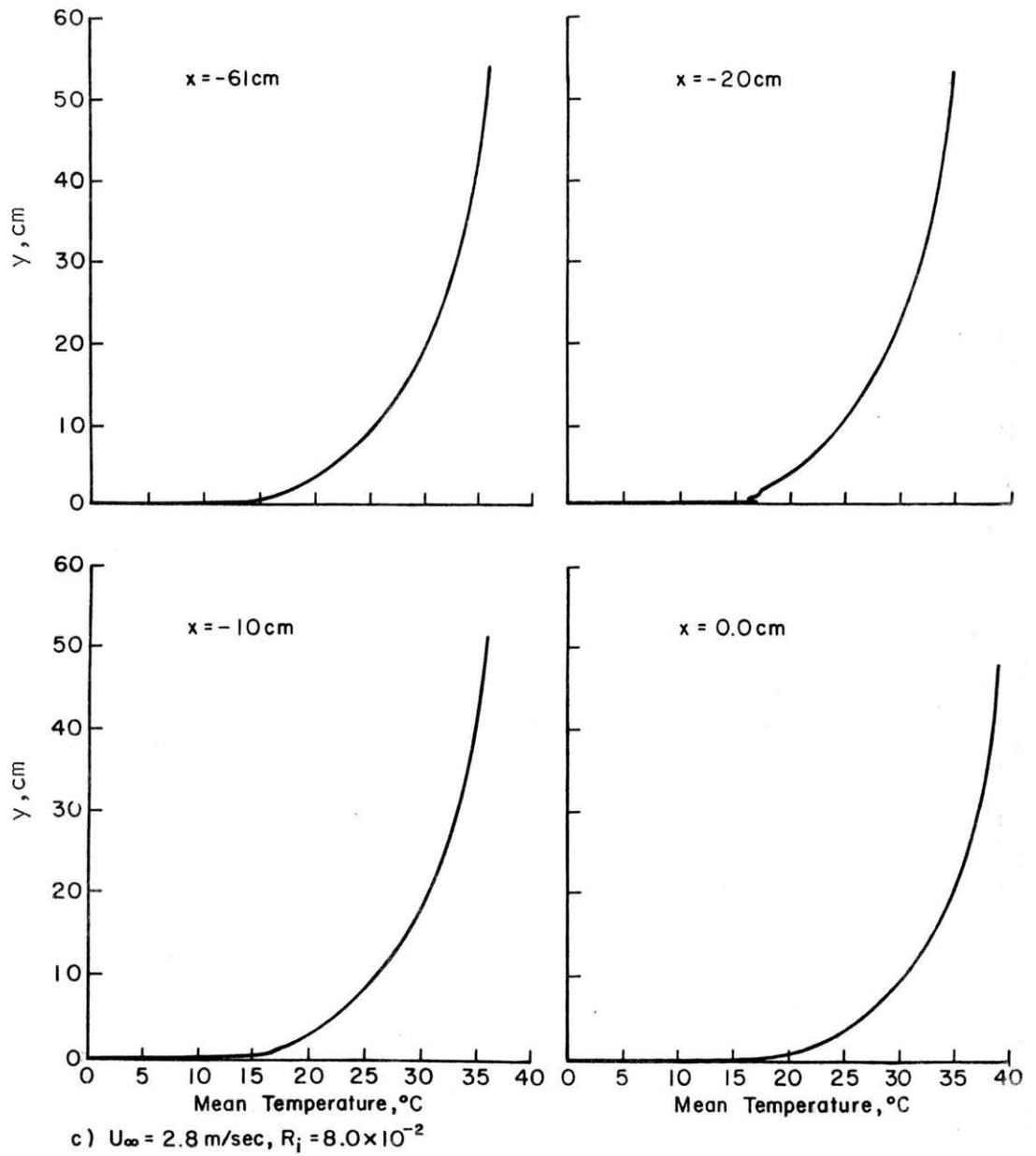


Figure C3 (concluded) Temperature distribution over the 1 to 4 slope ridge

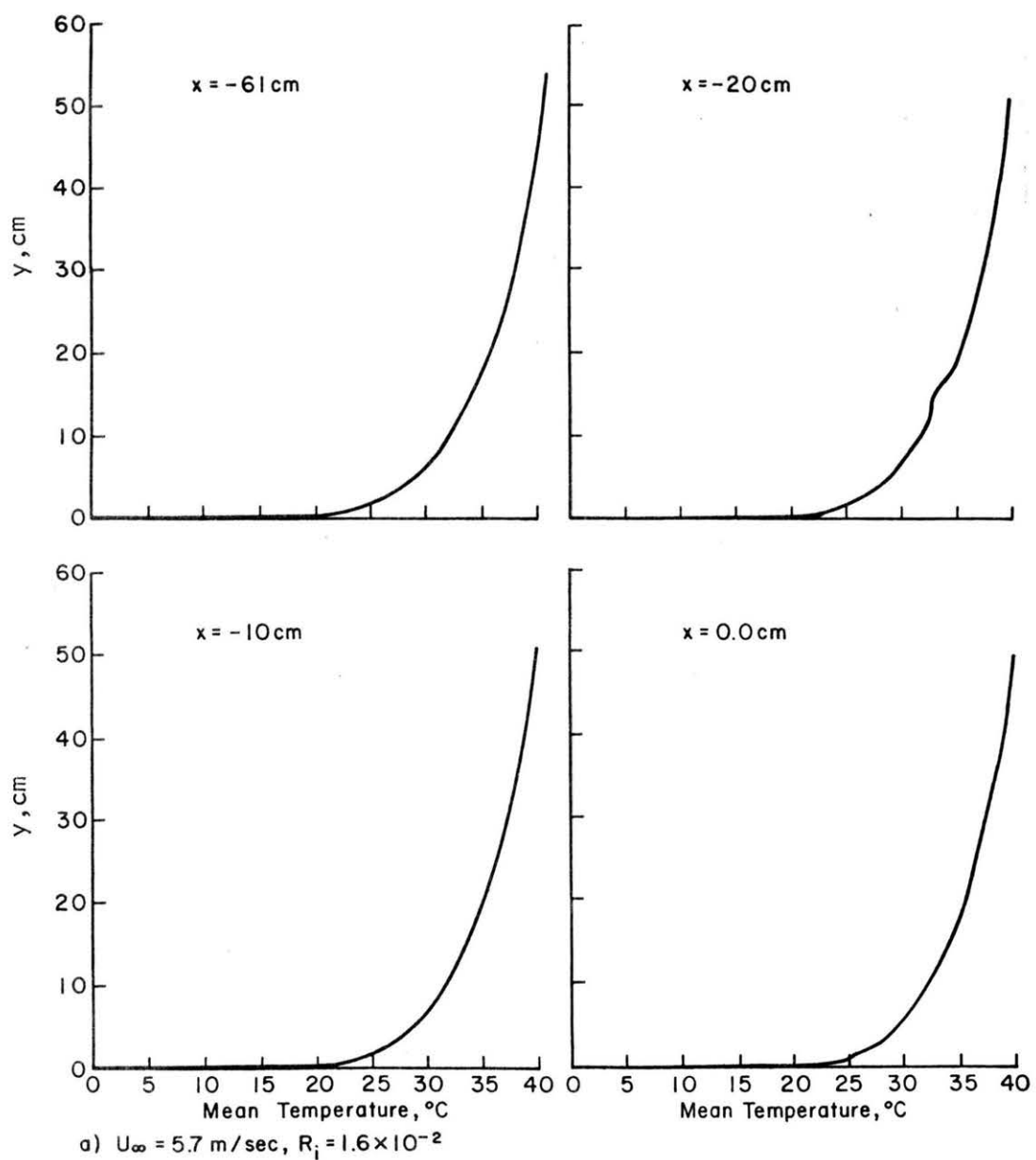


Figure C4 Temperature distributions over the 1 to 6 slope ridge

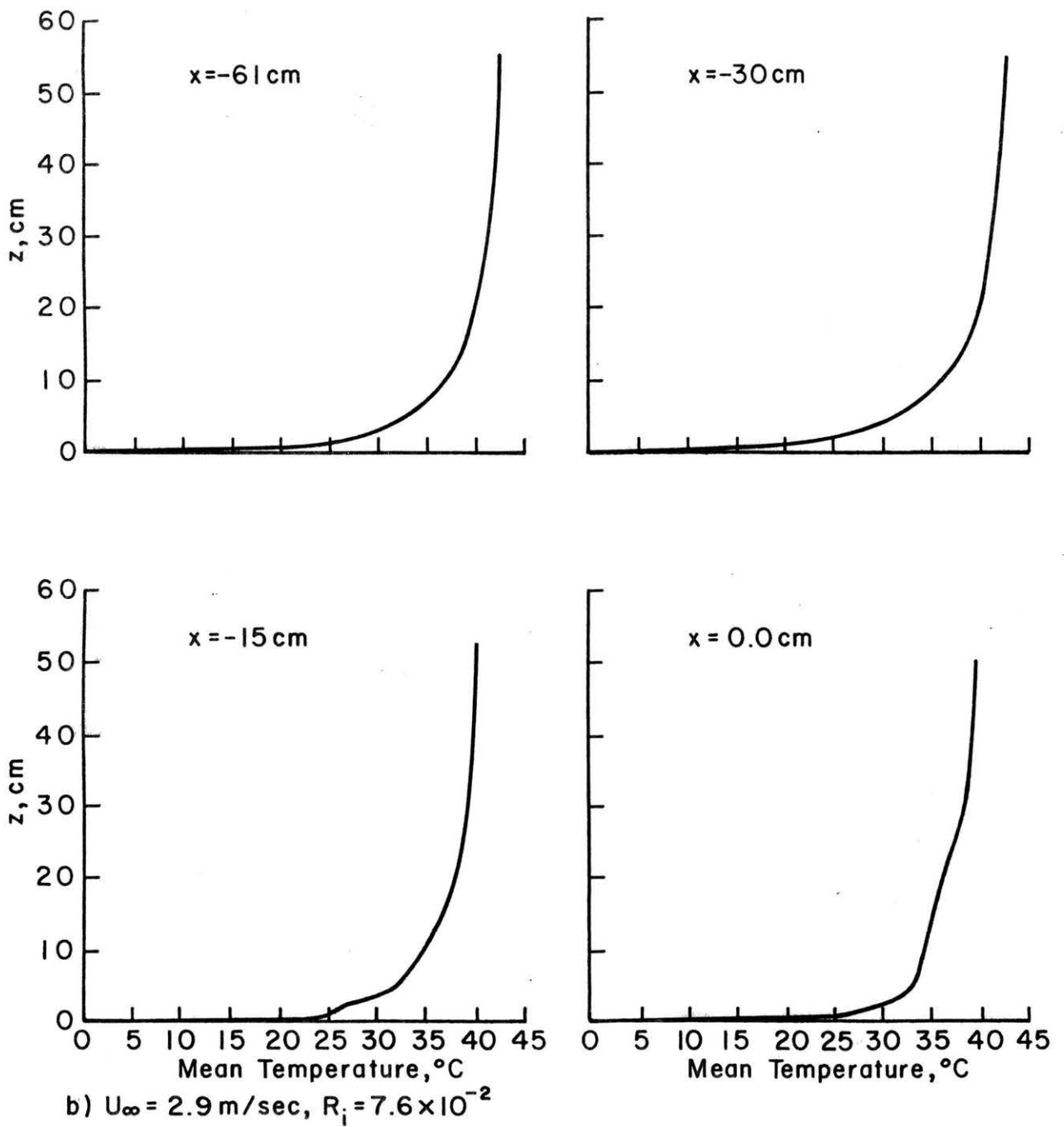


Figure C4 (concluded) Temperature distribution over the 1 to 6 slope ridge

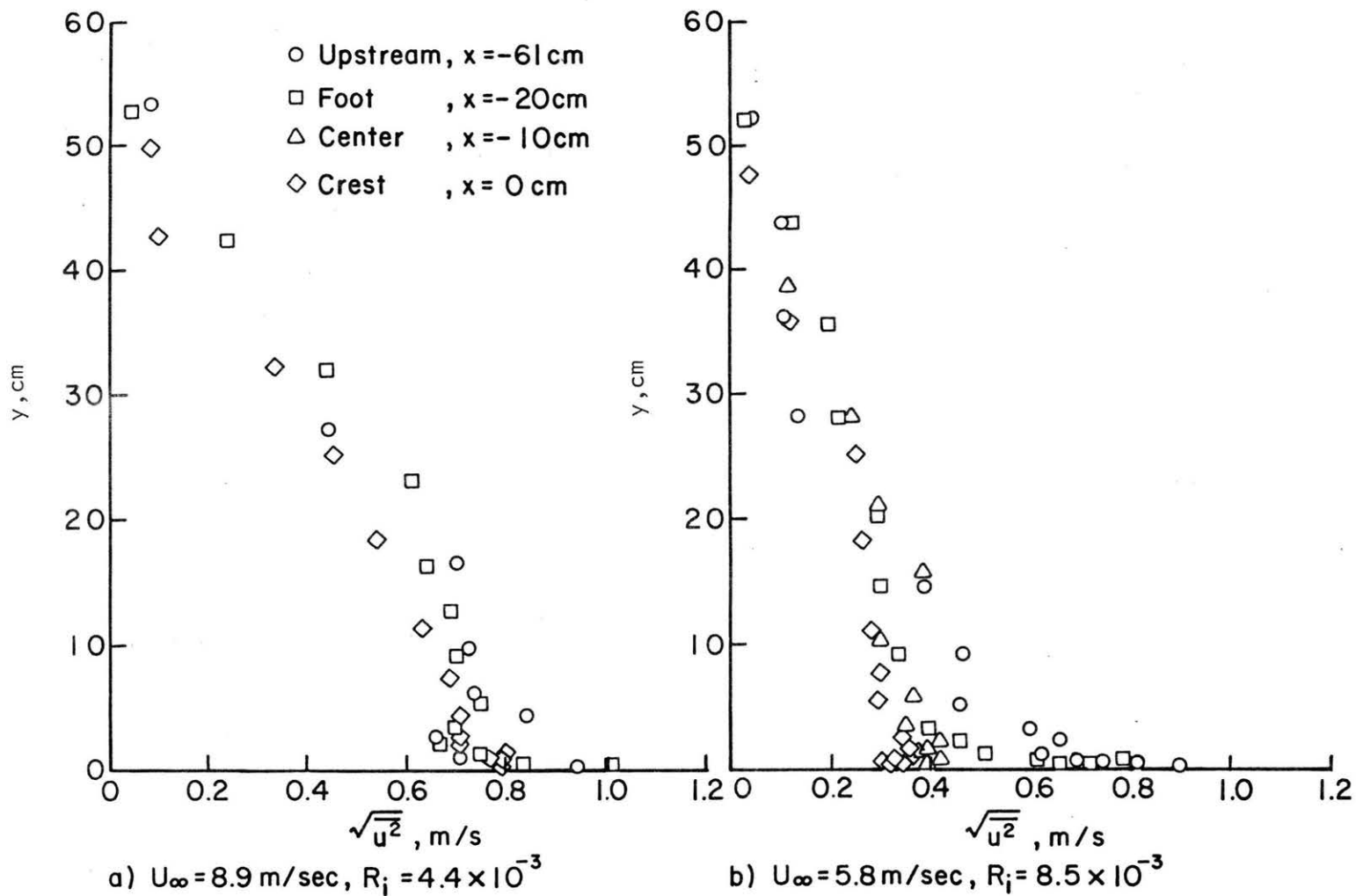
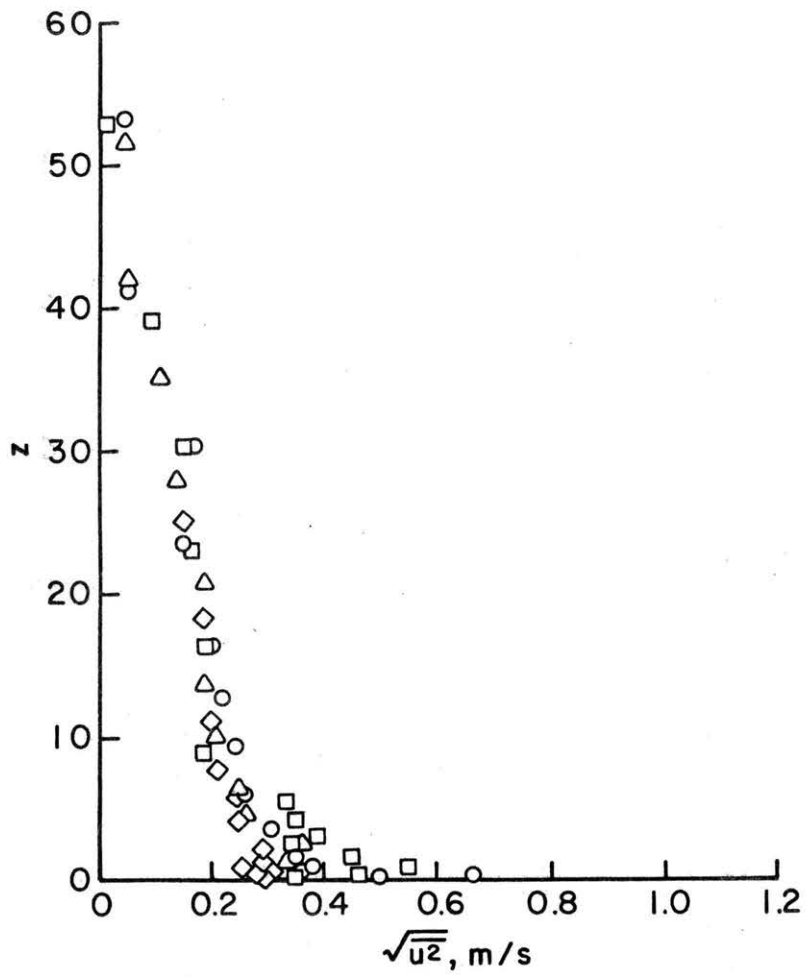


Figure C5 Longitudinal turbulence over the 1 to 4 slope ridge



c) $U_{\infty} = 2.8 \text{ m/sec}, R_i = 8.0 \times 10^{-2}$

Figure C5 (concluded) .Longitudinal turbulence over the 1 to 4 slope ridge

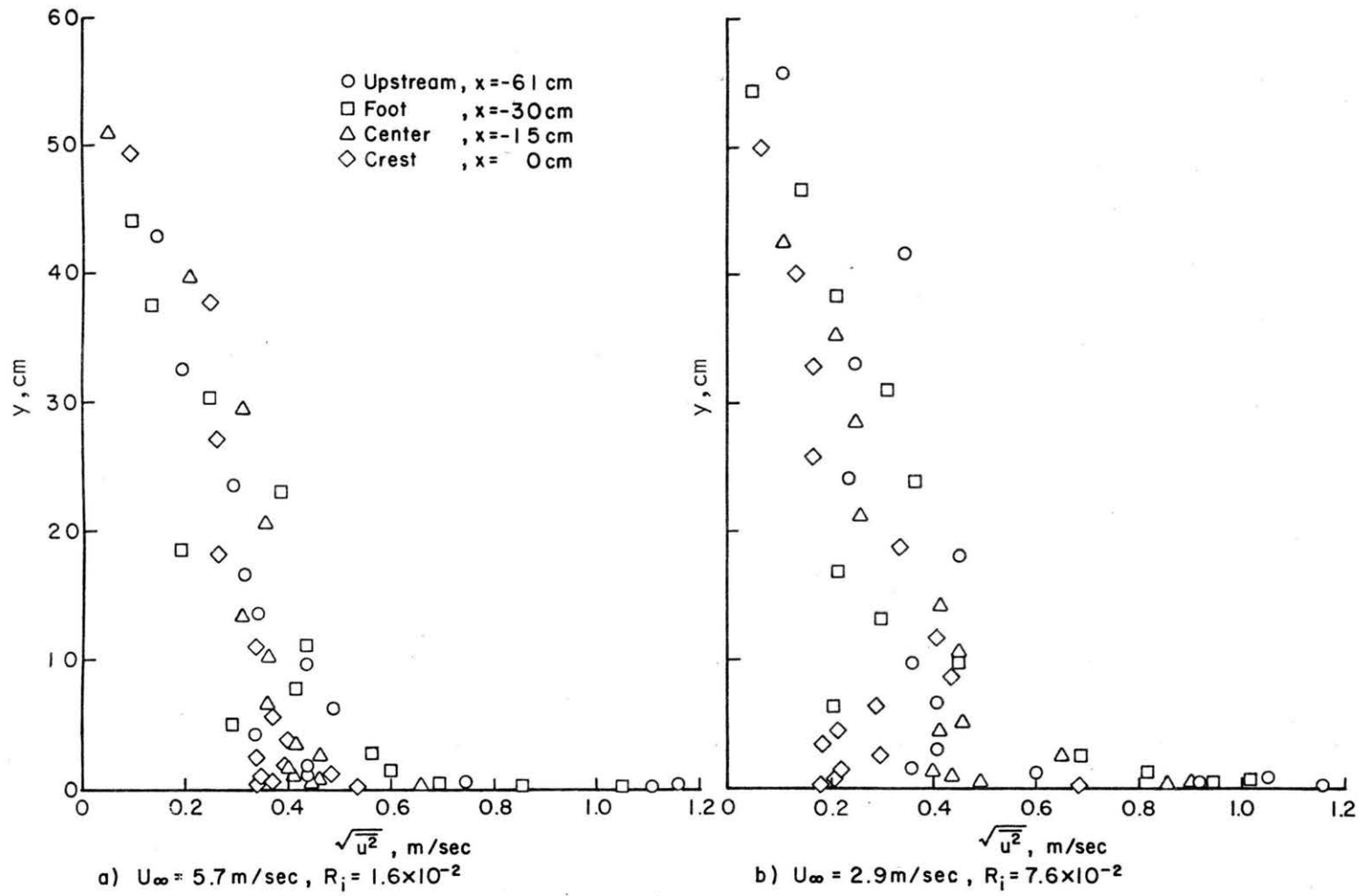


Figure C6 Longitudinal turbulence over the 1 to 6 slope ridge

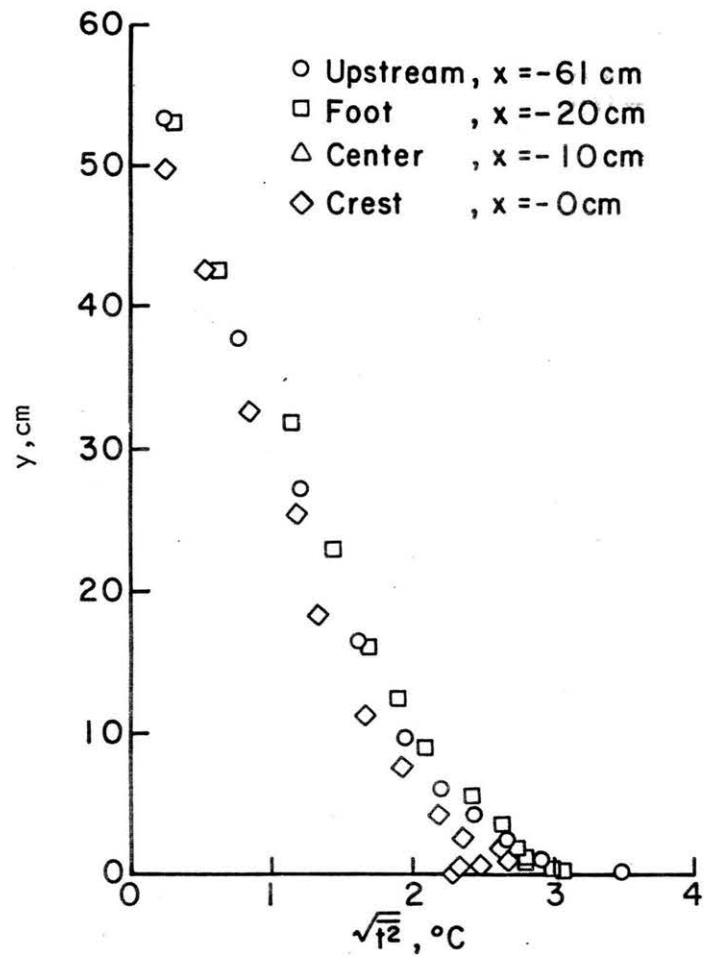
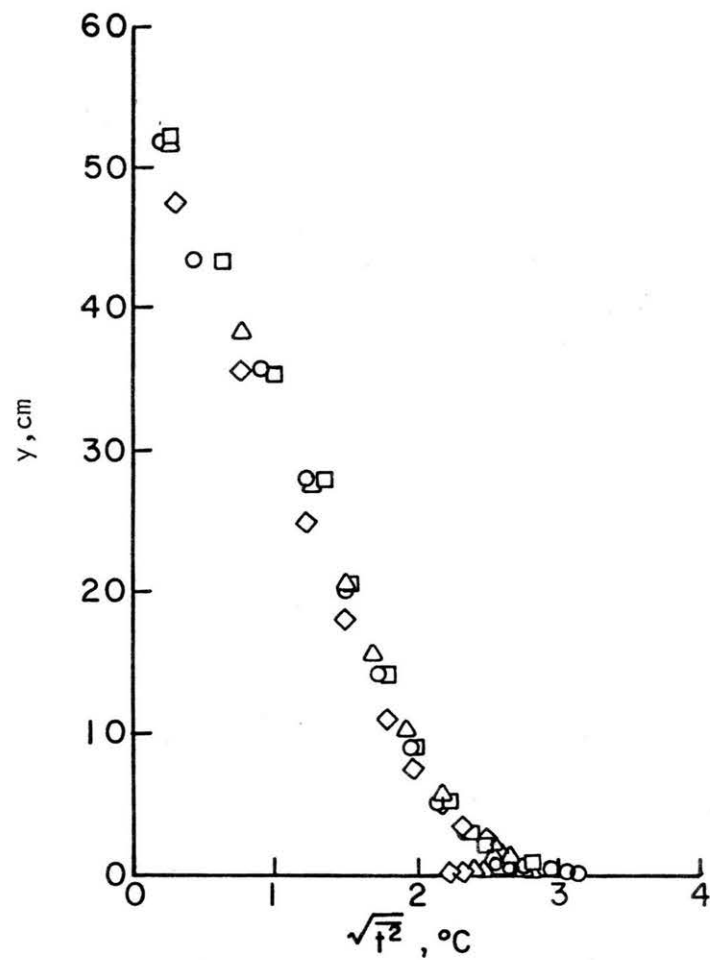
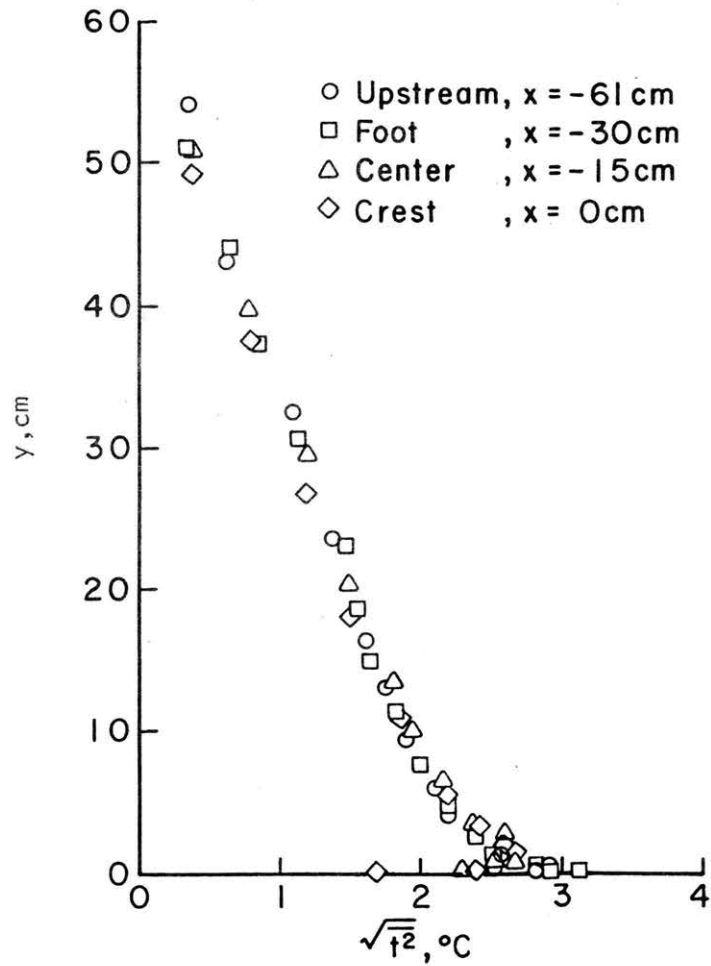
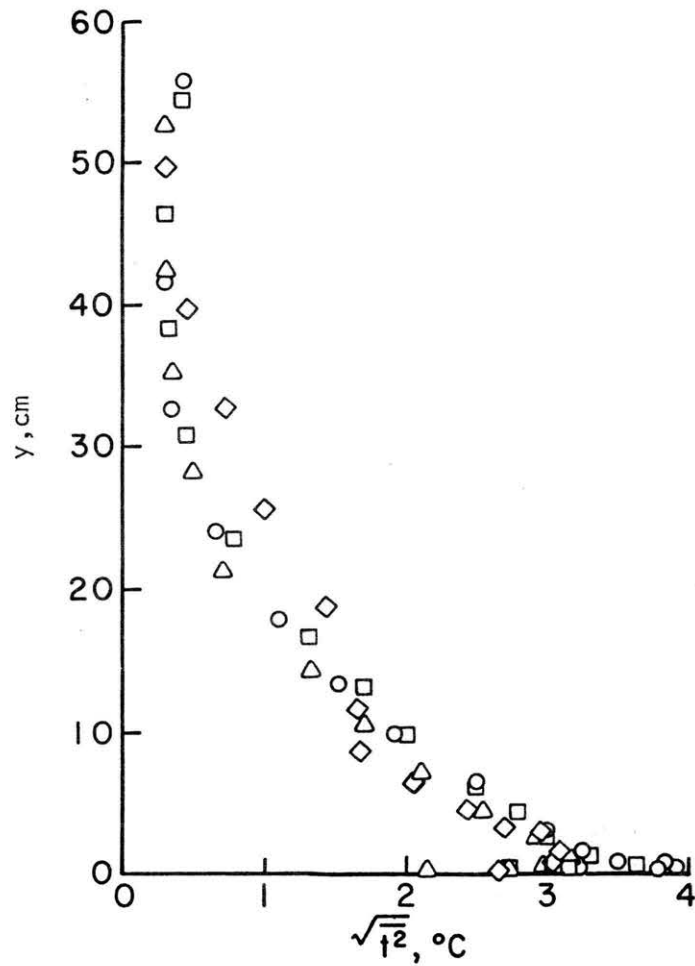
a) $U_\infty = 8.9 \text{ m/sec}$, $R_i = 4.4 \times 10^{-3}$ b) $U_\infty = 5.8 \text{ m/sec}$, $R_i = 8.5 \times 10^{-3}$

Figure C7 Temperature fluctuations over the 1 to 4 slope ridge



a) $U_\infty = 5.7$ m/sec, $R_i = 1.6 \times 10^{-2}$



b) $U_\infty = 2.9$ m/sec, $R_i = 7.6 \times 10^{-2}$

Figure C8 Temperature fluctuations over the 1 to 6 slope ridge

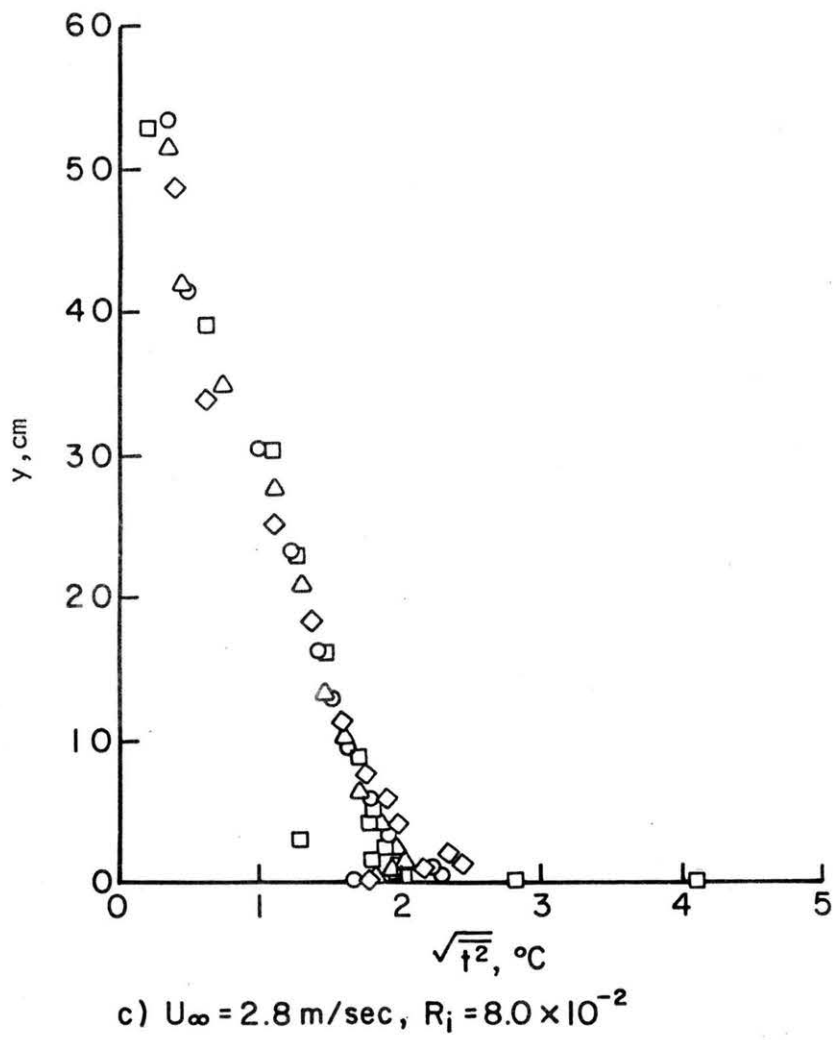


Figure C8 (concluded) Temperature fluctuations over the 1 to 6 slope ridge

APPENDIX D

MEASUREMENTS OF FLOW OVER MODEL, THREE-DIMENSIONAL HILLS

By Ho Chen Chien, V. A. Sandborn, R. J. B. Bouwmeester, and R. N. Meroney

SUMMARY

A set of velocity distribution measurements was made over an approximate Gaussian shaped hill, a 1 to 4 slope, and 1 to 3 slope, cone-shaped hill. The hills were approximately one tenth the height of the boundary layer thickness. Detailed velocity measurements were made for a free-stream velocity of 9.4 meters per second. A limited number of velocity profiles were also taken over the Gaussian hill for a free-stream velocity of 15.3 meters per second. The speedup of velocity near the surface of the isolated three-dimensional hills is less than the speedup observed for nearly all two-dimensional ridge configurations.

INTRODUCTION

Obvious sites for wind turbine installations will include both two- and three-dimensional topography. The isolated three-dimensional hill is commonly encountered in nature, and is a likely candidate for wind-power sites. The present study considers the ideal symmetrical Gaussian and cone-shaped hills. Information for these basic shapes is required to aid in the development of methods to predict the flow over local terrain. The present study is for hills that are small compared to the local boundary layer thickness (hill height to boundary layer thickness of approximately 0.1). Based on the previous studies of two-dimensional ridges of the same height, Ref. 1, the effect of the hill would be expected to produce a speedup of the local wind velocities near the surface. Due to the three-dimensional nature of the hill the local speedup at any particular location will not be as great as that observed for the two-dimensional ridge. The present models will correspond to atmospheric hill heights of the order of 30 to 100 meters high.

EXPERIMENTAL SETUP

The measurements were taken in the Meteorological Wind Tunnel located in the Fluid Dynamics and Diffusion Laboratory at Colorado State University. The purpose of this experiment was to survey the flow characteristics over models of three-dimensional hills emersed in deep turbulent layers. Experimental facilities and techniques are discussed in following sections.

WIND-TUNNEL FACILITY

As mentioned above, the measurements were performed in the recirculating Meteorological Wind Tunnel (see Figure B8). Details of the tunnel are discussed in Appendix B.

MODEL DESCRIPTION

The three, three-dimensional hills used in the tests are illustrated in Figure D1. The numbers used to distinguish these hills in this report are:

- Hill No. 1 Gaussian hill with crest height:radius = 1:6
- Hill No. 2 Cone-shaped hill with crest height:radius = 1:4
- Hill No. 3 Cone-shaped hill with crest height:radius = 1:3

The models were made of Plexiglas. Each of the models were instrumented with static pressure taps along a centerline of the hill.

INSTRUMENTATION

Details of the mean velocity and static pressure measurements for the present study are covered in Appendix B. The wind tunnel actuator-carriage system described in Appendix B was also employed for the present study.

STATIC PRESSURE MEASUREMENTS

A commercial cylindrical pitot-static tube was used along with the static pressure taps mounted in the surface of each hill to measure the local static pressure difference with respect to the freestream static pressure. For the Gaussian and 1:4 cone-shaped hill, the surface static pressures on diameters 0° , 45° and 90° with respect to the freestream flow direction were measured by rotating the model centerline static taps to the specific direction. The static pressure taps were drilled approximately normal to the surface. It was not possible in the case of the Gaussian hill to accurately align the perpendicular direction, so some uncertainty may exist in the local surface pressure measurements.

VELOCITY MEASUREMENTS

Three different probes were used to measure the total pressure: a commercial pitot-static tube, a commercial Kiehl probe and a hot-film probe. The pitot-static tube was mounted from the ceiling of the wind tunnel about 1 m upstream of the models. This probe was used not only as a reference static pressure for calculation of dynamic pressure but also for calibration of the hot-film probe. The Kiehl probe and hot-film probe were mounted on the actuator probe support similar to Figure B11 of Appendix B. Both probes were used for the measurement of mean velocity.

Velocity measurements were made for constant approach, freestream velocities. The dynamic pressure from the pitot-static tube was used to adjust and maintain the tunnel flow at a constant value. The Kiehl probe and hot-film probe were positioned at the desired point by adjusting the carriage manually. The mean velocity measurements at different heights were then calculated from the averaged pressure measured with the Kiehl probe and local static pressures or from the voltage drop across the hot-film probe. The hot-film was operated with a commercial constant temperature anemometer. The time-averaged signals were obtained using a digital minicomputer.

RESULTS

Tables DI through DIV list the results obtained for both the pressure distributions and mean velocity profiles. The velocity profiles were taken perpendicular to the smooth flat-plate approach surface and not perpendicular to the local hill surface. The normal vertical coordinate corresponds to the requirements of a wind-power site, but it is different from the usual boundary-layer coordinate system.

A limited flow visualization study was made for the surface flow around the Gaussian hill. Figure D3 shows a series of surface oil streak patterns observed for the Gaussian hill. The upstream portion of the hill was coated with a "light cooking" oil. White zinc oxide was mixed with the oil to make the movement visible. The surface streaks indicate the local flow directions around the hill. The region of separation in the rear of the hill is also readily observed from the photographs. The area of separation is not as uniform as expected, which may be partly due to some gravity effect of the flow of the oil. The included angle of separation was found to be approximately 35° . Although the character of the separation appears somewhat different for the different velocities the included angle of separation remained roughly the same.

From the oil pictures the region of highest shear appears to be just off the peak on either side and slightly downstream. Directly downstream of this high shear region the oil flow pattern was observed to turn sharply outward. Two different flow regions are observed in the oil pictures. A fairly uniform sheet of oil is observed over the forward part of the hill. This uniform sheet exists about to 100° from the forward centerline. Around an angle of 100° the patterns are very "streaky." The patterns apparently are a combination of gravity effects on the oil and local intermittent fluctuations of flow separation. The apparent intermittent characteristic of separation is more pronounced at the lower velocities. The region, which was assumed to be the location of a "true-mean-zero-surface-shear" separation, shows very distinct convolutions of the oil pattern. The convolutions would suggest organized vortex motions were present. The photograph for a freestream velocity of 12.2 m/sec is somewhat distorted, since the shear forces were too small.

Figure D4 shows typical smoke-streak patterns around the Gaussian hill. The smoke was produced by painting small spots and lines of $TiCl_4$ on the model surface. The $TiCl_4$ reacts with moisture in the air to produce a white smoke. The smoke study was done at a velocity of less than 1 m/sec. The smoke streaks show a distinct curl inward toward the separation region as they go over the hill. The motion near separation would appear to be in the opposite direction to the pattern of outward flow shown by the oil. The smoke indicates some vortex motion near separation; however, the pattern is not well defined.

Figures D5 through D13 are plots of the mean velocity distributions listed in Tables DIII and DIV. A speedup ratio of 0.57 was obtained at the crest of the Gaussian hill. It is possible that slightly higher speedup ratios may be obtained in the region just off the crest; however, the present grid of measurements did not cover the crest region in sufficient detail to indicate a maximum away from the crest. In general the speedup ratio is of the order of 0.30 or less away from the crest. The cone hills obtain maximum speedup ratios of the order of 0.3 at the crest. Compared to the two-dimensional ridges, the isolated three-dimensional hills do not appear to be a great deal better than bluff, two-dimensional ridges, discussed in Appendix A.

CONCLUDING REMARKS

The present study suggests that the round crest hill will be a better wind-power site than the sharp-crested cones. The flow visualization suggests that the region around the crest on the shoulders may also produce local high wind velocities. The static-pressure measurements on the Gaussian hill appear to indicate the higher velocities over a region of about $H/7$ to $H/2$ radius away from the crest at right angles to the flow direction. Thus, for the rounded three-dimensional hill it may not be necessary to mount the wind turbine directly at the crest. If, however, the prevailing windflow direction varies over large angles, the crest of the hill is suggested as the best location. The separation region on the downstream face of the hill does not quite reach to the crest of the Gaussian hill, but the large fluctuations associated with that separation are evident near the crest. If a choice is available two-dimensional ridges appear to be much better as wind-velocity amplifiers than the isolated three-dimensional hills.

REFERENCES

1. Meroney, R. N., Sandborn, V. A., Bouwmeester, R. J. B., and Rider, M. A., Sites for Wind-Power Installations, Second Annual Report, Colorado State University Report No. CER77-78 RNM-VAS-RB-MAR6, March 1977, 186 p.

Table DI Static pressure on the surface of Gaussian hill
 $\Delta p = (p_{\text{static}})_{\text{free stream}} - (p_{\text{static}})_{\text{local}} \text{ (N/cm}^2\text{)}$

Measuring Angle $\theta =$		0°	45°	90°
Tap No.	Radius (cm)	Δp	Δp	Δp
1	20.95	+0.049	-0.18	-0.192
2	17.15	-0.049	---	---
3	13.00	---	-0.183	-0.200
4	9.35	-0.048	-0.183	-0.210
5	6.67	-0.051	-0.193	-0.220
6	4.12	-0.109	-0.200	-0.225
7	2.54	-0.208	-0.215	-0.227
8	0.00 (crest)	-0.218	-0.218	-0.230
9	- .80	-0.198	-0.215	-0.235
10	- 2.54	-0.183	-0.208	-0.230
11	- 4.45	-0.157	-0.220	-0.220
12	- 6.19	-0.090	-0.212	-0.217
13	- 8.26	-0.051	-0.200	-0.207
14	-10.80	0.0	-0.195	-0.200
15	-13.97	+0.121	-0.180	-0.192
16	-17.46	+0.048	-0.188	-0.145
17	-20.95	-0.051	-0.183	-0.185
U_∞		9.4 m/s	9.4 m/s	9.75 m/s

Table DII. Static pressure on the surface of 1:4 cone hill, at $U_{\infty} = 9.4$ m/sec, $\Delta p = (p_{st})_{\text{free stream}} - (p_{st})_{\text{local}}$ (N/cm^2)

Measuring Angle $\theta =$		0°	45°	90°
Tap No.	Radius (cm)	Δp	Δp	Δp
1	14.35	---	-0.172	-0.185
2	12.07	-0.168	-0.175	-0.188
3	9.73	-0.170	-0.182	-0.192
4	7.29	-0.175	-0.185	-0.198
5	4.83	-0.185	-0.195	-0.205
6	3.81	-0.192	-0.198	-0.212
7	2.54	-0.195	-0.208	-0.215
8	1.27	-0.208	-0.215	-0.225
9	0.0 (crest)	-0.235	-0.240	-0.235
10	- 1.27	-0.225	-0.227	-0.225
11	- 2.54	-0.212	-0.215	-0.215
12	- 5.08	-0.187	-0.20	-0.205
13	- 7.62	-0.185	-0.195	-0.198
14	-10.16	-0.175	-0.168	-0.195
15	-12.70	---	-0.180	-0.188
16	-15.24	---	-0.175	-0.188

Table DIII Tabulated upstream velocity profiles for each hill.

UPSTREAM VELOCITY PROFILES

TUNNEL TEMPERATURE--T IN DEG. C BAROMETRIC PRESSURE--BAR IN NT/(CM.CM)
 BOUNDARY LAYER THICKNESS--DELTA IN CM REFERENCE VELOCITY--U(REF) IN M/S
 NONDIMENSIONAL HEIGHT--Y* = Y/DELTA NONDIMENSIONAL VELOCITY--U* = U(Y)/U(REF)
 RADIAL DISTANCE FROM CREST--R IN CM

R	52.22	28.65	20.32
DELTA	65.02	42.70	45.36
U(REF)	9.78	9.33	9.24
T	21.11	21.83	21.33
BAR	8.38	8.39	8.39
DATE	29/10/1977	5/11/1977	7/11/1977

Hill No. 1		Hill No. 2		Hill No. 3	
Y*	U*	Y*	U*	Y*	U*
.007	.532	.006	.574	.006	.553
.013	.551	.037	.652	.022	.569
.017	.575	.063	.689	.045	.638
.087	.707	.115	.733	.069	.672
.113	.725	.166	.746	.102	.723
.143	.733	.235	.769	.134	.727
.185	.754	.301	.800	.182	.765
.229	.776	.370	.824	.230	.790
.272	.785	.456	.843	.278	.803
.353	.812	.523	.875	.342	.815
.422	.830	.593	.889	.406	.836
.494	.854	.660	.902	.470	.875
.567	.894	.746	.938	.550	.894
.639	.916	.830	.953	.630	.921
.712	.941	.916	.979	.712	.947
.783	.956	1.000	1.000	.807	.962
.855	.963			.903	.989
.927	.991			1.000	1.000

Table DIV. Tabulated velocity profiles

FOR HILL NO. 1

MEASURING ANGLE -0 DEG. FROM FLOW DIRECTION

a) R	0.00	50.80
DELTA	52.27	51.82
U(REF)	13.73	15.67
T	21.11	21.11
BAR	8.38	8.38
DATE	29/10/1977	29/10/1977

Y*	U*	Y*	U*
.005	.846	.005	.578
.014	.879	.014	.615
.028	.868	.021	.647
.042	.879	.031	.665
.057	.873	.043	.677
.076	.846	.057	.710
.099	.851	.074	.720
.121	.844	.094	.728
.151	.844	.122	.739
.182	.846	.173	.770
.222	.857	.212	.792
.268	.862	.259	.800
.316	.868	.336	.831
.369	.893	.410	.860
.443	.905	.482	.893
.510	.926	.547	.912
.581	.950	.620	.930
.677	.967	.692	.949
.790	.992	.792	.973
.891	.995	.898	.988
1.000	1.000	1.000	1.000

Table DIV (continued) Tabulated velocity profiles

FOR HILL NO. 1		MEASURING ANGLE = 0 DEG. FROM FLOW DIRECTION				
b) R	31.90	20.80	9.25	4.60	0.00	
DELTA	47.96	45.59	45.34	40.51	50.34	
U(REF)	9.14	9.60	9.77	10.15	9.69	
T	21.11	21.11	21.22	21.22	21.22	
BAR	8.38	8.38	8.37	8.37	8.37	
DATE	29/10/1977	29/10/1977	29/10/1977	29/10/1977	29/10/1977	

Y*	U*	Y*	U*	Y*	U*	Y*	U*	Y*	U*
.007	.499	.011	.538	.012	.599	.012	.711	.010	.805
.013	.511	.013	.547	.019	.599	.021	.715	.021	.811
.017	.524	.017	.550	.027	.633	.030	.739	.035	.827
.035	.603	.020	.579	.035	.644	.040	.745	.043	.833
.061	.660	.025	.614	.041	.668	.048	.765	.056	.827
.087	.702	.033	.614	.056	.690	.050	.751	.064	.824
.114	.714	.041	.630	.073	.739	.067	.761	.071	.827
.143	.743	.057	.647	.084	.733	.075	.761	.078	.808
.183	.748	.073	.673	.093	.749	.094	.775	.085	.808
.230	.776	.088	.699	.100	.752	.111	.783	.100	.811
.272	.789	.120	.712	.112	.761	.129	.788	.115	.811
.353	.816	.153	.717	.132	.783	.146	.783	.129	.833
.422	.849	.184	.732	.148	.783	.166	.785	.161	.805
.494	.857	.232	.751	.165	.793	.192	.817	.202	.818
.568	.896	.329	.787	.180	.802	.219	.820	.245	.833
.639	.903	.376	.800	.211	.811	.245	.832	.303	.862
.711	.933	.423	.816	.244	.836	.272	.826	.364	.865
.783	.950	.473	.819	.276	.842	.300	.835	.422	.887
.855	.960	.519	.837	.309	.855	.334	.829	.495	.915
.927	.988	.568	.860	.340	.861	.371	.859	.569	.931
1.000	1.000	.616	.876	.373	.861	.409	.876	.640	.953
		.663	.895	.420	.880	.443	.865	.710	.965
		.713	.902	.469	.892	.498	.886	.781	.978
		.759	.926	.518	.911	.550	.919	.854	.984
		.807	.926	.566	.924	.604	.937	.929	.994
		.856	.941	.613	.939	.606	.955	1.000	1.000
		.903	.949	.662	.942	.713	.955		
		.951	.962	.710	.952	.769	.964		
		1.000	1.000	.757	.961	.820	.973		
				.806	.973	.874	.973		
				.854	.989	.929	.991		
				1.000	1.000	1.000	1.000		

Table DIV (continued) Tabulated velocity profiles

FOR HILL NO. 1

MEASURING ANGLE 45 DEG. FROM FLOW DIRECTION

c) R	20.80	9.25	4.60
DELTA	47.37	47.47	47.32
U(REF)	9.33	9.60	9.60
T	21.56	21.56	21.56
BAR	8.35	8.35	8.35
DATE	1/11/1977	1/11/1977	1/11/1977

Y*	U*	Y*	U*	Y*	U*
.007	.591	.004	.547	.006	.460
.025	.647	.019	.629	.020	.671
.040	.654	.035	.673	.037	.688
.055	.693	.050	.673	.054	.717
.071	.708	.073	.708	.071	.724
.085	.729	.096	.736	.087	.743
.100	.742	.117	.743	.104	.732
.117	.753	.142	.751	.120	.739
.133	.757	.164	.756	.139	.747
.147	.774	.187	.768	.155	.768
.171	.774	.219	.777	.177	.764
.193	.787	.250	.790	.204	.777
.216	.791	.280	.794	.236	.794
.248	.810	.311	.822	.260	.809
.278	.820	.341	.828	.302	.813
.309	.817	.373	.846	.336	.819
.355	.828	.418	.850	.370	.830
.402	.846	.463	.857	.402	.837
.447	.857	.510	.873	.452	.860
.494	.871	.556	.876	.535	.876
.539	.882	.602	.895	.585	.889
.585	.908	.648	.902	.634	.911
.631	.922	.693	.911	.684	.914
.693	.935	.754	.962	.736	.941
.754	.961	.817	.971	.833	.990
.816	.971	.876	.981	.901	.990
.877	.987	.938	.990	.951	1.000
.938	.990	1.000	1.000	1.000	1.000
1.000	1.000				

Table DIV (concluded) Tabulated velocity profiles

FOR HILL NO. 1

MEASURING ANGLE 90 DEG. FROM FLOW DIRECTION

d) R	20.80	9.25	4.60
DELTA	45.44	40.98	43.84
U(REF)	9.60	9.60	9.60
T	21.36	21.36	21.89
BAR	8.36	8.36	8.34
DATE	31/10/1977	31/10/1977	1/11/1977

Y*	U*	Y*	U*	Y*	U*
.033	.441	.006	.532	.006	.619
.049	.609	.023	.632	.020	.671
.064	.635	.041	.673	.037	.688
.078	.671	.059	.695	.054	.717
.093	.695	.077	.717	.071	.724
.110	.717	.095	.712	.087	.743
.127	.739	.112	.747	.103	.732
.143	.743	.131	.732	.120	.739
.174	.756	.148	.743	.139	.746
.190	.760	.165	.768	.155	.768
.206	.781	.193	.768	.177	.764
.222	.772	.255	.797	.204	.777
.238	.797	.246	.797	.236	.794
.254	.790	.272	.800	.269	.809
.270	.800	.308	.816	.302	.813
.294	.809	.344	.828	.336	.819
.318	.816	.380	.837	.370	.830
.343	.819	.415	.857	.402	.837
.365	.828	.450	.860	.452	.860
.389	.837	.486	.867	.534	.876
.423	.833	.521	.876	.585	.889
.454	.846	.627	.902	.634	.911
.487	.867	.670	.895	.684	.914
.518	.876	.736	.930	.735	.941
.567	.886	.786	.945	.833	.990
.615	.898	.893	.981	.901	.990
.663	.918	.946	.990	.951	1.000
.710	.922	1.000	1.000	1.000	1.000
.760	.945				
.808	.962				
.856	.981				
.904	.990				
1.000	1.000				

Table DV Tabulated velocity profiles.

FOR HILL NO. 2

MEASURING ANGLE = 0 DEG. FROM FLOW DIRECTION

a) R	12.85	7.62	0.00
DELTA	57.91	48.67	44.68
U(REF)	9.17	9.20	9.24
T	21.83	21.83	21.83
BAR	8.39	8.39	8.39
DATE	5/11/1977	5/11/1977	5/11/1977

Y*	U*	Y*	U*	Y*	U*
.006	.595	.006	.599	.009	.648
.032	.643	.028	.659	.024	.683
.060	.704	.058	.710	.040	.697
.090	.728	.089	.738	.056	.715
.131	.770	.119	.759	.080	.727
.173	.782	.148	.779	.108	.753
.215	.804	.192	.792	.139	.777
.270	.817	.238	.797	.170	.785
.313	.837	.282	.825	.204	.799
.369	.864	.357	.858	.254	.822
.430	.880	.433	.877	.300	.828
.509	.904	.507	.904	.349	.836
.581	.920	.581	.927	.417	.866
.652	.940	.656	.950	.480	.894
.719	.961	.730	.962	.547	.911
.807	.977	.820	.985	.610	.924
.900	.989	.912	.997	.678	.944
1.000	1.000	1.000	1.000	.756	.962
				.838	.974
				.919	.990
				1.000	1.000

Table DV. (continued) Tabulated velocity profiles.

FOR HILL NO. 2

MEASURING ANGLE 45 DEG. FROM FLOW DIRECTION

b) R	12.85	7.62
DELTA	48.77	49.86
U(REF)	9.24	9.42
T	22.00	22.00
BAR	8.36	8.36
DATE	6/11/1977	6/11/1977

Y*	U*	Y*	U*
.005	.537	.005	.532
.022	.638	.023	.631
.036	.672	.052	.659
.060	.723	.081	.730
.094	.745	.126	.746
.134	.781	.169	.761
.179	.781	.214	.796
.239	.812	.271	.812
.298	.828	.315	.824
.361	.851	.373	.849
.432	.866	.432	.870
.507	.898	.504	.893
.598	.927	.578	.913
.673	.947	.665	.936
.761	.962	.738	.959
.851	.978	.825	.990
.929	.993	.915	.990
1.000	1.000	1.000	1.000

Table DV (concluded) Tabulated velocity profiles

FOR HILL NO. 2

MEASURING ANGLE 90 DEG. FROM FLOW DIRECTION

c) R	22.86	12.85	7.62
DELTA	43.51	47.73	48.77
U(RFF)	9.42	9.24	9.33
T	22.00	22.00	22.00
BAR	8.36	8.36	8.36
DATE	6/11/1977	6/11/1977	6/11/1977

Y*	U*	Y*	U*	Y*	U*
.006	.527	.005	.440	.005	.522
.030	.616	.025	.623	.022	.642
.056	.644	.040	.660	.036	.689
.081	.670	.062	.695	.060	.720
.116	.713	.086	.732	.095	.745
.149	.746	.123	.761	.134	.761
.180	.742	.161	.765	.179	.787
.213	.753	.268	.815	.239	.817
.247	.774	.314	.822	.299	.832
.298	.792	.390	.848	.361	.852
.349	.812	.466	.848	.432	.886
.397	.828	.542	.875	.507	.899
.464	.858	.618	.931	.598	.915
.535	.880	.710	.950	.673	.957
.599	.903	.802	.989	.762	.979
.668	.916	.893	.989	.850	.990
.748	.959	1.000	1.000	.930	.990
.817	.970			1.000	1.000

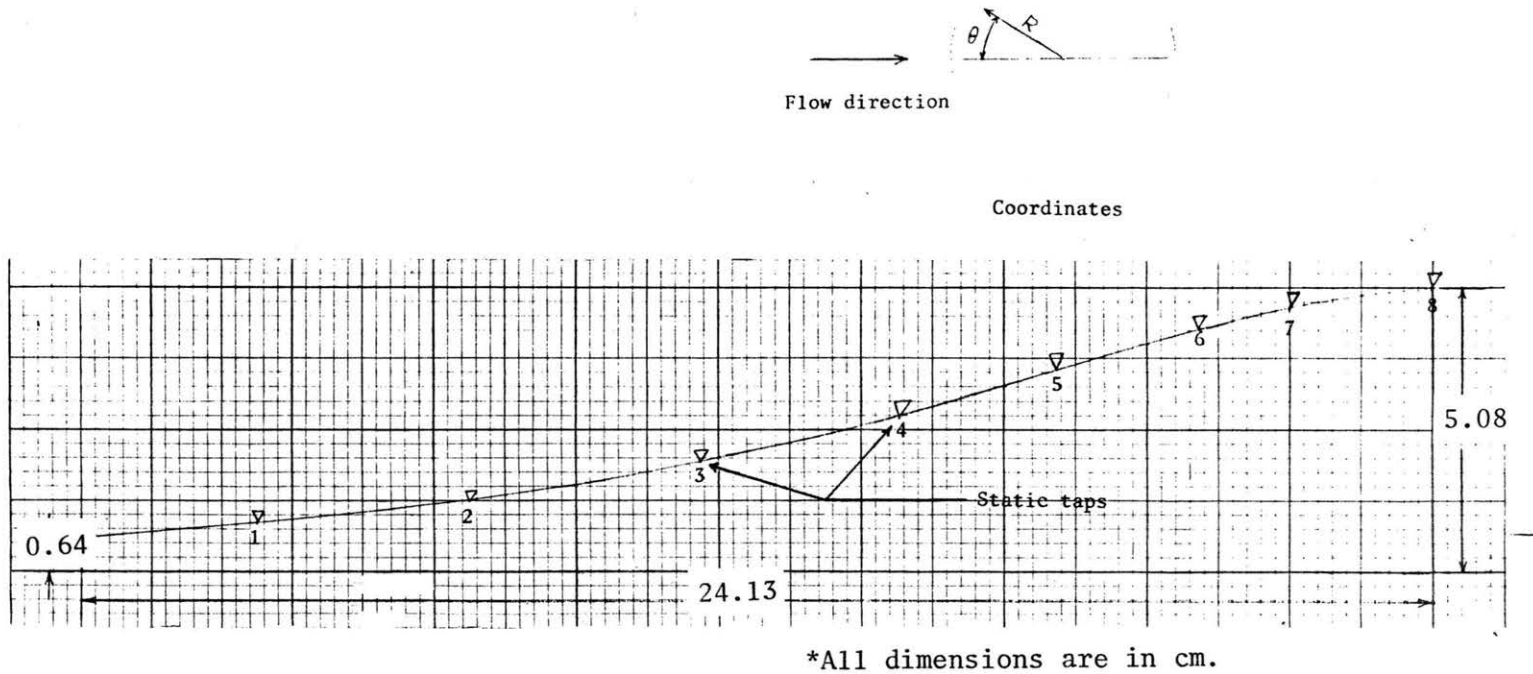
Table DVI Tabulated velocity profiles

FOR HILL NO. 3

MEASURING ANGLE -0 DEG. FROM FLOW DIRECTION

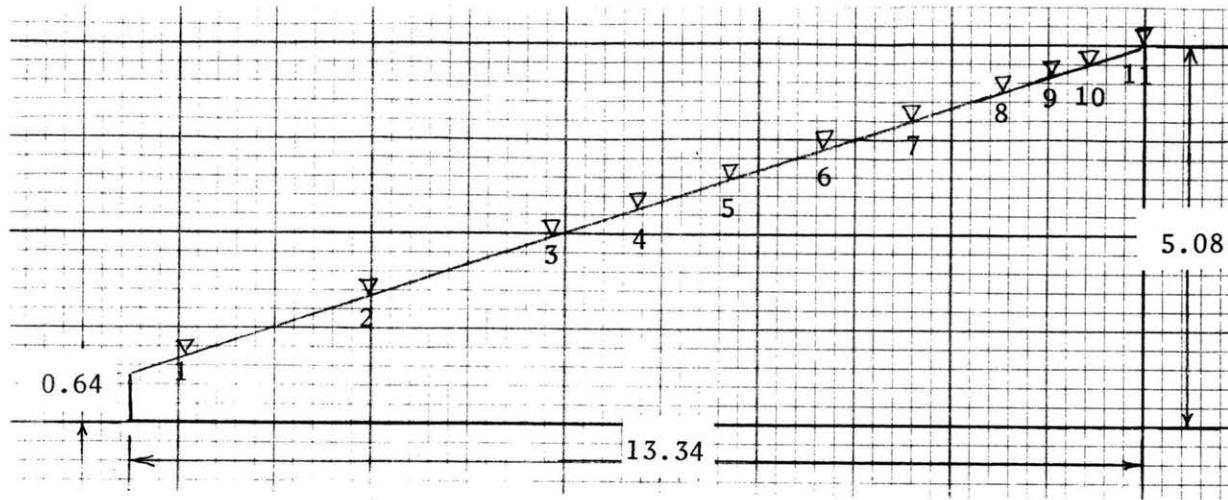
R	10.16	4.32	0.00
DELTA	50.70	46.23	46.36
U(REF)	9.13	9.42	8.96
T	21.33	21.33	21.33
BAR	8.39	8.39	8.39
DATE	7/11/1977	7/11/1977	7/11/1977

Y*	U*	Y*	U*	Y*	U*
.005	.586	.006	.611	.005	.647
.021	.635	.024	.670	.018	.693
.045	.670	.048	.686	.041	.749
.071	.723	.080	.717	.074	.763
.105	.749	.134	.750	.104	.784
.138	.765	.182	.774	.136	.792
.189	.781	.229	.796	.168	.819
.241	.808	.292	.812	.199	.837
.291	.828	.354	.835	.245	.847
.359	.845	.417	.841	.292	.862
.426	.864	.480	.874	.339	.874
.493	.885	.544	.896	.403	.897
.578	.911	.607	.900	.466	.922
.662	.935	.685	.929	.529	.932
.746	.961	.763	.948	.606	.959
.830	.989	.843	.963	.685	.976
.916	1.000	.921	.971	.764	1.000
1.000	1.000	1.000	1.000		

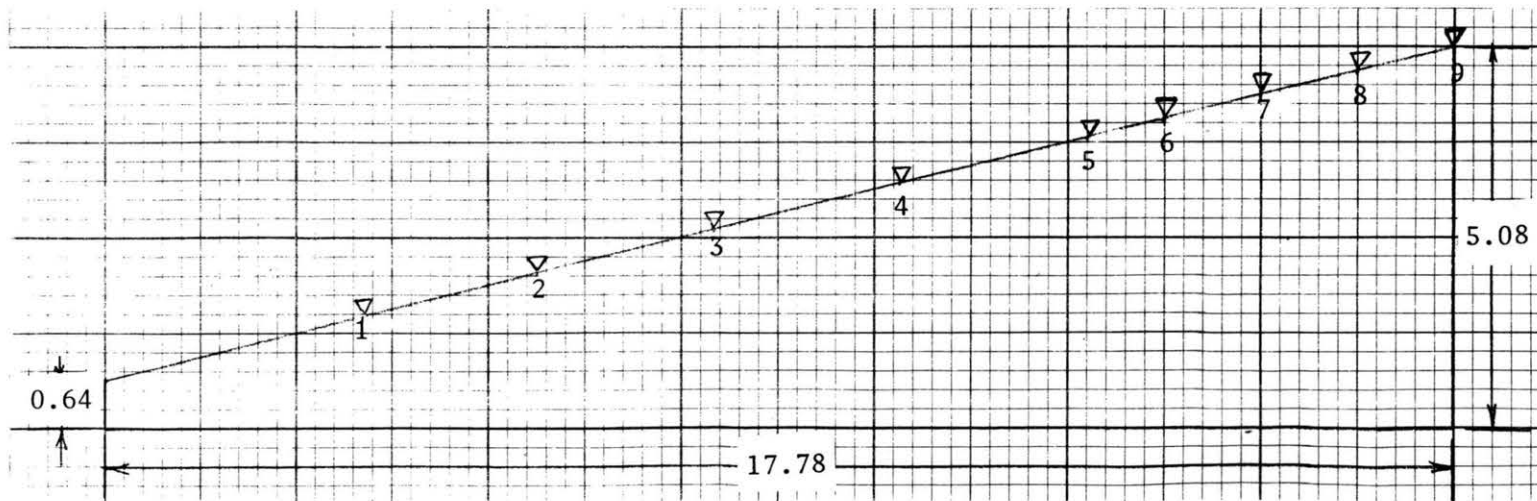


(a) Gaussian Hill (approximate).

Figure DI. Dimension of 3 dimensional hills and location of static taps on their surfaces (Real scale).



(b) Cone shaped hill with 1:4 slope.



(c) Cone shaped hill with 1:3 slope.

Figure DI (concluded) Dimension of 3-dimensional hills and location of static taps on their surfaces (Real scale)



a) 12.1 m/sec



b) 15.2 m/sec



c) 18.3 m/sec

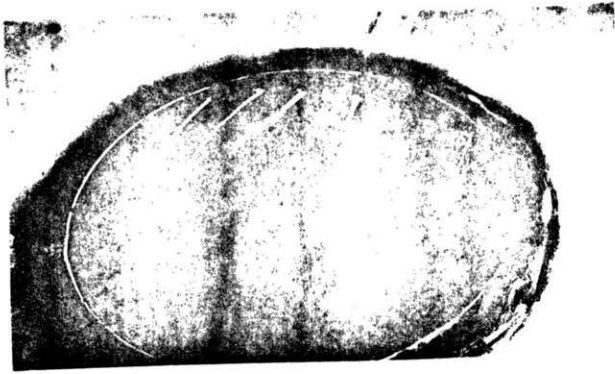


d) 21.2 m/sec

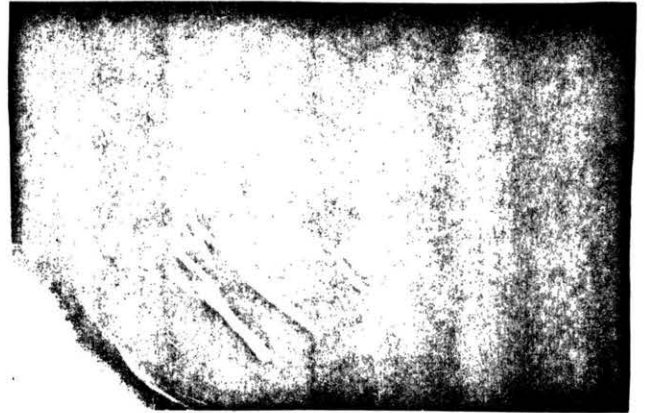


Flow direction

Figure D2 Surface
oil streak patterns
over the Gaussian
hill. (top view)



a) Upstream smoke streaks.



b) Side view.



c) Downstream separation effect.

Figure D3 Smoke streak patterns over the Gaussian hill

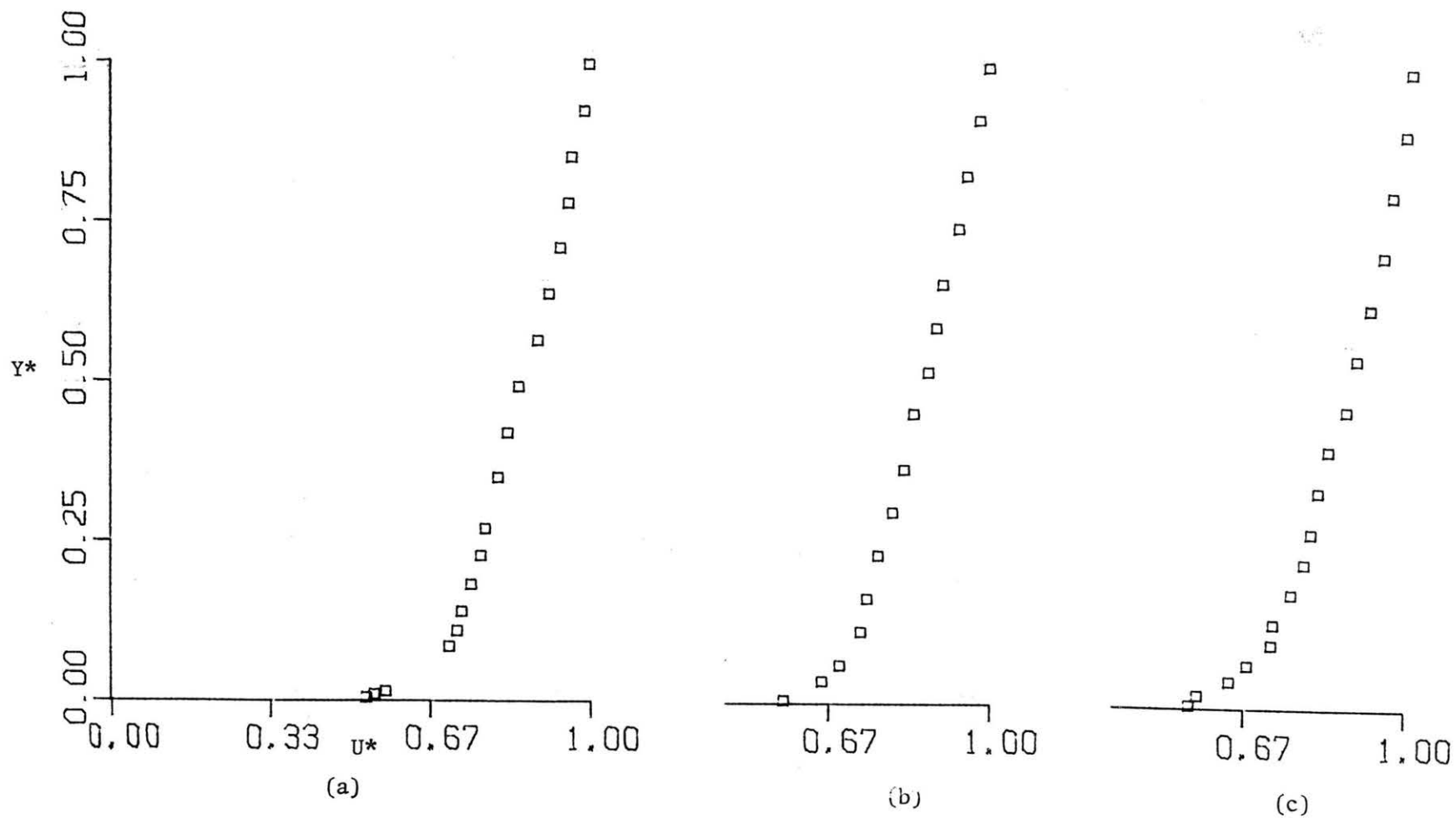
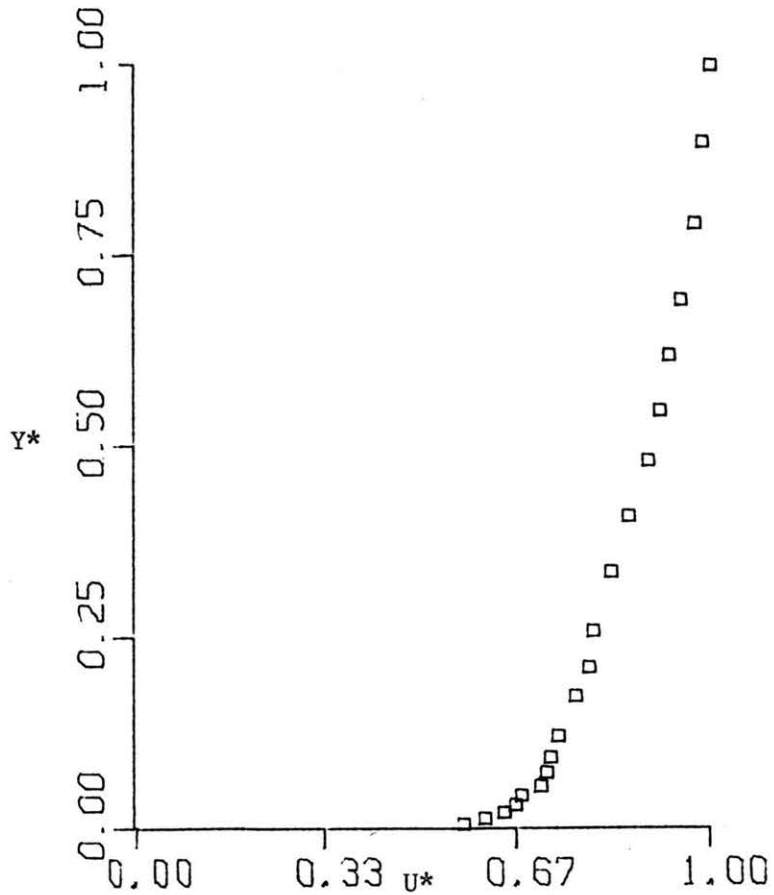
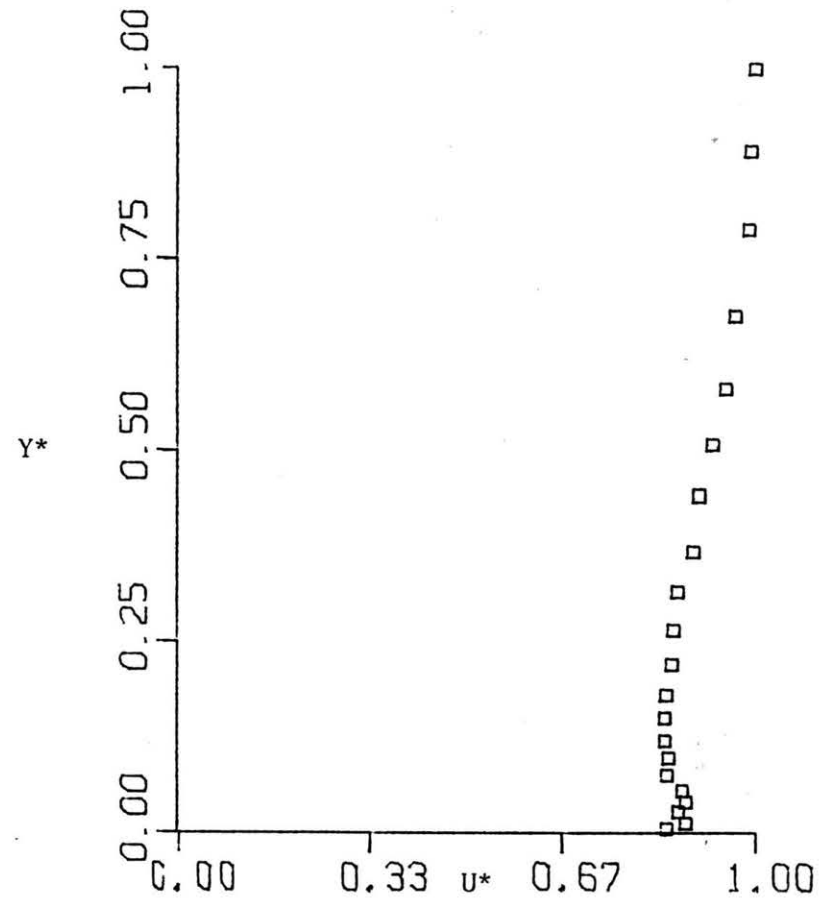


Figure D4 Upstream velocity profiles. (a) 50.8 cm upstream crest of Hill No. 1 -- Gaussian hill $U(\text{REF}) = 9.78$ m/s. (b) 28.7 cm upstream crest of Hill No. 2 -- 1:4 hill $U(\text{REF}) = 9.33$ m/s. (c) 20.3 cm upstream crest of Hill No. 3 -- 1:3 hill $U(\text{REF}) = 9.24$ m/s



(a)



(b)

Figure D5 Velocity profiles for Hill No. 1 at $U_{FS} = 15.25$ m/s and measuring angle 0° from flow direction. (a) 50.8 cm upstream crest of hill, (b) crest of hill

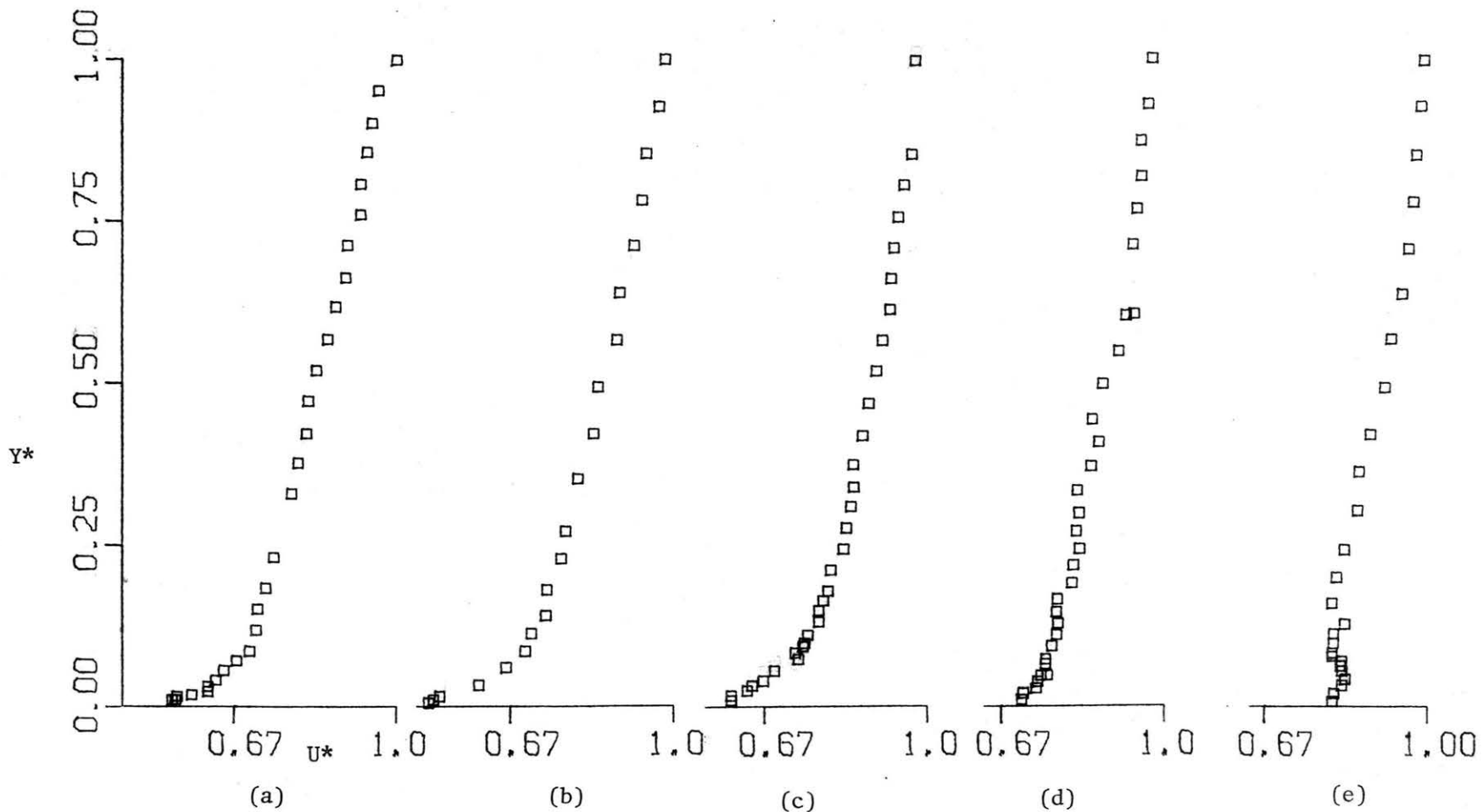


Figure D6 Velocity profiles for Hill No. 1 at $\theta = 0^\circ$, (a) $R = 31.90$ cm, $U(\text{REF}) = 9.14$ m/s, (b) $R = 20.80$ cm, $U(\text{REF}) = 9.60$ m/s, (c) $R = 9.25$ cm, $U(\text{REF}) = 9.77$ m/s, (d) $R = 4.60$ cm, $U(\text{REF}) = 10.15$ m/s, (e) crest of the hill, $U(\text{REF}) = 9.69$ m/s

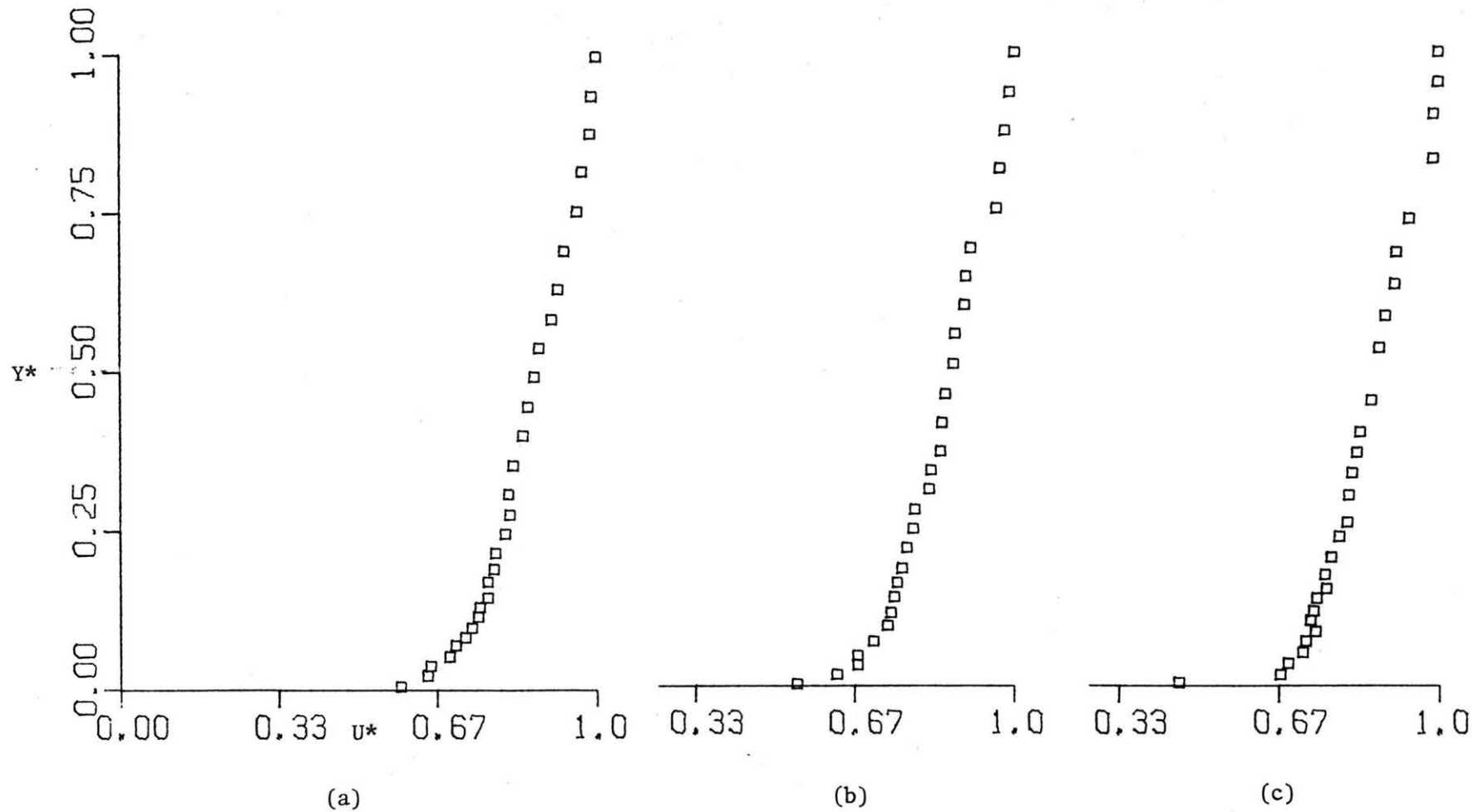


Figure D7 Velocity profiles for Hill No. 1 at $\theta = 45^\circ$, $V = 9.4$ m/s
 (a) $R = 20.80$ cm, $U(\text{REF}) = 9.33$ m/s.
 (b) $R = 9.25$ cm, $U(\text{REF}) = 9.60$ m/s.
 (c) $R = 4.60$ cm, $U(\text{REF}) = 9.60$ m/s.

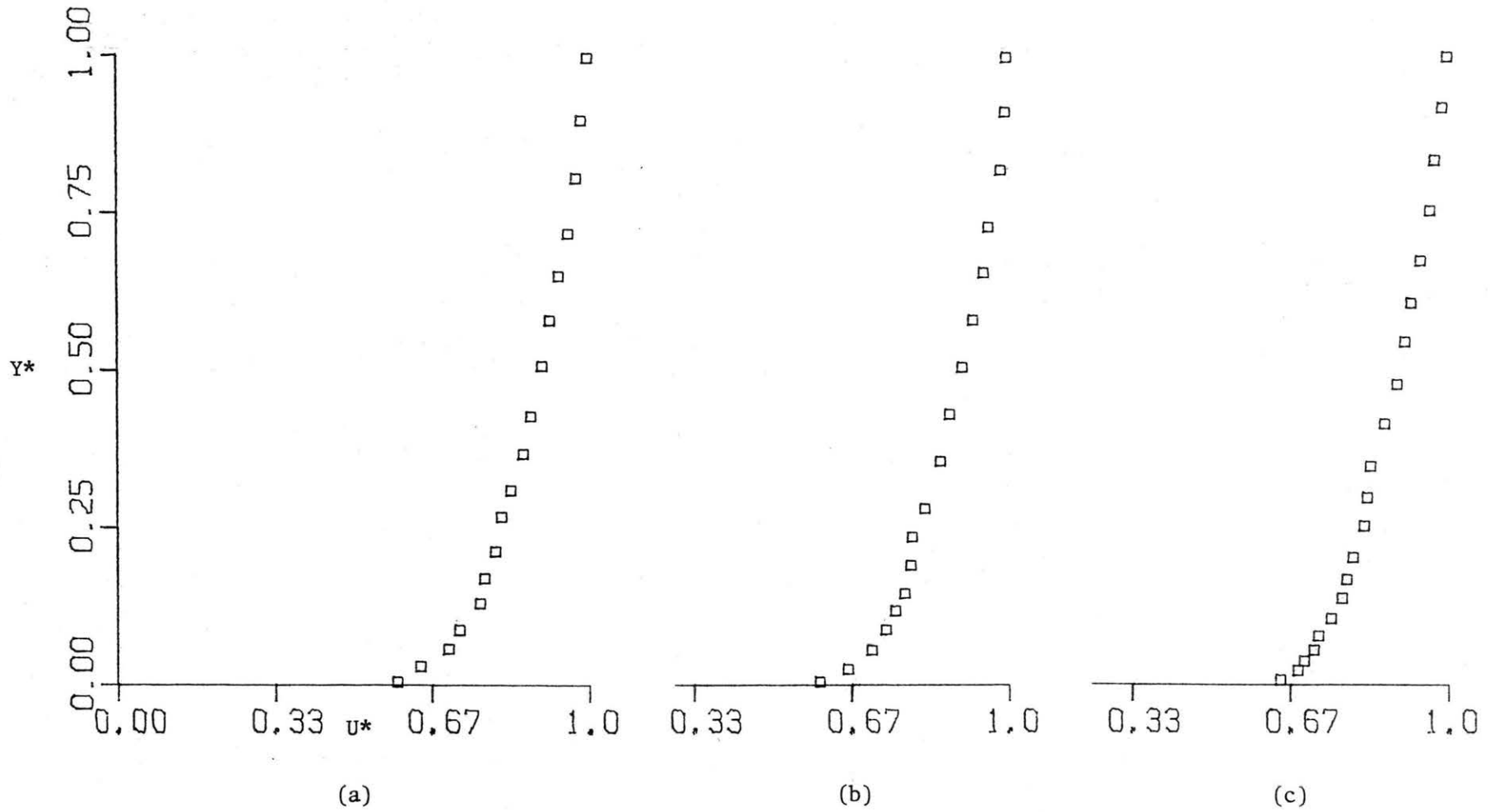


Figure D8 Velocity profiles for Hill No. 1 at $\theta = 90^\circ$
 (a) $R = 20.80$ cm, $U(\text{REF}) = 9.60$ m/s.
 (b) $R = 9.25$ cm, $U(\text{REF}) = 9.60$ m/s.
 (c) $R = 4.60$ cm, $U(\text{REF}) = 9.60$ m/s.

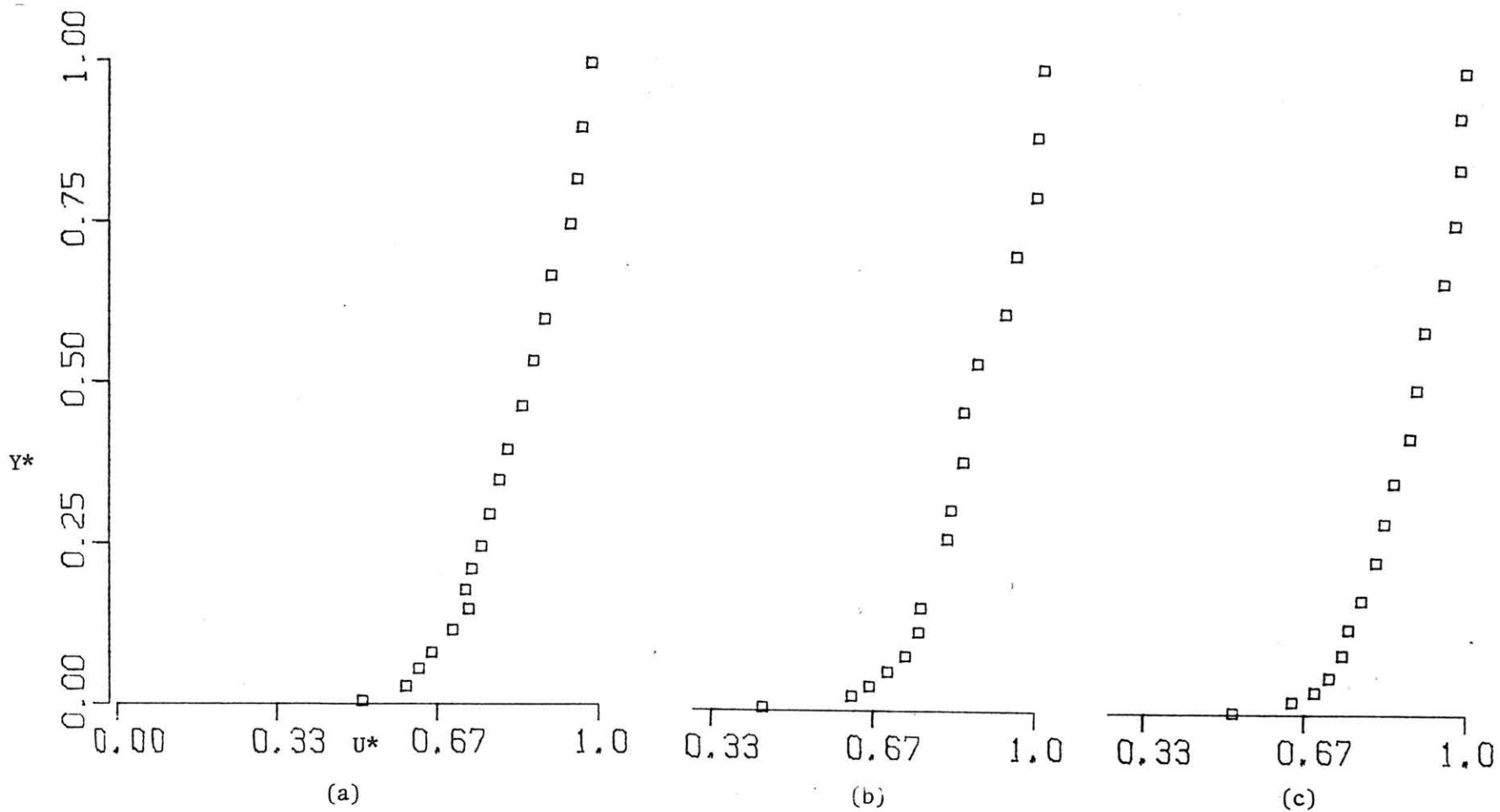
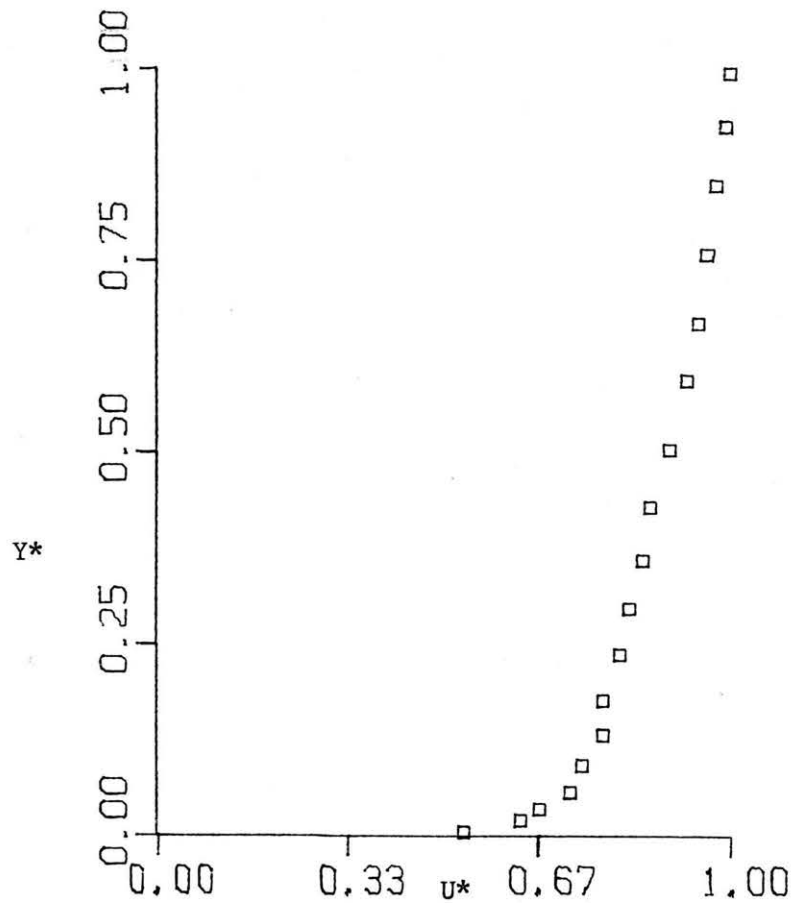
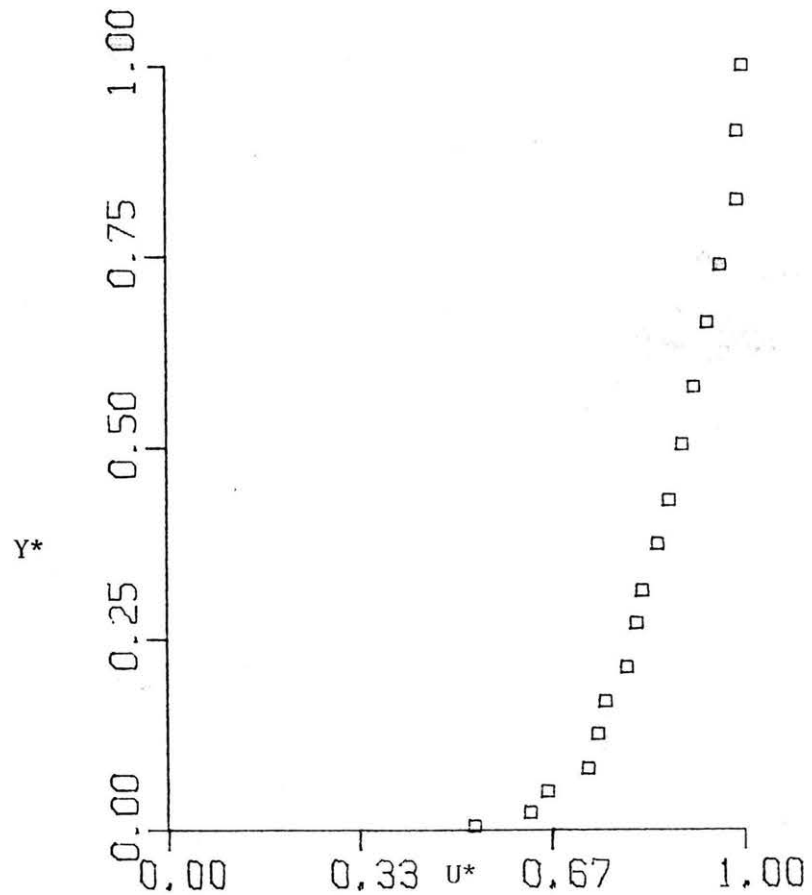


Figure D9 Velocity profiles for Hill No. 2, at $\theta = 0^\circ$
 (a) $R = 12.85$ cm, $U(\text{REF}) = 9.17$ m/s.
 (b) $R = 7.62$ cm, $U(\text{REF}) = 9.20$ m/s.
 (c) crest of hill, $U(\text{REF}) = 9.24$ m/s.



(a)



(b)

Figure D10 Velocity profiles for Hill No. 2 at $\theta = 45^\circ$ (a) $R = 12.85$ cm, $U(\text{REF}) = 9.24$ m/s.(b) $R = 7.62$ cm, $U(\text{REF}) = 9.42$ m/s.

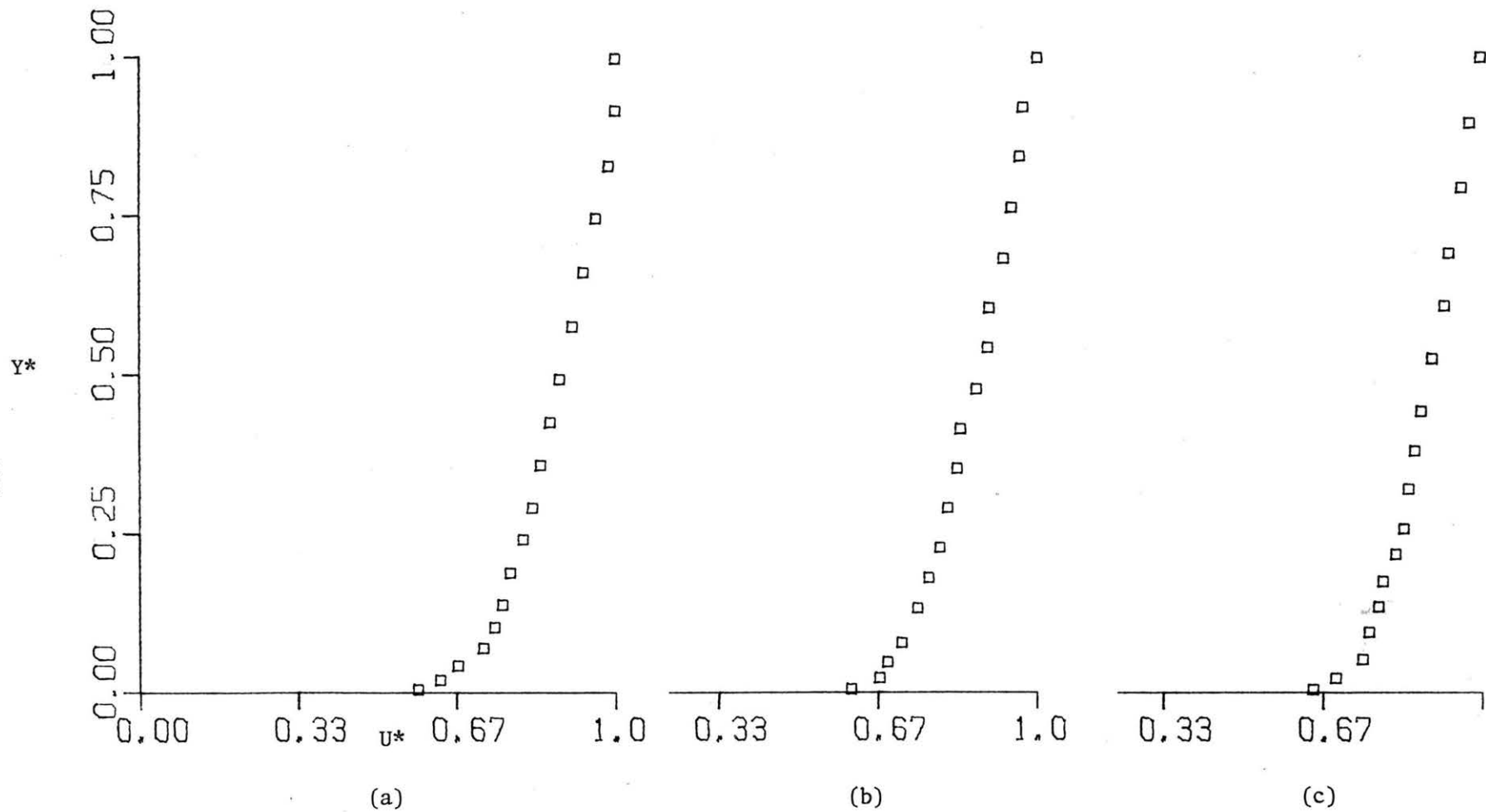


Figure D11 Velocity profiles for Hill No. 2 at $\theta = 90^\circ$
 (a) $R = 22.86$ cm, $U(\text{REF}) = 9.42$ m/s.
 (b) $R = 12.85$ cm, $U(\text{REF}) = 9.24$ m/s.
 (c) $R = 7.62$ cm, $U(\text{REF}) = 9.33$ m/s.

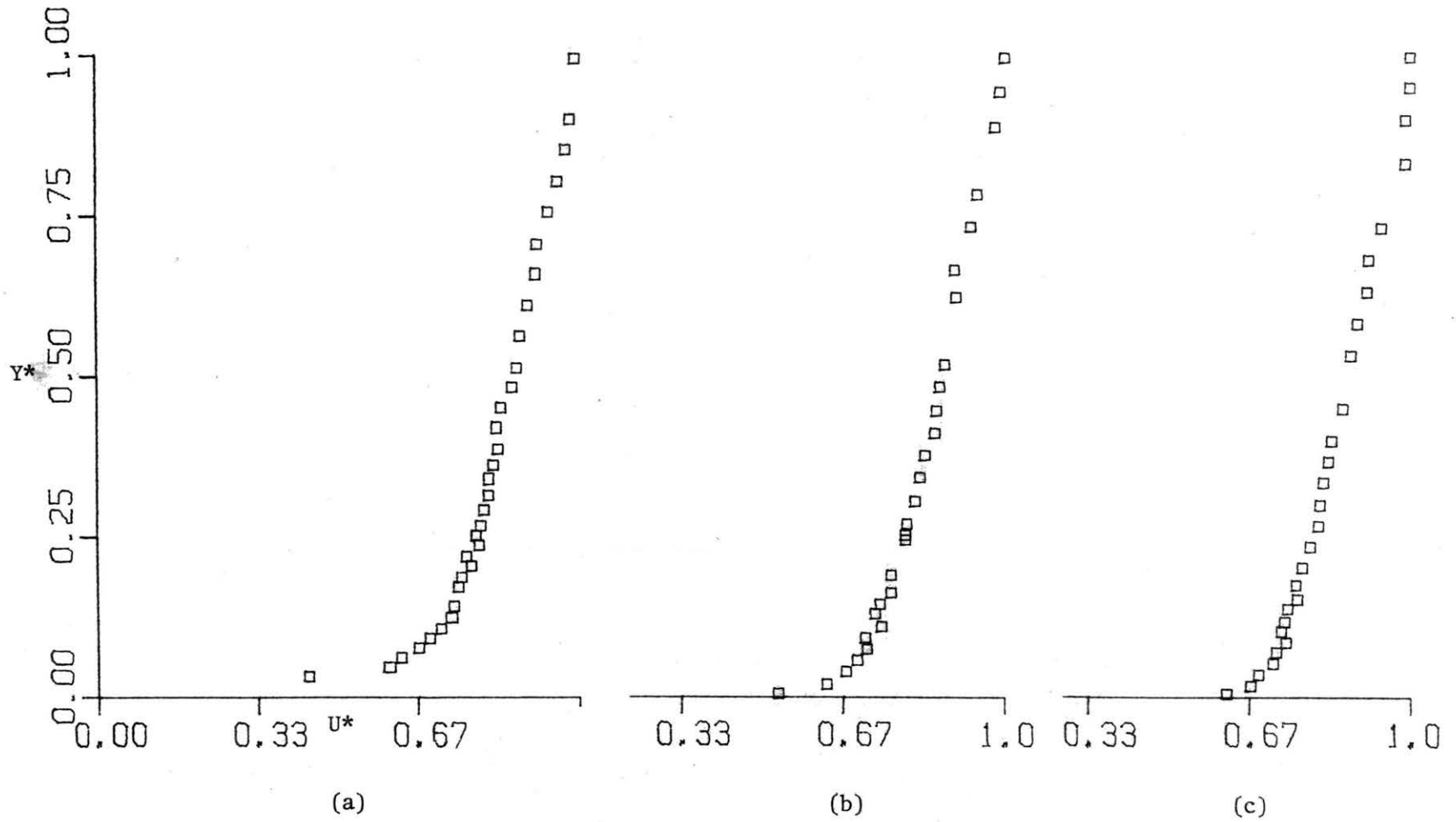


Figure D12 Velocity profiles for Hill No. 3 at $\theta = 0^\circ$
 (a) $R = 10.16$ cm, $U(\text{REF}) = 9.13$ m/s.
 (b) $R = 4.32$ cm, $U(\text{REF}) = 9.42$ m/s.
 (c) Crest of hill, $U(\text{REF}) = 8.96$ m/s.

APPENDIX E

EFFECTS OF ALTERNATE RIDGE SHAPES

By V. A. Sandborn and H. C. Chien

SUMMARY

Measurements of the velocity distributions near the upstream edge of bluff, two-dimensional ridges are reported. The extent of the separation bubble observed at the upwind edge of the bluff-step type ridge was evaluated. The maximum height of the separation bubble was approximately one step height from the forward edge of the ridge. The results also indicate the separation bubble extends for about 0.4 step heights out from the surface. It appears that wind power systems should be located at least 3 step heights downstream of the bluff to be out of the separation effects.

INTRODUCTION

An experimental survey of the speedup of winds over a number of different ridge shapes were reported in Appendix A. The general result was that triangular ridges produced the greatest speedup ratios. Alternate shapes, such as sine waves produced speedups of comparable magnitude as the triangular ridge. Thus, either sharp crested or round crested ridges will be the best for wind power applications.

BLUFF RIDGES

The original survey of Rider and Sandborn (1977) (Appendix A) demonstrated that bluff ridges, either with a "step" rise or a very sharp slope, failed to produce speedup ratios comparable to the gentle slope (1 to 3 or greater) triangular ridge. From smoke flow visualization the step ridge was shown to have a flow separation bubble at the top of the step. Employing the same test facility and models as reported previously, a detailed set of measurements were made in the separation region on top of the step ridge. Figure E1 shows the measured velocity distributions in the region above the separation bubble for $U_{\infty} = 17.4$ meters per second. As shown in Figure E2 the separation bubble extends back from the forward edge approximately 4 H. The region of separated flow extends out approximately 0.4 H or less from the surface. The location of maximum height of the separation is approximately 1 H back from the forward edge of the ridge. Thus, for wind power applications it is necessary to be at least 3 ridge heights downstream of a bluff to insure that the wind turbine is not operating in a separated flow region. Information on the effect of flow Reynolds number on the separation is also shown on Figure E2. The present model study was shown by Rider and Sandborn (1977) (Appendix A) to give similar value of the speedup ratio for triangular hills as a study made in an order of magnitude larger Reynolds number.

Thus, the effect of Reynolds number was not expected to be a major factor in defining the shape of the separation bubble. Increasing the Reynolds number of the present test case by increasing the velocity produced slightly smaller separation bubbles. Thus, it would appear that the present case will produce a larger bubble of separation than that encountered at higher Reynolds numbers. The present separation bubble dimensions should represent a conservative estimate of similar separation bubbles encountered in the atmosphere.

A detailed set of velocity profiles were also taken for a steep slope (1 to 1.5) ridge, Figure E3. This steep ridge indicated a modest speedup in the initial investigation. The smoke visualization study suggested a possible near separation directly at the foot of this ridge. The separation is limited to the region directly at the foot of the ridge. Half way up the forward face of the ridge the velocity profile is well on its way to recovering the lost momentum near the surface. At the initial crest of the ridge the velocity near the surface is greater than the original approach velocities. However, the recovery of the boundary layer velocity near the surface cannot reach values obtained with the smaller slopes triangular ridges. The shear layer extends well out beyond usable wind power heights, so the wind turbine will be forced to operate in a wind gradient for this type of ridge, Figure E3b, develop like a flat plate boundary layer, which progressively loses momentum to the surface.

Figure E3c shows velocity profiles measured in the separation region behind the ridge. The initial profile ($x = 12.7$ cm) at the start of the rearward ramp shows a slight tendency for the velocity gradient to decrease in the region of interest for wind power. The presence of a separation downstream may act to smooth out the velocity gradient near the surface.

Table EI Velocity profiles. Bluff step ridge

a)		b)		c)	
$x = .13 \text{ CM}$		$x = 3.18 \text{ CM}$		$x = 4.98 \text{ CM}$	
$U_{\infty} = 17.87 \text{ M/S}$		$U_{\infty} = 17.87 \text{ M/S}$		$U_{\infty} = 17.87 \text{ M/S}$	
Y	U(Y)	Y	U(Y)	Y	U(Y)
.25	0.00	.25	0.00	.25	0.00
.27	0.00	.49	0.00	.58	0.00
.40	8.39	.89	0.00	.76	1.16
.71	9.01	.97	0.00	1.50	8.23
1.17	10.01	1.29	6.98	2.18	10.41
1.99	11.04	1.71	9.87	3.59	12.09
2.95	12.20	2.16	10.79	4.71	12.85
3.76	12.64	2.69	11.52	5.95	13.67
5.28	13.67	3.45	12.20	7.82	14.53
6.55	14.25	4.69	13.37	9.81	15.43
8.07	14.99	5.98	14.06	12.10	16.62
9.60	15.70	7.27	14.53	13.62	17.02
11.35	16.29	8.54	15.08	14.98	17.41
13.12	17.02	9.81	15.52	16.10	17.57
14.64	17.49	11.43	16.37	17.40	17.87
15.81	17.80	13.55	17.10		
17.17	17.87	15.77	17.72		
		17.39	17.87		
d)		e)		f)	
$x = 7.37 \text{ CM}$		$x = 8.26 \text{ CM}$		$x = 12.27 \text{ CM}$	
$U_{\infty} = 17.87 \text{ M/S}$		$U_{\infty} = 18.10 \text{ M/S}$		$U_{\infty} = 18.17 \text{ M/S}$	
Y	U(Y)	Y	U(Y)	Y	U(Y)
.25	0.00	.25	0.00	.25	4.94
.33	2.02	.70	5.20	.49	6.27
.74	4.94	1.15	6.78	.80	7.17
1.12	6.58	1.56	8.55	1.13	8.06
1.63	8.86	2.16	10.41	1.52	9.01
2.12	10.28	2.68	11.16	2.02	10.01
3.36	11.86	3.43	12.09	2.75	11.28
4.68	12.96	4.44	12.96	3.45	12.31
5.97	13.67	5.81	13.77	4.64	13.27
7.20	14.34	7.06	14.53	5.99	14.06
8.46	14.90	8.52	15.08	7.33	14.81
9.75	15.43	9.80	15.70	8.70	15.35
11.62	16.29	11.05	16.20	9.88	15.95
13.57	17.02	12.32	16.94	11.16	16.45
14.85	17.41	13.49	17.49	12.40	16.94
16.06	17.72	14.81	17.57	13.71	17.41
17.36	17.87	16.13	17.87	14.95	17.72
		17.35	18.10	16.21	17.95
				17.52	18.17

Table EII Velocity profiles 1:1.5 slope ridge

a)		b)		c)		d)	
X = -19.37 CM		X = -2.26 CM		X = 0.00 CM		X = 2.54 CM	
U _∞ = 17.41 M/S		U _∞ = 17.41 M/S		U _∞ = 17.41 M/S		U _∞ = 17.41 M/S	
Y	U(Y)	Y	U(Y)	Y	U(Y)	Y	U(Y)
.25	7.98	.15	7.89	.25	9.73	.25	5.93
.44	8.55	.43	8.39	.60	10.14	.58	9.73
.68	9.01	.69	8.86	.85	10.28	.86	10.14
.94	9.59	.96	9.31	1.10	10.66	1.11	10.54
1.43	10.54	1.20	9.59	1.36	10.91	1.35	10.79
2.22	11.40	1.45	10.01	1.61	11.16	1.61	11.04
2.98	11.75	1.70	10.41	1.85	11.40	1.86	11.04
3.48	12.09	1.97	10.54	2.11	11.63	2.13	11.40
4.76	12.74	2.22	10.91	2.87	12.31	2.61	11.86
6.00	13.37	2.47	11.16	4.16	12.96	2.88	11.98
7.29	13.77	2.74	11.28	5.42	13.47	4.15	12.64
8.56	14.25	3.48	11.75	6.69	14.15	5.42	13.37
9.83	14.81	4.00	12.20	7.96	14.53	6.68	13.96
11.10	15.26	5.26	12.85	9.23	14.99	7.96	14.53
12.36	15.78	6.53	13.37	10.51	15.70	9.23	14.99
13.65	16.12	7.82	13.86	11.77	16.12	10.49	15.61
14.90	16.70	9.07	14.34	13.05	16.70	11.77	15.95
16.17	17.02	10.35	14.90	14.32	17.02	13.05	16.54
17.45	17.41	11.62	15.35	15.59	17.26	14.30	16.94
		12.88	15.70	16.83	17.41	15.58	17.26
		14.16	16.45			16.83	17.41
		15.41	16.94				
		14.16	17.26				
		17.96	17.41				

Table EII (concluded) Velocity profiles 1:1.5 slope ridge

e)		f)		g)		h)	
$x =$	5.08 CM	$x =$	12.70 CM	$x =$	14.61 CM	$x =$	16.51 CM
$U_{\infty} =$	17.41 M/S	$U_{\infty} =$	17.80 M/S	$U_{\infty} =$	17.57 M/S	$U_{\infty} =$	18.25 M/S
Y	U (Y)	Y	U (Y)	Y	U (Y)	Y	U (Y)
.25	7.27	.25	7.36	.38	0.00	.38	0.00
.57	9.59	.42	9.01	.53	0.00	.74	0.00
.82	10.14	.68	10.01	.67	0.00	1.23	0.00
1.08	10.54	.93	10.54	.92	0.00	1.75	0.00
1.34	10.91	1.19	10.79	1.17	0.00	2.46	0.00
1.57	11.16	1.44	11.04	1.43	0.00	2.64	5.93
1.85	11.16	1.69	11.16	1.52	0.00	3.02	9.59
2.11	11.40	1.95	11.40	1.69	6.05	3.27	10.54
2.35	11.63	2.19	11.52	1.93	9.31	3.54	11.16
2.60	11.86	2.45	11.75	2.18	10.28	3.78	11.40
2.84	12.09	2.95	12.09	2.45	10.79	4.05	11.63
3.37	12.42	1.68	12.85	2.70	11.04	4.54	11.86
4.11	12.74	5.49	13.67	2.96	11.40	5.04	12.20
5.41	13.37	6.76	14.15	3.22	11.40	5.81	12.74
6.68	14.15	8.04	14.62	3.72	11.75	7.08	13.47
7.93	14.53	9.31	15.17	4.22	12.09	8.36	14.06
9.20	15.08	10.57	15.61	4.99	12.64	9.63	14.81
10.47	15.61	11.84	16.12	6.25	13.37	10.90	15.35
11.74	16.12	13.10	16.70	7.52	14.06	12.15	15.87
13.01	16.70	14.38	17.10	8.80	14.62	13.44	16.29
14.27	17.02	15.67	17.33	10.07	15.17	14.71	16.94
15.55	17.33	16.93	17.57	11.34	15.61	15.97	17.33
16.83	17.41	18.20	17.80	12.59	15.78	17.24	17.72
				13.87	16.12	18.51	17.95
				15.13	16.70	19.78	18.10
				16.41	16.94	21.06	18.25
				17.69	17.26		
				18.96	17.49		
				20.20	17.57		

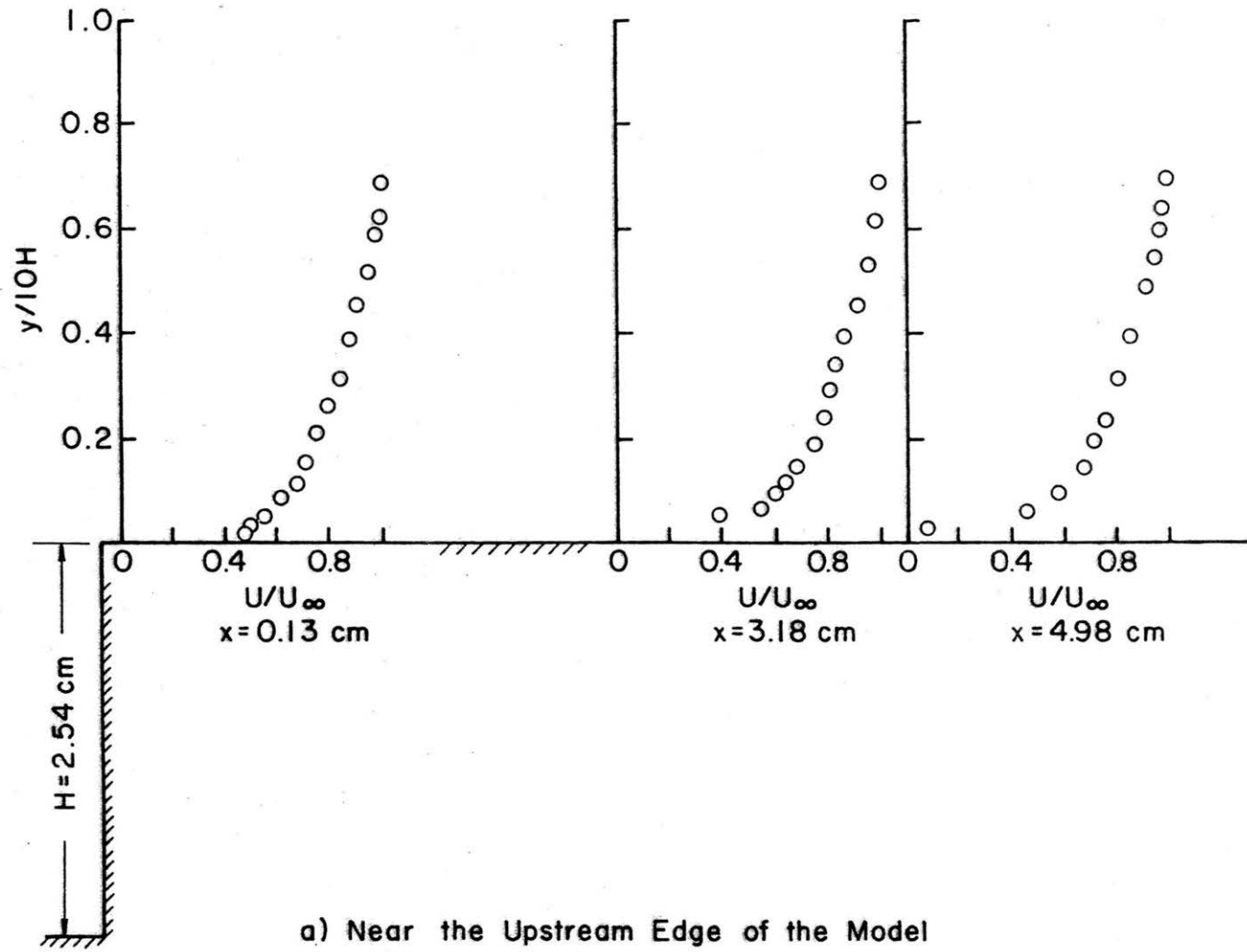


Figure EI Velocity profiles along the top of a bluff-step ridge

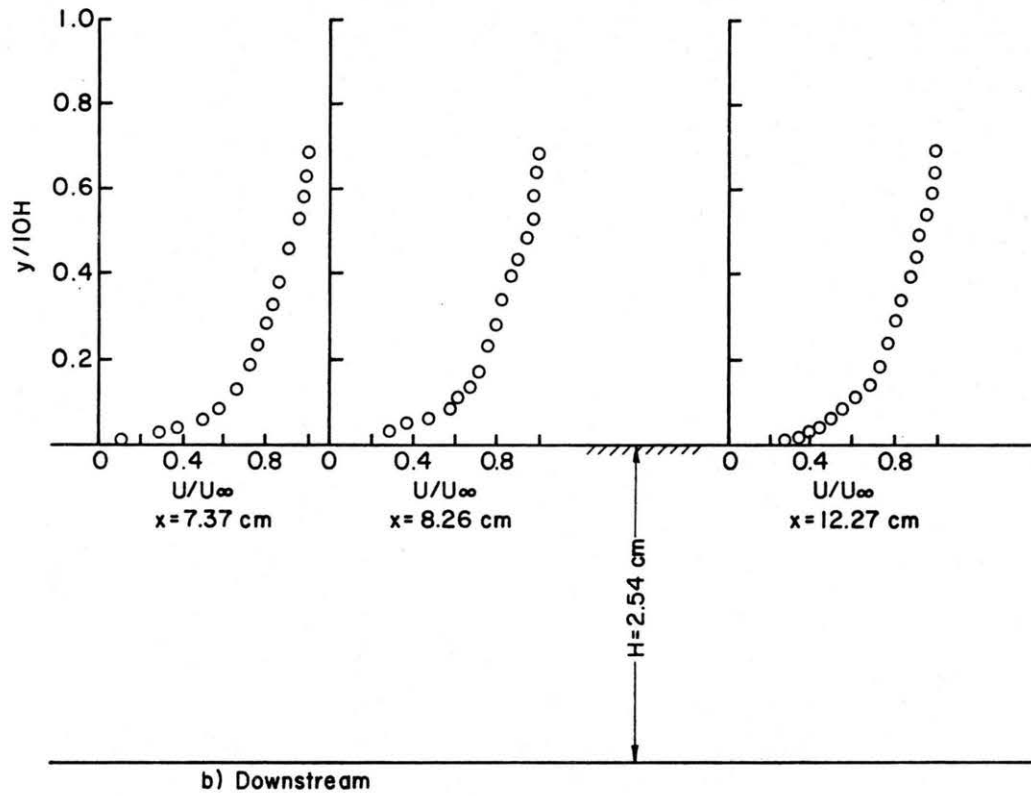


Figure E1 (continued) Velocity profiles along the top of a bluff-step ridge

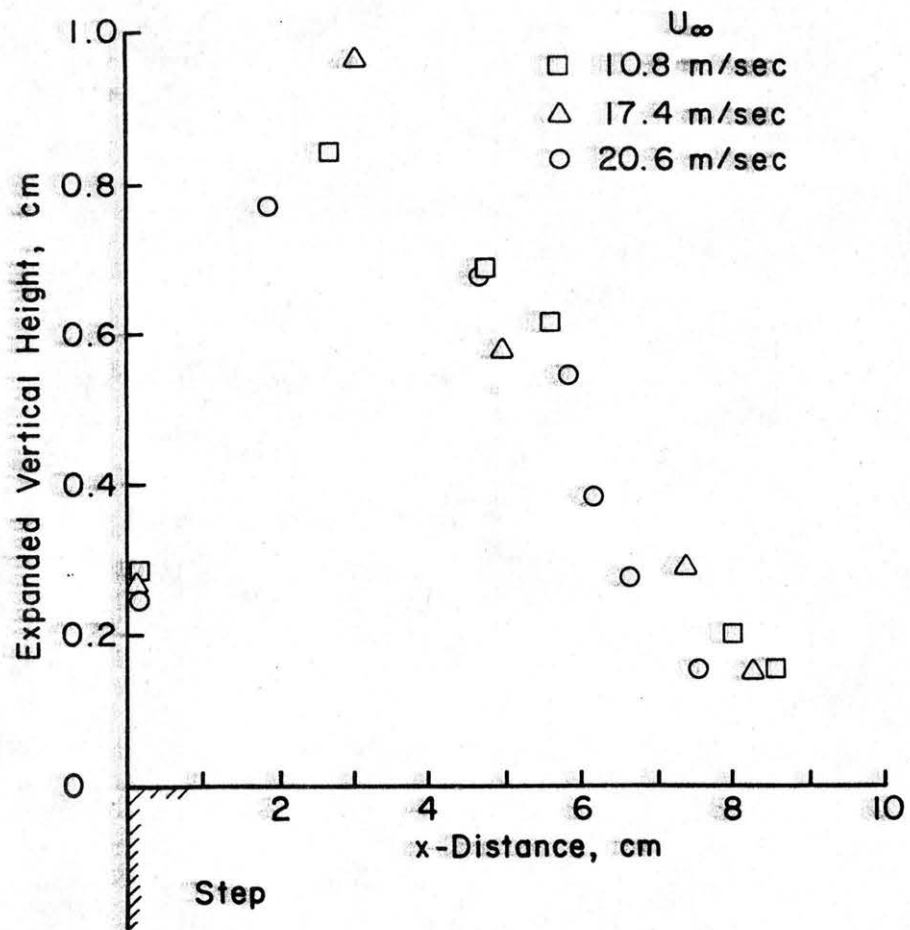


Figure E2 Measured separation bubble extent at the forward edge of a bluff-step ridge

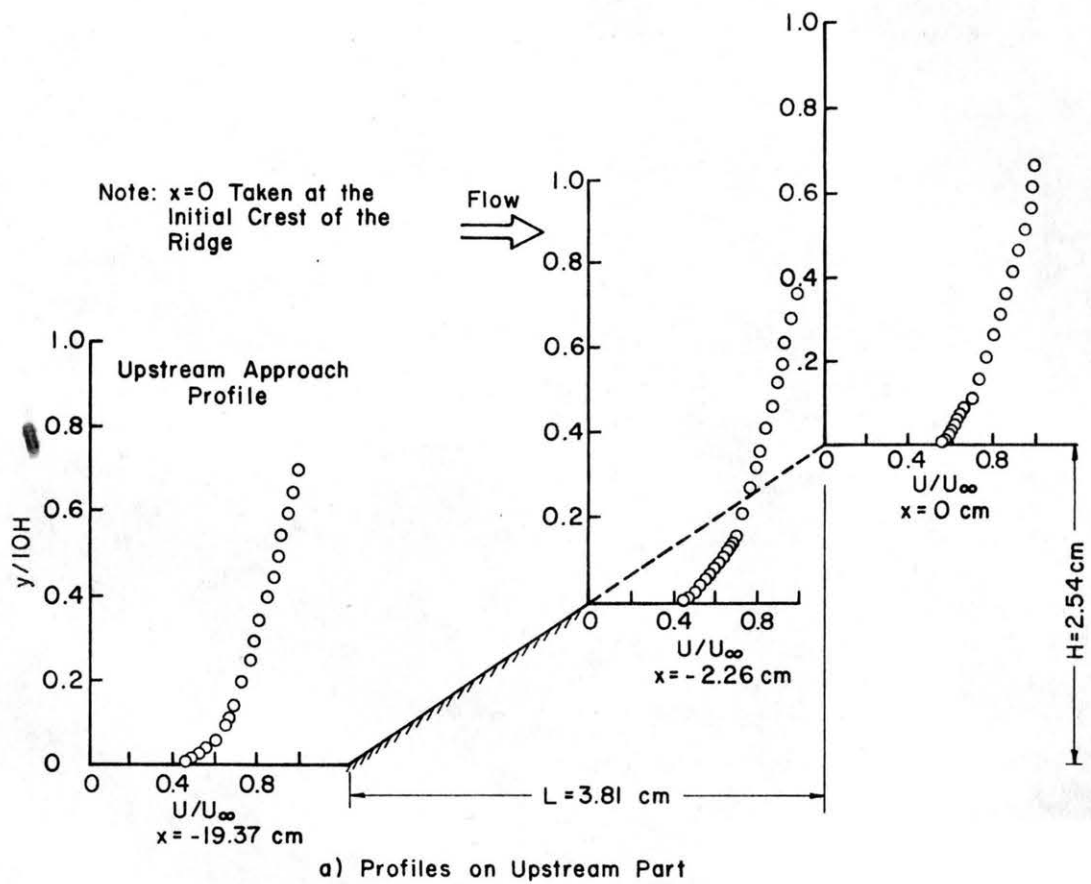


Figure E3 Velocity distributions over a bluff-step sloped ridge